





25098653



This is to certify that the

dissertation entitled

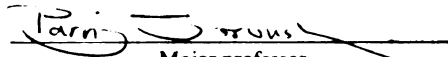
"Constitutive Modeling And Flexural Analysis  
of Steel Fiber Reinforced Concrete for  
Structural Applications."

presented by

Mr. Cha-Don Lee

has been accepted towards fulfillment  
of the requirements for

Ph.D. degree in Civil Engineering

  
Major professor

Date Jan. 2, 1990

**PLACE IN RETURN BOX to remove this checkout from your record.  
TO AVOID FINES return on or before date due.**

DATE DUE	DATE DUE	DATE DUE
APR 25 1998	_____	_____
Jul 12	_____	_____
SEP 27 1998 244	_____	_____
MAR 09 2001	_____	_____
_____	_____	_____
_____	_____	_____
_____	_____	_____
_____	_____	_____

MSU is An Affirmative Action/Equal Opportunity Institution

**CONSTITUTIVE MODELING AND FLEXURAL ANALYSIS  
OF STEEL FIBER REINFORCED CONCRETE  
FOR STRUCTURAL APPLICATIONS**

By

**Cha-Don Lee**

A DISSERTATION

Submitted to  
Michigan State University  
in partial fulfillment of the requirements  
for the degree of

DOCTOR OF PHILOSOPHY

Department of Civil and Environmental Engineering

1990

**ABSTRACT****CONSTITUTIVE MODELING AND FLEXURAL ANALYSIS  
OF STEEL FIBER REINFORCED CONCRETE  
FOR STRUCTURAL APPLICATIONS***by***Cha-Don Lee**

The objective of this study was to develop techniques for predicting the effects of steel fibers on the tensile, compressive and flexural behavior of concrete.

A refined concept ("interaction concept") was proposed for predicting the tensile strength of SFRC. This concept accounts for the contributions of fibers through their pull-out action and also by arresting the growth of microcracks in cementitious matrices. A constitutive model was also developed for predicting the complete tensile stress-strain relationship of SFRC. The modeling of post-peak performance takes into account the contributions of fibers crossing the critical section through their pull-out action as well as that of matrix in its post-peak softening range of behavior.

A simple and practical model was also developed for predicting the compressive constitutive behavior of steel fiber reinforced concrete. The model accounts for the effects of fiber volume fraction, aspect ratio and type (straight vs. hooked), and the matrix compressive strength, on the compressive behavior of

SFRC.

A flexural analysis procedure, with some simplifying assumptions made to simulate the flexural behavior in the vicinity of the cracked section, was developed which gives due consideration to the behavior at and near the critical (cracked) section. The tensile and compressive constitutive models of SFRC developed in this study were used in this flexural analysis procedure. Analytical studies were conducted using the developed flexural analysis procedure in order to derive relationships between the tensile constitutive behavior and the flexural strength of SFRC.

The complexity and instability associated with testing cementitious materials in direct tension have led to extensive use of flexural testing for assessing the tensile behavior of SFRC. It is thus important to analyze flexural test results in order to derive information regarding tensile performance of SFRC. For this purpose, a "System Identification" approach was adopted in this investigation.

The "System Identification" technique was used together with the developed flexural analysis procedure in order to derive information on the tensile behavior of SFRC using flexural test results. This technique was successful in obtaining optimum sets of parameters which provide satisfactory matches between the measured and predicted flexural load-deflection relationships. The tensile characteristics of SFRC obtained from analysis of flexural test results by "System Identification" were superior to those obtained from direct tension test results. This phenomenon was attributed to the positive effects of strain gradient existing in SFRC under flexural loads.

*To Young-Soon and Uihwan*

## **ACKNOWLEDGMENT**

I wish to express my sincere appreciation to those who have contributed to the development of this dissertation by their academic guidance and by encouragement. In particular, I would like to thank my academic advisor Dr. Parviz Soroushian, Associate Professor of Civil and Environmental Engineering, for his constant help throughout this research. Thanks are also extended to the other members of the thesis committee; Dr. W. Bradley, Dr. N. Altiero, and Dr. G. Ludden for their interest and their comments during this research.

The financial support for this project was provided by the Research Excellence Fund of the State of Michigan, the DEED Research Program of the American Public Power Association, and the GE Faculty Development Program in Computer Aided Engineering. These contributions are gratefully acknowledged.

## TABLE OF CONTENTS

LIST OF TABLES .....	viii
LIST OF FIGURES .....	ix
Chapter 1: INTRODUCTION .....	1
Chapter 2: MECHANICAL PROPERTIES OF STEEL FIBER REINFORCED CONCRETE: A REVIEW OF THE LITERATURE .....	4
2.1 INTRODUCTION .....	4
2.2 STEEL FIBER REINFORCED CONCRETE UNDER TENSION .....	6
2.2.1 Microcracking in Mortar and Concrete under Tension .....	7
2.2.2 Microcracking in Steel Fiber Reinforced Concrete under Tension .....	10
2.2.3 Pull-Out Mechanism of Steel Fibers in SFRC under Tension .....	13
2.2.4 Tensile Behavior of Steel Fiber Reinforced Concrete .....	16
2.2.5 Constitutive Models .....	19
2.3 STEEL FIBER REINFORCED CONCRETES UNDER COMPRESSION .....	27
2.3.1 Microcracking in Mortar and Concrete under Compression .....	27
2.3.2 Compressive Behavior of Steel Fiber Reinforced Concrete .....	30
2.3.3 Analytical Modeling .....	33
2.4 STEEL FIBER REINFORCED CONCRETE UNDER FLEXURE .....	35
2.4.1 Flexural Properties of SFRC .....	36
2.4.2 Analysis of Steel Fiber Reinforced Concrete Beams under Flexure .....	38
Chapter 3: THE CONSTITUTIVE MODEL FOR STEEL FIBER REINFORCED CONCRETE UNDER TENSION .....	40
3.1 INTRODUCTION .....	40
3.2 EFFECTS OF FIBER REINFORCEMENT VARIABLES ON TENSILE BEHAVIOR OF STEEL FIBER REINFORCED CONCRETE .....	41
3.3 DEVELOPMENT OF EXPRESSIONS FOR THE NUMBER OF STEEL FIBERS CROSSING UNIT CROSS-SECTIONAL AREA IN SFRC .....	44
3.3.1 Development of Theoretical Expressions .....	45
3.3.2 Experimental Assessment of the Orientation Factor .....	55
3.3.3 Theoretical Values vs. Experimental Measurements .....	60
3.4 PREDICTION OF TENSILE STRENGTH: "INTERACTION CONCEPT" .....	62
3.4.1 "Interaction Concept" .....	64
3.4.2 Empirical Coefficients .....	66

3.4.3 "Interaction Concept" vs. Composite Material and Spacing Concept .....	69
3.5 PRE-PEAK CONSTITUTIVE MODELING .....	72
3.6 POST-PEAK CONSTITUTIVE MODELING .....	74
3.7 COMPARISON WITH TEST RESULTS .....	86
3.8 SUMMARY AND CONCLUSION .....	89
Chapter 4: THE CONSTITUTIVE MODEL FOR STEEL FIBER REINFORCED CONCRETE UNDER COMPRESSION .....	92
4.1 INTRODUCTION .....	92
4.2 EFFECTS OF VARIABLES ON COMPRESSIVE BEHAVIOR .....	93
4.3 EXPERIMENTAL RESULTS .....	96
4.4 THE CONSTITUTIVE MODELS FOR STEEL FIBER REINFORCED CONCRETE .....	100
4.5 COMPARISON WITH TEST RESULTS AND PARAMETRIC STUDIES .....	106
4.6 SUMMARY AND CONCLUSION .....	113
Chapter 5: FLEXURAL ANALYSIS OF STEEL FIBER REINFORCED CONCRETE .....	115
5.1 INTRODUCTION .....	115
5.2 FLEXURAL ANALYSIS .....	117
5.2.1 Curvature Distributions .....	117
5.2.2 Analysis of the Critical Section .....	121
5.2.3 Nonlinear Flexural Analysis of the Critical (Cracked) Section .....	126
5.2.4 Comparison with Test Results .....	129
5.3 FLEXURAL BEHAVIOR OF CRITICAL (CRACKED) SFRC SECTION .....	132
5.4 A PARAMETRIC STUDY OF SFRC BEAM FLEXURAL BEHAVIOR .....	136
5.5 SUMMARY AND CONCLUSION .....	153
Chapter 6: INTERPRETATION OF FLEXURAL TEST RESULTS USING "SYSTEM IDENTIFICATION" .....	157
6.1 INTRODUCTION .....	157
6.2 "SYSTEM IDENTIFICATION" .....	158
6.3 DEFINITION OF ERROR FUNCTION .....	161
6.4 METHOD OF OPTIMIZATION .....	162
6.5 SELECTION OF PARAMETERS IN "SYSTEM IDENTIFICATION" .....	173
6.6 RESULTS OF "SYSTEM IDENTIFICATION" .....	174
6.7 SUMMARY AND CONCLUSION .....	184

<b>Chapter 7: SUMMARY AND CONCLUSION .....</b>	<b>188</b>
<b>LIST OF REFERENCES .....</b>	<b>199</b>

## LIST OF TABLES

2.1 Application of Steel Fiber Reinforced Concrete .....	5
3.1 Mean Values of Fiber Orientation at Different Location on Cross Section and for Different Fiber Types .....	58
3.2 Direct Tensile Test Specimen and Results .....	67
3.3 Average, Standard Deviations and Sum Total of Squares of Normalized Errors for Different Concepts .....	71
3.4 Pull-Out Load-Deflection Relationship for Straight-Round Steel Fibers .....	77
3.5 Conditions of Some Direct Tension Test Results of SFRC .....	86
4.1 Fiber Reinforced Concrete Mixtures .....	98
5.1 Flexural Test Conditions .....	130
5.2 Effects of Material-Related Factors .....	140
5.3 Effects of Constitutive Behavior-Related Factors .....	140
5.4 Effects of Material-Related Factors ( $2^k$ Factorial Design) .....	152
5.5 Effects of Material-Related Factors in Order .....	152
6.1 Test Conditions and Optimized Values from System Identification .....	175
6.2 Comparison of the Tension Test Results with the Optimum Values of Parameters in Analysis of Flexural Test Results Using System Identification .....	176
6.3 Derived Tensile Strength of Matrices and Composites in Direct Tension and System Identification .....	183

## LIST OF FIGURES

2.1 Propagation of Cracks in Cementitious Matrix .....	8
2.2 Tortuosity of Crack Path .....	9
2.3 Branching of Microcracks inside the Cement Paste and Shattering of Grains by Crossing Microcracks .....	9
2.4 Interaction of Microcracks with Steel Fibers .....	10
2.5 Continuous Nature of Shifted Microcracks around a Steel Fiber .....	11
2.6 Schematic Description of the Microstructure of Steel Fiber-Cement Interface .....	12
2.7 Debonding and Pseudo-Debonding of Steel Fibers in Cementitious Materials .....	12
2.8 Interaction of a Crack with a Number of Randomly Oriented Steel Fibers .....	13
2.9 A Typical Relationship between Average Bond Stress and Pull-Out Deflection in Pull-Out Tests on Straight-Round Steel Fibers .....	15
2.10 Effect of Fiber Types on Pull-Out Behavior .....	15
2.11 Deviation from Linear Behavior in SFRC, Resulting from Gradual Microcrack Propagation .....	16
2.12 Typical Direct Tensile Stress-Strain Relationships for Concrete and Mortar Matrices .....	17
2.13 Two Theoretical Types of SFRC Direct Tensile Behavior in the Post-Peak Region .....	18
2.14 Fiber Reinforced Composite .....	20
2.15 Verification of the Composite Material Concept .....	24
2.16 Verification of the Spacing Concept .....	26
2.17 Localization of Microcracks .....	28
2.18 Microcracks in the Post-Peak Region .....	29
2.19 Typical Compressive Stress-Strain Curves for Plain Concrete and Reinforced with 1% Volume Fraction of Steel Fibers .....	30
2.20 Effects of Fiber Reinforced and Confinement by Transverse Steel on Compressive Behavior of Concrete .....	31
2.21 Typical Comparison between Compressive Behavior of Fibrous and Equivalent Confined Concretes .....	32
2.22 The Compressive Constitutive Model of Reference 5 .....	33
2.23 Analytical Model of Reference 5 vs. Test .....	34
2.24 Flexural Behavior of Steel Fiber Reinforced Concrete Beam under Flexure .....	37
2.25 One Major Crack at Critical Section in Steel Fiber Reinforced Concrete Beam .....	37
2.26 Hypothetical Stress-Strain Distributions .....	38
3.1 Effects of Fiber Volume Fraction on Tensile Behavior of Steel Fiber Reinforced Concrete .....	41
3.2 Influence of Fiber Aspect Ratio on Direct Tensile Behavior of Steel Fiber Reinforced Concrete .....	42
3.3 Effects of Fiber Diameter on Direct Tensile Strength of SFRC .....	43

<b>3.4 Effects of Steel Fiber Deformation on Direct Tensile Behavior of SFRC</b> .....	<b>44</b>
<b>3.5 Number of Fibers per Unit Area</b> .....	<b>46</b>
<b>3.6 Orientation of Steel Fibers in Concrete</b> .....	<b>47</b>
<b>3.7 Three Dimensional Fiber Orientation</b> .....	<b>48</b>
<b>3.8 Two Dimensional Orientation of Fibers</b> .....	<b>49</b>
<b>3.9 Different Conditions with Two Boundaries</b> .....	<b>51</b>
<b>3.10 Effect of Height on Orientation Factor in Cases with Two Boundaries</b> .....	<b>51</b>
<b>3.11 Effects of Cross-Sectional Dimensions on Orientation Factor in Cases with Four Boundaries</b> .....	<b>53</b>
<b>3.12 Different Conditions with Four Boundaries</b> .....	<b>54</b>
<b>3.13 Comparisons between Exact and Approximate Expressions of Orientation Factor in Different Conditions</b> .....	<b>55</b>
<b>3.14 Measurement of the Number of Fibers per Unit Area</b> .....	<b>57</b>
<b>3.15 Measured vs. Normal Distribution</b> .....	<b>59</b>
<b>3.16 2-D and 3-D Orientation Factors for Different Geometric Conditions</b> .....	<b>62</b>
<b>3.17 Influences of Fibers on Cracking Characteristics and Tensile Behavior of Concrete</b> .....	<b>63</b>
<b>3.18 Comparisons of the Proposed "Interaction Concept" with Tensile Strength Test Results</b> .....	<b>68</b>
<b>3.19 Comparisons of the Composites Material and the Spacing Concept Predictions with Tensile Strength Test Results</b> .....	<b>70</b>
<b>3.20 Simulation of the Steel Fiber Reinforced Concrete Tensile Behavior upon Cracking at Peak Load</b> .....	<b>73</b>
<b>3.21 Increase in Strain at Peak-Tensile Stress in the Presence of Steel Fibers as a Function of Some Fiber Reinforcement Properties (<math>N_f \cdot d_f \cdot l_f</math>)</b> .....	<b>73</b>
<b>3.22 Comparisons of the Average Stress vs. Average Crack Width Relationship in the Post-Peak Region with Test Results</b> .....	<b>76</b>
<b>3.23 Typical Experimental Plot of Fiber Pull-Out vs. Displacement (Slippage) Relationship</b> .....	<b>76</b>
<b>3.24 Model of Pull-Out Load-Deflection Relationship for Straight-Round Steel Fibers</b> .....	<b>77</b>
<b>3.25 Pull-Out Test Procedure</b> .....	<b>78</b>
<b>3.26 Simulation of Pre-Peak Pull-Out Behavior of Straight-Round Steel Fibers</b> .....	<b>79</b>
<b>3.27 Comparison of the Experimental Pull-Out Load-Deflection Relationships in the Post-Peak Region with the Empirically Derived Model for This Study</b> .....	<b>81</b>
<b>3.28 Effects of Fiber Concentration, Volume Fraction and Orientation on Pull-Out Strength</b> .....	<b>82</b>

3.29 Comparisons of Experimental Tensile Stress-Deformation Relationships with Predictions of the Model Developed in This Study .....	87
4.1 Effects of Different Fibers on Compressive Behavior of SFRC .....	94
4.2 Experimental Compressive Stress-Strain Relationship .....	99
4.3 General Form of the Compressive Constitutive Model of SFRC .....	101
4.4 Comparison between Empirical Expressions on Test Results for Different Variables of Compressive Constitutive Model .....	104
4.5 Analytical Model vs. Test (1 Mpa = 145 psi) .....	106
4.6 Effects of Fiber Reinforcement Index and Concrete Compressive Strength on Compressive Behavior of SFRC as Predicted by the Proposed Constitutive Model (1 Mpa = 145 psi) .....	111
5.1 Crack Patterns and Possible Curvature Distributions .....	116
5.2 Moment and Curvature Distributions .....	118
5.3 Actual and Assumed Crack Shapes .....	122
5.4 Deformation Compatibility after Cracking .....	123
5.5 Estimation of the Initial Strain Configuration .....	127
5.6 Improvements of Regula-Falsi Method .....	128
5.7 Comparisons between Experimental and Analytical Deflection Curves .....	131
5.8 Typical Load-Deflection Curves ( $V_f = 0.5\%$ and $1.2\%$ ) .....	133
5.9 Strain and Stress Distributions at the Critical Section .....	134
5.10 Material-Related and Constitutive Behavior-Related Factors .....	137
5.11 Definitions of Four Different Criteria .....	141
5.12 Influence of Matrix Strength on Load-Deflection Curve .....	144
5.13 Influence of Matrix Softening in Tension on Load-Deflection Curve .....	145
5.14 Influences of Fiber Dimensions and Fiber Volume Fraction .....	147
5.15 Influence of Fiber Pull-Out Behavior .....	149
6.1 Error Surface in Parameter Space (Case of $N = 2$ ) .....	159
6.2 The Iterative Minimization Procedure .....	163
6.3 Main Theorems Used in Powell's Algorithm .....	168
6.4 Main Theorems in Powell's Algorithm for $N = 2$ .....	170
6.5 Quadratic Line Search .....	172
6.6 Comparisons between Experimentally Obtained and Theoretically Optimized Flexural Load-Deflection Curves .....	177

# CHAPTER 1

## INTRODUCTION

Reinforcement of concrete with short, randomly distributed steel fibers leads to improvements in the tensile strength, and tensile and compressive ductility of the material [1-6].\* Improvements in the stiffness, cracking characteristics, strength and toughness of reinforced concrete structural elements in the presence of steel fibers under flexural, shear, torsional and axial forces are direct consequences of the improvements in the tensile and compressive performance of the material [7-9].

The advantages associated with the use of steel fibers in load-bearing structural elements can be realized in large scales only if structural engineers are provided with structural design equations and guidelines for optimizing the use of steel fibers in conjunction with conventional reinforcing bars in structural elements. The very basic tools required for analytical studies on fiber reinforced concrete structural elements are reliable constitutive models of fibrous concrete which have been verified using comprehensive sets of experimental results. In many applications steel fiber reinforced concrete is subjected to flexural forces. It is thus important to develop analytical techniques to predicting the flexural behavior of steel fiber reinforced concrete which is marked by nonlinear stress distribution and dominance of a cracked section in deciding the post-peak performance.

---

\* Numbers in square brackets refer to the list of references.

The objective of this research was to: (1) develop tensile and compressive constitutive models for steel fiber reinforced concrete which reflect the current level of our understanding of the physics of the material behavior under different stress systems and are refined using the available experimental data; and (2) develop analytical techniques for flexural analysis of steel fiber reinforced concrete, and for deriving information on the direct tensile and compressive performance characteristics of steel fiber reinforced concrete based on the flexural test data.

A comprehensive review of the literature on mechanical properties and constitutive modeling of steel fiber reinforced concrete under compression and tension is presented in Chapter 2. This chapter also critically reviews some popular concepts used in predicting the tensile strength of steel fiber reinforced concrete, and presents the background and analysis procedures for steel fiber reinforced concrete behavior under flexure. The development of an experimental model for predicting the constitutive behavior of steel fiber reinforced concrete under tension is described in Chapter 3. In Chapter 4, an empirical compressive constitutive model is presented for compressive behavior of steel fiber reinforced concrete. In both Chapters 3 and 4, parametric studies are conducted using the developed constitutive models in order to assess the performance characteristics of steel fiber reinforced concrete.

Chapter 5 describes the process of incorporating the developed tensile and compressive constitutive models into an approximate nonlinear flexural analysis procedure which takes into account the formation of one major crack at the flexural section and the nonlinear distributions of stresses and curvatures in the vicinity of this crack.

The system identification technique is used in Chapter 6 together with the developed flexural analysis procedure and tensile/compressive constitutive models

in order to identify characteristic tensile and compressive values of the stress-strain characteristics of steel fiber reinforced concrete using the flexural load-deflection relationship. Finally, Chapter 7 summarizes the research program and presents the conclusions; suggestions are also made for future research in this area.

## CHAPTER 2

### MECHANICAL PROPERTIES OF STEEL FIBER REINFORCED CONCRETE: A REVIEW OF THE LITERATURE

#### 2.1 INTRODUCTION

Stress system produced in concrete by external loads (compression, tension, flexure or multi-axial) lead to a tendency towards the propagation and interconnection of microcracks in cementitious materials [10-13]. The ease with which microcracks can propagate in concrete results in a brittle failure which is generally considered to be a major shortcoming of cementitious materials.

Reinforcement of concrete with short, randomly distributed steel fibers results in improvements in tensile strength and tensile and compressive toughness of the material. This is due to the fact that propagating microcracks in cementitious matrices tend to be arrested or deflected [1,5,10,11,14] by fibers. Debonding and pull-out actions of fibers under tension and the confinement of cementitious matrices by steel fibers under compression are also important mechanisms through which steel fibers improve the mechanical behavior of concrete [1,5,10,11,14]. Improvements in the flexural performance of concrete in the presence of steel fibers are direct consequences of the corresponding improvements in the tensile and compressive performance of the material.

The desirable mechanical properties of steel fiber reinforced concrete have encouraged the use of steel fiber reinforced concrete in wide ranges of non-structural and structural applications [15] (see Table 2.1 ).

Table 2.1 Application of Steel Fiber Reinforced Concrete

	APPLICATIONS	EXPERIMENTAL APPLICATIONS	EXPERIMENTS
CAST IN PLACE	HIGHWAY CONSTR. & REPAIR		
	AIRPORT RUNWAYS, TAXIWAYS, APRONS		
	INDUSTRIAL FLOORS		
	DAM CONST. & REPAIR		
	REFRACTORY CASTABLES		
	BRIDGE DECK CONSTR. & REPAIR		
		FLUID CONTAINMENT	
	CANAL, RESERVOIR LINING		
	MINE & TUNNEL LINING		
			STRUCTURAL BLDG. ELEMENTS
	SECURITY VAULTS		
	CAISSON & PILE REPAIR		
PRE-CAST			RAILROAD TIES
		PIPE	
	SUBTERRANIAN VAULTS		
	MODULAR PANELS		
	REFRACTORY PRECAST		
		STRUCTURAL PRECAST	
	BREAKWATERS		
	CRIB BLOCK		
			MACHINE BASES & FRAMES

In order to design or analyze the reinforced concrete structural elements incorporating steel fibers, it is important to understand and to be able to predict the stress-strain and load-deformation properties of the material under tensile, compressive and flexural loads. The remainder of this chapter presents a comprehensive review of the literature on the failure mechanisms of plain and steel fiber reinforced concrete under compression, tension and flexure. The available tensile and compressive constitutive models and flexural analysis procedures developed for steel fiber reinforced concrete are also critically reviewed.

## **2.2 STEEL FIBER REINFORCED CONCRETE UNDER TENSION**

The pre-peak tensile behavior of SFRC may be characterized by the process of microcracking of the matrix prior to the formation of a continuous crack system across the section which marks the peak load and the appearance of a macrocrack. These propagating microcracks tend to be arrested by fibers leading to increased stiffness and peak tensile strength of steel fiber reinforced concrete.

The peak tensile load is typically marked by the appearance of one major crack at the critical section, after which the pull-out of fibers bridging the critical crack tends to dominate the behavior in the post-peak region. The fiber pull-out process generally provides the composite material with important post-peak ductility and toughness.

In the following discussion, first some observations regarding the nature of microcracking in mortar and concrete are presented and the interaction mechanisms of fibers with microcracks are described. The fiber pull-out process and the tensile constitutive behavior of steel fiber reinforced concrete are also discussed.

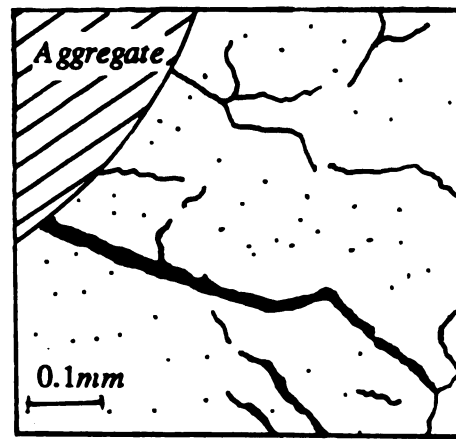
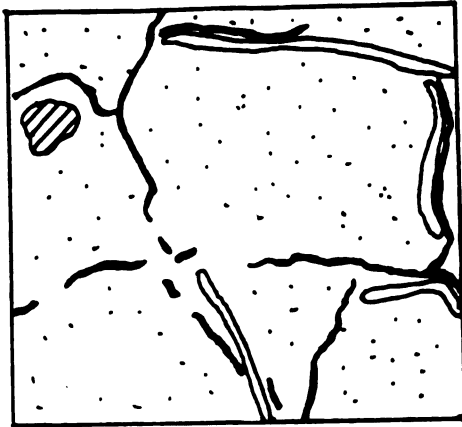
### 2.2.1 Microcracking in Mortar and Concrete under Tension

For air dried mortar and concrete, shrinkage-induced bond cracks around large aggregate particles appear prior to any loading (Figure. 2.1(a)). In concrete, multiple cracking around sand grains is frequently observed (Figure. 2.1(b)), and this phenomenon seems to be more pronounced between adjacent sand grains than around isolated ones.

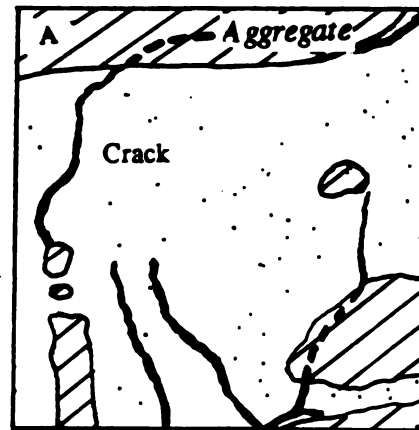
In mortar, under tensile loads, microcracks tend to propagate along the segments of cement-sand grain interface and also around the air voids (Figure 2.1(c)). It can be shown that cracks under tension change orientation when encountering aggregates under tensile stress in order to pass around aggregates without crossing (see the microcrack in Figure 2.1(d) encountering aggregate "A"). This suggests that aggregate surfaces may act as crack arrestors, causing microcracks to stop prior to reaching aggregate surfaces. In the presence of aggregates, the crack path is thus never straight (see Figure 2.2 for mortar). The overall tortuosity of the crack pattern in concrete is higher than that in mortar, because concrete cracks must propagate around the densely spaced aggregate pieces as well as sand grains.

Other phenomena sometimes observed in the microcracking process include the branching of microcracks inside the paste, and shattering of aggregate particles crossed by microcracks. Branching (Figure 2.3(a)) occurs at the crack tip, and usually only one of these branches is activated and increases in width with further loading. In some cases a crack is observed to run through, rather than around, an aggregate grain (Figure 2.3(b)). This might cause the aggregate grain to shatter.

The reorientation, branching and multiple cracking associated with the interaction of microcracks with aggregate particles lead to the dissipation of large amounts of energy, which is beneficial to tensile behavior of the material.



(a) Shrinkage Induced Bond Cracks (b) Multiple Cracking



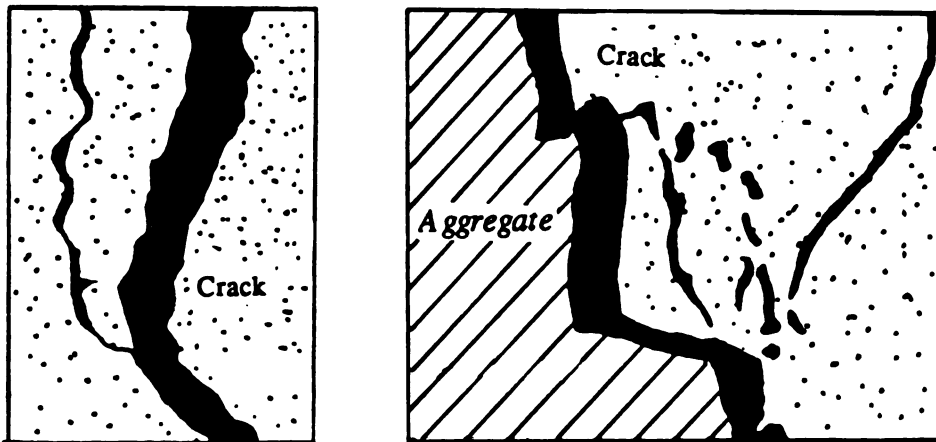
(c) Crack Propagation

(d) Reorientation of Cracks

Figure 2.1 Propagation of Cracks in Cementitious Matrix



Figure 2.2 Tortuosity of Crack Path



(a) Microcrack Branching

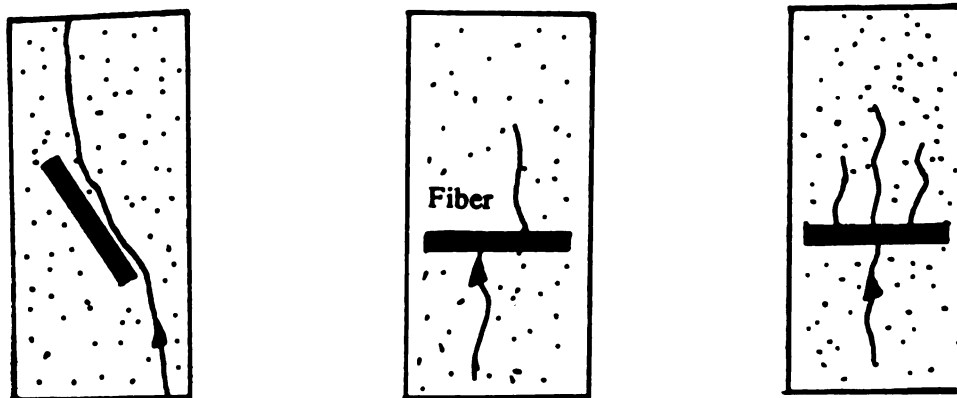
(b) Aggregate Shattering

Figure 2.3 Branching of Microcracks inside the Cement Paste and Shattering of Grains by Crossing Microcracks

### 2.2.2 Microcracking in Steel Fiber Reinforced Concrete Under Tension.

The propagation mechanism of microcracks tends to be influenced by the presence of fibers. Cracks approaching fibers in a direction almost parallel to them tend to run parallel to such fibers for at least some distance along the length (Figure 2.4(a)) and those cracks advancing in a direction inclined with respect to steel fibers are either shifted (Figure 2.4(b), which occurs in 30% of events in steel fibers) or branched out into multiple post-fiber cracks (Figure 2.4(c), observed in 50% of events in steel fiber).

The microcrack encountering a fiber stays continuous, making the lateral shifts around the fibers, as can be clearly seen in the picture of the groove under a steel fiber which intersected microcracks in Figure 2.5.



(a) Parallel Running

(b) Shifting

(c) Branching

Figure 2.4 Interaction of Microcracks with Steel Fibers.

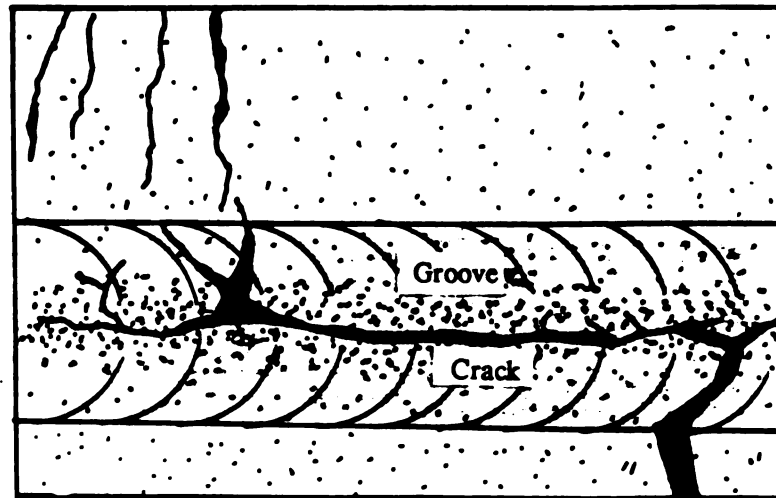


Figure 2.5 Continuous Nature of Shifted Microcracks around a Steel Fiber.

The intersection of microcracks with steel fibers is strongly influenced by the nature of fiber-matrix interfacial zone [11]. This zone in steel fiber reinforced concrete consists of 3 regions (Figure 2.6): (1) a thin duplex film in actual contact with steel fibers; (2) outside this, 10 to 30 micrometer-thick porous region incorporating massive calcium hydroxide crystals; and (3) outside this, a highly porous layer parallel to the interface; pseudo-debonding may occur in this very porous region due to the tensile stresses in a direction parallel to the crack generated near the crack tip.

The microcrack propagation in the vicinity of fibers (at the fiber-matrix interface) might take place at the interface itself leading to the separation of the matrix from the fiber (debonding, Figure 2.7(a)), or it might occur (as discussed earlier, see Figure 2.4(c)) at a small distance (about 20 micro-meter) from the fiber and parallel to it (pseudo-debonding, Figure 2.7(b)) [11]. The nature of pseudo-debonding (Figure 2.7(b)) leads to branching and lateral shifting of the advancing crack, and sometimes causes some true debonding between places

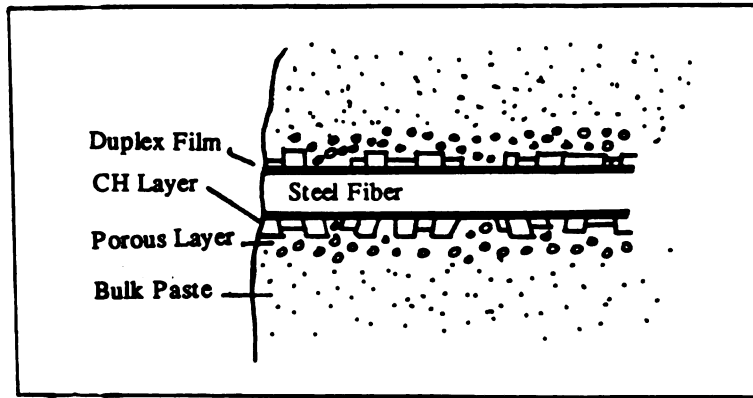
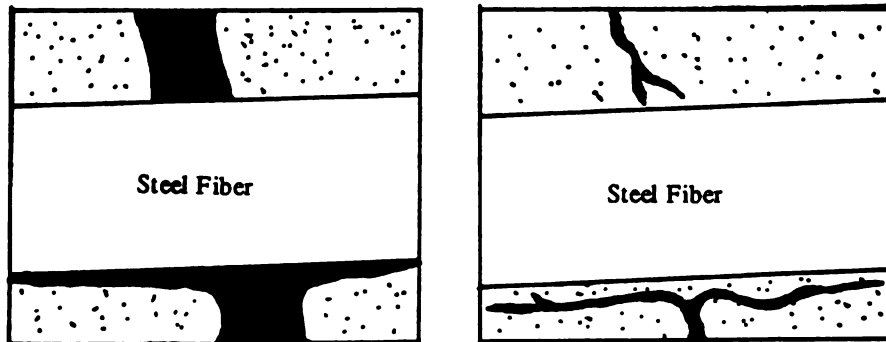


Figure 2.6 Schematic Description of the Microstructure of Steel Fiber-Cement Interface [11]



(a) Debonding

(b) Pseudo-debonding

Figure 2.7 Debonding and Pseudo-debonding of Steel Fibers in Cementitious Materials [11].

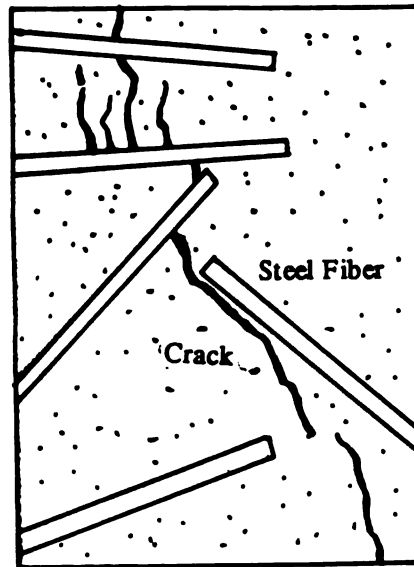


Figure 2.8 Interaction of a Crack with a Number of Randomly Oriented Steel Fibers [11].

where parallel secondary cracks run past the fiber. The propagation of a microcrack when encountering a number of randomly oriented fibers might take place with a mixture of fiber-matrix interaction types (see Figure 2.4 for these types), as shown in Figure 2.8.

The branching, shifting and parallel running of microcracks involve dissipation of extra energy from the stressed system and illustrate an important mechanism through which fibers enhance the pre-peak stiffness and the ultimate tensile strength of fiber reinforced concrete.

### 2.2.3 Pull-Out Mechanism of Steel Fibers in SFRC Under Tension

The pre-peak behavior and maximum tensile strength of the composite material depends on local bond characteristics at the fiber-matrix interface, while the post-peak behavior is dominated by an average bond behavior in pull-out action of fibers bridging the critical crack. Thus, pull-out tests on individual

fibers embedded in concrete matrix seem to provide information which are more relevant to average bond behavior in the post-peak tensile behavior of steel fiber reinforced concrete [16].

Fiber-matrix interfacial bond strength is provided by a combination of adhesion, friction and mechanical interlocking [17]. Fiber debonding from the matrix at early stages of loading in the pre-peak region is resisted by the adhesion of matrix to fibers. Following debonding, the frictional stress transfer between fiber and matrix and mechanical bonding tend to dominate the pull-out performance and the corresponding energy dissipation which characterize the post-peak behavior of the composite. In the post-peak region under tensile stresses, following the appearance of macrocracks, the resistance to pull-out is provided in fibers aligned in the tensile stress direction primarily by shear stresses along the interfaces. For inclined fibers, the progressive bending of successive sections of the fiber will require an additional effort which depends on the rigidity and yielding properties of fibers. Inclined fibers may also produce a normal stress component on part of the sliding surface of embedded fibers thus slightly increasing the frictional resistance [17].

It is worth mentioning that an excessive increase in interfacial bond strength may actually cause fiber rupture (instead of fiber pull-out) to dominate the failure of the composite material, leading to a drop in toughness (which benefits from the energy dissipated by the fiber pull-out process).

A typical relationship between average bond stress and pull-out deformation obtained from pull-out tests on straight-round steel fibers is presented in Figure 2.9 [18-21]. The pull-out behavior is observed to be linear before the peak pull-out load is reached. In the post-peak region the fibers are observed to gradually slip out at decreasing pull-out loads until the completion of fiber pull-out. Mechanical deformations of steel fibers can modify the pull-out

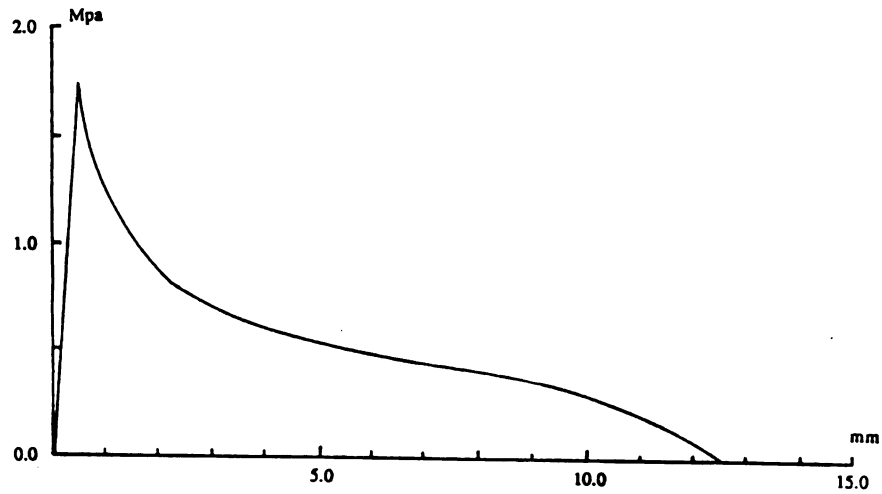


Figure 2.9 A Typical Relationship between Average Bond Stress and Pull-Out Deflection in Pull-Out Tests on Straight-Round Steel Fibers [18-21].

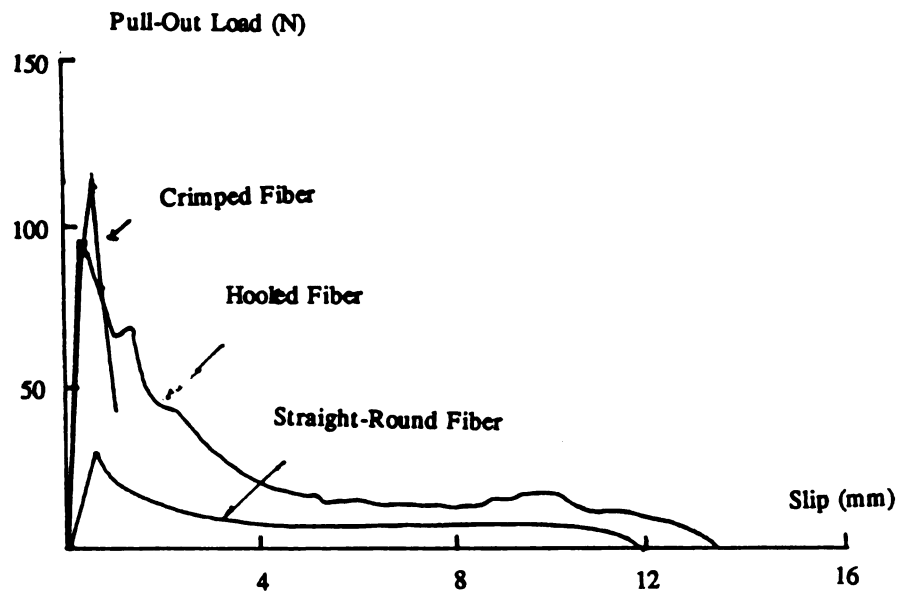


Figure 2.10 Effect of Fiber Types on Pull-Out Behavior

load-deformation relationships (Figure 2.10).

#### 2.2.4 Tensile Behavior of Steel Fiber Reinforced Concrete

Fibers, with their microcrack arresting action, tend to increase the fracture energy and consequently the tensile strength of concrete. With the progress of microcracking process in SFRC, deviation from the linear behavior occurs in tensile stress-strain relationship of the material (see Figure 2.11) [22,23].

The deviation from linear behavior under tension in SFRC takes place at about 80% of the tensile strength [24]. The increase in the tensile strength of the matrix resulting largely from the microcrack-arrest action of steel fibers at a typical volume fraction of 1 to 2% is usually about 20 to 50% [24,25].

The peak load under direct tensile stress in SFRC seems to be reached when a catastrophic microcrack propagation takes place and a continuous system of microcracks forms at a critical cross section. Reference 24, based on microscopic

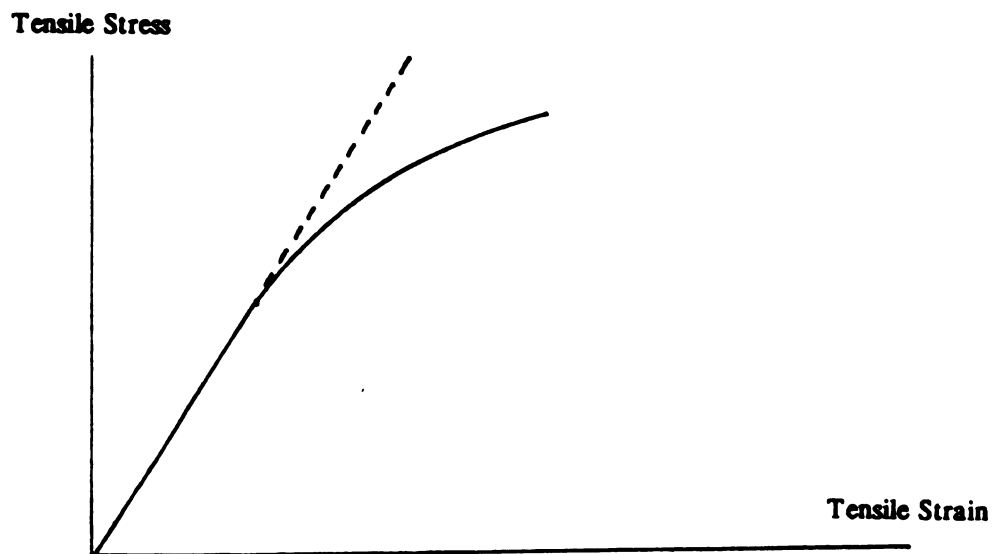


Figure 2.11 Deviation from Linear Behavior in FRC, Resulting from Gradual Microcrack Propagation.

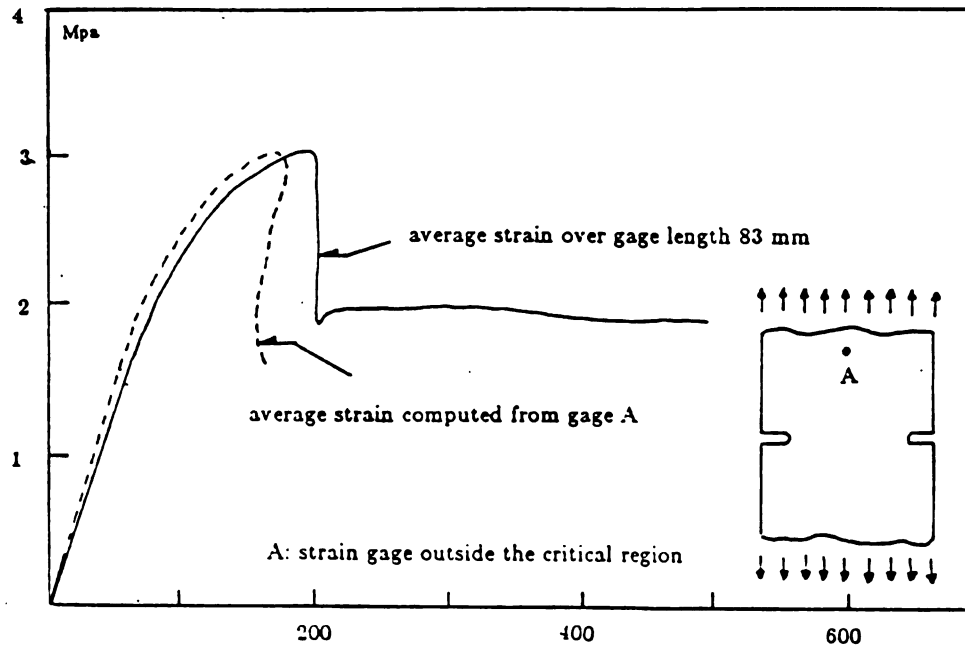


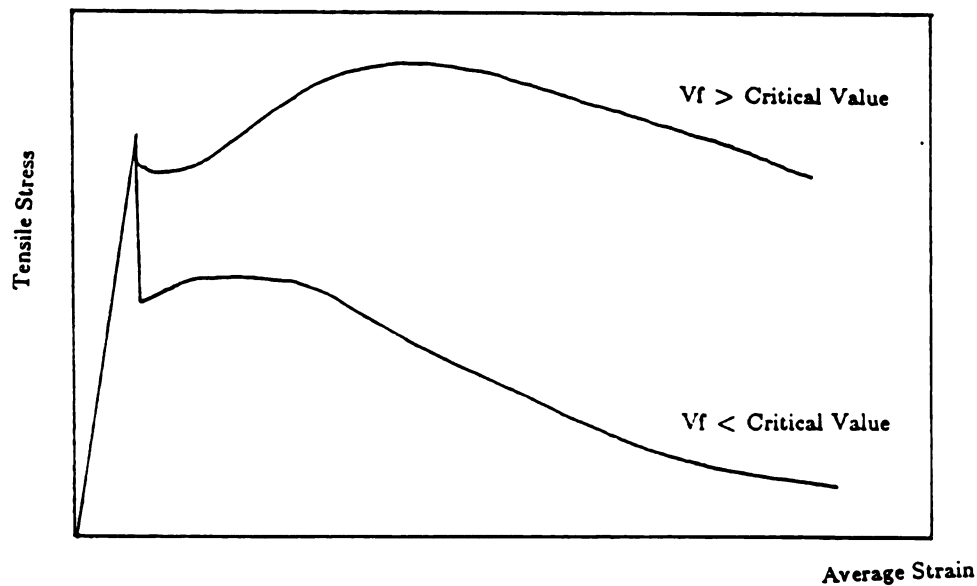
Figure 2.12 Typical Direct Tensile Stress-Strain Relationships for Concrete and Mortar Matrices.

measurements, has concluded that immediately after peak load a single crack becomes visible in steel fiber reinforced concrete specimens under direct tension. Thereafter, tensile deformations tend to be localized in the cracked location, and unloading takes place outside the cracked region (Figure 2.11). Increasing deformations at this stage result in gradual pull-out or rupture of fibers crossing the crack.

The crack opening under tension is resisted at this stage by fibers bridging the crack and also by the remainder of the tensile resistance of the matrix at the crack in its softening zone of behavior. Fiber pull-out mechanism in post-peak stage provides steel fiber reinforced concrete with greatly increased ductility compared to plain concrete under tension. A typical direct tensile stress-deformation relationship for concrete matrix, which demonstrates the post-cracking tensile resistance and softening behavior of cementitious matrices is

shown in Figure 2.12 [10].

In spite of matrix contributions to tensile resistance at cracks, either fiber pull-out or rupture of fibers tends to dominate the post-cracking failure mechanism of SFRC under direct tension, depending on fiber length and fiber-matrix interfacial bond characteristics. The longer fibers with better bond to cementitious matrices tend to have higher pull-out forces, and thus they rupture before pulling out. Theoretically speaking, following the appearance of macrocrack and the activation of the pull-out performance of fibers, two types of behavior might be observed: the tensile resistance might continue to increase with increasing tensile deformations, or it might progressively drop following a sudden drop at the peak load (see Figure 2.13). The first case (increasing resistance after



(a)  $V_f \geq V_{crit.}$

(b)  $V_f < V_{crit.}$

Figure 2.13 Two Theoretical Types of SFRC Direct Tensile Behavior in the Post-Peak Region [26].

peak) can take place if the fiber volume fraction is above a critical volume needed for maintaining the tensile resistance of the composite material after cracking by the pull out action of fibers. This critical fiber volume fraction depends on the geometry, aspect ratio, orientation, and tensile strength of fibers in addition to the fiber-matrix interfacial bond characteristics.

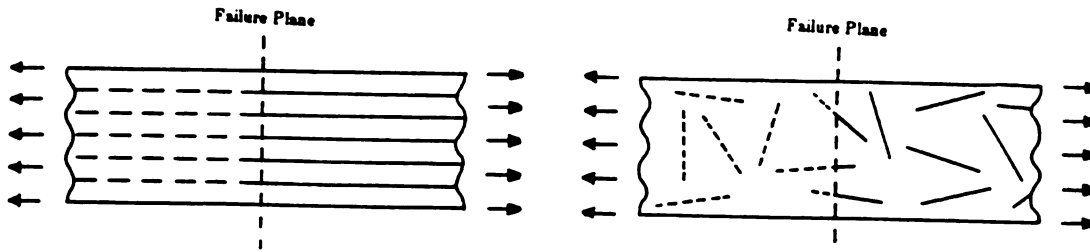
For concretes reinforced with steel fibers in a 3-D random manner and constructed with conventional mixing techniques, the volume fraction of fibers that can be incorporated into concrete within constraints of sufficient workability and fiber dispersability is normally less than the critical volume fraction. Hence, a sudden dropping of tensile resistance at peak tensile stress followed by gradual softening in the post peak region tends to dominate the direct tensile behavior of SFRC [26]. The tensile resistance is expected to reach zero when the last fiber is completely pulled out of the matrix, and this takes place at relatively large crack widths comparable to half the fiber length.

Direct tensile behavior of steel fiber reinforced concrete has been observed to be influenced by fiber volume fraction, aspect ratio (length over diameter) and fiber shape (mechanical deformation) among other factors. A detailed discussion on the effects of these factors on the tensile behavior of steel fiber reinforced concrete is presented in Chapter 3.

### **2.2.5 Constitutive Models**

There are two popular concepts for analytical simulation of the failure mechanism in fiber reinforced concrete under direct tension: composite material concept and spacing concept.

The composite material concept attributes the increase in tensile strength of concrete resulting from steel fiber reinforcement to the mobilization of the fiber-to-matrix interfacial bond resistance through the pull-out action of steel fibers at



(a) Continuous, Aligned

(b) Uniformly Dispersed, Randomly Oriented

Figure 2.14 Fiber Reinforced Composite

peak tensile stress [1,3,27-29]. The composite material concept was originally developed for matrices reinforced with aligned, continuous fibers with perfect bond to the matrix (Figure 2.14(a)), assuming that the Poisson's ratios of fibers and matrix are similar [28,30-33]:

$$\sigma_c = \sigma_m' \cdot (1 - V_f) + \sigma_f \cdot V_f \quad (2.1)$$

where :

$\sigma_m'$  = matrix tensile strength ;

$\sigma_f$  = fiber tensile stress at composite failure ; and

$V_f$  = fiber volume fraction.

In the case of matrices reinforced with short randomly oriented fibers (Figure 2.14(b)), the composite material concept should be refined to account for: (1) the randomness of the orientation and location of fibers with respect to the failure plane which tends to reduce their efficiency in providing resistance against the applied tensile stresses; (2) the failure plane crossing short fibers at random locations along the length, leaving less than half of the fiber length in one side of the crack to resist pull-out forces; and (3) partial effectiveness of matrix in contributing to the tensile resistance at cracks. These factors result in the following expression for predicting the tensile strength of steel fiber reinforced concrete:

$$\sigma_c = \eta_1 \cdot \sigma_m' \cdot (1 - V_f) + \eta_2 \cdot \eta_3 \cdot \sigma_f' \cdot V_f \quad (2.2)$$

where :

$\eta_1$  = *the fraction of matrix tensile strength effective at the composite peak tensile stress*

$$\approx 1.0 [3];$$

$\eta_2$  = *orientation efficiency factor*

$$= 0.41 \text{ for fibers randomly oriented in space [9,12,16];}$$

$\eta_3$  = *fiber location factor*

$$= 0.5 [3];$$

$\sigma_f'$  = *smaller of the fiber fracture and pull-out strengths*

$$= 2 \cdot \tau_u \cdot l_f / d_f \leq \sigma_{fu} ;$$

$\tau_u$  = *average fiber-to-matrix interfacial bond stress at peak*

*pull-out resistance ;*

$\sigma_{fu}$  = *fiber tensile strength ;*

$l_f = \text{fiber length ; and}$

$d_f = \text{fiber diameter .}$

In the above expression (Equation (2.2)), the values of  $\eta_1$  and  $\tau$  are found empirically through normalizing expression of Equation (2.2) with respect to  $V_f \cdot l_f / d_f$ :

$$\frac{\sigma_c}{V_f \cdot l_f / d_f} = \eta_1 \cdot \frac{\sigma_m' \cdot (1 - V_f)}{V_f \cdot l_f / d_f} + 2 \cdot \eta_2 \cdot \eta_3 \cdot \tau_u \quad (2.3)$$

Figure 2.15(a) shows how the above expression fits the test results presented by Mangat (1976) [3] with  $\eta_1$  equal to 1.1 and  $\tau_u$  equal to 1 Mpa (145 psi) for concrete reinforced with straight-round steel fibers.

A closer analysis of Figure 2.15(a) indicates that this figure represents the strong dependence of the composite material tensile strength on the matrix tensile strength rather than fiber pull-out strength. Contrary to the assumption of the composite material concept that a relatively large fraction of fiber pull-out strength should be mobilized at the composite material peak stress, the measured values of strain and crack width at peak tensile stress in steel fiber reinforced concrete are not sufficiently large to mobilize the pull-out action of fibers [28]. The discrepancy becomes clear when the increase in tensile strength resulting from the presence of fibers is directly related to fiber reinforcement properties:

$$\sigma_c - \eta_1 \cdot \sigma_m' (1 - V_f) = 2 \eta_2 \cdot \eta_3 \cdot \tau_u V_f \cdot l_f / d_f \quad (2.4)$$

Assuming a value of 1.1 for  $\eta_1$ , 1 Mpa (145 psi) for  $\tau_u$  and 0.34 for  $(2 \cdot \eta_2 \cdot \eta_3)$  ( derived from Figure 2.15(a) for the same set of data ), considerable

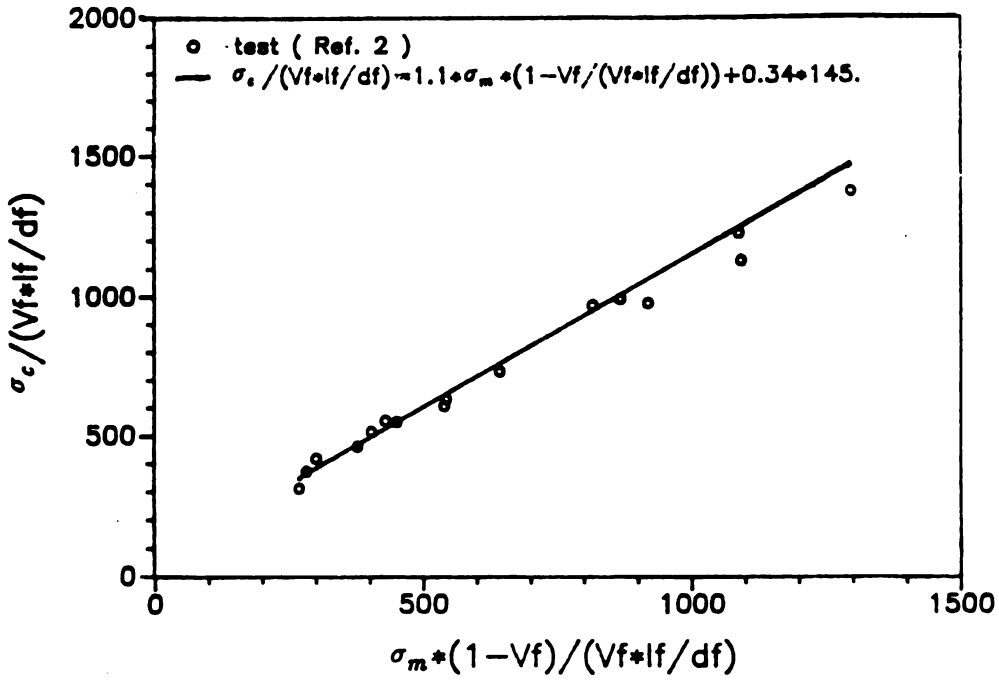
discrepancies between test results and analytical predictions can be observed in Figure 2.15(b) compared to Figure 2.15(a). This leads to the conclusion that composite material concept (Equation (2.2)) can not satisfactorily describe the trends observed in the tensile strength of cement composites reinforced with steel fibers.

The spacing concept for predicting the tensile strength of steel fiber reinforced concrete is, on the other hand, based on the assumption that the dominant factor deciding the effectiveness of fibers in contributing to the tensile strength of concrete is the number of fibers available in unit volume of the composite to disrupt the propagation of microcracks. Fiber count has been represented in the literature [34,35] by different measures of the average spacing of fibers, or by the number of fibers at unit cross sectional area. Once the parameter representing fiber spacing is defined, test results are used in this so called "fiber spacing" approach to derive the empirical relationship between the tensile strength of fiber concrete and this parameter.

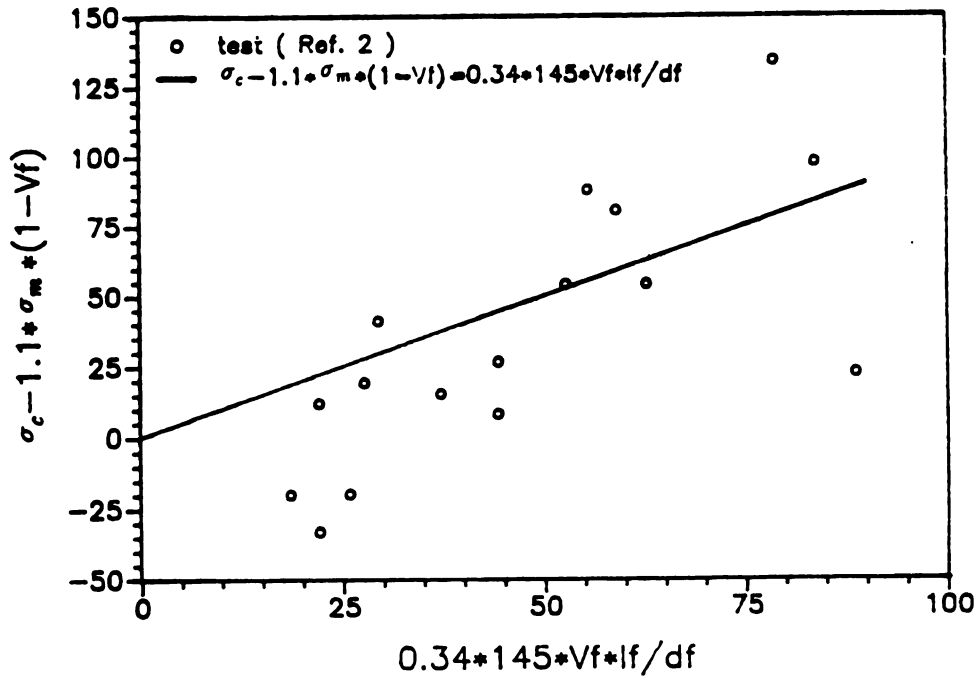
Romualdi and Mandel (1964) [34] have derived an expression for average fiber spacing based on the assumption that the projectiles of randomly distributed fibers in the direction parallel to that of tensile stress decide the effectiveness of fibers in increasing the tensile strength of concrete. The expression for fiber spacing derived in this reference is an average of the spacings of projectiles in a plane normal to the tensile stress direction :

$$S = 13.8 \cdot d_f / \sqrt{V_f \times 100} \quad (2.5)$$

An alternative approach based on the spacing concept has been introduced by Soroushian and Lee (1989) [36]. This approach suggests that the fibers in any orientation with respect to tensile stress can play the microcrack-arresting



(a) Conventional Verification [3]



(b) New Verification of the Composite Material Concept

Figure 2.15 Verification of the Composite Material Concept

role, and the number of fibers ( $N_1$ ) per unit cross-sectional area in the composite (irrespective of their orientation) is the factor representing the effectiveness of fibers in increasing the tensile strength of concrete :

$$N_1 = \alpha \cdot V_f / A_f \quad (2.6)$$

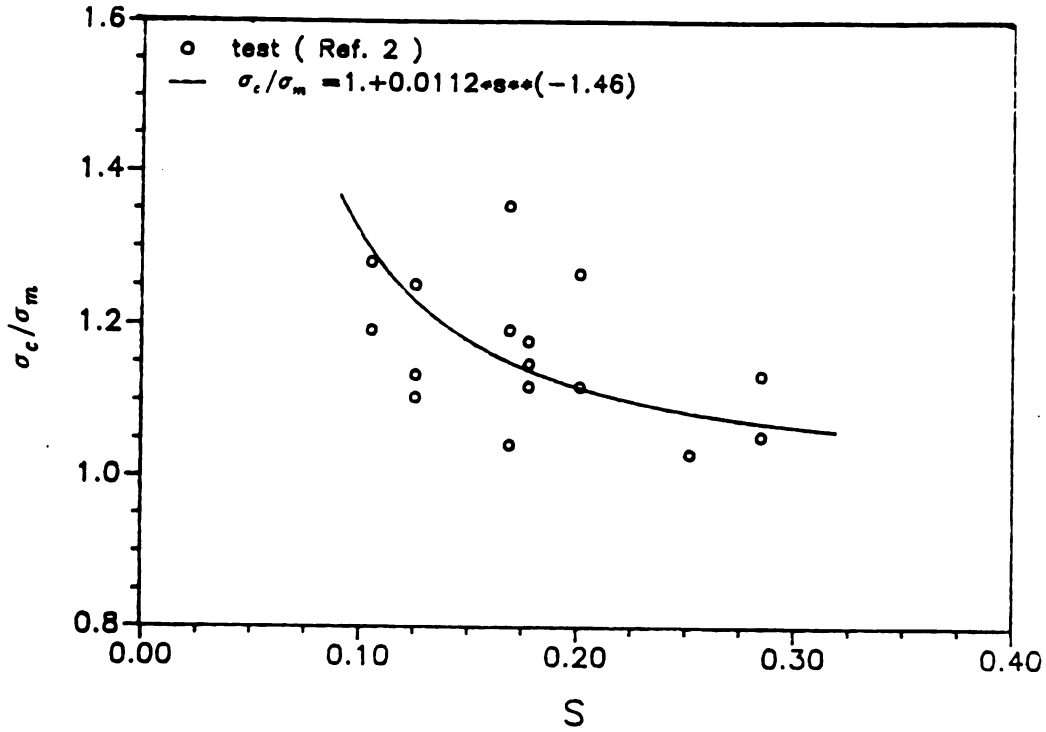
where:

$\alpha$  = *orientation factor (depends on the section geometry and fiber length as described in the next Chapter) and*

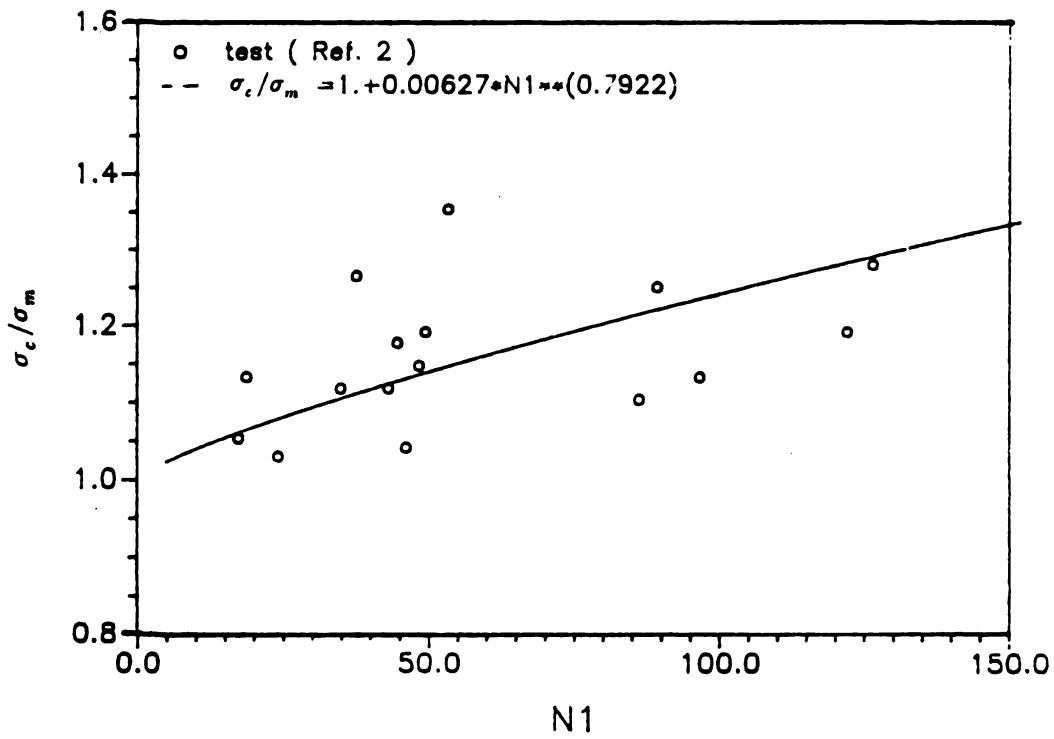
$$\begin{aligned} A_f &= \text{fiber cross-sectional area} \\ &= \pi d_f^2 / 4. \end{aligned}$$

Figure 2.16(a) and 2.16(b) present typical relationships between tensile strength test results (the same ones used in Figure 2.15) and different measures related to fiber spacing. The correlations between tensile strength test results and different measures related to fiber spacing in Figures 2.16(a) and 2.16(b) show that the spacing concept has deficiencies in representing the failure conditions of steel fiber reinforced concrete at peak tensile stress. One factor leading to these deficiencies is the disregard of the spacing concept for the effects of fiber-to-matrix interfacial bond characteristics on the composite material performance.

It can be concluded from the above discussion that a new approach to the prediction of SFRC tensile strength is needed. This approach should take into account contribution of fibers to tensile strength of the composite through both microcrack arrest and pull-out action. Steps taken towards this goal in this investigation are described in the next Chapter.



(a) Fiber Spacing (Equation (2.5))



(b) Fiber Spacing (Equation (2.6))

Figure 2.16 Verification of the Spacing Concept.

## **2.3 STEEL FIBER REINFORCED CONCRETE UNDER COMPRESSION**

In compression, fibers improve the post-peak ductility, energy absorption capacity and, to some extent, the strength of concrete [37]. These improvements result from the arrest of microcrack propagation by fibers as well as the confinement effects of fibers in the cementitious matrix.

This section presents the nature of microcracking in plain concrete, the role of steel fibers in confining concrete matrices, and the experimentally observed performance characteristics of steel fiber reinforced concrete under compression. No literature is available on the microcracking behavior of steel fiber reinforced concrete under compression.

### **2.3.1 Microcracking in Mortar and Concrete under Compression**

The internal stresses at aggregate-matrix interfaces resulting from external compressive loading generally consist of components normal to the aggregate (compressive or tensile) and those acting parallel to the aggregate (i.e. in shear) [13,38]. Bond cracks at aggregate-matrix interfaces and their propagation, which lead to the nonlinear behavior of concrete in compression, are thus caused by either tensile or shear stresses [38].

Under increasing uniaxial compressive stresses, the extent of microcracking at stresses below 85% of peak stress in the pre-peak region is limited primarily to cracks at the interface between the coarse aggregates and mortar matrix [13,38].

At about 85% of ultimate compressive load, the bond microcracks begin to increase substantially. This marks the increase in Poisson's ratio and the deviation of stress-volumetric strain relationship from linearity. Mortar cracks tend

to bridge between the nearby bond cracks and the appearance of continuous microcracks indicates that the so-called critical load is reached, where significant nonlinearities tend to occur and the volume of compressed concrete starts to increase rather than continue to decrease. As some load paths become inoperative due to microcracking under compressive stress, alternative load paths (either entirely through mortar or partly through mortar and partly through aggregates) continue to be available for carrying increasing compressive loads [38]. The decrease in the number of load paths available would eventually bring concrete to the post-peak region of behavior when compressive resistance decreases with extensive continuous microcracking [38].

Just prior to peak and immediately after it, a localization of microcracks seems to take place (Figure 2.17) [39]. This stage is also distinguished by formation of continuous microcracks (in which mortar cracks interconnect the bond



Figure 2.17 Localization of Microcracks



Figure 2.18 Microcracks in the Post-Peak Region

microcracks). This involves sharp increase in mortar cracks at or near the peak stress. In the post peak region, microcracks are continuous, uniform and extensive in all directions (Figure 2.18) [39]. The continuous microcracks tend to be roughly in the loading direction, particularly if the transverse friction forces at the ends (where external compressive stresses are applied) are completely removed [39].

A contribution to the ultimate strength might be provided also by mechanical interlocking of the coarse aggregates after cracking. Factors like this might influence the trends in the effects of coarse aggregates on concrete compressive behavior.

The idea that microcracks in concrete under compression are the major cause of nonlinearity has been challenged lately [40]. The nonlinearity of concrete appears to be highly dependent on the nonlinear softening response

characteristics of cement paste and mortar (due to submicrocracking) rather than bond cracks at the coarse aggregate-matrix interface which penetrate into mortar. More studies are needed to fully understand the nature of failure in concrete materials under compression.

### 2.3.2 Compressive Behavior of Steel Fiber Reinforced Concrete

Short, randomly distributed fibers, when added to concrete, confine the material and delay the crack propagation, thus producing increases in the peak strength, strain at the peak stress, ductility and energy absorption capacity (Figure 2.19) [2,5,14]. The strain at peak compressive stress tends to increase in the presence of steel fibers [5].

The confinement effect of steel fibers in concrete is shown in Figure 2.20 [41] which compares the effects of increasing the fiber reinforcement index (Figure 2.20(a)) with the effects of increasing the confinement of non-fibrous concrete by transverse reinforcement (Figure 2.20(b)). Soroushian and Lee (1987) [41], using

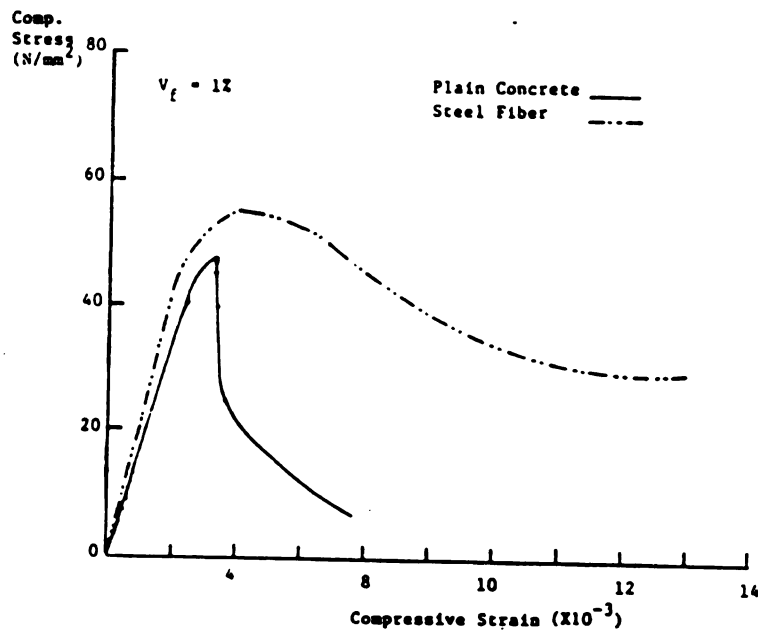
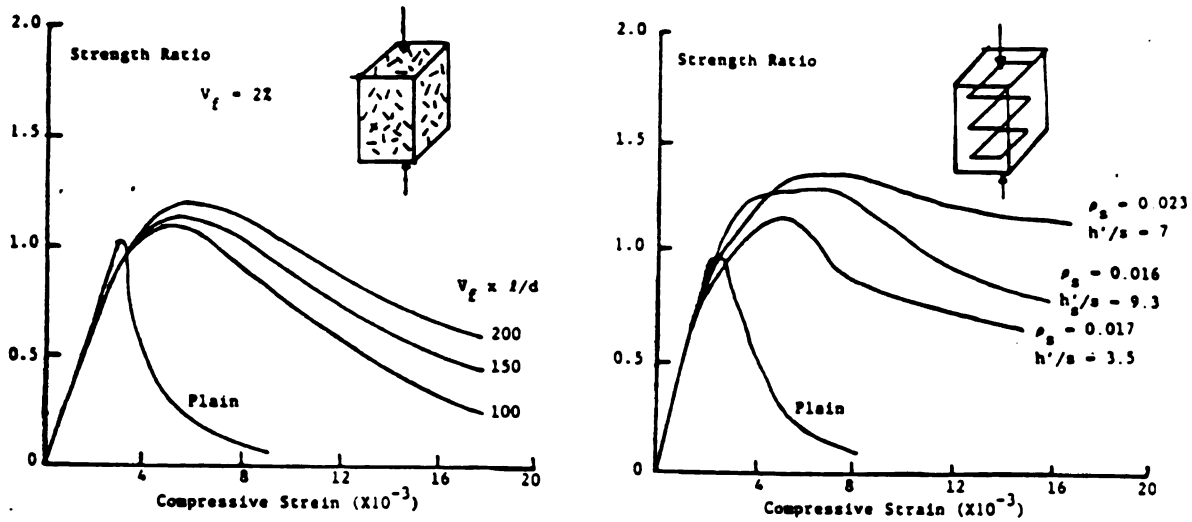


Figure 2.19 Typical Compressive Stress-Strain Curves for Plain Concrete and Reinforced with 1% Volume Fraction of Steel Fibers[33]



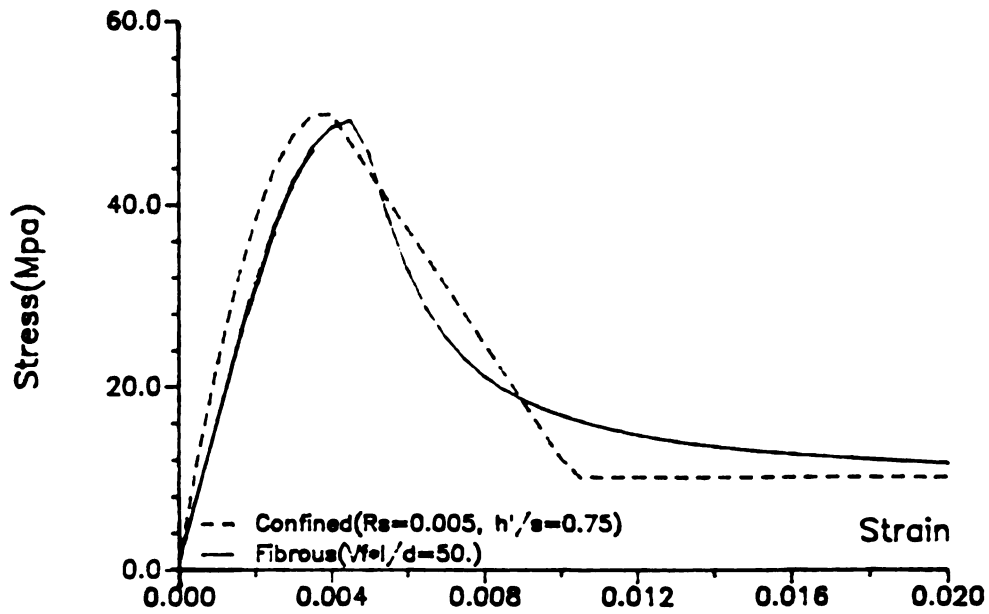
(a) Fiber Reinforcement

(b) Transverse Reinforcement

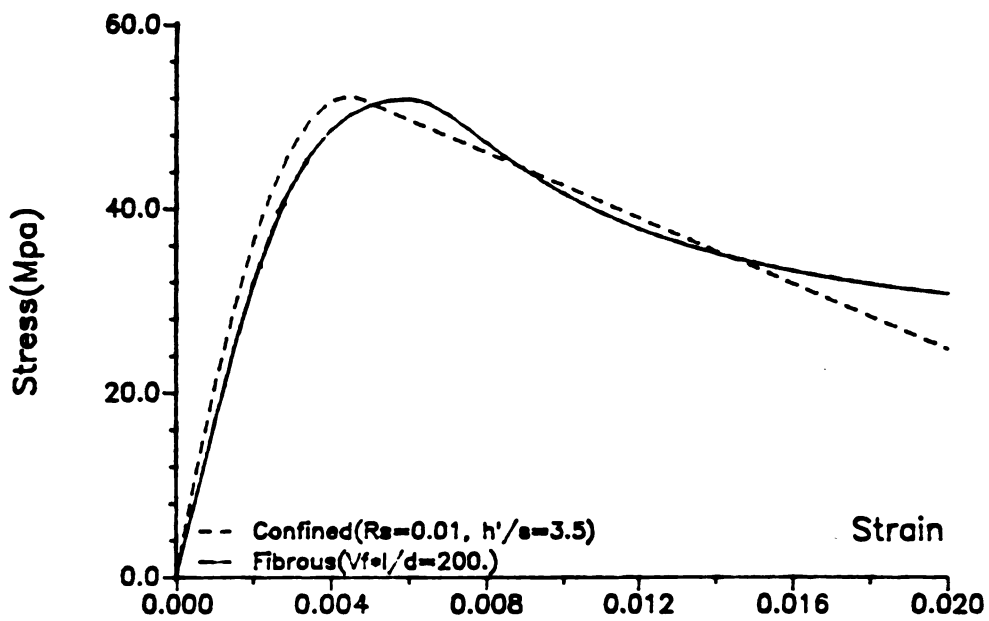
Figure 2.20 Effects of Fiber Reinforced and Confinement by Transverse Steel on Compressive Behavior of Concrete

the empirical constitutive models presented in Reference 5 for fibrous concrete and in Reference 42 for confined concrete, showed that the improvements in ductility and energy absorption capacity resulting from the increase in fiber reinforcement index are comparable to those resulting from the increased confinement of non-fibrous concrete by transverse reinforcement. Figure 2.21 [41] shows typical comparison between the compressive constitutive relationships of the fibrous and equivalent confined concretes.

The behavior of steel fiber reinforced concrete is dependent on the volume fraction and aspect ratio of steel fibers, mechanical deformation of fibers, matrix mix proportions and maximum aggregate size, specimen geometry, and loading versus casting direction [3,5]. The effects of these variables on the compressive behavior of steel fiber reinforced concrete will be discussed in detail in



(a) Steel Fiber



(b) Steel Fiber

Figure 2.21 Typical Comparison between Compressive Behavior of Fibrous and Equivalent Confined Concretes.

conjunction with discussions on compressive constitutive modeling of steel fiber reinforced concrete in Chapter 4.

### 2.3.3 Analytical Modeling

Very few analytical studies on the compressive constitutive behavior of steel fiber reinforced concrete have been reported in the literature. Reference 5 has presented a compressive stress-strain diagram for steel fiber reinforced mortar, the details of which are shown in Figure 2.22. This model consists of two curvilinear portions, one for the pre-peak and the other for the post-peak regions. The constant coefficients in the curvilinear equations have been derived using some characteristic stress and strain values as the boundary conditions. These characteristic values have been expressed, using experimental stress-strain relationships, as functions of the fiber reinforcement index and the compressive strength of plain mortar.

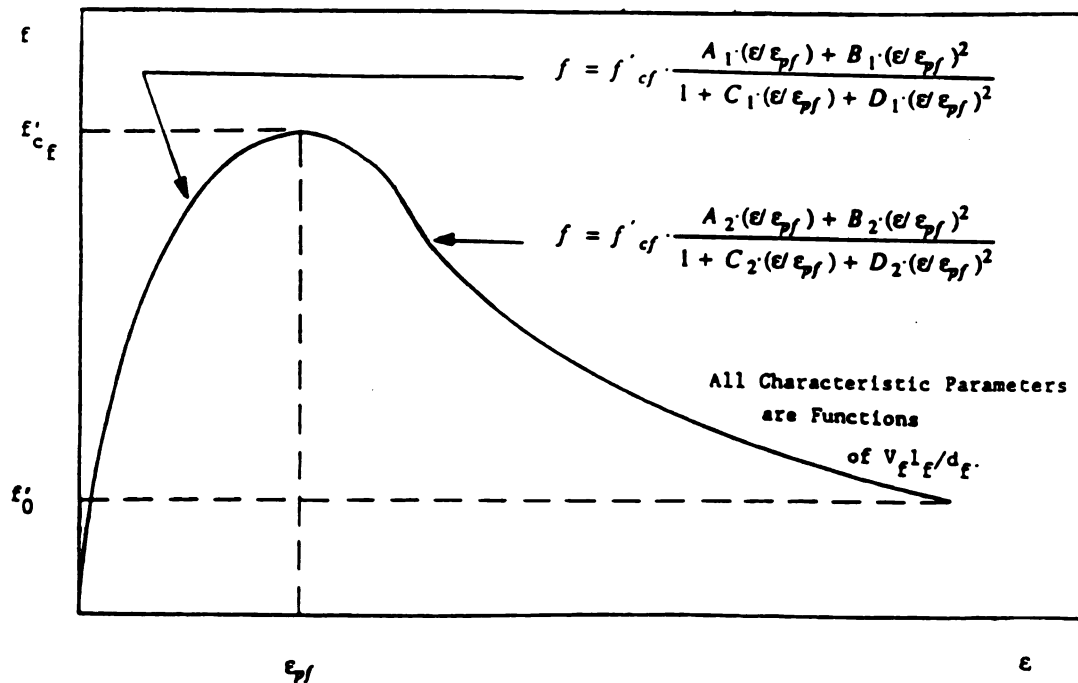
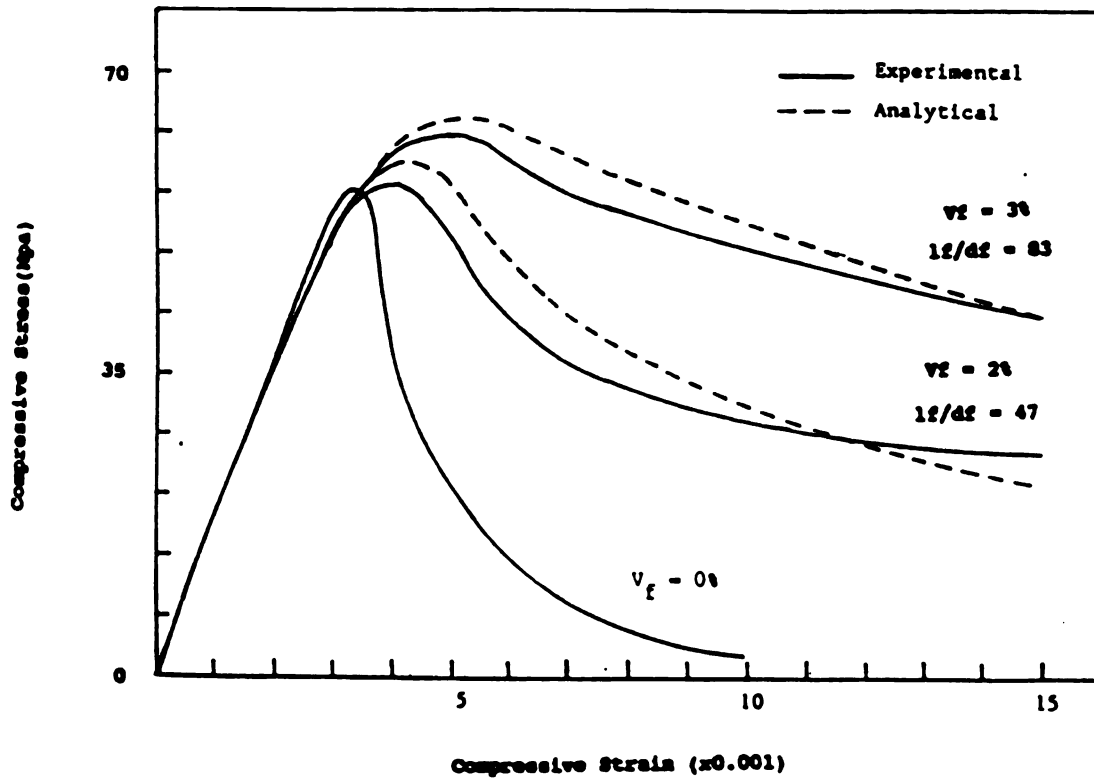


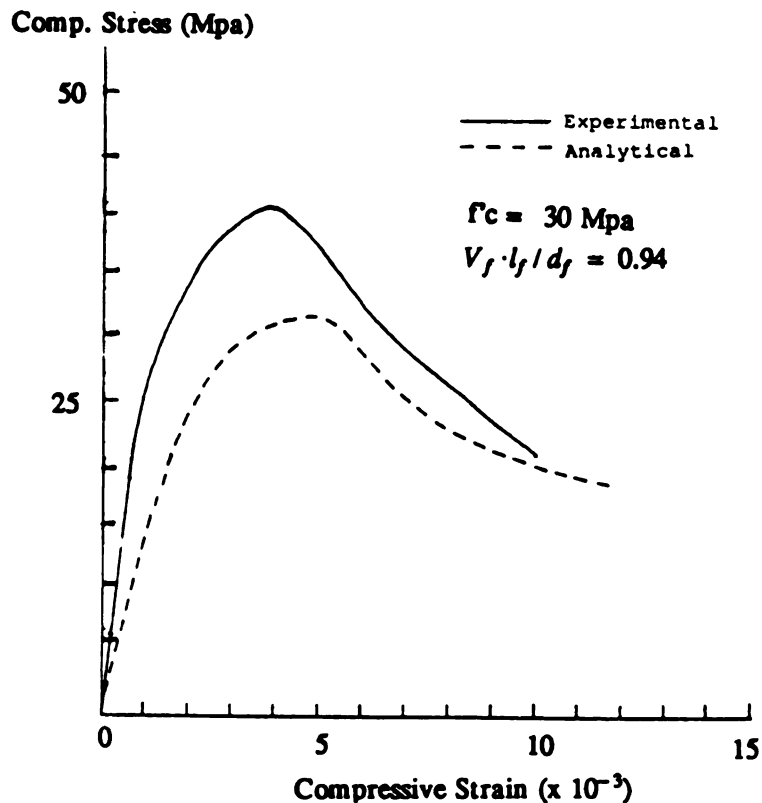
Figure 2.22 The Compressive Constitutive Model of Reference 5

The model of Reference 5 has been based on an experimental strain measurement technique which has possibly led to strain values (e.g., at peak stress) greater than the typical values reported in the literature. Hence, although this model compares reasonably well with the test results based on which it has been developed (Figure 2.23(a), it can not successfully predict the experimental compressive stress-strain relationships reported in the literature (Figure 2.23(b)). It should also be emphasized that the model of Reference 5 has been developed for steel fiber reinforced mortar, which behaves differently from steel fiber reinforced concrete.



(a) Test Data from Reference 5

Figure 2.23 Analytical Model of Reference 5 vs. Test



(b) Test Data from Reference 70

Figure 2.23 Analytical Model of Reference 5 vs. Test(cont'd)

## 2.4 STEEL FIBER REINFORCED CONCRETE UNDER FLEXURE

An important advantage of using steel fibers in concrete is related to the improvements in flexural behavior, which result directly from the improvements in the tensile and compressive behavior of steel fiber reinforced concrete. Mechanisms determining the improved flexural behavior of steel fiber reinforced concrete are, however, more complex than those responsible for improvements in the tensile and compressive behavior of the material. This partly illustrates why the improvements in flexural behavior of concrete resulting from steel fiber reinforcement are more pronounced than those in tensile and compressive

behavior.

The experimentally observed behavior of steel fiber reinforced concrete and flexural analysis procedures applied to the material will be discussed in the following sections. The main advantage of the use of steel fiber reinforced concrete is its high performance related to its flexural behavior. This benefit is the direct outcome of improvements in its mechanical properties of tension and compression. Mechanisms behind the flexural behavior of steel fiber reinforced concrete, however, are quite different from that of plain concrete or conventionally reinforced concrete. This section will describe experimentally observed behavior of steel fiber reinforced concrete beam and present reviews on some of the approaches to analyze it.

#### **2.4.1 Flexural Properties of SFRC**

The improvements of SFRC performance in compression and in tension result in significantly higher improvements in the flexural strength and ductility of SFRC [43-45]. A typical comparison between the flexural load-deflection relationships of plain and steel fiber reinforced concrete is presented in Figure 2.24.

SFRC exhibits an obvious deviation from linear load-deflection behavior prior to the peak flexural load. This point of deviation from linearity has been called the first-crack load ( $P_{cr}$  in Figure 2.24). Beyond the first cracking, the flexural load continues to increase at a lower stiffness due to the formation and propagation of a macrocrack at the critical section in matrix until the ultimate load ( $P_u$ ) is reached. In plain concrete once the deflection corresponding to the ultimate flexural load of plain concrete is exceeded, failure is brittle and the post-peak load-deflection curve shows a sharp descending behavior. Steel fiber reinforced concrete, on the other hand, is able to sustain a considerable fraction

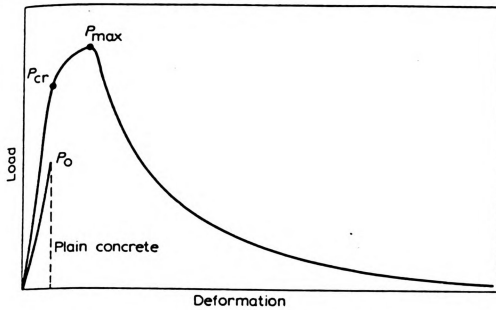


Figure 2.24 Flexural Behavior of Steel Fiber Reinforced Concrete Beam under Flexure

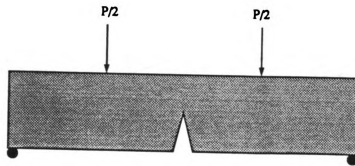


Figure 2.25 One Major Crack at Critical Section in Steel Fiber Reinforced Concrete Beam

of its flexural resistance even at deflections considerably larger than those corresponding to the peak load.

In the post-peak region, only one major crack occurs at a critical section in SFRC (see Figure 2.25). This can imply that curvature tends to become concentrated at this critical section. The critical section may be subject to severe distortions and plane sections may no longer remain plane after bending at this location.

#### 2.4.2 Analysis of Steel Fiber Reinforced Concrete Beams under Flexure

Limited analytical studies have been reported in the literature on predicting the flexural behavior of steel fiber reinforced concrete. Some investigators [46-50] have assumed hypothetical stress-strain and strain distributions across the critical section at the ultimate condition (see Figure 2.26) in order to compute

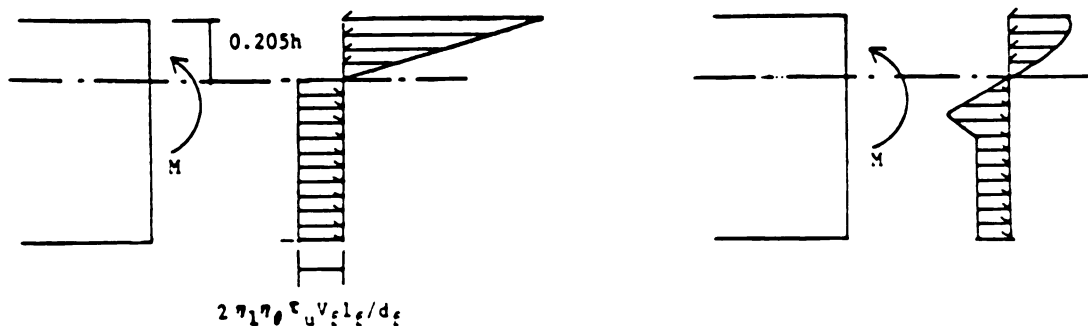


Figure 2.26 Hypothetical Stress-Strain Distributions [46-50]

flexural strength by considering equilibrium conditions at the critical section.

Very limited number of attempts have been made to simulate complete flexural load-deformation relationship of SFRC [45,51]. Studies in this area have been typically based on conventional beam theory, which assumes that plane sections normal to the beam axis remain plane after bending. An overall flexural analysis of SFRC beams, however, should account for the opening of a crack at the critical section, where flexural deformation tends to be concentrated. The nonlinearities occurring in the vicinity of the crack should also be taken into account.

## CHAPTER 3

# THE CONSTITUTIVE MODEL FOR STEEL FIBER REINFORCED CONCRETE UNDER TENSION

### 3.1 INTRODUCTION

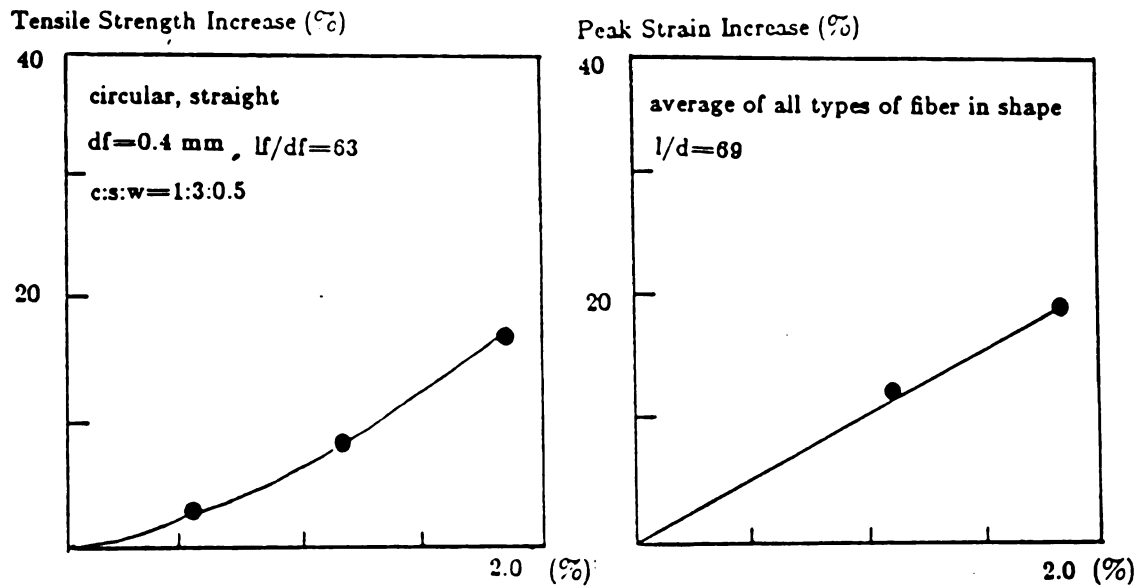
Direct tensile tests on SFRC have shown that reinforcement of concrete with short, randomly distributed steel fibers leads to improvements in tensile strength and tensile ductility of the cementitious material. These improvements can be attributed to the microcrack-arresting and pull-out actions of fibers [1,5,10,11,14]. Both of these actions of steel fibers in concrete tend to be dependent on the number of fibers crossing unit cross-sectional area in concrete [35]. Consequently, accurate expressions for computing the number of fibers in unit area are required for the modeling of SFRC under tension.

In spite of the significances of the tensile behavior in structural applications of SFRC, very few tensile constitutive models have been developed [24,26,52]. In this chapter, an empirical constitutive model for SFRC under tension is proposed, which reflects our understanding of the physics of SFRC tensile behavior and also takes advantage of the tensile test results reported by different investigators. The developed model accounts for both of the microcrack-arresting and pull-out actions of steel fibers in concrete.

### 3.2 EFFECTS OF FIBER REINFORCEMENT VARIABLES ON TENSILE BEHAVIOR OF STEEL FIBER REINFORCED CONCRETE

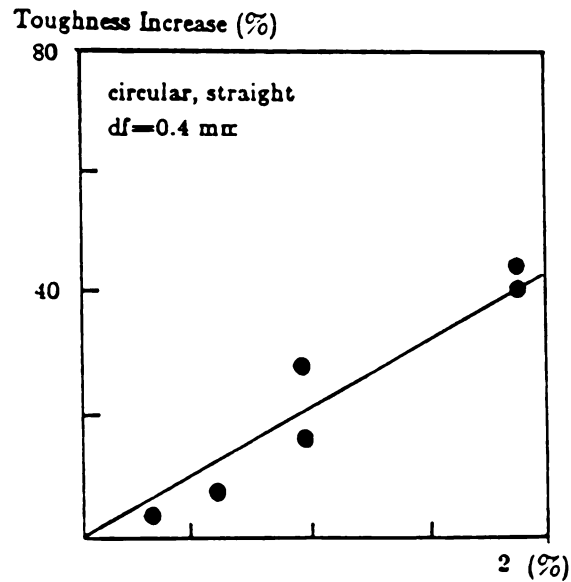
Direct tensile behavior of steel fiber reinforced concrete has been observed to depend on the fiber volume fraction, aspect ratio and deformation type. The increase in fiber volume fraction up to a certain limit (beyond which problems with workability and fiber dispersability start to dominate the behavior) tends to increase the direct tensile strength (Figure 3.1(a)), strain at peak tensile stress (Figure 3.1(b)) and post-peak energy absorption capacity (Figure 3.1(c)) of steel fiber reinforced concrete.

At a specified fiber volume fraction, the increase in fiber aspect ratio (defined as the ratio of the fiber length to its diameter) also increases the direct tensile strength (Figure 3.2(a)), strain at peak stress (Figure 3.2(b)) and also energy absorption capacity of steel fiber reinforced concrete [2,24,28,52,53].



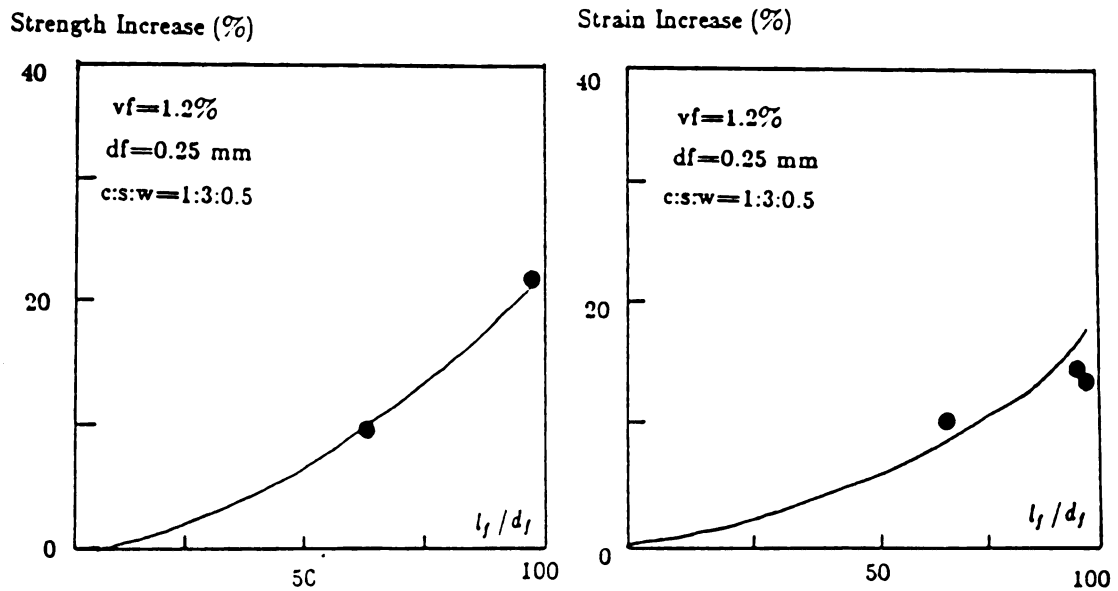
(a) Tensile Strength (b) Strain at Peak Tensile Stress

Figure 3.1 Effects of Fiber Volume Fraction on Tensile Behavior of Steel Fiber Reinforced Concrete [52]



(c) Energy Absorption Capacity

Figure 3.1 Effects of Fiber Volume Fraction on Tensile Behavior of Steel Fiber Reinforced Concrete [52] (cont'd)



(a) Direct Tensile Strength (b) Strain at Peak Stress

Figure 3.2. Influence of Fiber Aspect Ratio on Direct Tensile Behavior of Steel Fiber Reinforced Concrete [52].

Fibers with high aspect ratios are, however, more difficult to disperse in concrete and have more pronounced adverse effects on fresh mix workability. Hence, at each fiber volume fraction, there is a limit on aspect ratio beyond which the problems with fresh mix workability and fiber disperability tend to decide the tensile behavior of SFRC.

Some limited test results [25] have also indicated that the direct tensile strength of steel fiber reinforced concrete increases with decreasing fiber diameter at a constant aspect ratio (Figure 3.3).

Steel fibers are generally mechanically deformed for achieving a better mechanical bonding to the matrix. Reference 4 has reported experimental tensile stress-strain relationships for steel fiber reinforced concrete incorporating straight-round, hooked and paddled fibers. The results presented in Figure 3.4 are indicative of some differences in the overall tensile stress-strain relationship

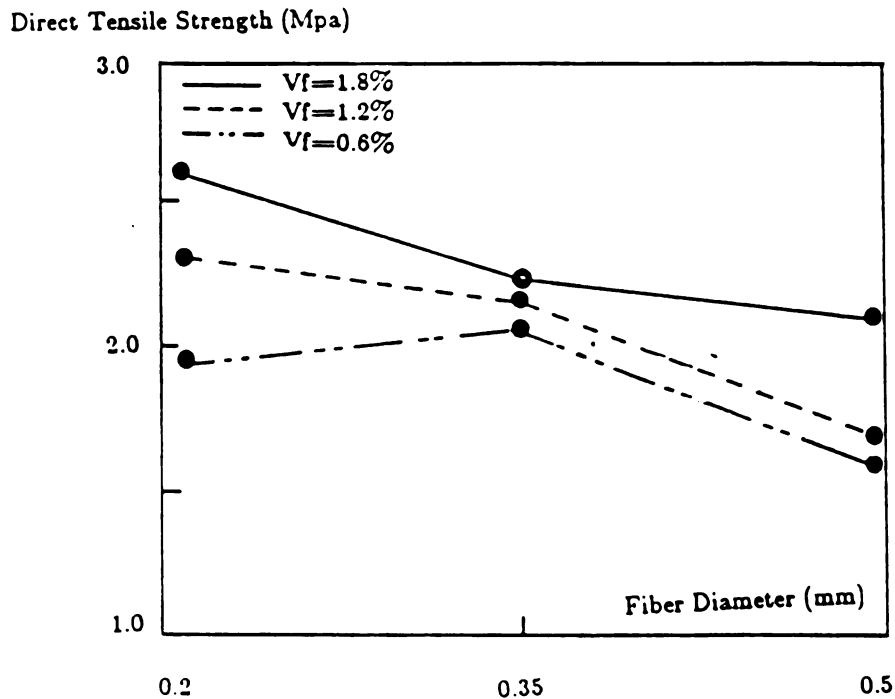


Figure 3.3 Effect of Fiber Diameter on Direct Tensile Strength of SFRC [25].

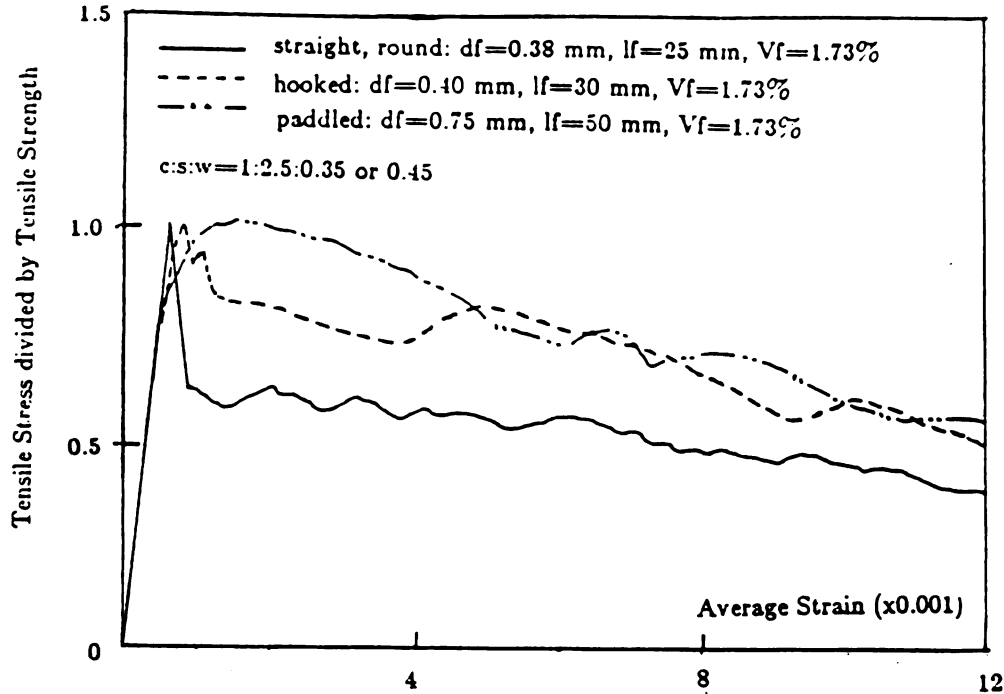


Figure 3.4 Effects of Steel Fiber Deformations On Direct Tensile Behavior of SFRC [4].

of steel fiber reinforced concrete, incorporating fibers with different mechanical deformations.

### 3.3 DEVELOPMENT OF EXPRESSIONS FOR THE NUMBER OF STEEL FIBERS CROSSING UNIT CROSS-SECTIONAL AREA IN SFRC

Both microcrack-arresting and pull-out action of fibers in concrete which contribute to the improvements in tensile strength and tensile ductility of steel fiber reinforced concrete are dependent on the number of fibers crossing unit cross-sectional area in concrete [1,5,10,14,35]. In the following discussion,

theoretical expressions are derived for the number of fibers per unit cross sectional area in fiber reinforced concrete, with due consideration given to the effects of the surrounding boundaries. Measurements are made on the number of fibers per unit cross-sectional area in steel fiber reinforced concrete specimens incorporating various volume fractions of fibers of different types. Based on statistical evaluation of the measured values, the differences in fiber concentration at different locations on the cross section are assessed. The effects of vibration on reorientation of steel fibers in concrete are investigated through comparisons between the computed and measured values of number of fibers per unit cross-sectional area.

### 3.3.1 Development of Theoretical Expressions

The average number of fibers per unit area may be considered as the total number of fibers times the possibility of one randomly located fiber crossing the unit area. This probability can be computed using a so-called fiber orientation factor ( $\alpha$ ), which is basically the average ratio, for all possible fiber orientations, of the projected fiber length in the tensile stress direction (for cross-sections normal to the tensile stress direction) to the fiber length itself.

Given the orientation factor as  $\alpha$ , the average number of fibers per unit area can be obtained as follows:

$$\begin{aligned}
 N_1 &= p N & (3.1) \\
 &= \alpha \frac{V_f}{A_f}
 \end{aligned}$$

where :

$p$  = possibility of one fiber crossing unit cross sectional area

$$= \frac{\alpha l_f}{l b f} \quad \text{in Figure 3.5 ; and}$$

$N$  = total number of fibers

$$= \frac{V_f}{A_f l_f} b h l \quad \text{in Figure 3.5.}$$

It can be shown from Equation (3.1) that finding the orientation factor with reasonable accuracy under different geometric conditions is important in the development of tensile constitutive models for SFRC.

The value of orientation factor is affected by different factors: (a) boundaries of the specimen restricting the orientation of fibers (see Figure 3.6); (b) vibration during concrete construction which may cause reorientation of fibers in

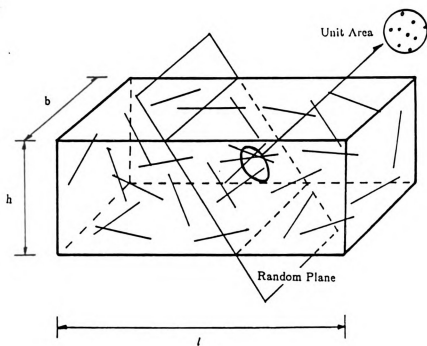
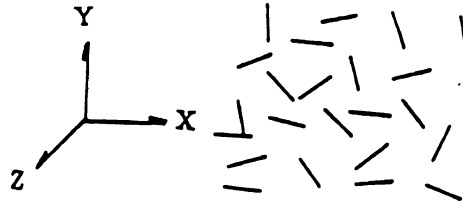
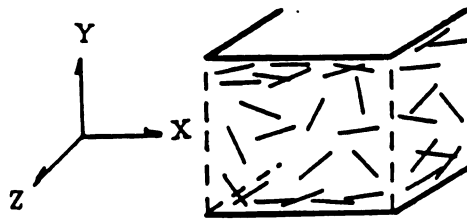


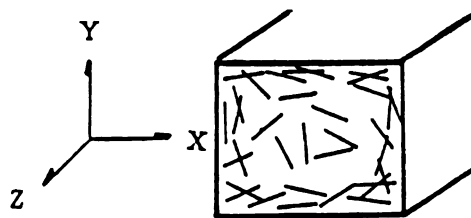
Figure 3.5 Number of Fibers per Unit Area



(a) Three-Dimensional



(b) Two Boundaries



(c) Four Boundaries

Figure 3.6 Orientation of Steel Fibers in Concrete

horizontal planes; (c) fiber types; and (d) location in cross section (top vs. bottom) with respect to the casting and vibration directions. Results of analytical and experimental investigations of these factors are presented in this section.

Steel fibers when uniformly dispersed in an infinitely large volume of concrete, are expected to be randomly oriented, with equal probabilities of being oriented in different directions in space. The orientation factor in this condition ( $\alpha$  representing  $\alpha$  in Equation (3.1)) can thus be expressed as follows (see Figure 3.7, where projectile is taken along the z-direction);

$$\alpha_0 = \frac{\int_0^{\pi/2} \int_0^{\pi/2} l_f \cos\theta \cos\phi d\theta d\phi}{(\pi/2)^2 l_f} \quad (3.2)$$

$$= 0.405$$

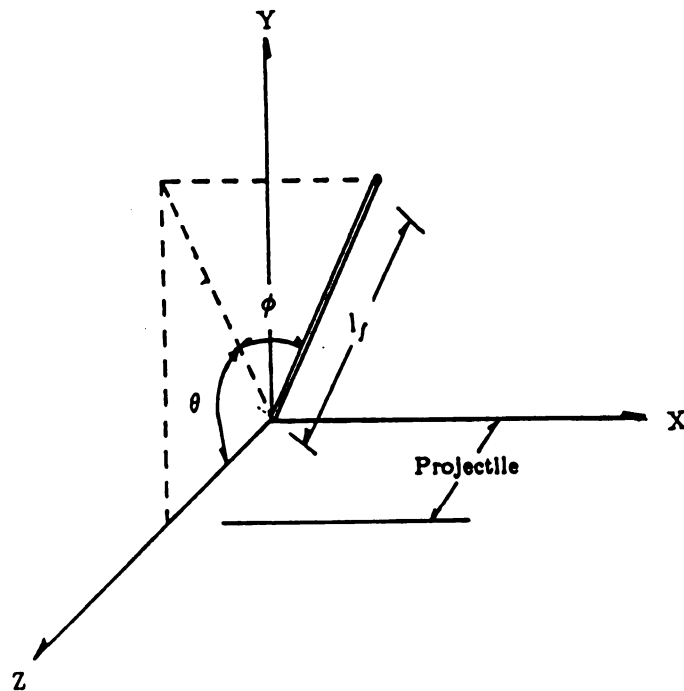


Figure 3.7 Three Dimensional Fiber Orientation

Application of steel fiber reinforced concrete to thin product (e.g., panels) may practically restrict fibers to a two-dimensional distribution. In a pure 2-D distribution (Figure 3.8), with two boundaries restricting the orientation of fibers in the plane, the following equation can be used to derive the orientation factor ( $\alpha_{2D}$ ):

$$\alpha_{2D} = \begin{cases} \frac{\int_{d_r/2}^{b/2} \beta_3 dx}{b/2} & \text{for } b \leq l_f \\ \frac{l_f}{b} \frac{\int_{d_r/2}^{l_f/2} \beta_3 dx}{l_f/2} + (1 - \frac{l_f}{b})0.64 & \text{for } b > l_f \end{cases} \quad (3.3)$$

where ;

$$\beta_3 = \frac{\int_0^\gamma l_f \cos\theta d\theta}{l_f \int_0^\gamma d\theta} ; \quad \text{and}$$

$$\gamma = \sin^{-1}\left(\frac{2x}{l_f}\right).$$

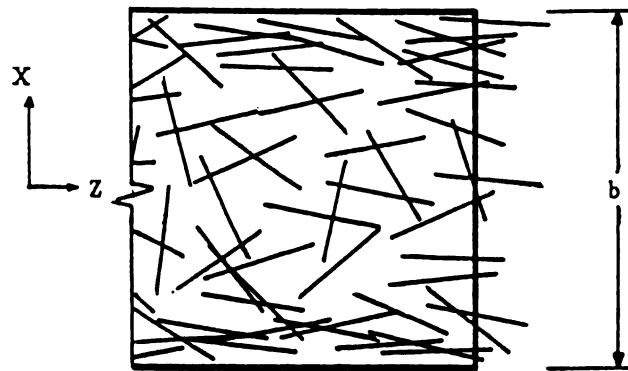


Figure 3.8 Two Dimensional Orientation of Fibers

The above expressions give a lower limit for 2-D orientation factor equal to 0.64 when the width ( $b$  in Equation (3.3)) becomes infinity, and an upper limit equal to 1.0 when the width becomes close to zero.

Where two boundaries are present to restrict the fiber orientation (Figure 3.6(a)), the orientation factor ( $\alpha_2$  representing  $\alpha$  in this condition) in the  $z$ -direction, which is a typical direction of tensile stresses, can be obtained by considering the effects of these two parallel boundaries:

$$\alpha_2 = \begin{cases} \frac{\int_{d_f/2}^{h/2} \beta_1 dy}{h/2} & \text{for } h < l_f \text{ ( Figure 3.9(a) )} \\ \frac{l_f}{h} \frac{\int_{d_f/2}^{l_f/2} \beta_1 dy}{l_f/2} + (0.405)(1 - l_f/h) & \text{for } h \geq l_f \text{ ( Figure 3.9(b) )} \end{cases} \quad (3.4)$$

where :

$$\beta_1 = \frac{\int_0^{\pi/2} \int_{\gamma_0}^{\gamma} l_f \cos\theta \cos\phi d\theta d\phi}{l_f (\pi/2) \gamma}$$

$$\gamma_0 = \sin^{-1}(d_f / l_f)$$

$$\gamma = \sin^{-1}(2y / l_f)$$

The result is shown in Figure 3.10 and it indicates that at thicknesses smaller than the fiber length, the obtained fiber orientation factor ( $\alpha_2$ ) is very close to a 2-D condition, and for thickness greater than two times the fiber length, there is a gradual approach to 3-D fiber orientation.

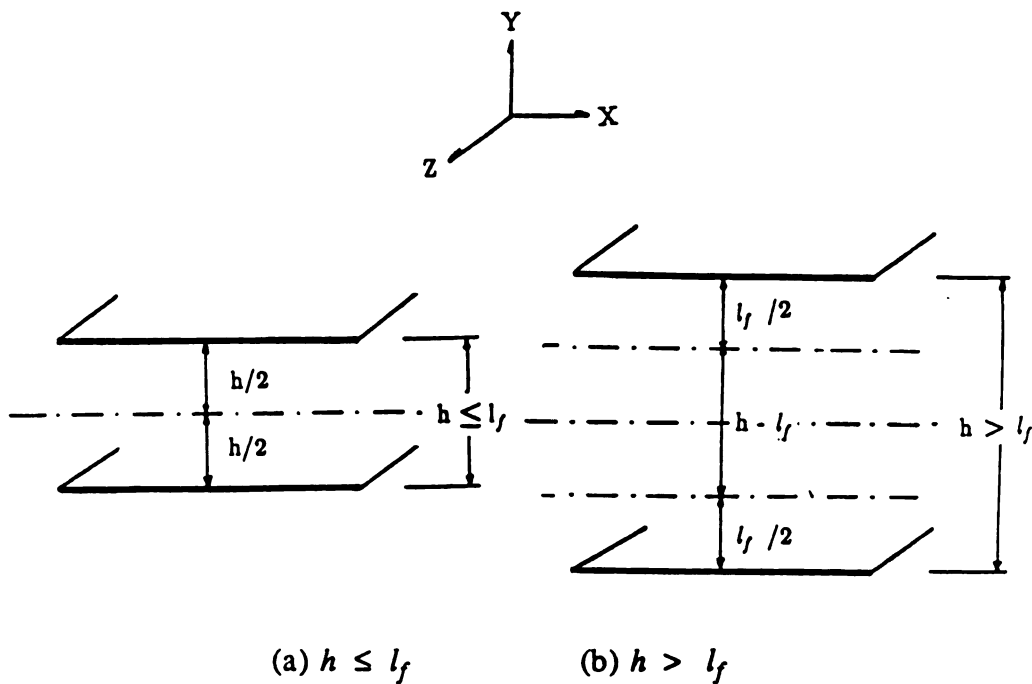


Figure 3.9 Different Conditions with Two Boundaries

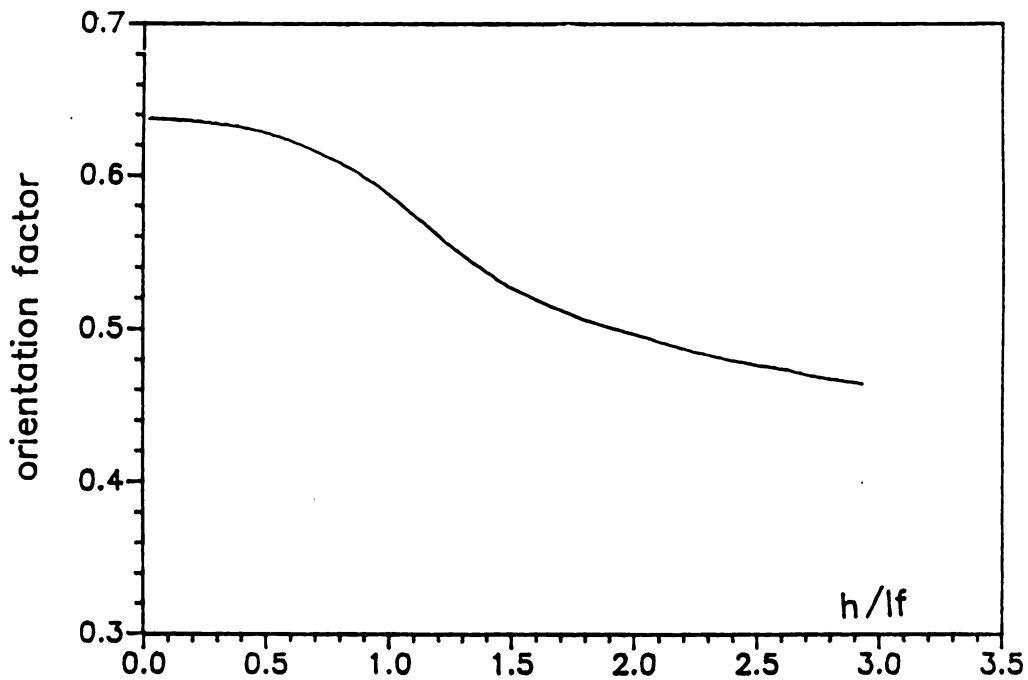


Figure 3.10 Effect of Height on Orientation Factor in Cases with Two Boundaries

In the condition where four boundaries are present (Figure 3.6(c)), the following expressions can be used to derive the orientation factor ( $\alpha$ ) in the z-direction:

$$\alpha = \begin{cases} f(b, h) & \text{for both sides } (b, h) < l_f \\ \frac{l_f}{b} f(l_f, h) + (1 - l_f/b) \frac{\int_{d_f/2}^{h/2} \beta_1 dy}{h/2} & \text{for only one side } (h) \leq l_f \\ \frac{l_f^2}{bh} f(l_f, l_f) + \frac{l_f(b+h-2l_f)}{bh} \frac{\int_{d_f/2}^{l_f/2} \beta_1 dy}{l_f/2} + \frac{(0.405)(b-l_f)(h-l_f)}{bh} & \text{for both sides } (b, h) \geq l_f \end{cases} \quad (3.5)$$

where :

$$f(m, n) = \int_{d_f/2}^{m/2} \int_{d_f/2}^{n/2} \frac{\beta_2 dx dy}{(m/2)(n/2)} ;$$

$$\beta_2 = \frac{\int_{\gamma_0}^{\gamma} \int_{\gamma_0}^{\delta} l_f \cos\theta \cos\phi d\theta d\phi}{l_f \int_{\gamma_0}^{\gamma} \int_{\gamma_0}^{\delta} d\theta d\phi} ;$$

$$\gamma_0 = \sin^{-1}(d_f / l_f) ;$$

$$\gamma = \sin^{-1}(2y / l_f) ;$$

$$\delta = \sin^{-1}(2x / l_f) ; \text{and}$$

$$\beta_1 = \text{given in illustration of Equation (3.4).}$$

Figure 3.11 presents the effects of cross sectional dimensions on the fiber orientation factor ( $\alpha$ ) for typical cases representing conditions having four boundaries as shown in Figure 3.12. Three cases with width-to-height ( $b/h$ ) ratios equal to 1, 3 and 6 are considered. It may be concluded from Figure 3.11 that the width-to-height ratio plays an important role in deciding the fiber orientation factor at cross sectional dimensions close to or smaller than fiber length. The fiber orientation seems to gradually approach a 3-D conditions as the cross sectional dimensions exceed two times the fiber length.

Approximate equations for 2-D and 3-D orientation factors (which are rather convenient to use) are presented below. These expressions were derived using Taylor Expansions of exact expressions. Comparisons between exact and approximate expressions are given in Figure 3.13.

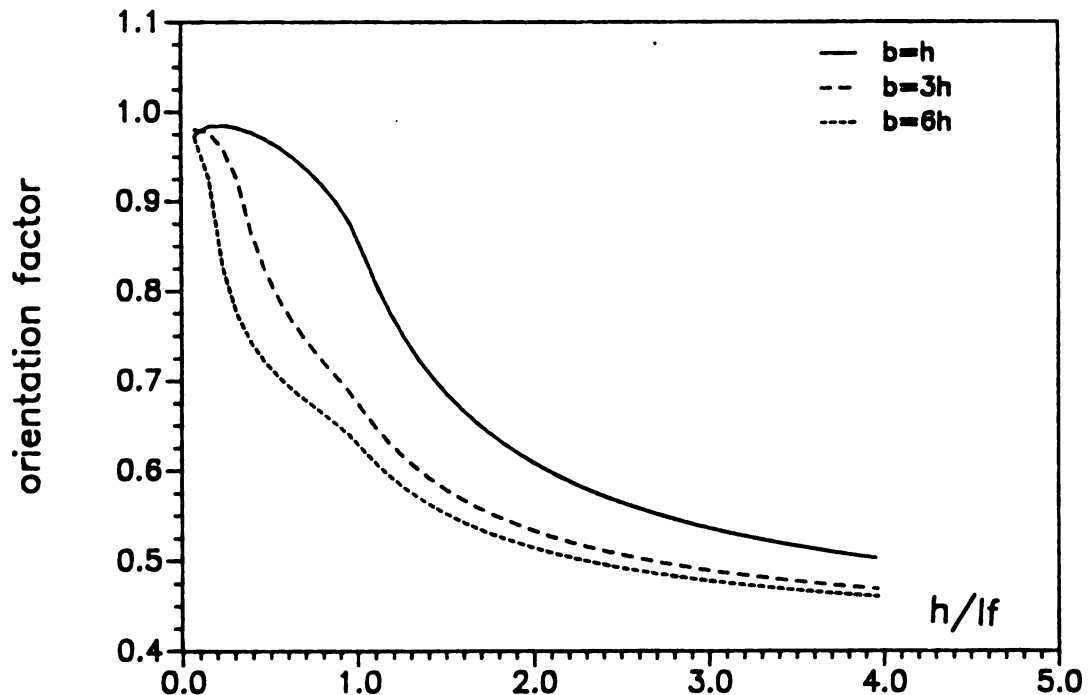


Figure 3.11 Effects of Cross-Sectional Dimensions on Orientation Factor in Cases with Four Boundaries

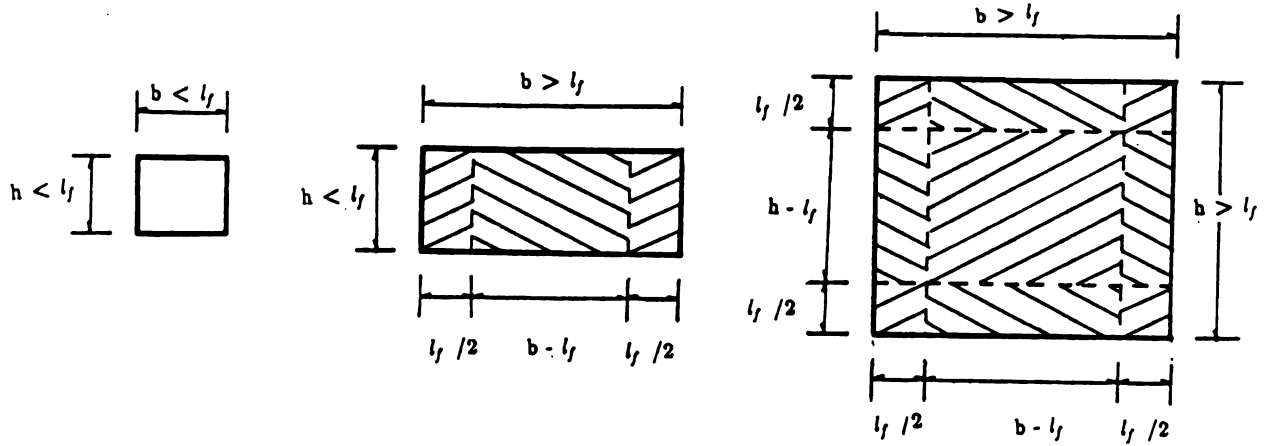


Figure 3.12 Different Conditions with Four Boundaries

$$\alpha = \begin{cases} 6 \cdot \frac{l_f^2}{b \cdot h} \cdot \tan^{-1}\left(\frac{b}{\sqrt{6} \cdot l_f}\right) \cdot \tan^{-1}\left(\frac{h}{\sqrt{6} \cdot l_f}\right) & \text{for both } b, h \leq l_f \\ \frac{l_f}{h} \cdot \tan^{-1}\left(\frac{h}{\sqrt{6} \cdot l_f}\right) \cdot (1.56 + 0.766 \cdot \frac{l_f}{b}) & \text{for only } h \leq l_f \\ 0.098 \cdot \frac{l_f^2}{b \cdot h} + 0.2 \cdot l_f \cdot \frac{(b+h)}{b \cdot h} + 0.405 & \text{for both } b, h > l_f \end{cases} \quad (3.6)$$

$$\alpha_{2D} = \begin{cases} \sqrt{6} \cdot \frac{l_f}{b} \cdot \tan^{-1}\left(\frac{b}{\sqrt{6} \cdot l_f}\right) & \text{for } b \leq l_f \\ 0.31 \cdot \frac{l_f}{b} + 0.64 & \text{for } b > l_f \end{cases} \quad (3.7)$$

orientation factor

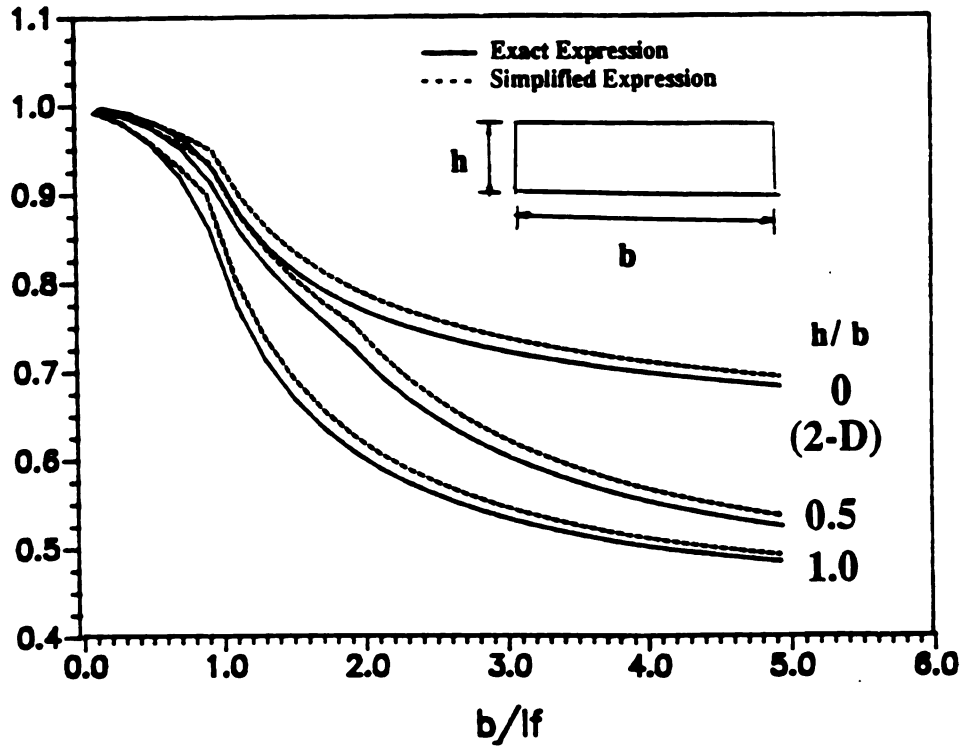


Figure 3.13 Comparisons between Exact and Approximate Expressions of Orientation Factor in Different Conditions

### 3.3.2 Experimental Assessment of the Orientation Factor

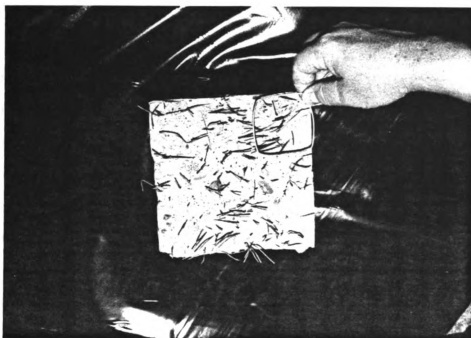
Orientation of steel fibers in concrete and consequently the number of fibers per unit area are influenced not only by the boundaries restricting the random orientation of fibers, but also by the fact that steel fibers tend to settle down and reorient in horizontal planes when fibrous concrete is vibrated during placement. Hence, as a result of vibration, the orientation of steel fibers in concrete moves further away from a 3-D condition and tends to approach a 2-D condition. In order to assess the degree of fiber reorientation during vibration, a comparison was made between the values for the number of fibers per unit area obtained theoretically from Equation (3.5) and measured experimentally. This section presents the results of measurements made in this study on the number of fibers per unit area. These results are compared with the theoretical values

in order to derive more representative expressions for the actual fiber orientation conditions in concrete.

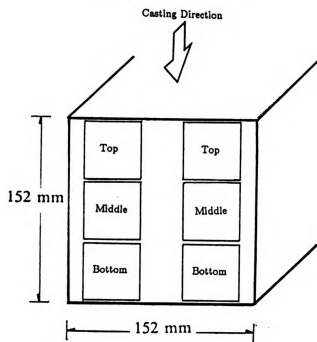
The measurements of the number of fibers per unit area were performed on fractured cross-sectional surfaces of 152 mm by 152 mm by 457 mm (6 in. by 6 in. by 18 in.) steel fiber reinforced concrete beams tested in flexure. The concrete matrices had a water/binder ratio of 0.40, fly ash (type F)/binder ratio of 0.3, aggregate/binder ratio of 4.0, fine-to-coarse aggregate ratio of 1.0, and superplasticizer (solid content)/binder ratio of 0.01 by weight. The fiber volume fractions were 0.5, 1.0, 1.5 and 2.0%, and the fibers were either straight (51 mm = 2 in. length and 0.5 mm = 0.02 in. diameter) or hooked (51 mm = 2 in. length and 0.5 mm = 0.02 in. diameter). The specimens were vibrated externally, and were tested in flexure after 28 days of air curing (at 40% Relative Humidity and 22°C, 72°F). The flexural loading was continued until complete separation occurred.

A total of 19 flexural specimens were tested in this investigation. For each specimen, the number of fibers per unit area was measured using a 51 mm (2 in.) square frame (Figure 3.14(a)), noting that the number of fibers per unit area at a certain location is the sum total of the number of fibers appearing on one side and the number of pulled out fibers on the corresponding opposite side.

Measurements were made at six locations on each specimen (Figure 3.14(b)). These locations were categorized as top, middle, and bottom with respect to the casting direction, as shown in Figure 3.14(b). The measured values of the number of fibers per unit area were then normalized as follows :



(a) Measurement Technique



(b) Measurement Location

Figure 3.14 Measurement of the Number of Fibers per Unit Area

$$\alpha = \frac{N_1}{V_f/A_f} \quad (3.8)$$

where  $\alpha$ , the normalized value, is actually the orientation factor in Equation (3.1). The theoretical values for  $\alpha$  ( $\alpha_0$ ,  $\alpha_2$  and  $\alpha$  in Equations (3.2),(3.4) and (3.5), respectively) were influenced only by the boundary conditions, but not the vibration of concrete. The differences between the measured and theoretical values of  $\alpha$  will thus mainly represent the consequences of fiber reorientation in fresh mix under vibration.

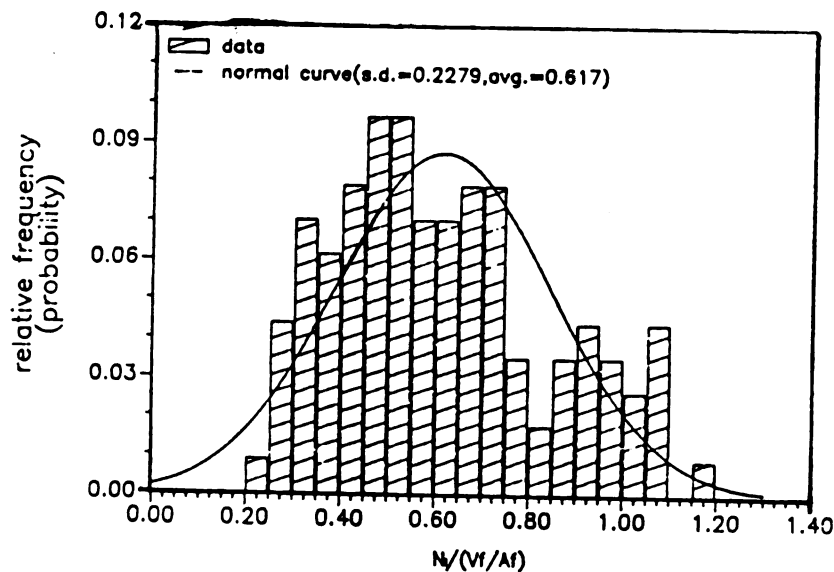
Table 3.1 summarizes the measurements made in this study for the number of fibers per unit cross sectional area in a total of 19 specimens. The means and standard deviations of the orientation factors (obtained by normalizing the number of fibers per unit area following Equation (3.1)) are given in this table for different locations on cross section and for different fiber types.

In order to verify if there is any statistically significant difference between the fiber orientation factors, and consequently the number of fibers per unit area,

Table 3.1 Mean Values of Fiber Orientation at Different Location on Cross Section and for Different Fiber Types

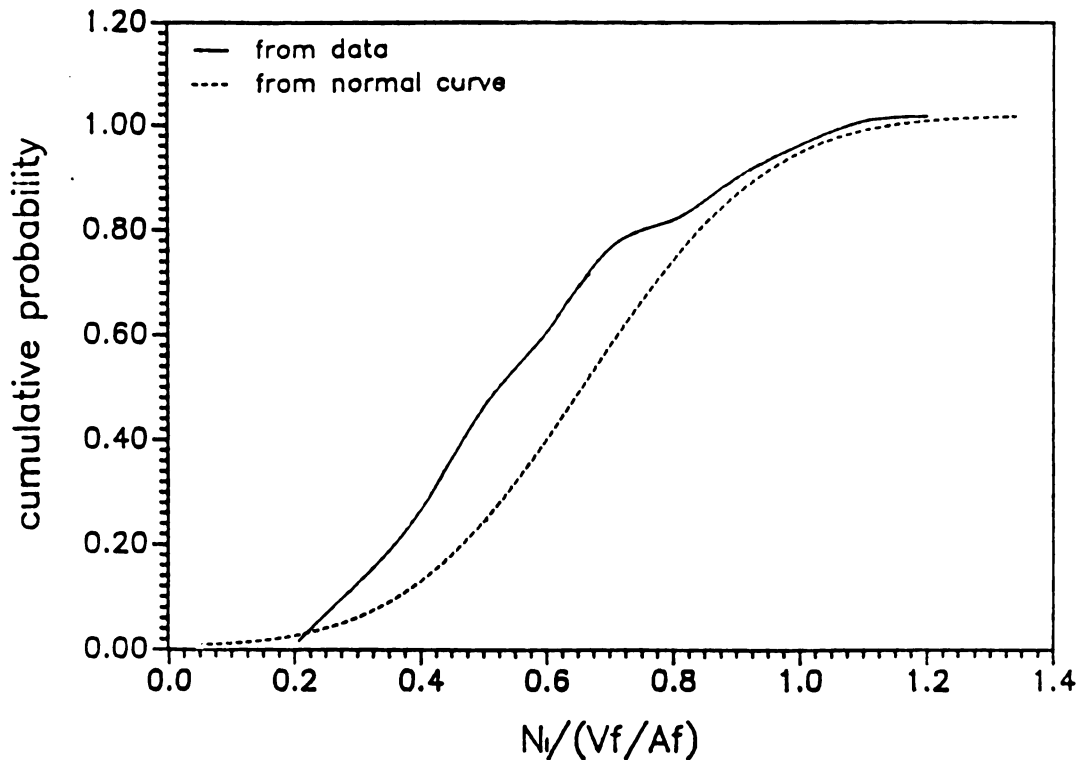
Fiber Type (No. of Specimen)	Mean and Standard Deviation of alpha(Eq.8)							
	Top		Middle		Bottom		All	
	Mean	Std. Dev.	Mean	Std. Dev.	Mean	Std. Dev.	Mean	Std. Dev.
Straight (16 Specimens)	0.609	0.231	0.587	0.235	0.654	0.240	0.617	0.235
Hooked (3 Specimens)	0.605	0.211	0.476	0.0773	0.776	0.214	0.619	0.179
All (19 Specimens)	0.608	0.225	0.569	0.221	0.673	0.237	0.617	0.228

at different locations on cross section or for different fiber types, the hypothesis that there are no effects of location and fiber type was tested statistically using the measured values of fiber orientation factor. T-tests [54] indicated that at a significance level of 0.05, given the measurements made on the available specimens, there are no statistically significant effects of location on cross section (top vs. bottom) or fiber type (straight vs. hooked) on orientation factor and consequently on the number of fibers per unit area. Hence, the mean and standard deviation of fiber orientation factor can be derived using all the measurements made in this study, irrespective of the location or fiber type. The resulting values of mean and standard deviation (given in the last two columns of the last row in Table 3.1) are 0.617 and 0.228, respectively. Figures 3.15(a) and 3.15(b) compare the frequency and cumulative frequency distributions of the measured orientation factors with the corresponding normal distribution curves. Some degree of similarity between the measured values and normal distribution curves can be observed.



(a) Frequency Distribution

Figure 3.15 Measured vs. Normal Distribution



(b) Cumulative Frequency Distribution

Figure 3.15 Measured vs. Normal Distribution (cont'd)

F-tests [54] on measurements made at different locations on cross section and for different fiber types also showed no statistically significant effects of location and fiber type (at 0.05 significant level) on the standard deviation of the measured values of orientation factor.

### 3.3.3 Theoretical Values vs. Experimental Measurements

The theoretical value of orientation factor obtained from Equation (3.5) for the parameters chosen in this study ( fiber length of 51 mm = 2 in., and cross sectional dimensions of 152 mm by 152 mm = 6 in. by 6 in.) is 0.537. The difference between the measured mean value of fiber orientation (0.617) and the calculated value of 0.537 is about 4 times the standard error of the measured

mean value. This significant difference can not be simply attributed to the variation of steel fiber concentration inside concrete. The relatively large value of orientation factor in actual measurements may result from the modification of fiber orientation during the vibration of fresh mix [55]. Vibration effects cause a reorientation of steel fibers inside concrete and encourage a tendency toward 2-D distribution of fibers in horizontal planes. This effect of vibration may be used to illustrate the difference between the measured and theoretical values of number of fibers per unit area (and orientation factor).

It should be noted that, for the conditions of test specimens in this study (152 mm = 6 in. square section, 51 mm = 2 in. fiber length), a pure 2-D distribution in horizontal planes (considering the boundary effects), would lead to a horizontal orientation factor of 0.74 (see section 3.3.1 for theoretical expressions for 2-D fiber orientation) which is larger than the measured value of 0.617. Noting that this measured value (0.617) is at the same time larger than the corresponding 3-D fiber orientation factor of 0.537 obtained theoretically (considering the boundary effects), it may be concluded that the actual fiber orientation factor after vibration of concrete is in between the corresponding 2-D and 3-D orientation factors (calculated considering the boundary effects). Approximate values of orientation factors in specimens with different geometries and fiber lengths can be derived from Figure 3.16. This figure shows values for orientation factors in 2-D conditions with two boundaries (calculated using Equation (3.3)) and 3-D conditions (with different height-to-width ratios calculated using Equation (3.5)), in terms of the ratio of specimen width to fiber length. For each geometric condition, given the specimen width to fiber length ratio and also the ratio of specimen height to its width, Figure 3.16 can be used to derive theoretical values of orientation factor for 2-D and 3-D conditions. The experimental results of this study indicate that the actual orientation factor would fall

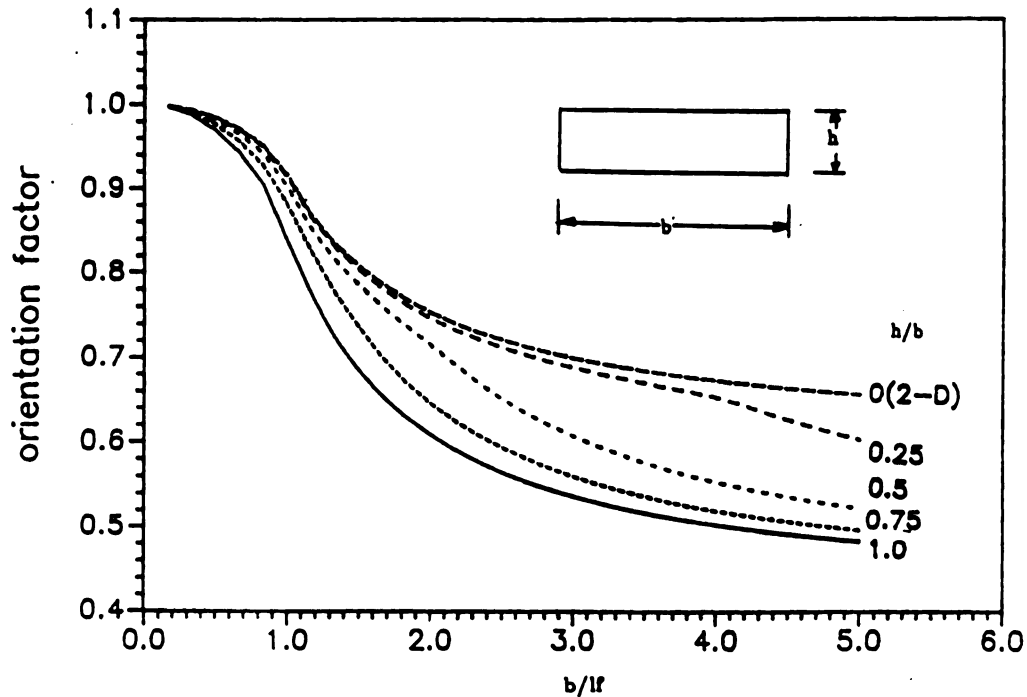


Figure 3.16 2-D and 3-D Orientation Factors for Different Geometric Conditions

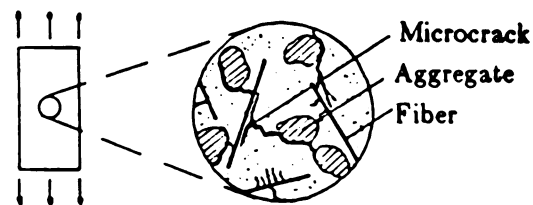
between the 2-D and 3-D values (an average of the two may be used as a rough approximation).

### 3.4 PREDICTION OF TENSILE STRENGTH: "INTERACTION CONCEPT"

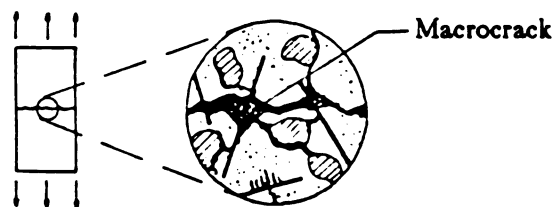
As mentioned earlier, there are two dominant analytical simulations of fiber reinforced concrete failure mechanism under direct tension. One considers the pull-out action of fibers as the key mechanism through which fibers contribute to the tensile strength of material (generally referred to as the composite material concept or the law of mixture) [1,3,27-29,56]. The second approach (usually referred to as the spacing concept) suggests that the spacing of fibers, not their

bonding to matrix and pull-out behavior, is the key factor which decides the effectiveness of fibers in concrete [34,35]. One may consider that the spacing concept is based on the assumption that at the composite peak stress fibers act mainly to arrest microcracks (Figure 3.17) rather than to bridge the macrocracks, while the opposite applies to the composite material concept.

Figures 2.18(b) and 2.19 presented in Chapter 2 are indicative of shortcomings of the composite material and spacing concepts, respectively, in describing the performance of steel fiber reinforced concrete at peak tensile stress. The deficiencies of the composite material concept may have been caused by disregard for the microcrack-arresting action of steel fibers (Figure 3.17(a)) and the inherent assumption at the composite material approach that the pull-out



(a) Arrest of Microcracks



(b) Bridging of Macrocracks

Figure 3.17 Influences of Fibers on Cracking Characteristics and Tensile Behavior of Concrete

resistance of fibers is almost fully mobilized at peak tensile stress (where the strains and crack openings are insufficient to do so) [28]. The spacing concept, on the other hand, disregards any partial mobilization of bond stresses (Figure 3.17(b)) at peak tensile stress, which could be the key reason for its discrepancies when compared to test results.

### 3.4.1 "Interaction Concept"

The formulation presented below for the prediction of SFRC tensile strength can potentially account for the contributions of both the microcrack-arresting and partial pull-out actions of steel fibers at the peak tensile stress of the composite material:

$$\sigma_c = A \cdot \sigma_m' + 0.25\pi \cdot d_f \cdot l_f \cdot \tau \cdot N_1 \quad (3.9)$$

where :

$$A = 1 + a \cdot N_1^{1/3} ;$$

$$\tau = \textit{interfacial bond stress at the composite peak tensile stress}$$

$$= t \cdot \sigma_m ; \textit{ and}$$

$a , t = \textit{coefficients to be derived empirically.}$

The contribution of matrix at peak tensile stress in the above equation is represented by  $A \cdot \sigma_m'$ , where  $A$  is dependant on the number of fibers per unit cross-sectional area ( $N_1$ ). This reflects the fact that a higher number of fibers (with a smaller fiber spacing) is more effective in arresting microcracks (Figure 3.17(a)) and thus in increasing the contribution of the matrix to the composite material tensile strength. Equation (3.8) can be used to derive  $N_1$ , with the

orientation factor ( $\alpha$ ) being a function of the fiber reinforcement properties (geometry and volume fraction) and the cross-sectional dimensions of test specimen as described in section 3.3 in this Chapter.

The contribution of fiber pull-out at peak tensile stress is represented in Equation (3.9) by the multiplication of the average fiber interfacial area resisting pull-out ( $0.25\pi \cdot d_f \cdot l_f$ ) times the average fraction of bond stress mobilized at the composite peak tensile stress ( $\tau$ ) times the number of fiber per unit area ( $N_1$ ). The proportionality of  $\tau$  and matrix tensile strength ( $\sigma_m'$ ) reflects the fact that stronger matrices may be capable of activating a larger fraction of fiber pull-out force at peak tensile stress. It is assumed that the inclination of fibers with respect to the tensile stress direction has a negligible effect on the pull-out action of fibers. It is worth mentioning that the decisions on the dependence of the matrix contribution to tensile strength of the composite on the number of fibers per unit cross-sectional area ( $N_1$ ), and also the dependence of the fiber pull-out contribution on the matrix tensile strength ( $\sigma_m$ ) were made based on the physics of the composite material behavior at peak tensile stress, and also based on an extensive trial and adjustment verification of different concepts for describing the composite material performance at peak tensile stress.

The proposed approach to the prediction of SFRC tensile strength accounts for the physical interactions that exist between fibers and matrix at peak tensile stress, and it may thus be referred to as the "interaction concept" for predicting the tensile strength of fiber reinforced concrete.

Coefficients  $a$  and  $t$  of the "interaction concept" in Equation (3.9) have to be decided empirically using tensile stress test results. A comprehensive set of test data was used for this purpose.

### 3.4.2 Empirical Coefficients

A total of 50 SFRC tensile strength test results were used to derive the empirical coefficients of the proposed "interaction concept" equation for the prediction of SFRC tensile strength (Equation (3.9)). The direct tension test results used in this study were obtained for mortars reinforced with straight (round or rectangular) steel fibers [24,25,29,52,57]. These tests were performed on specimens with rectangular cross sections of different dimension. Table 3.2 summarizes the following properties of the tension test specimens : (a) cross sectional dimensions ; (b) fiber reinforcement properties ; and (c) matrix mix proportion and tensile strength test results.

Least square fitting of the "interaction concept" expression (Equation (3.9)) to the test data presented in Table 3.2 provided the basis for calculating coefficients  $a$  and  $t$  of Equation (3.9), which were found to be equal to 0.138 and 0.2, respectively. Hence, the proposed "interaction concept" leads to the following equation for calculating the tensile strength of steel fiber reinforced concrete :

$$\sigma_c = \sigma_m' \cdot (1 + 0.138 \cdot N_1^{1/3} + 0.05\pi \cdot d_f \cdot l_f \cdot N_1) \quad (3.10)$$

Figure 3.18 shows the desirable comparisons between predictions of the proposed "interaction concept" (Equation (3.10)) and SFRC tensile strength test results.

The bond stress mobilized at the composite tensile strength is represented in Equation (3.9) by  $t \cdot \sigma_m'$ . An empirical value of 0.20 for  $t$  indicates that, for a typical matrix tensile strength of 2.41 Mpa (350 psi), the bond stress developed at the composite material tensile strength is typically 0.48 Mpa (70 psi), which is

Table 3.2 Direct Tensile Test Specimen and Results

Ref.	matrix			fiber			specimen size widthxdepth (mm x mm)	composite	
	c:s:w	tensile strength (Mpa)	strain at peak (x0.0001)	diameter (mm)	length (mm)	Vf (%)		tensile strength (Mpa)	strain at peak (x0.0001)
24	1:2:0.5	2.8	1.74	0.41	25.4	0.5-1.5	76x19	3.0-3.6	1.9-2.2
25	1:2.5:0.6	1.68	*	0.25	18.8	1-3	38x51	2.0-2.5	*
	"	"	*	0.25	12.7	1-3	"	1.8-2.1	*
	*	"	*	0.25	25.4	1-3	"	2.2-2.7	*
29	1:3:0.5	3.38	1.43	0.25	19.1	0.6-1.7	102x102	3.7-4.0	1.6-1.8
	"	"	"	"	38.1	0.3-1.7	"	3.5-3.8	1.5-1.9
	"	"	"	"	25.4	0.3-1.7	"	3.0-4.3	1.6-2.2
	"	"	"	0.41	13.8	0.6-1.7	"	3.4-3.5	1.5-1.6
	"	"	"	"	25.4	0.6-1.7	"	3.6-4.0	1.5-1.8
	"	"	"	"	38.1	0.6-1.7	"	3.8-4.5	1.7-2.0
	"	"	"	0.43	15.2	1.7	"	3.7	1.6
	"	"	"	"	30.5	1.2-1.7	"	3.5-4.1	1.7
	"	"	"	"	45.7	0.6-1.7	"	3.7-4.6	1.6-1.8
34	1:2:0.45	1.74	0.85	0.5	50	0.6-1.8	16x100	1.9-2.6	1.2-2.1
	"	"	"	0.35	35	0.6-1.8	"	1.9-2.4	1.1-2.2
	"	"	"	0.25	25	0.6-1.8	"	1.6-2.0	0.9-1.7
35	*	2.8	*	0.43	12.7	1-3	12.7x76	3.6-5.3	1.6-4.4
	*	"	*	"	19.1	1-3	"	2.7-4.6	1.2-6.6
	*	"	*	"	25.4	1-3	"	3.5-5.3	1.3-6.0

\* Not Reported

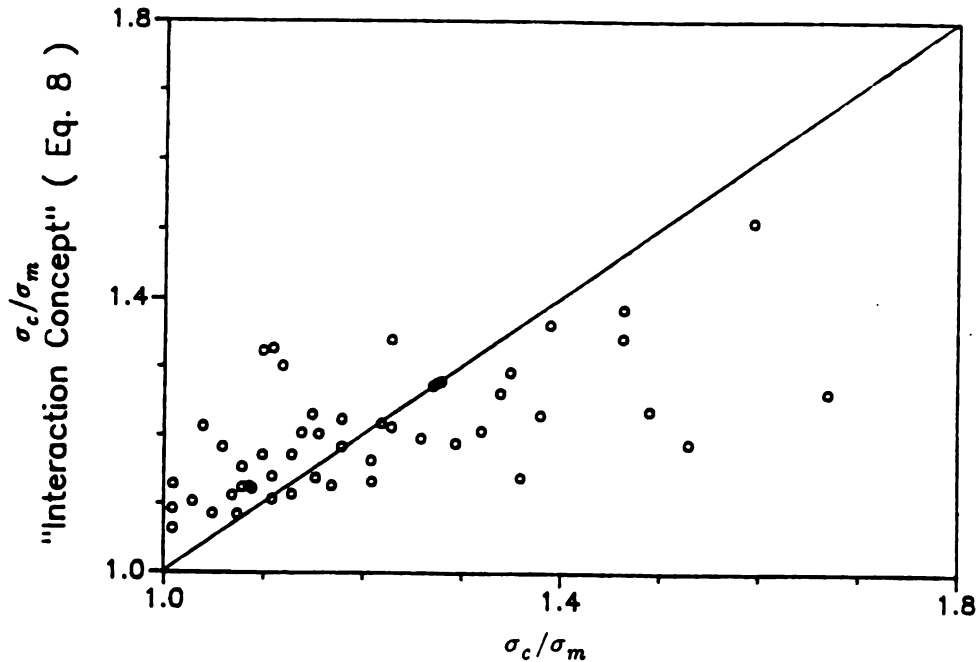


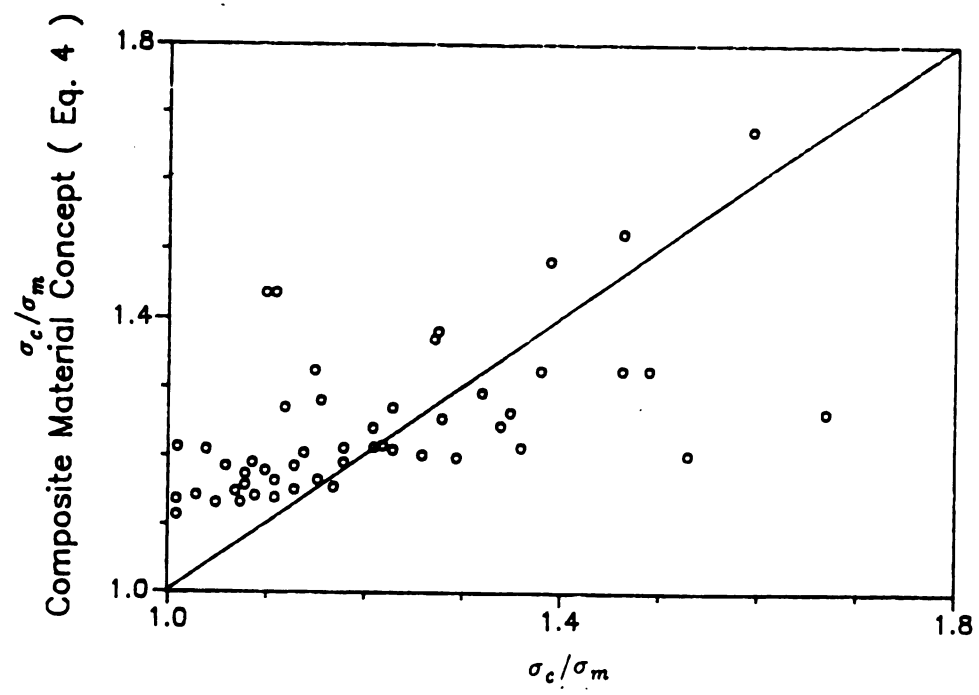
Figure 3.18 Comparisons of the Proposed "Interaction Concept" with Tensile Strength Test Results

only about 25% of a typical fiber-to-matrix bond strength of about 2 Mpa (reported in Reference 28). This result is compatible with the discussion made earlier on strains and crack openings at the peak tensile stress of the composite indicating that they are not large enough to fully mobilize the pull-out action and interfacial bond strength of steel fibers in concrete.

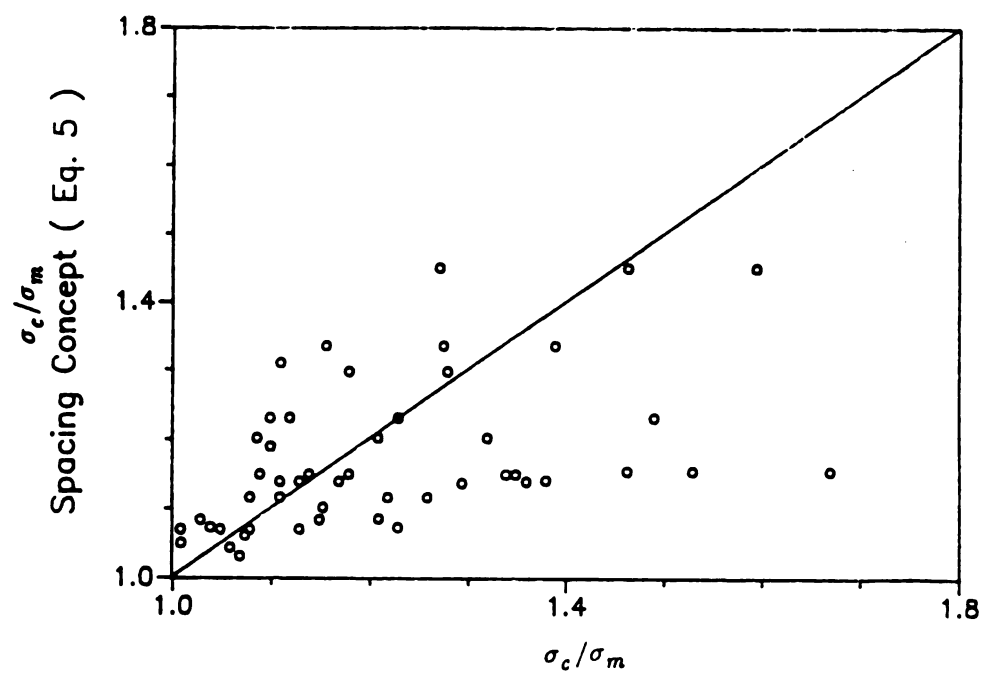
The matrix contribution to tensile strength is represented in Equation (3.9) by  $\sigma_m' \cdot (1 + a \cdot N_1^{1/3})$ . With the empirical value of 0.138 for  $a$ , at a typical value of 0.047 for  $N_1$  (corresponding to a volume fraction of 1% in a direct tension test specimen with typical cross-sectional dimensions), the contribution of matrix to the composite material tensile strength is 1.05 times the matrix tensile strength. This increase in the tensile strength of matrix may be attributed to the microcrack-arresting action of fibers inside the matrix which tends to strengthen the matrix under the action of tensile stresses.

### 3.4.3 "Interaction Concept" vs. Composite Material and Spacing Concepts

This section uses tensile strength test results presented in Table 3.2 to perform a comparative study on the accuracy of the proposed "interaction concept" versus those of the composite material concept (Equation 2.4 [3]) and the spacing concept (Equation 2.5 [34]) and modified spacing concept (Equation 2.6 [35]) in predicting the tensile strength of SFRC. The comparison between predictions of the new "interaction concept" and test results is presented in Figure 3.18. Figures 3.19(a), (b), and (c) compare the same test results with the predictions of the composite material concept (Equation 2.4), spacing concept (Equation 2.5), and modified spacing concept (Equation 2.6), respectively. Relatively large scatters between test results and predictions based on the composite material and spacing concepts are observed in Figure 3.19. The sum total of the squares of normalized errors ( the normalized error represents the difference between theoretical and experimental tensile strength values normalized with respect to the experimental strength ) for each of the four approaches introduced in Figures 3.18 and 3.19 are as follows : 0.429 for the "interaction concept" (Equation (3.10)), 0.553 for the composite material concept (Equation (2.4)), 0.567 for the spacing concept (Equation (2.5)), and 0.551 for the modified spacing concept (Equation (2.6)). This confirms the favorable comparison of the "interaction concept" prediction with test results. The average and standard deviation of errors (differences between normalized theoretical and experimental values) are presented in Table 3.3. The average error of the "interaction concept" prediction is observed to be closer to zero and the standard deviation of its errors is also

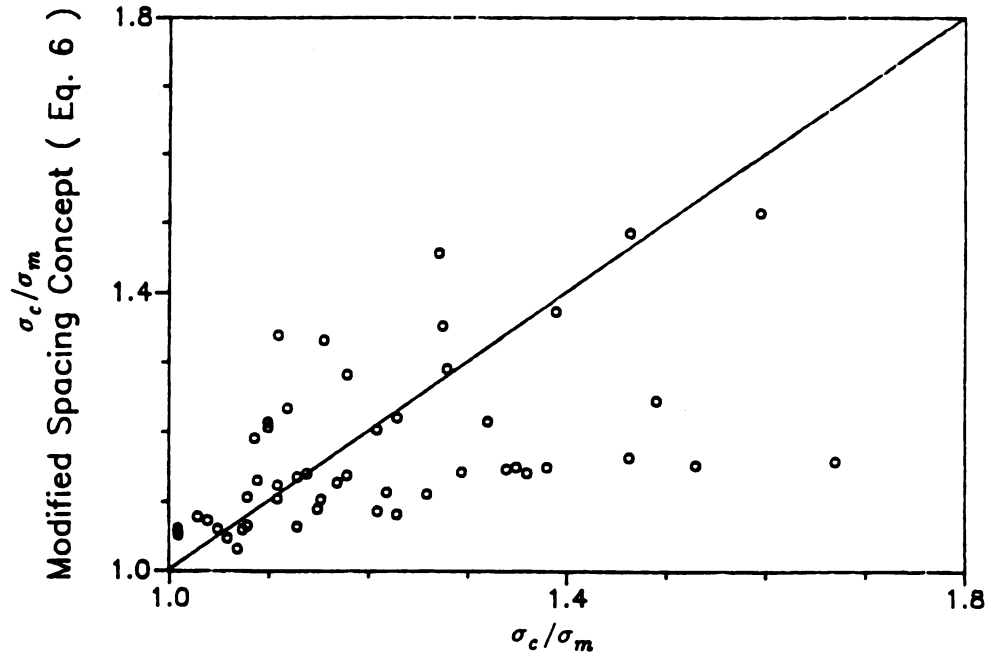


(a) Composite Material Concept (Equation (2.4))



(b) Spacing Concept (Equation (2.5))

Figure 3.19 Comparisons of the Composites Material and the Spacing Concept Predictions with Tensile Strength Test Results



(c) Modified Spacing Concept (Equation (2.6))

Figure 3.19 Comparisons of the Composites Material and the Spacing Concept Predictions with Tensile Strength Test Results (cont'd)

Table 3.3 Average, Standard Deviations, and Sum Total of Squares of Normalized Errors for Different Concepts

Concept	Avg.	Std. Dev.	Sum Total of Sqrs.
" Interaction Concept " (Equation 3.10)	-0.0014	0.0925	0.429
Composite Material (Equation 2.4)	0.0456	0.0945	0.553
Spacing (Equation 2.5)	0.0248	0.104	0.567
Modified Spacing (Equation 2.6)	0.0234	0.102	0.551

seen to be the lowest, when compared with those obtained for the other concepts. Hence, Equation (3.10) based on the "interaction concept" seems to predict the direct tensile strength of steel fiber reinforced concretes with a more reasonable accuracy.

### 3.5 PRE-PEAK CONSTITUTIVE MODELING

The pre-peak tensile behavior of steel fiber reinforced concrete deviates from linearity when microcrack propagation has already occurred (see Figure 2.14). Thus, as shown in Figure 3.20, the behavior was assumed (based on the reported tension test results) to be linear, with a slope equal to the elastic modulus of the matrix, up to the matrix tensile strength ( $\sigma_m'$ ). At this point, due to major microcrack propagation in the matrix, the stiffness was assumed to be reduced, and the stress-strain relationship was continued linearly up to the peak tensile stress.

Strain at peak tensile stress was derived empirically, using the test data summarized in Table 3.2, as a function of some fiber reinforcement properties:

$$\epsilon_c = \epsilon_m \cdot (1 + 0.35 \cdot N_f \cdot d_f \cdot l_f) \quad (3.11)$$

where:

$\epsilon_c$  = composite tensile strain at peak

tensile stress ; and

$\epsilon_m$  = matrix tensile strain at peak

tensile stress.

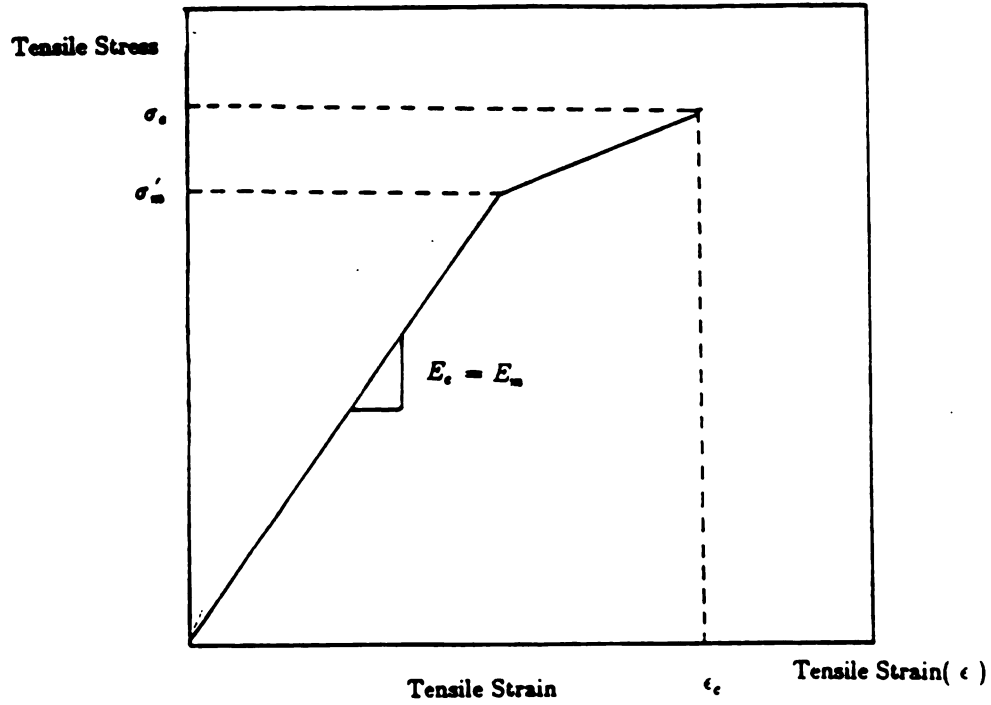


Figure 3.20 Simulation of the Steel Fiber Reinforced Concrete Tensile Behavior upon Cracking at Peak Load

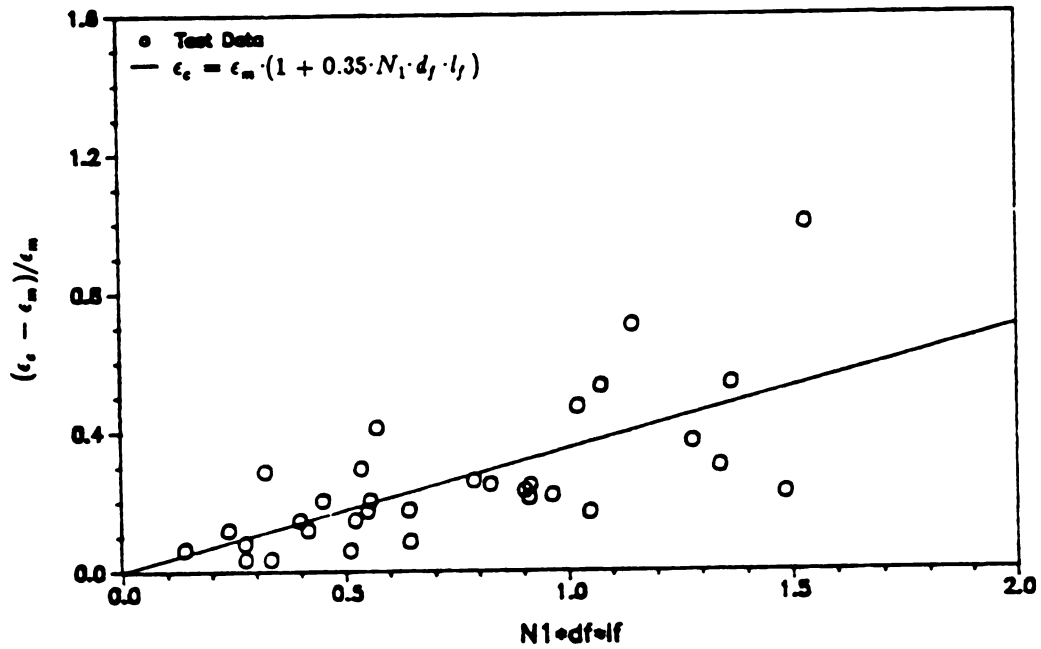


Figure 3.21 Increase in Strain at Peak-Tensile Stress in the Presence of Steel Fibers as a Function of Some Fiber Reinforcement Properties ( $N_1 \cdot d_f \cdot l_f$ )

Figure 3.21 presents the relatively desirable comparison between predictions of the above equation and the reported test results for strain at peak tensile stress in steel fiber reinforced mortar.

### 3.6 POST-PEAK CONSTITUTIVE MODELING

In the pre-peak region the matrix and fibers interact and both contribute to the tensile resistance of fibrous concrete. Crack opening at the peak load, however, sharply reduces the contribution of matrix and tends to transfer tensile loads mainly to the fibers bridging the crack. The matrix contributes to the post-peak tensile resistance of the composite through its softening behavior. The tensile behavior of the composite in the post-peak region can thus be simulated by superimposing the pull-out performance of fibers with the matrix softening behavior.

Due to difficulties in direct tensile testing of concrete only limited experimental data are available in this area. In the interpretation of the direct tension test results it should be considered that the post-peak deformations in fiber reinforced concrete tend to localize in one major crack at the critical section. The tensile behavior of fiber reinforced concrete can thus be represented by a stress-strain relationship in the pre-peak region, and an average stress vs. average crack width (deformation) relationship in the softening (post-peak) region [10,24,58]. An empirical model presented in Reference 10 for the softening (post-peak) behavior of the matrix was simplified (by a bilinear presentation of the curvilinear model) to represent the contribution of the matrix to the post-peak behavior of fiber reinforced concrete:

$$\sigma_m = \begin{cases} \sigma_m' - 0.6 \cdot \frac{\sigma_m'}{s_{sr}} \cdot s & 0 \leq s \leq s_{cr} \\ 0.4 \cdot \sigma_m' \cdot \frac{s_{c0} - s}{s_{c0} - s_{cr}} & s_{cr} \leq s \leq s_{c0} \end{cases} \quad (3.12)$$

where:

$\sigma_m$  = tensile stress (in post-peak region);

$\sigma_m'$  = peak tensile stress;

$s$  = crack opening;

$s_{cr}$  = crack width at  $\sigma_m$  equal to  $0.4 \cdot \sigma_m'$   
= 0.015 mm ; and

$s_{c0}$  = crack opening at  $\sigma_m$  equal to zero.

The above equation is compared with test results in Figure 3.22. It should be noted that a more elaborate modeling may require the consideration of fiber effects on the matrix post-peak tensile behavior.

Upon the cracking of matrix at the peak tensile strength of the composites a crack starts to open and the pull-out mechanism of fibers tends to be mobilized. Typical experimental plots of fiber pull-out versus displacement (slippage) relationships for straight round steel fibers are given in Figure 3.23. Based on 36 experimental pull-out load-slip relationships reported in References 16,18,19,59-61, an empirical expression for pull-out behavior was developed in this investigation (Figure 3.24). The model consists of three straight lines: a linear pre-peak ascending portion, and a bilinear post-peak descending branch. This trilinear model includes two characteristic bond values ( $\tau_u$  and  $\tau_r$  in Figure 3.24) and three characteristic pull-out slip values ( $s_{pk}$ ,  $s_r$  and  $s_0$ ).

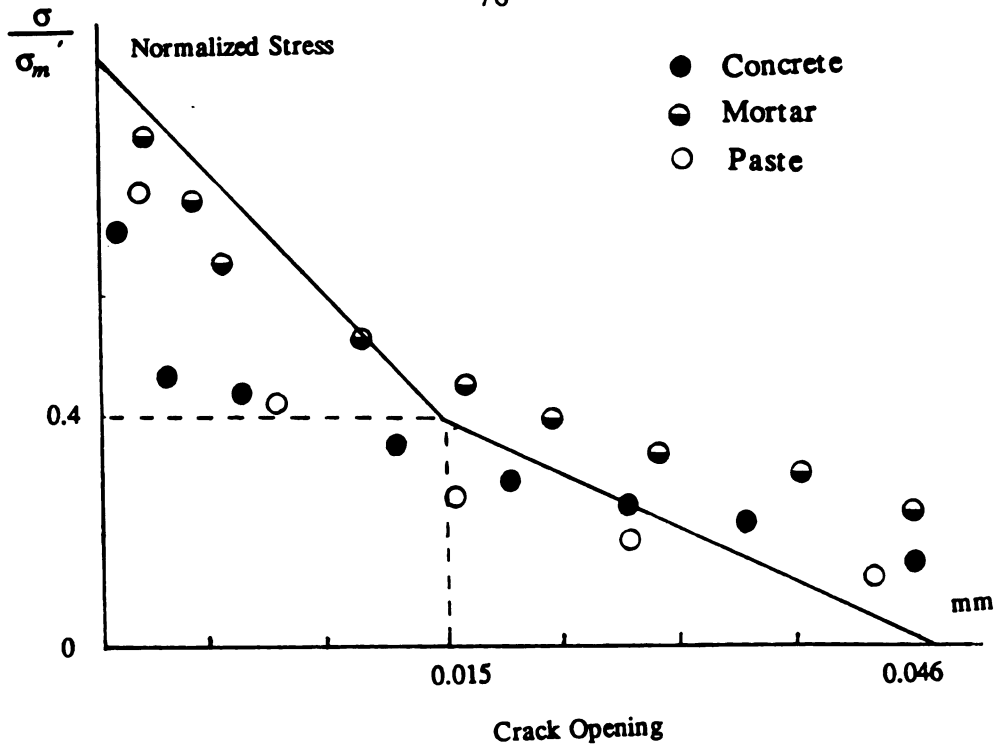


Figure 3.22 Comparisons of the Average Stress vs. Average Crack Width Relationship in the Post-Peak Region with Test Results

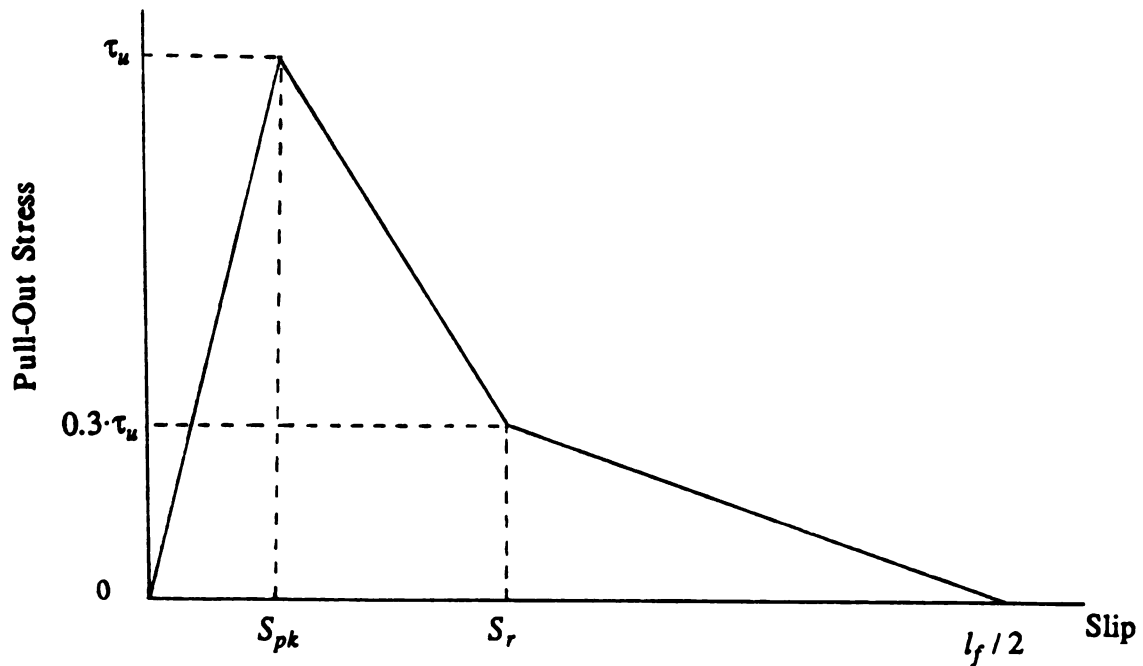


Figure 3.23 Typical Experimental Plot of Fiber pull-out vs. Displacement (Slip-page) Relationship

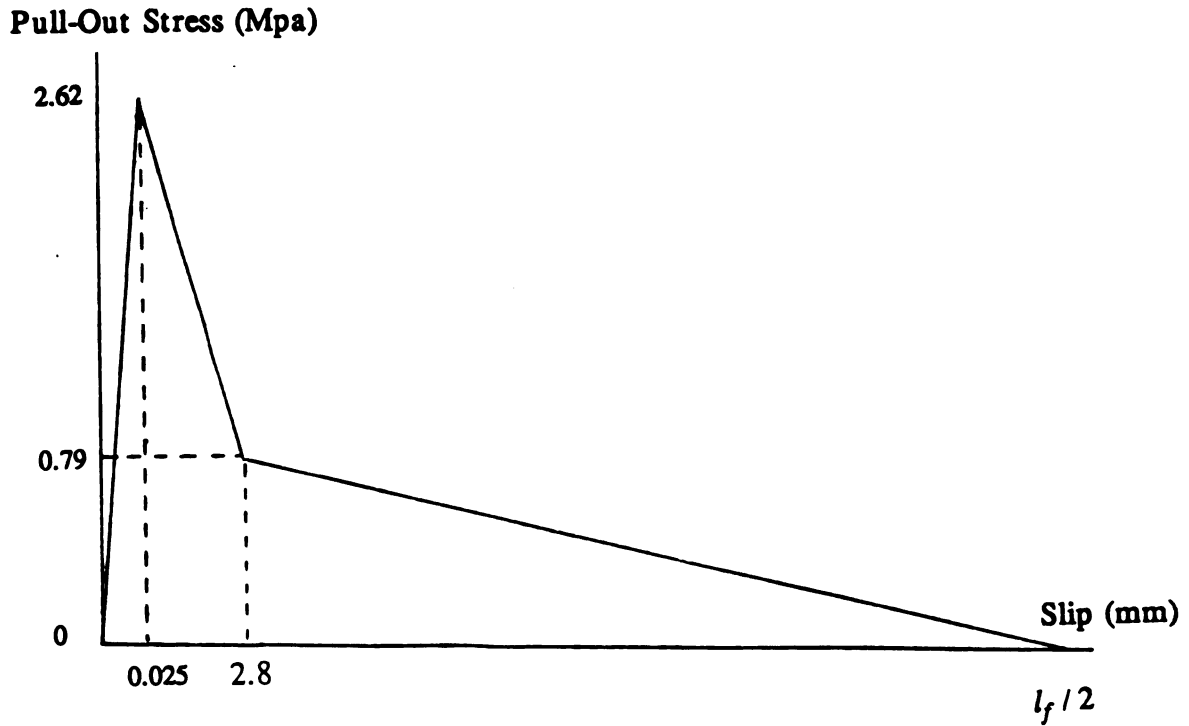


Figure 3.24 Model of Pull-Out Load-Deflection Relationship for Straight-Round Steel Fibers

Table 3.4 Pull-Out Test Conditions and Results [16,18,19,59,60,61]

Ref.	matrix	fiber		avg. bond strength (Mpa)	peak displacement (mm)
	c:s:w	diameter (mm)	embedment length (mm)		
16	1:4:0.5	0.38	50.8	1.8	*
18	1:2.5:0.55	0.4	12.7	2.62	*
	1:2.5:0.6	0.25	12.7	2.62	0.51
	1:2.5:0.55	0.15	12.7	1.02	*
	"	0.4	12.7	2.25	*
19	1:3:0.31	0.4	20.1	2.4	0.04
	or	0.4	30.	2.4	*
		0.4	20.	2.4	*
	1:3:0.65	0.3	30.	2.4	*
		0.3	20.	2.3	*
59	1:2:0.4	0.64	31	2.1	*
	1:0:0.31	0.64	50.8	0.64	*
60	1:0:0.55	0.38	30.3	*	0.203
	"	0.51	*	*	0.45
	"	0.41	*	*	0.23
61	1:2.5:0.4	0.4	12.5	0.194	0.2
	1:2.5:0.6	0.4	12.5	0.42	0.2

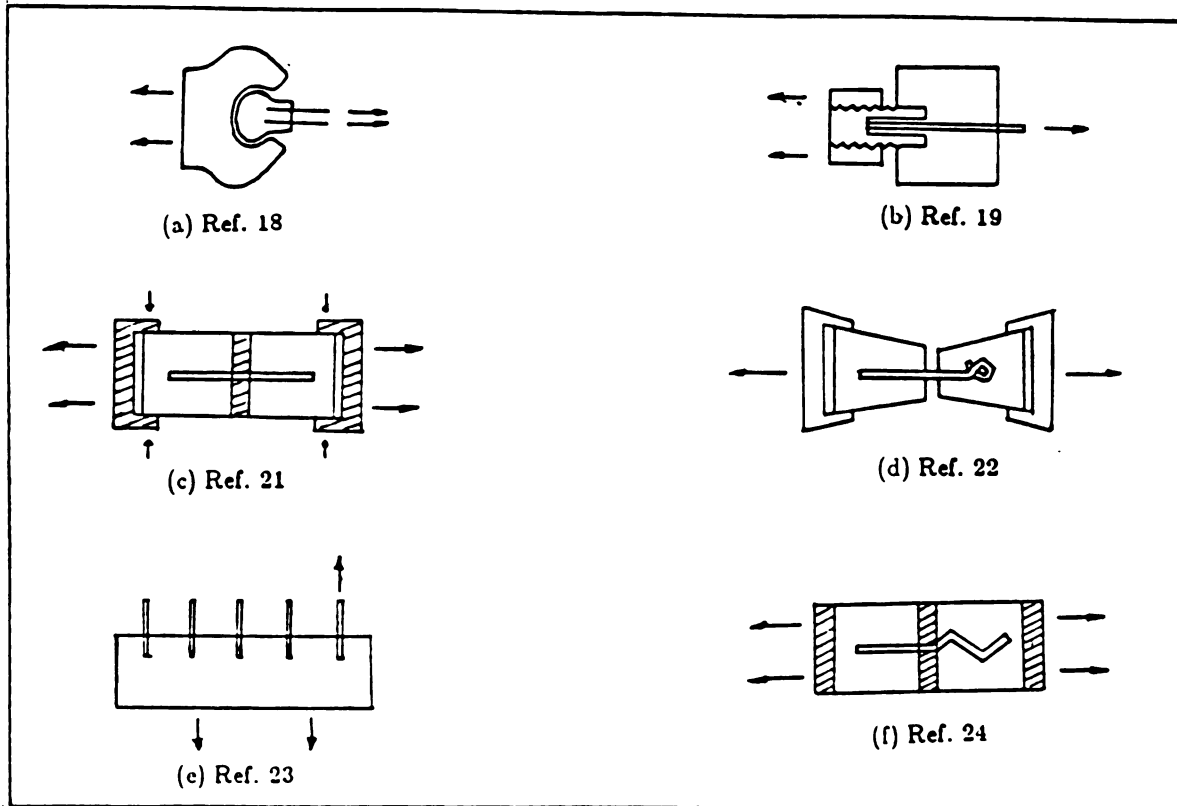


Figure 3.25 Pull-Out Test Procedure

Several pull-out test results reported in the literature were used to derive the characteristic bond stress and slip values of the proposed model. Table 3.4 summarizes some fiber and matrix properties and experimental procedures (see Figure 3.25) as well as test results for the pull-out tests used in this study.

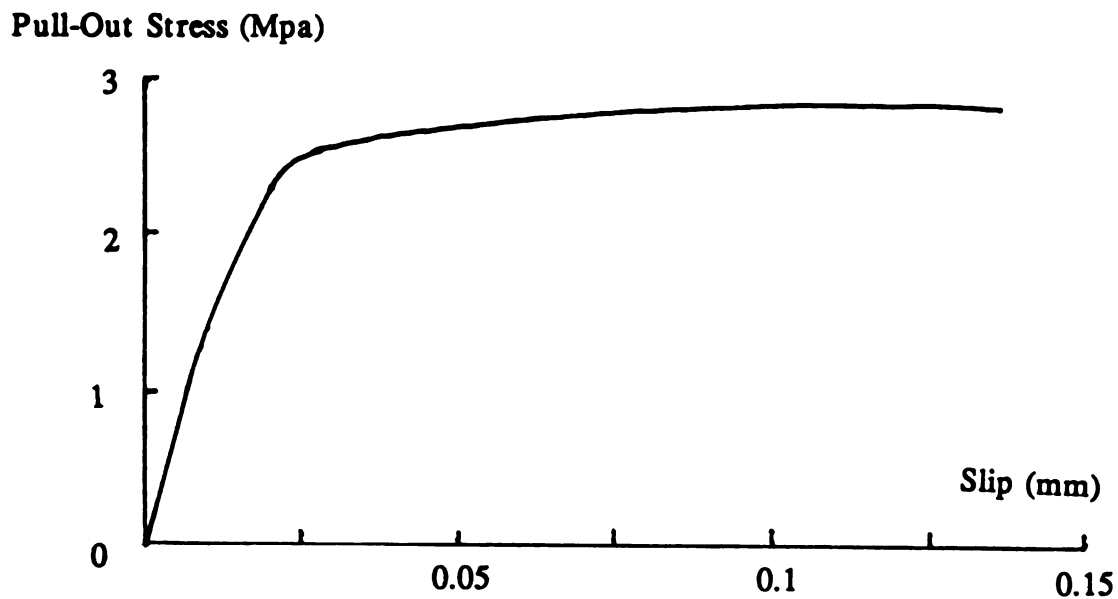
The average characteristic bond stress values derived from pull-out test results are as follows:

$$\tau_u = 2.62 \text{ Mpa (380psi)} ; \text{ and} \quad (3.13)$$

$$\tau_r = 0.3 \cdot \tau_u$$

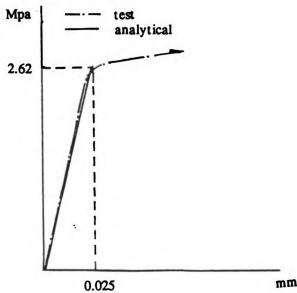
While the stability of the pull-out test is vital to proper monitoring of the

fracture behavior and pull-out deformations, most pull-out tests have not been conducted under stable test conditions [62]. It was pointed out in Reference 62 that with the method of crosshead or overall displacement-controlled tests, very low initial stiffnesses, and thus large slip values at the peak pull-out load, are generally recorded. To avoid the problems addressed above, slip-controlled tests which ensure greater stability during specimen softening were performed and the typical results are shown in Figure 3.26(a) for the pull-out behavior of straight-round steel fibers. It has been reported in this reference that considerable scatter observed in the measured peak slip values possibly result from the flat nature of the load-slip characteristics in the vicinity of the peak-load. Pull-out test results of Reference 62 are distinguished from others [16,18,19,59-61] by a much larger initial pull-out stiffness. Based on the test results reported in Reference 62, the fiber pull-out slip at peak pull-out load ( $s_{pk}$ ) was selected to



(a) Pull-Out Test Results in Reference 62

Figure 3.26 Simulation of Pre-Peak Pull-Out Behavior of Straight-Round Steel Fibers



(b) Pre-Peak Pull-Out Model vs. Test Results from Reference 62  
 Figure 3.26 Simulation of Pre-Peak Pull-Out Behavior of Straight-Round Steel Fibers (cont'd)

be 0.025 mm (0.001 in.) for use in the model of this investigation. The model is shown in Figure 3.26(b) to closely simulate the initial pull-out stiffness in the pull-out test results of Reference 62 (see Figure 3.26(b)). It is worth mentioning that this value of slip at peak pull-out load is roughly five times the maximum crack opening at the peak tensile stress of SFRC under direct tension as given in Reference 28.

With the limited fiber pull-out data available, the other characteristic pull-out slip value at residual strength ( $s_r$  in Figure 3.24 corresponding to a bond strength of  $\tau_r$ ) was obtained as the average of test results reported in the literature ( $s_r = 2.8mm$ ) [18,19,60,61]. The slip at zero pull-out load ( $s_0$  in Figure 3.24) was assumed to occur when complete pull-out has been made (i.e., when

the slip value equals half of the fiber length). A summary of the selected values for characteristic bond stress and slip values is given below:

$$s_{pk} = 0.025\text{mm} \text{ (0.001 in. )}; \quad (3.14)$$

$$s_r = 2.8\text{mm} \text{ (0.11 in. )}; \text{ and}$$

$$s_0 = l_f / 2.$$

Typical comparisons between the post-peak branch of the proposed fiber pull-out model with the above empirical characteristic values of bond stress and slip and experimental post-peak results are observed in Figure 3.27 to be reasonable. In the pull-out tests used in this investigation, except for Reference 62 (where multiple fibers were pulled out simultaneously), a single straight-round

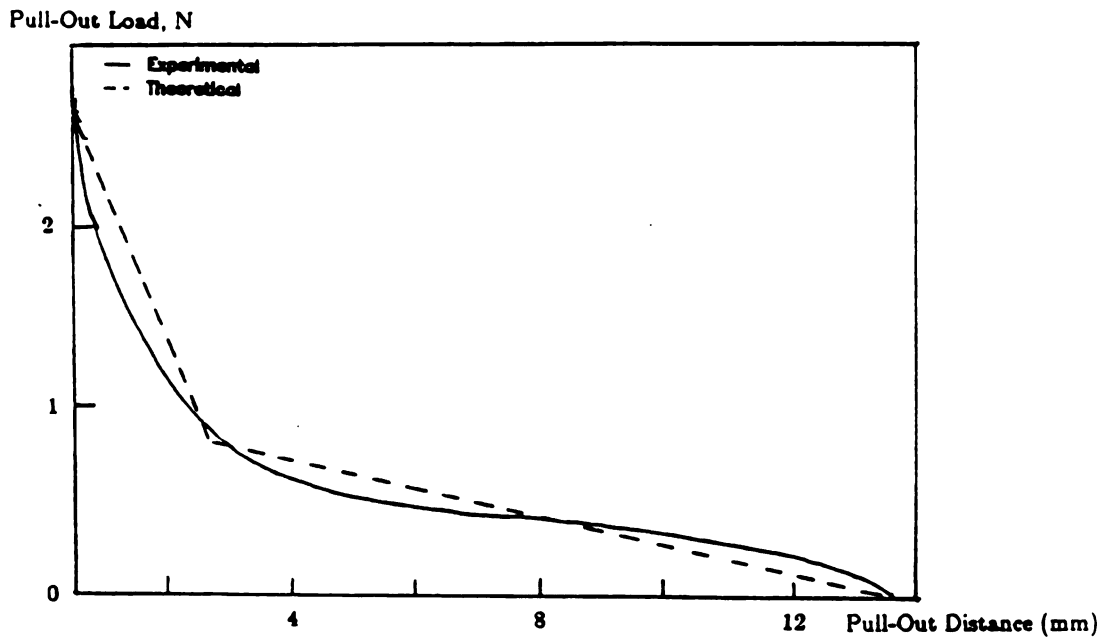
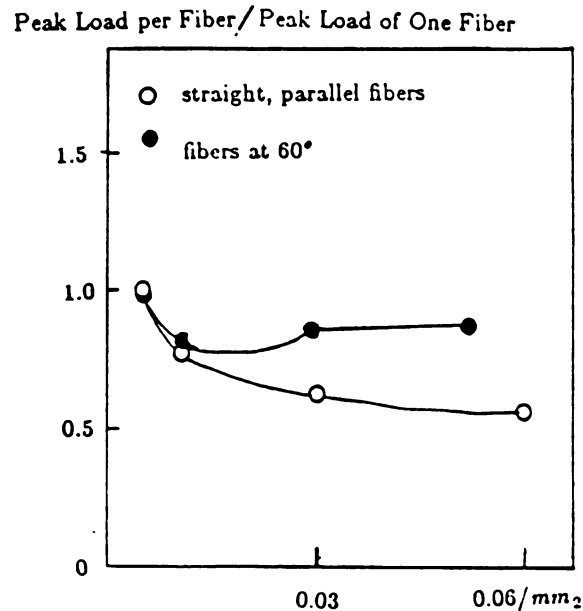
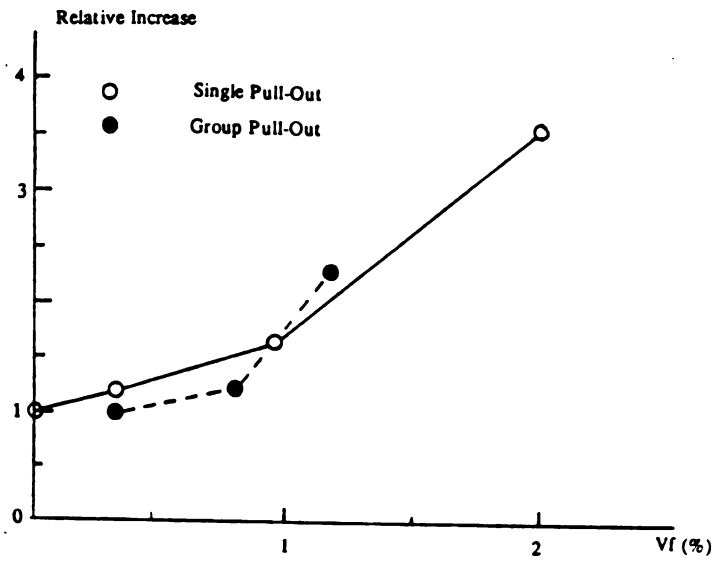


Figure 3.27 Comparison of the Experimental Pull-Out Load-Deflection Relationships in the Post-Peak Region with the Empirically Derived Model of This Study

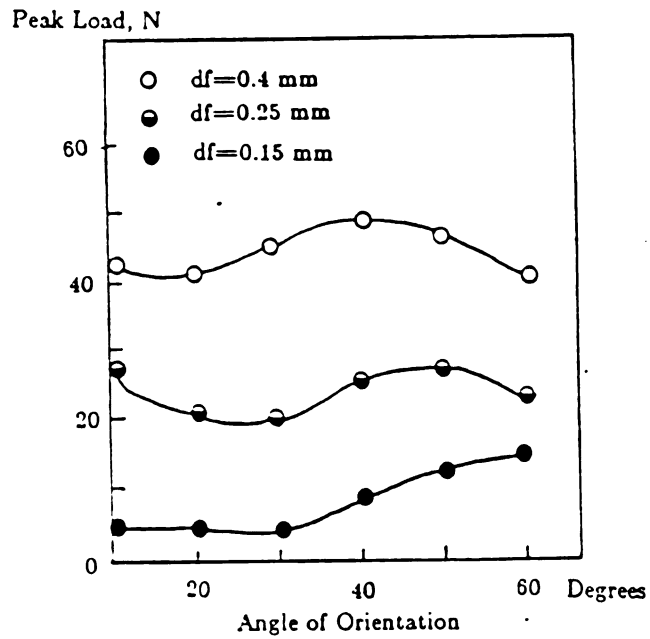
steel fiber (which was aligned in the loading direction) was pulled out of the matrix. In the actual conditions of the composite material, however, fibers are closely spaced and also randomly oriented. An increase in the number of fibers per unit cross sectional area has been shown to reduce the pull-out strength of fibers (Figure 3.28(a)). Another observation has been made by Reference 60 that, as the volume fraction in matrix (and thus the number of fibers per unit cross sectional area) increases, the pull-out strength of fibres tends to increase (see Figure 3.28(b)). More comprehensive test results are needed if the effects of the number of fibers per unit cross-sectional area on the pull-out performance of fibers are to be considered.



(a) Fiber Concentration (No. of Fibers per Area)  
 Figure 3.28 Effect of Fiber Concentration, Volume Fraction and Orientation on Pull-Out Strength



(b) Fiber Volume Fraction



(c) Fiber Orientation

Figure 3.28 Effect of Fiber Concentration, Volume Fraction and Orientation on Pull-Out Strength (cont'd)

As far as the fiber orientation effects on pull-out strength are concerned, as shown in Figure 3.28(c), the increase in fiber inclination (with respect to the pull-out load direction) first increases the pull-out strength and then starts to reduce the pull-out resistance. Based on this observation it was assumed that the pull-out performance of fibers aligned in the direction of pull-out load roughly represents an average performance for randomly oriented fibers.

The composite material post-peak behavior was simulated assuming that the fiber slippage in the pre-peak region is negligible. This assumption was made based on the discussions presented in Reference 28, where it is stated that the crack opening at peak load is too small to significantly mobilize pull-out action of fibers. The composite material post-peak behavior may thus be assumed to depend on the pull-out behavior of fibers crossing the critical section (with fiber pull-out starting near the peak load) and the matrix softening behavior in the post-peak region:

$$\sigma = \sigma_f + \sigma_m \quad (3.15)$$

where:

$\sigma$  = *total resistance after peak tensile strength; and*

$\sigma_f$  = *average tensile stress provided by the pull-out resistance of fibers across the critical section.*

In the use of fiber pull-out behavior for simulating the post-peak behavior of composite materials, it was assumed that the fiber embedment length is equal to the statistically derived average value of  $l_f/4$ . The tensile resistance provided by fibers can thus be derived through multiplying the average value of bond stress by the interfacial area of all fibers crossing the cracked section

assuming an average embedment length of  $l_f/4$  :

$$\sigma_f = \tau \cdot \pi \cdot d_f \cdot \frac{l_f}{4} \cdot N_1 \quad (3.16)$$

where:

$\tau$  = average interfacial bond stress.

The value of  $\tau$  in the above expression can be obtained, using the proposed fiber pull-out constitutive model, as a function of the crack opening ( $s$ ) in the post-peak region:

$$\tau = \begin{cases} \frac{\tau_u}{s_{pk}} \cdot s & \text{for } 0 \leq s \leq s_{pk} \\ \frac{\tau_r - \tau_u}{s_r - s_{pk}} \cdot s + \frac{\tau_u \cdot s_r - \tau_r \cdot s_{pk}}{s_r - s_{pk}} & \text{for } s_{pk} < s \leq s_{sr} \\ -\frac{\tau_r}{s_0 - s_r} \cdot s + \frac{\tau_r \cdot s_0}{s_0 - s_r} & \text{for } s_r < s \leq s_0 \end{cases} \quad (3.17)$$

The contribution of matrix to post-peak tensile resistance ( $\sigma_m$ ) can also be expressed as a function of the post-peak crack opening at the critical section using the proposed softening model for the post-peak constitutive behavior of the matrix (see Equation (3.12)).

### 3.7 COMPARISON WITH TEST RESULTS

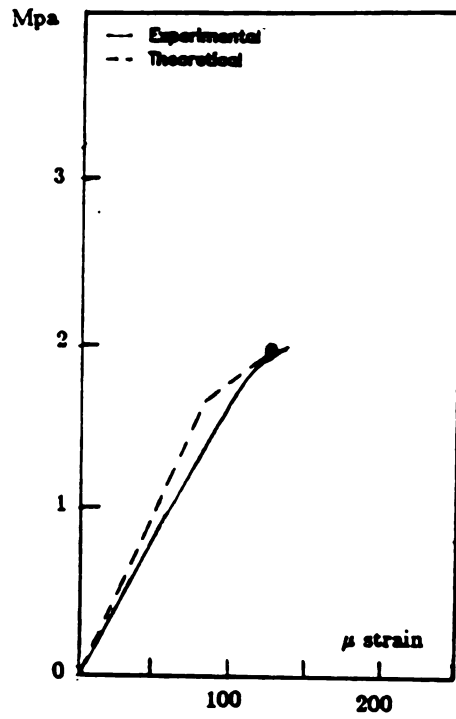
Complete tensile stress-deformation relationships for SFRC (covering both the pre-peak and post-peak regions) have been reported in References 4,24,29 and 63. Table 3.5 presents some key test conditions and Figure 3.29 compares the experimental tensile stress-deformation relationships with the predictions of the constitutive model developed in this study.

The proposed model is observed to predict experimental results with reasonable accuracy.

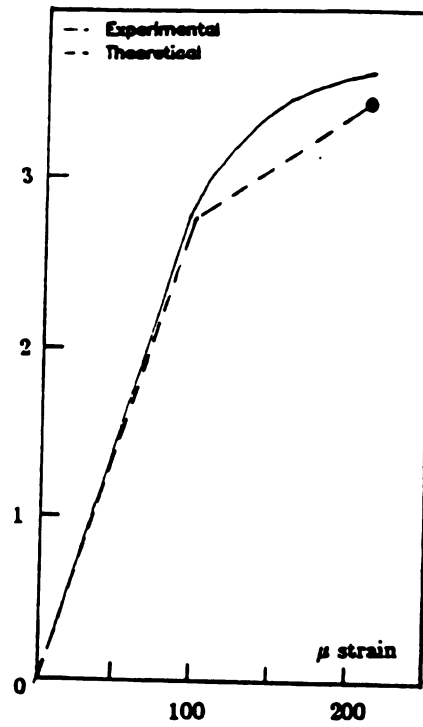
Table 3.5 Conditions of Some Direct Tension Test Results of SFRC.

Ref.	test No.	matrix			fiber			specimen		composite	
		crw	tensile strength (Mpa)	strain at peak (x0.0001)	diameter (mm)	length (mm)	VF (%)	width (mm)	depth (mm)	tensile strength (Mpa)	strain at peak (x0.0001)
4	1	1:2:0.5	2.8	1.74	0.41	25.4	0.5	76	19	3.0	1.9
	2		-	-	-	-	1.0			3.2	2.0
	3		-	-	-	-	1.5			3.6	2.2
8	4	1:2:0.45	1.74	0.85	0.5	50	0.6-1.8	16	100	1.9-2.6	1.2-2.1
	5		-	-	0.35	35	0.6-1.8			1.9-2.4	1.1-2.2
	6		-	-	0.25	25	0.6-1.8			1.6-2.0	0.9-1.7
9	7	1:2.5:0.45	*	*	0.38	25	1.73	50	100	2.3	4
13	8	1:2.5:0.6	1.68	*	0.26	19	1.0	50	50	2.03	*
	9		-	*	0.26	19	2.0			2.17	*
	10		-	*	0.26	19	3.0			2.5	*
34	11	1:2.5:0.6	1.68	*	0.15	12.7	1.0	50	50	2.1	*
	12		-	*	0.15	12.7	2.0			2.2	*
	13		-	*	0.15	12.7	3.0			2.56	*

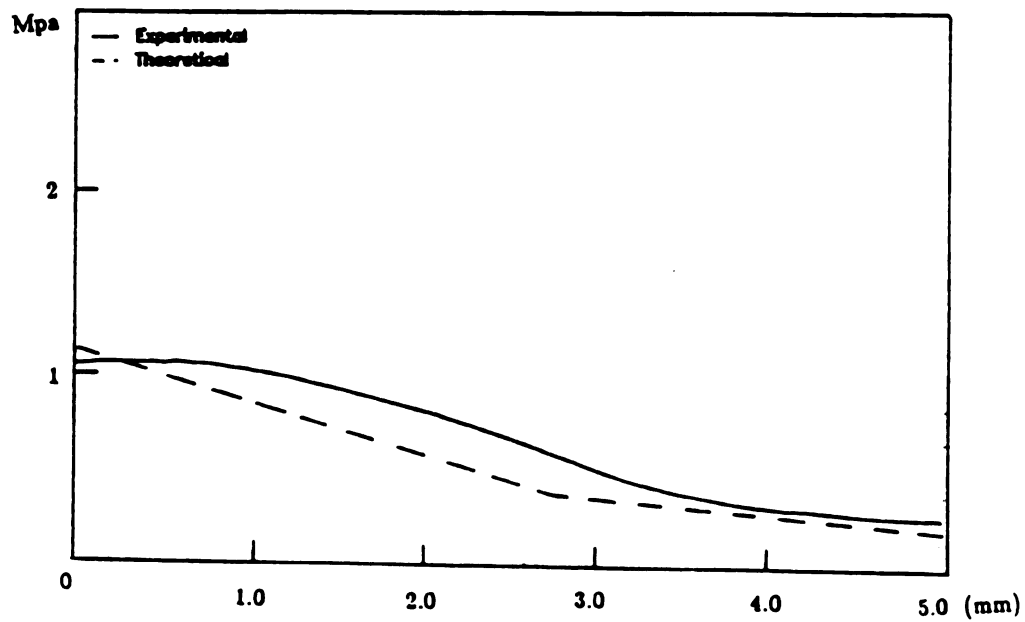
\* Not Reported



(a) Reference 63 (Pre-Peak)

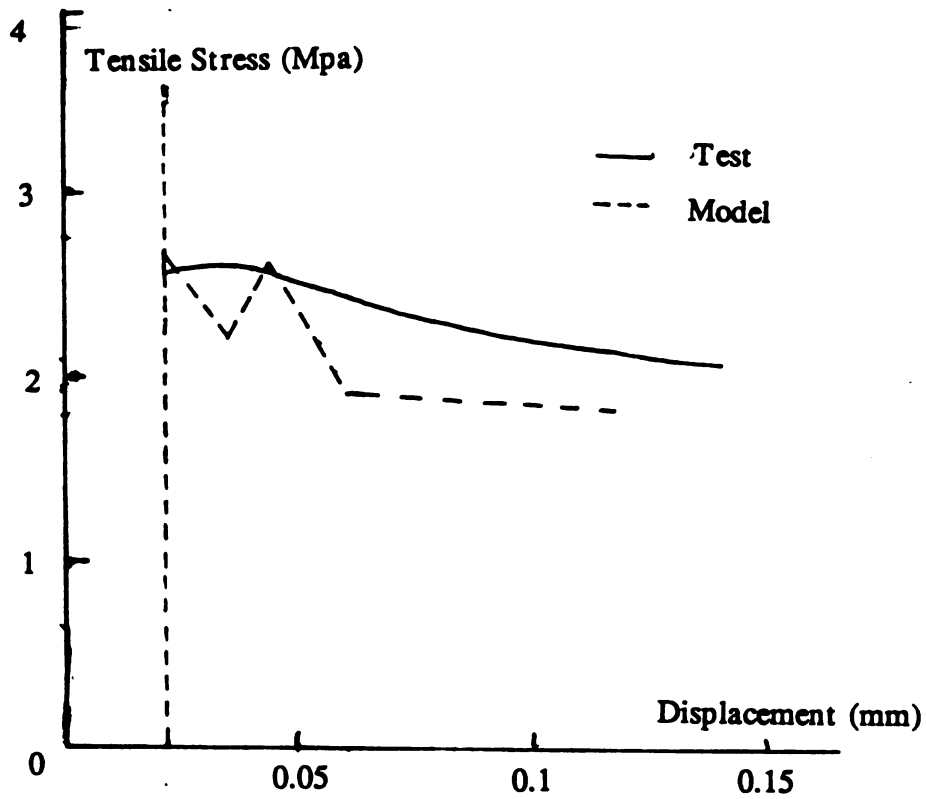


(b) Reference 24 (Pre-Peak)

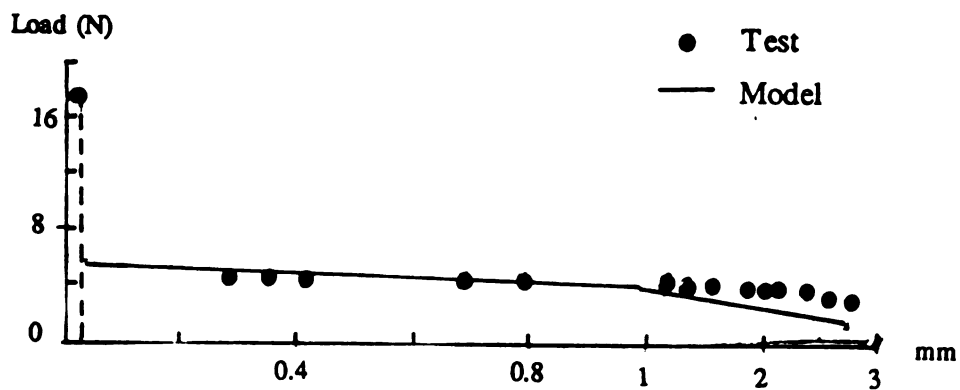


(c) Reference 29 (Post-Peak)

Figure 3.29 Comparison of Experimental Tensile Stress-Deformation Relationships with Predictions of the Model Developed in This Study



(d) Reference 29 (Post-Peak)



(e) Reference 24 (Post-Peak)

Figure 3.29 Comparisons of Experimental Tensile Stress-Deformation Relationships with Predictions of the Model Developed in This Study (cont'd)

### 3.8 SUMMARY AND CONCLUSIONS

Theoretical expressions were derived for the number of fibers per unit cross sectional area in fiber reinforced concrete as a function of fiber volume fraction and length, assuming that cross sectional boundaries are the only factors disturbing the 3-D random orientation of fibers. Measurements were made on fractured surfaces of steel fiber reinforced concrete specimens in order to assess the actual values for the number of fibers per unit area in steel fiber reinforced concrete. Nineteen steel fiber reinforced concrete specimens incorporating different fiber volume fractions and different fiber types were considered in this investigation. Statistical studies were conducted on the measured values of the number of fibers per unit area for determining the possible effects of fiber type and location on the number of fibers per unit area. Comparisons were also made between the theoretical and measured values of the number of fibers per unit area in order to determine the effects of reorientation of steel fibers inside concrete during vibration. Recommendations were made, based on the findings of this research, for approximating the number of fibers per unit cross sectional area in steel fiber reinforced concrete.

The following conclusions were derived from the results of this investigation:

(1) The type of steel fiber (straight vs. hooked) and the location in cross section with respect to the casting direction (top vs. bottom) did not have any statistically significant effect on the measured value of number of fibers per unit area.

(2) Vibration of steel fiber reinforced concrete seems to reorient the fibers, resulting in a tendency towards orienting the fibers in horizontal planes. This phenomenon illustrates the higher values for number of fibers per unit area in

actual measurements when compared with theoretical predictions.

(3) The number of fibers per unit cross sectional area in steel fiber reinforced concrete after vibration is between the theoretical values derived for 3-D and 2-D random orientation conditions considering the boundary effects.

A refined concept ("interaction concept") was proposed for predicting the tensile strength of SFRC. This concept accounts for the partial mobilization of the fiber pull-out action (interfacial bond stresses) at the composite material tensile strength, and also considers the microcrack arresting action of fibers and the consequent strengthening of matrix in the presence of steel fibers. The proposed "interaction concept" leads to an expression for predicting the tensile strength of steel fiber reinforced concrete, which incorporates some empirical coefficients to be determined empirically. These coefficients were decided in this study using a relatively large number of SFRC tensile strength test results.

The theoretical predictions based on the proposed "interaction concept", when compared with those of the composite material and spacing concepts, show a reasonable correlation with test results. More importantly, the relative matrix and fiber contributions to the composite material tensile strength in the proposed "interaction concept" are representative of the physical performance of the composite material at peak tensile stress.

The model used more stable test results for the post-peak region. Matrix softening behavior and fiber pull-out actions both expressed in terms of crack opening and fiber slip, are superimposed to simulate post-peak behavior of the composite. The comparisons with test results were satisfactory. Further research, however, is to be needed for the consideration of effect of fibers crossing the composite cross section.

A constitutive model was also developed for predicting the pre-peak tensile stress-strain relationship as well as the post-peak tensile stress-deformation

relationship of steel fiber reinforced concrete. The developed post-peak constitutive model accounts for the contributions of fibers crossing the critical section through their pull-out action as well as that of matrix in its post-peak softening range of behavior. Empirical fiber pull-out load-slip and matrix post-peak constitutive models were combined to derive the composite material post-peak tensile stress-deformation model. The pre-peak constitutive model of the composite material developed in this study was an empirical one based on the tension test results reported in the literature for steel fiber reinforced concrete. The proposed constitutive model is shown to compare reasonably well with tension test results performed on steel fiber reinforced concrete in both the pre- and post-peak region.

## CHAPTER 4

# THE CONSTITUTIVE MODEL FOR STEEL FIBER REINFORCED CONCRETE UNDER COMPRESSION

### 4.1 INTRODUCTION

Short, randomly oriented steel fibers, through their crack-arresting action and confining properties, improve the post-peak ductility, energy absorption capacity and, to some extent, the strength of concrete under compression (Figure 2.19). The strain at peak compressive stress also tends to increase in the presence of fibers [5], but the pre-peak compressive behavior of fibrous concrete is only slightly different from that of plain concrete.

In order to develop structural analysis and design procedures for fiber reinforced concrete load-bearing elements, it is important to develop constitutive models for fiber reinforced concrete.

Very few analytical studies on the compressive behavior of steel fiber reinforced concrete have been reported in the literature. Fanella and Naaman (1985) [5] have presented a compressive stress-strain diagram for steel fiber reinforced mortar (see Figure 2.22). It should be emphasized that this model has been developed for steel fiber reinforced mortar (the compressive behavior of which differs from that of steel fiber reinforced concrete). In particular, fiber reinforced mortar has a higher strain at peak-stress, and fibers are more effective in concrete than in mortar. Soroushian and Lee (1987) [41] have tried to simulate the steel fiber reinforcement effects on compressive behavior with the confinement of concrete by transverse reinforcement.

The research reported herein has used a relatively large number of experimental compressive stress-strain relationships to derive an empirical constitutive model for compressive behavior of steel fiber reinforced concrete. The developed model accounts for the effects of steel fiber volume fraction, aspect ratio and type (straight vs. hooked), and the concrete compressive strength, on performance characteristics of steel fiber reinforced concrete in compression.

#### 4.2 EFFECTS OF VARIABLES ON COMPRESSIVE BEHAVIOR

The improvements in concrete compressive behavior resulting from steel fiber reinforcement are dependent on the volume fraction and aspect ratio of steel fibers, mechanical deformations of fibers, matrix mix proportions, specimen geometry (height-to-depth ratio), and the loading versus casting direction [14,33].

The increase in fiber volume fraction is observed in Figure 4.1(a) to enhance the strength and especially post-peak ductility of steel fiber reinforced concrete under compression. Excessively high fiber volume fractions, however, lead to harsh mixes with increased air entrapment, and thus damage the compressive performance of steel fiber reinforced concrete. Fanella and Naaman (1985) [5] have found a consistent correlation between this damage and the reduction in matrix density (which could be attributed to increased air entrapment) at high fiber volume fractions.

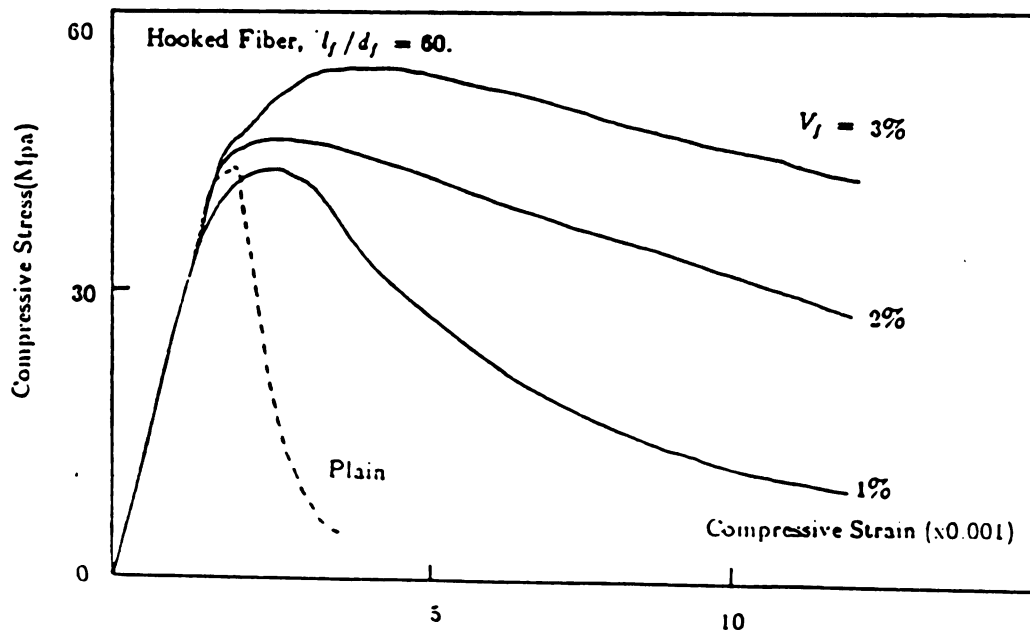
Figure 4.1(b) shows that the improvements in compressive behavior of steel fiber reinforced concrete resulting from the increase in fiber aspect ratio are similar to those obtained with increasing the fiber volume fraction. Excessively high aspect ratios at a constant fiber volume fraction can adversely influence the fresh

mix workability and thus hardened material properties of fiber reinforced concrete.

Since the increase in fiber volume fraction ( $V_f$ ) and aspect ratio ( $l_f/d_f$ ) have similar effects on compressive behavior of steel fiber reinforced concrete, their multiplication ( $V_f \cdot l_f/d_f$ ), generally referred to as the fiber reinforcement index, can be used as a single variable representing the fiber reinforcement effects on compressive behavior of concrete.

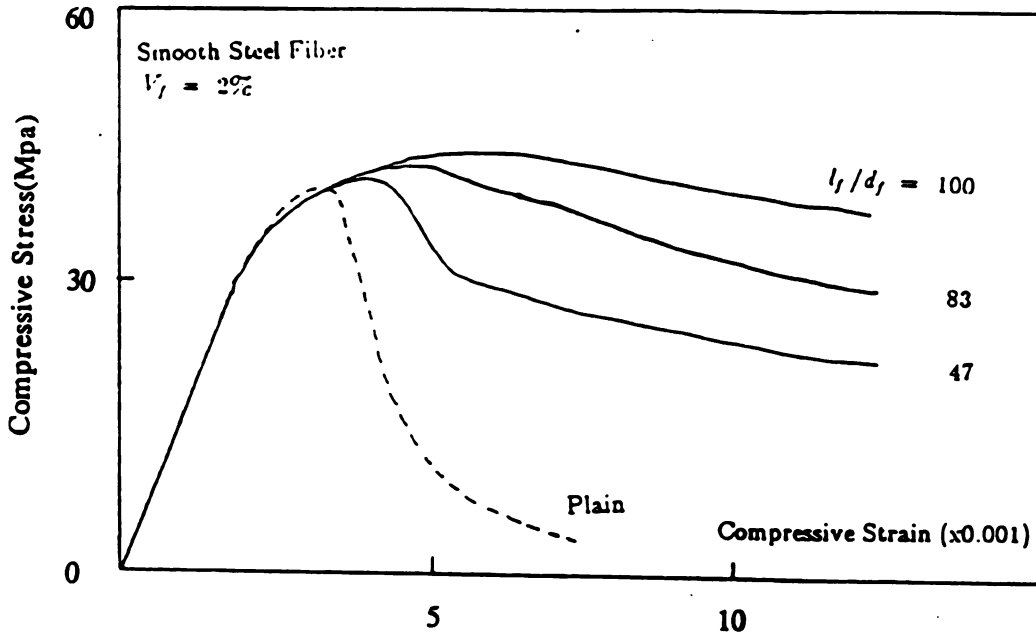
The efficiency of steel fiber actions in concrete tend to be improved when mechanically deformed fibers are used instead of the straight ones, mainly due to better mechanical bonding of deformed fibers to concrete (see Figure 4.1(c)).

Steel fibers are also found to be more effective in increasing the compressive strength of coarse aggregate concrete when compared with fine aggregate mortar.



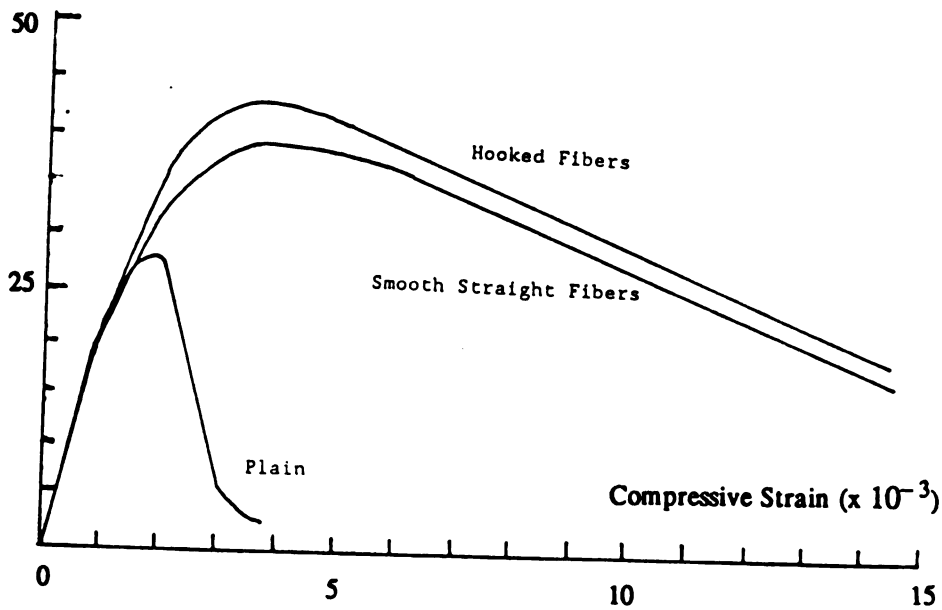
(a) Effects of Fiber Volume Fraction

Figure 4.1 Effects of Different Fibers on Compressive Behavior of SFRC



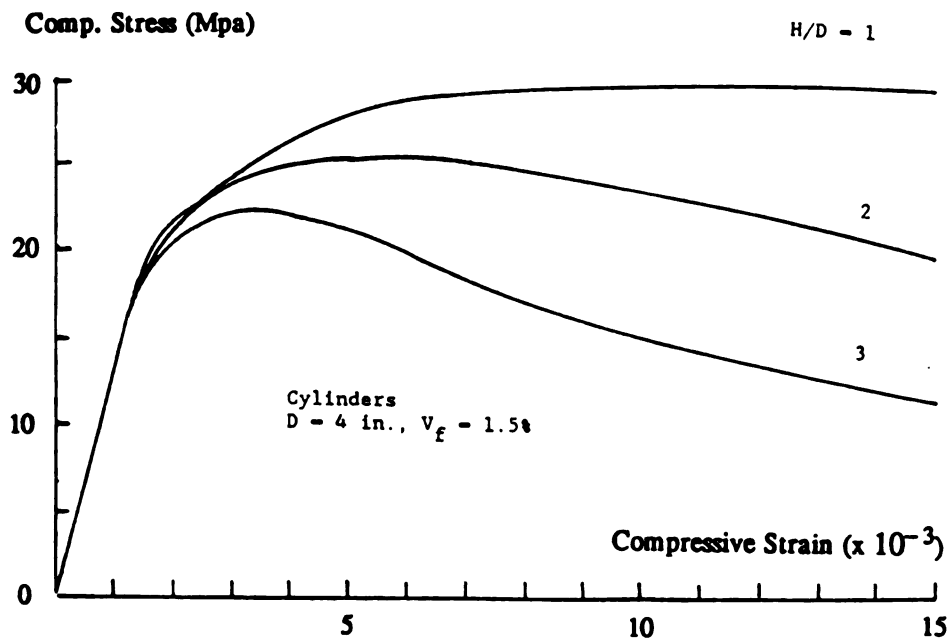
(b) Effects of Fiber Aspect Ratio

Comp. Stress (Mpa)



(c) Effects of Different Fibers on Compressive Behavior of SFRC

Figure 4.1 The Improvements in Concrete Compressive Behavior Resulting from Steel Fiber Reinforcements (1 Mpa = 145 psi) (cont'd)



(d) Effects of Height-to-Depth Ratio on Compressive Behavior of SFRC

Figure 4.1 The Improvements in Concrete Compressive Behavior Resulting from Steel Fiber Reinforcements (1 Mpa = 145 psi) (cont'd)

Another factor influencing the compressive ductility and energy absorption capacity of steel fiber reinforced concrete under compression is the height-to-depth ratio of specimens; the greater this ratio, the less desirable would be the compressive performance of steel fiber reinforced concrete (Figure 4.1(d)).

### 4.3 EXPERIMENTAL RESULTS

The compression test data used in this study for empirical modeling of fiber reinforced concrete constitutive behavior were selected from the literature [4,6,64,65], and also from the experimental data reported by Soroushian and Bayasi [4,64-66]. The steel fibers used in the selected test data were straight or

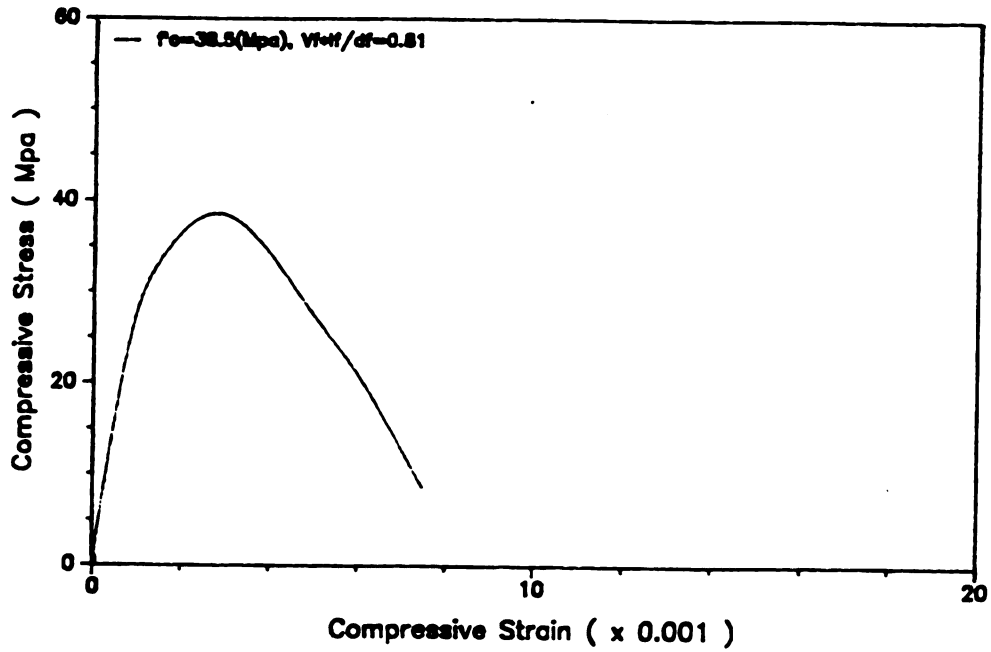
hooked with different aspect ratios. Table 4.1 presents some information on the concrete matrices and fiber reinforcement conditions in the selected test data. A total of ninety eight compression test results on steel fiber reinforced concrete were used in this study. The results covered fibrous concretes with wide ranges of matrix properties and fiber geometries. Only the compressive strength was reported for some of the fibrous mixtures, while for others the complete stress-strain relationships were available (see Figure 4.2 for some typical experimental results). It should be noted that the compression load in tests used in this study were unanimously applied in the direction of casting. This is generally considered to be a desirable loading condition, because fibers tend to be oriented horizontally when compacted by vibration, and would thus be more effective in confining concrete when the compression load is applied normal to the fiber orientation plane.

All the specimens included in this study were 150 mm (6 in.) in diameter and 300 mm (12 in.) in height. All the fibrous mixtures incorporated coarse aggregates with maximum particle sizes ranging from 9.5 mm (3/8 in.) to 19 mm (3/4 in.). The specimens were typically air-cured following about 7 days of curing in a moist environment, and were tested at an age of about 28 days. The fibers were carbon steel and had a tensile strength of about 1000 Mpa (145 Ksi). The compression load was applied quasi-statically.

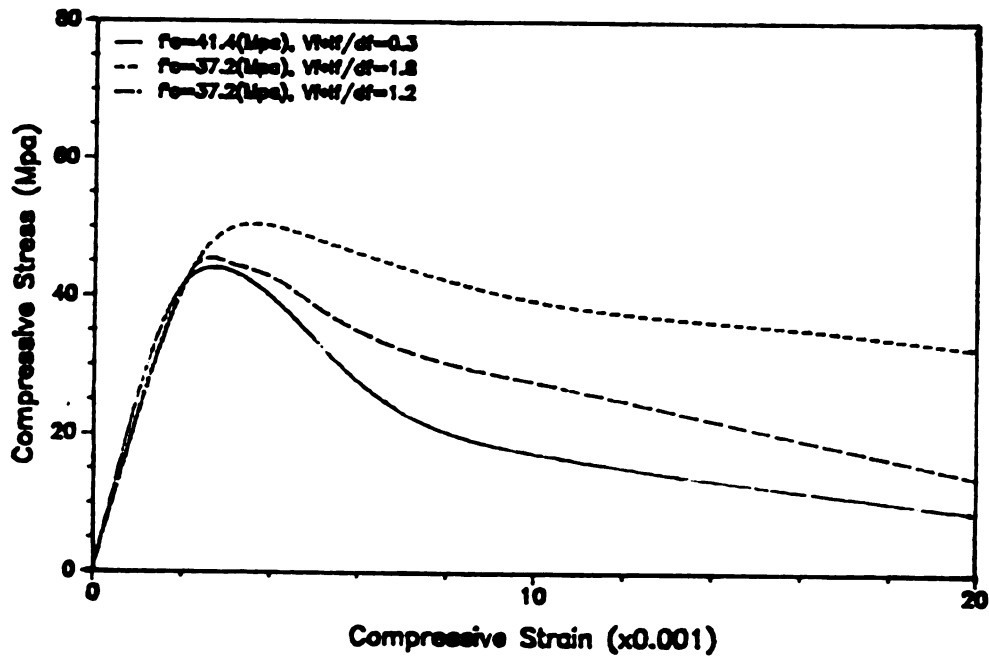
Table 4.1 Fiber Reinforced Concrete Mixtures

Ref.	Fiber Type	No. of Tests	matrix compressive strength (Mpa)	max. aggregate size (mm)	fiber			composite	
					Vf	aspect ratio (lf df)	reinforcement index (Vf lf df)	compressive strength (Mpa)	strain at peak ( $\times 0.0001$ )
4	straight	8	38.5	16.0	0.012	65.8	0.79	41	2.5
6	straight	4	55.8	9.5	0.01	59.3	0.593	58.6	*
		4	55.8	9.5	0.015	59.3	0.89	61.4	*
		4	55.8	9.5	0.02	59.3	1.186	62.1	*
		4	55.8	19.1	0.025	59.3	1.483	64.8	*
		4	48.3	19.1	0.01	59.3	0.593	55.2	*
		4	48.3	19.1	0.015	59.3	0.89	60	*
		4	48.3	19.1	0.02	59.3	1.186	58.6	*
		4	48.3	19.1	0.025	59.3	1.483	60	*
64	straight	2	42.0	19.1	0.01	57	0.57	48	2.0
		2	42.0	19.1	0.03	57	1.71	48.4	3.5
		2	57.2	19.1	0.01	83	0.83	53.1	2.6
		2	57.2		0.02	83	1.66	55.2	3.0
		2	57.2		0.03	83	2.49	56.5	3.2
		2	58.6		0.02	47	0.94	58.6	2.6
		2	58.6		0.02	83	1.66	60.7	4.0
		2	58.6		0.02	100	2.0	64.5	5.0
		2	62.1		*	*	0.47	62.7	2.6
		2	62.1		*	*	0.83	63.8	2.8
		2	62.1		*	*	1.66	64.8	2.9
		2	62.1		*	*	2.49	67.0	3.0
		2	62.1		*	*	2.00	69.0	4.5
		2	41.4		0.02	43	0.86	44.1	2.0
	2	41.4	0.01		57	0.57	45.5	2.4	
	2	41.4	0.02		57	1.14	42.7	2.8	
	2	41.4	0.02	72	1.44	43.4	3.0		
	2	41.4	0.03	57	1.71	48.2	4.25		
	hooked	2	37.2	19.1	0.01	60	0.6	41.4	2.2
		2	37.2	19.1	0.02	60	1.2	45.4	3.0
		2	37.2	19.1	0.03	60	1.8	60.3	3.8
		2	41.4	19.1	0.005	60	0.3	50.3	3.0
crimped	2	41.4	19.1	0.01	57	0.57	51.7	3.0	
	2	41.4	19.1	0.02	57	1.14	45.4	3.0	
65	straight	4	23.1	9.5	0.013	88.2	1.147	31.1	3.25
66	straight	3	40	19.1	0.02	57	1.14	42.1	2.0
		3	40	19.1	0.02	72	1.14	42.8	2.2

\* Not Reported

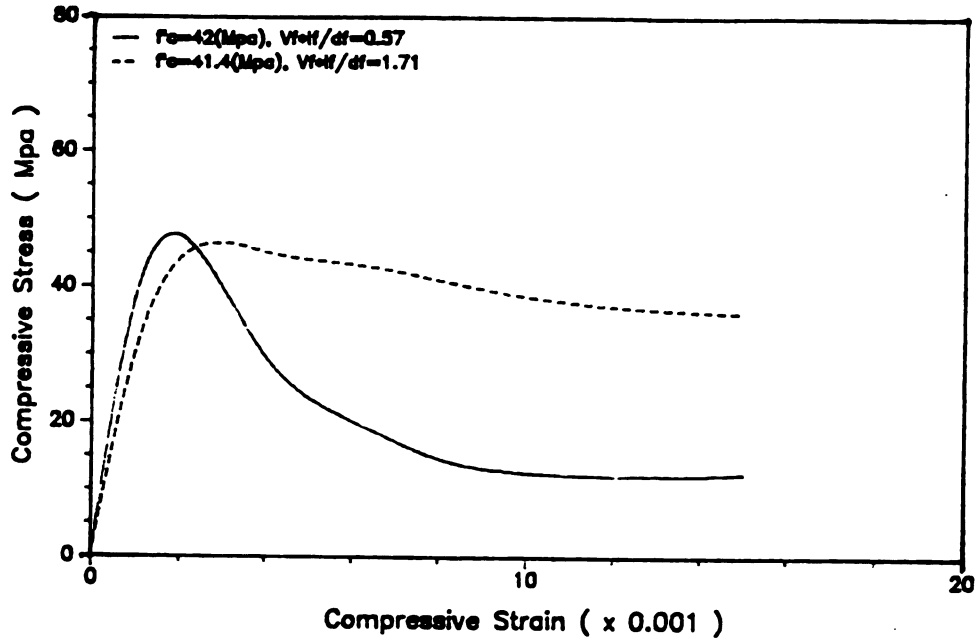


(a) Shah, Stroeven, Dalhuisen and Van Stekelenburg (Straight Fibers) [4]



(b) Soroushian and Bayasi (Straight Fibers) [64,66]

Figure 4.2 Experimental Compressive Stress-Strain Relationship



(c) Soroushian and Bayasi (Hooked Fibers) [64,66]

Figure 4.2 Experimental Compressive Stress-Strain Relationship (cont'd)

#### 4.4 THE CONSTITUTIVE MODEL FOR STEEL FIBER REINFORCED CONCRETE

An empirical model was developed for predicting the complete compressive stress-strain relationship of concretes reinforced with straight or hooked steel fibers as a function of the matrix strength and the reinforcement index of straight or hooked fibers ( $V_f \cdot l_f / d_f$ ). The constitutive model, which is a modified version of the model used earlier for plain concrete by Scott, Park and Priestley (1982) [67] and Soroushian and Sim (1986) [68] consists of a curvilinear ascending portion followed by a bilinear descending branch (Figure 4.3) :

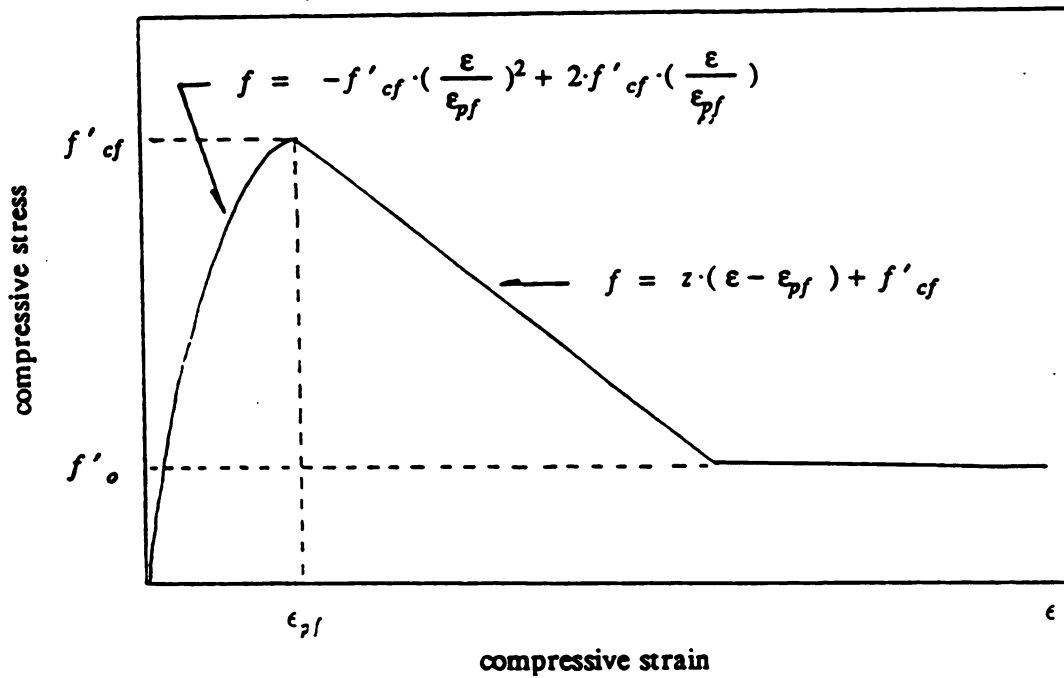


Figure 4.3 General Form of the Compressive Constitutive Model of SFRC

$$f = \begin{cases} -f'_{cf} \cdot \left(\frac{\epsilon}{\epsilon_{pf}}\right)^2 + 2 \cdot f'_{cf} \cdot \left(\frac{\epsilon}{\epsilon_{pf}}\right) & \text{for } \epsilon \leq \epsilon_{pf} \\ z \cdot (\epsilon - \epsilon_{pf}) + f'_{cf} \geq f'_o & \text{for } \epsilon > \epsilon_{pf} \end{cases} \quad (4.1)$$

where:

$f$  = concrete compressive stress ;

$\epsilon$  = concrete compressive strain ;

$f'_{cf}$  = compressive strength of steel

fiber reinforced concrete ;

$\epsilon_{pf}$  = strain at peak stress ; and

$z \cdot f'_o$  = coefficients derived empirically in terms of the compressive strength and fiber reinforcement index.

Coefficients  $z$  and  $f'_o$ , and the stress and strain at peak compressive stress ( $f'_{cf}$  and  $\epsilon_{pf}$ ) in this model were derived empirically for different fiber types as functions of the matrix compressive strength and the fiber reinforcement index.

The empirical expressions for different variables of the proposed model are given below (see Figure 4.3). These expressions have been derived through least square fitting of curves to experimental results. Figure 4.4 presents comparisons between the empirical expressions given below and test results.

Compressive Strength,  $f'_{cf}$  (see Figure 4.4(a)) :

$$f'_{cf} = f'_c + \alpha \cdot V_f \cdot l_f / d_f \quad (4.2)$$

where ;

$$\alpha = \begin{cases} 3.6 \text{ Mpa (515 psi) for straight fibers} \\ 6.0 \text{ Mpa (872 psi) for hooked fibers} \end{cases}$$

Residual Compressive Strength,  $f'_o$  (see Figure 4.4(b)) :

$$f'_o = 0.12 \cdot f'_{cf} + \beta \cdot V_f \cdot l_f / d_f \quad (4.3)$$

where ;

$$\beta = 11.8 \text{ Mpa (1700 psi) for both straight and hooked fibers}$$

Slope of the Descending Branch,  $z$  (see Figure 4.4(c)) :

$$z = -343 \cdot f'_c \cdot (1 - \gamma \cdot V_f \cdot l_f / d_f) \leq 0 \quad (4.4)$$

where ;

$$\gamma = \begin{cases} 0.66 & \text{for straight fibers} \\ 0.70 & \text{for hooked fibers} \end{cases}$$

Strain at Peak Stress,  $\epsilon_{pf}$  (see Figure 4.4(d)) :

$$\epsilon_{pf} = \epsilon_p + \delta V_f \cdot l_f / d_f \quad (4.5)$$

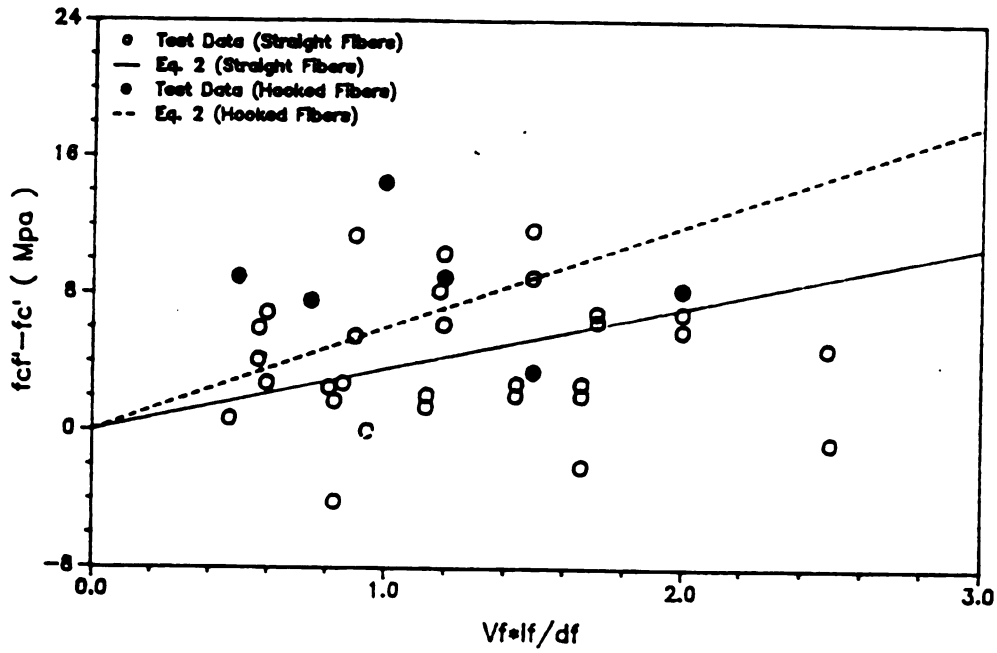
where ;

$$\delta = \begin{cases} 0.0007 & \text{for straight fibers} \\ 0.0017 & \text{for hooked fibers} \end{cases}$$

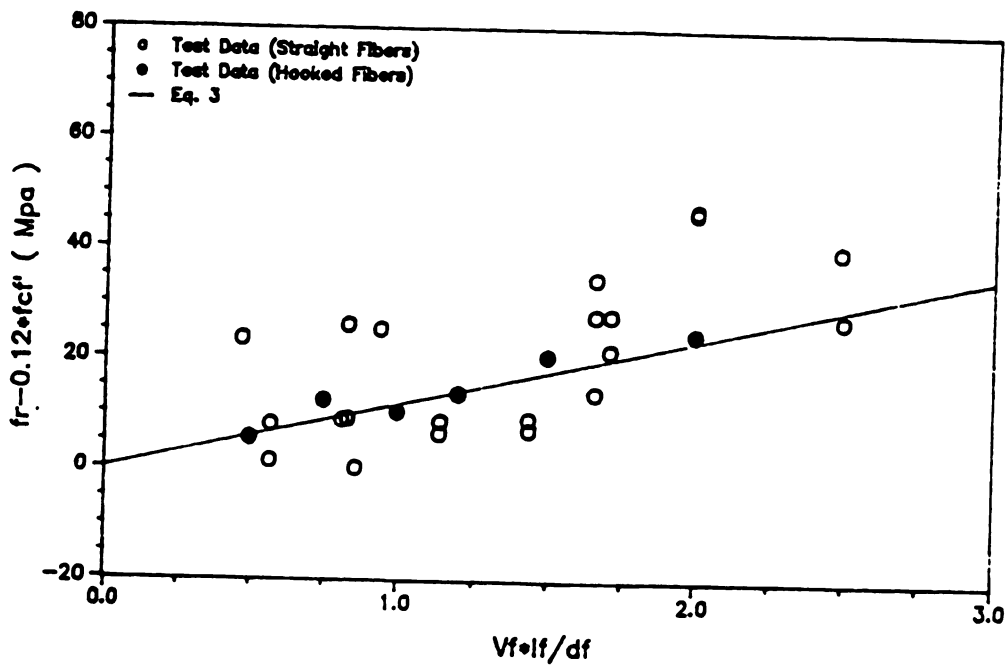
$$\epsilon_p = \text{strain at peak stress for plain concrete}$$

$$= 0.0021$$

It should be mentioned that variations in specimen geometry, loading versus casting direction, rate of loading, and maximum aggregate size (e.g. mortar versus concrete) will modify the compressive constitutive behavior of fibrous concrete. More test results are needed in order to refine the developed model for considering the effects of these factors.

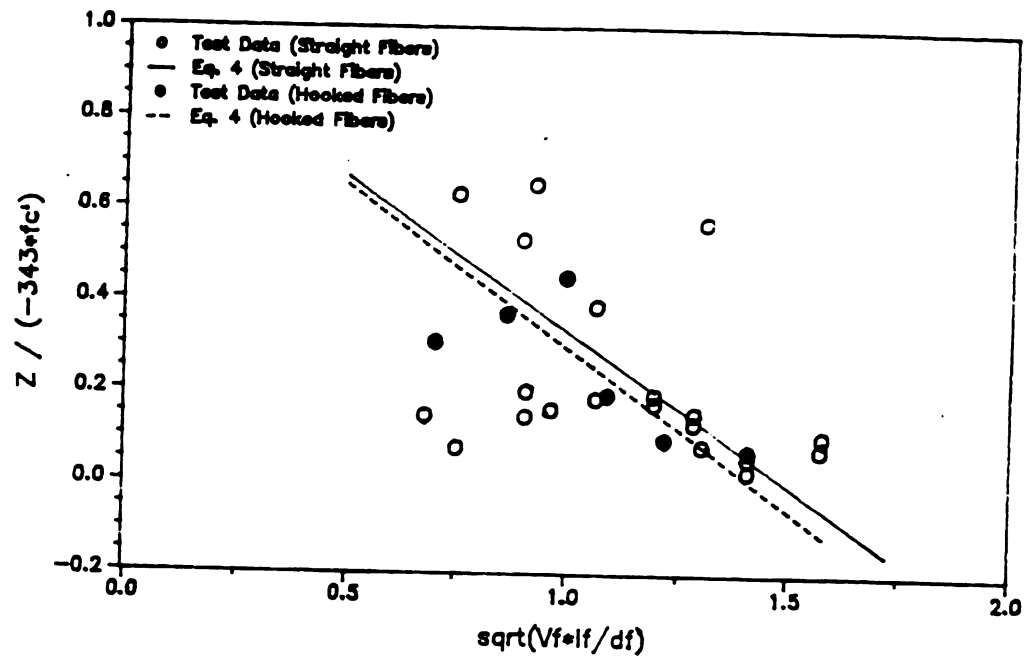


(a) Compressive Strength

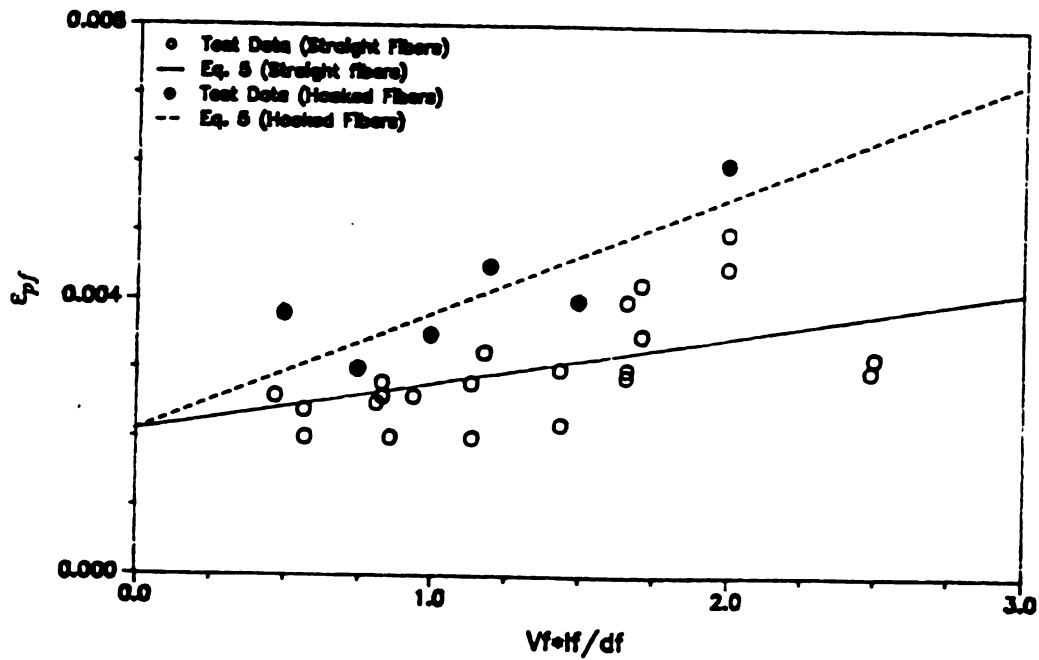


(b) Residual Compressive Strength

Figure 4.4 Comparison between Empirical Expressions on Test Results for Different Variables of Compressive Constitutive Model



(c) Slope of the Descending Branch

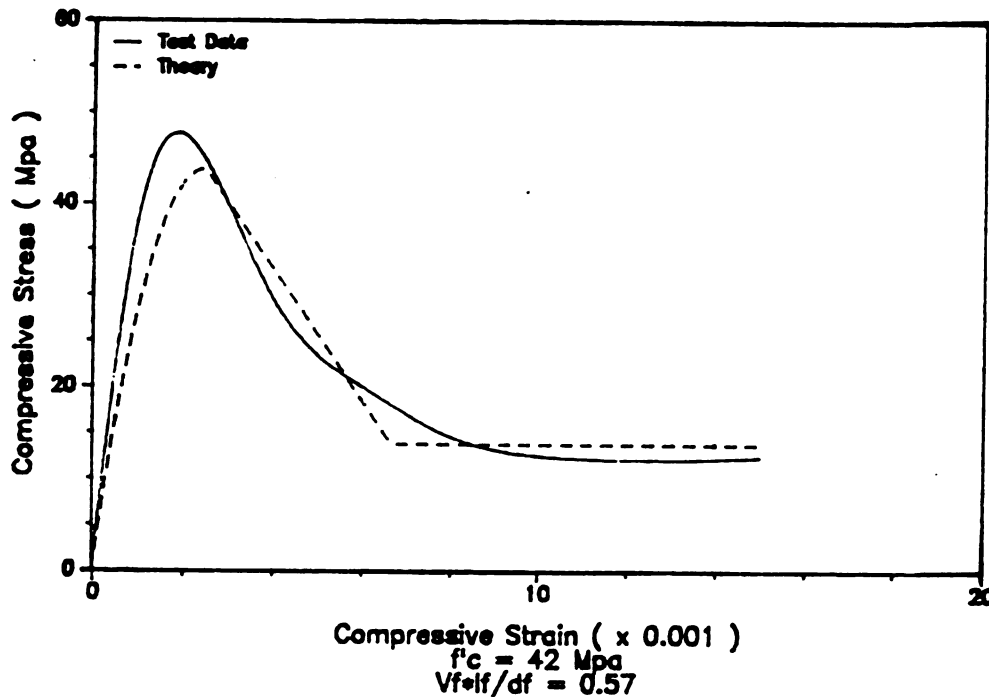


(d) Strain at Peak Stress

Figure 4.4 Comparison between Empirical Expressions on Test Results for Different Variables of Compressive Constitutive Model (cont'd)

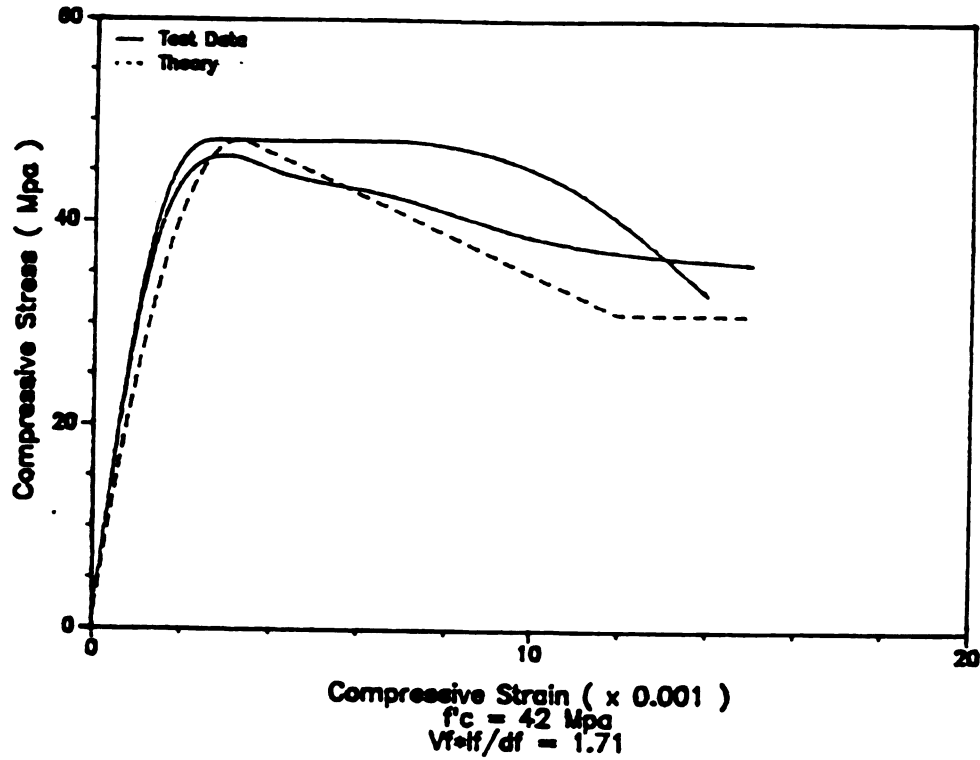
#### 4.5 COMPARISON WITH TEST RESULTS AND PARAMETRIC STUDIES

Typical comparisons between the predictions of the constitutive model developed in this study and the experimental compressive stress-strain relationships for 150 mm by 300 mm (6 in. by 12 in.) concrete cylindrical specimens reinforced with straight fibers are given in Figures 4.5(a) through 4.5(e). The experimental results presented in this figure cover wide ranges of fiber reinforcement index ( $V_f \cdot l_f / d_f$ ) and concrete compressive strength. The proposed model is observed to predict experimental results with a reasonable accuracy. Limited compression test results on crimped fibers have been reported in Reference 64. Figure 4.5(f) shows that the model developed for straight fibers satisfactorily predicts the compressive performance of concretes reinforced with crimped fibers.

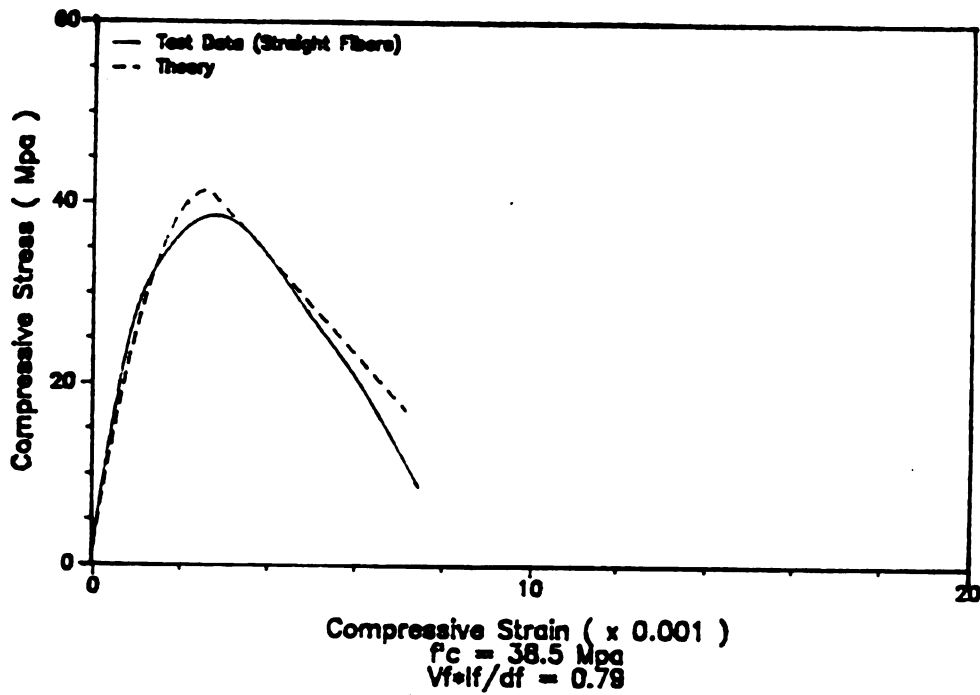


(a) Test Data from Reference 64 (Straight Fibers)

Figure 4.5 Analytical Model vs. Test (1 Mpa = 145 psi)

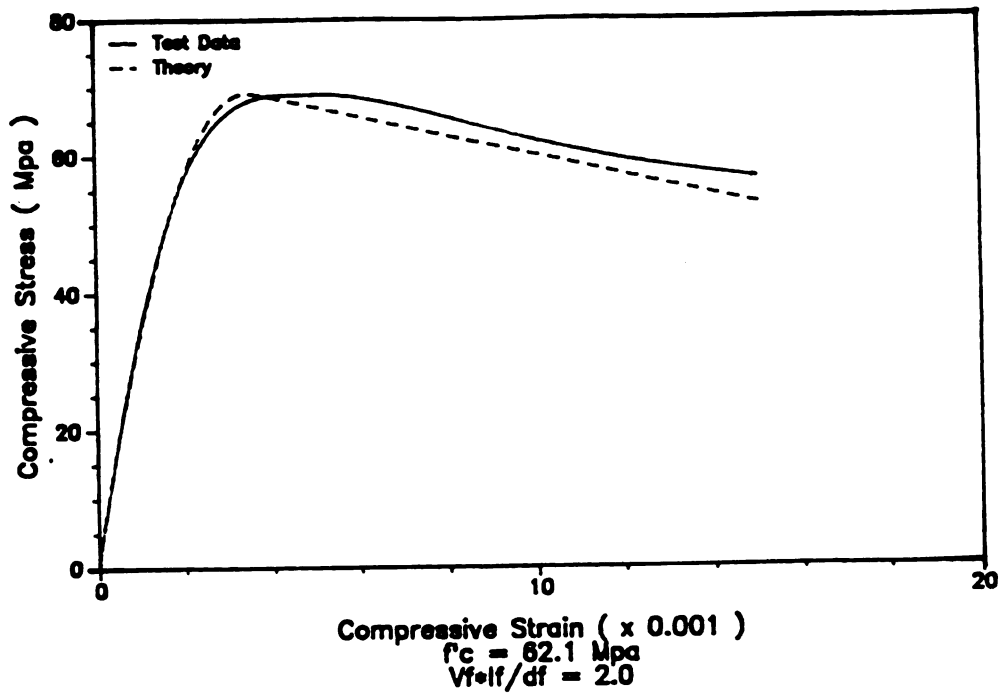


(b) Test Data from Reference 64 (Straight Fibers)

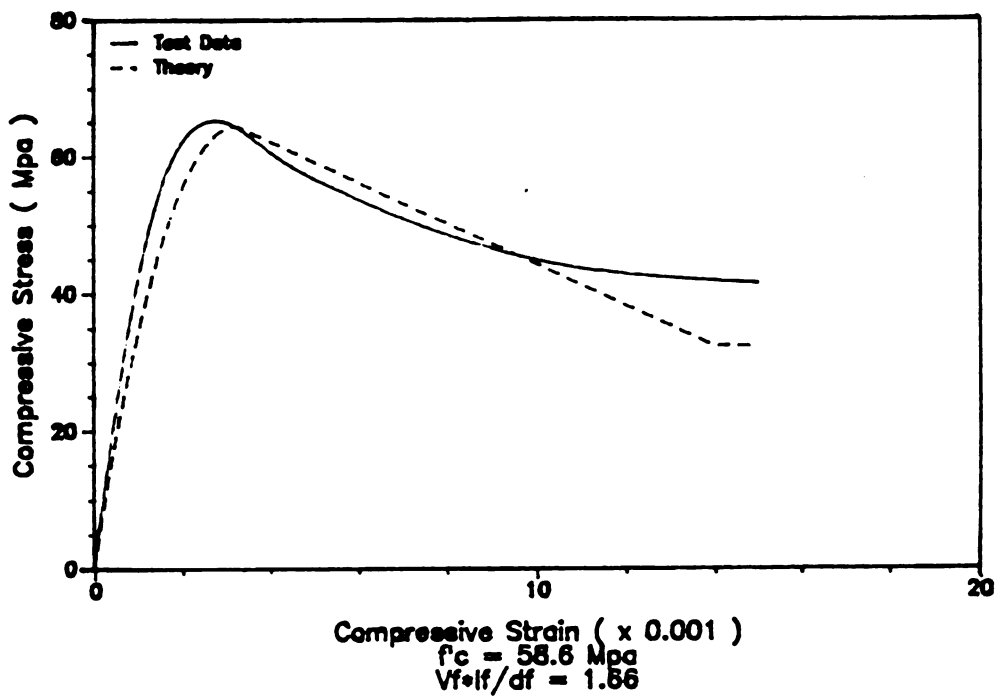


(c) Test Data from Reference 4 (Straight Fibers)

Figure 4.5 Analytical Model vs. Test (1 Mpa = 145 psi) (cont'd)

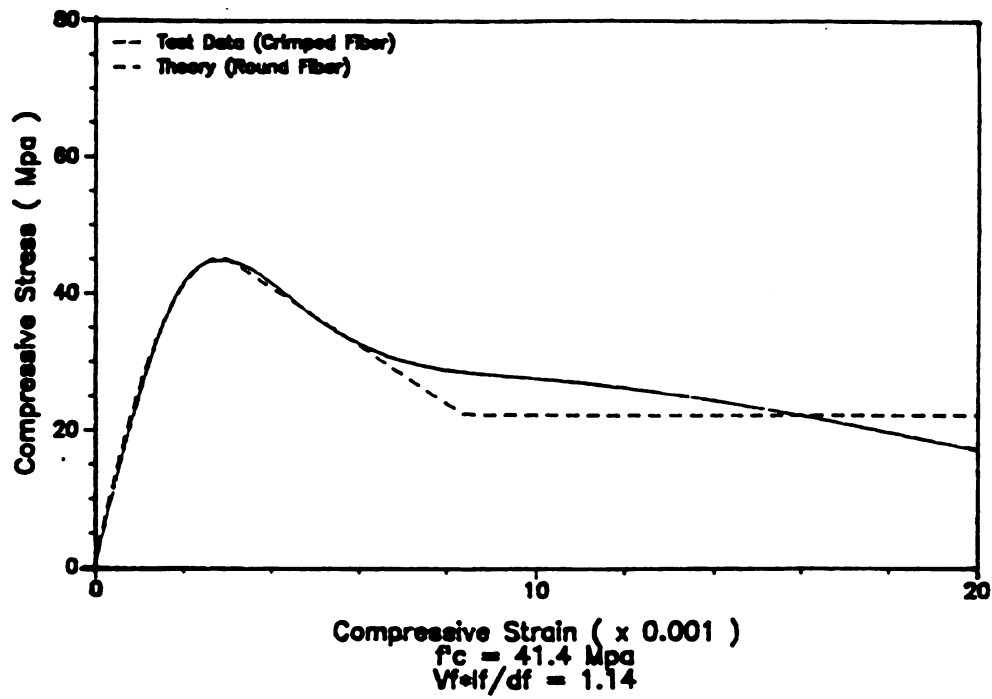


(d) Test Data from Reference 64 (Straight Fibers)

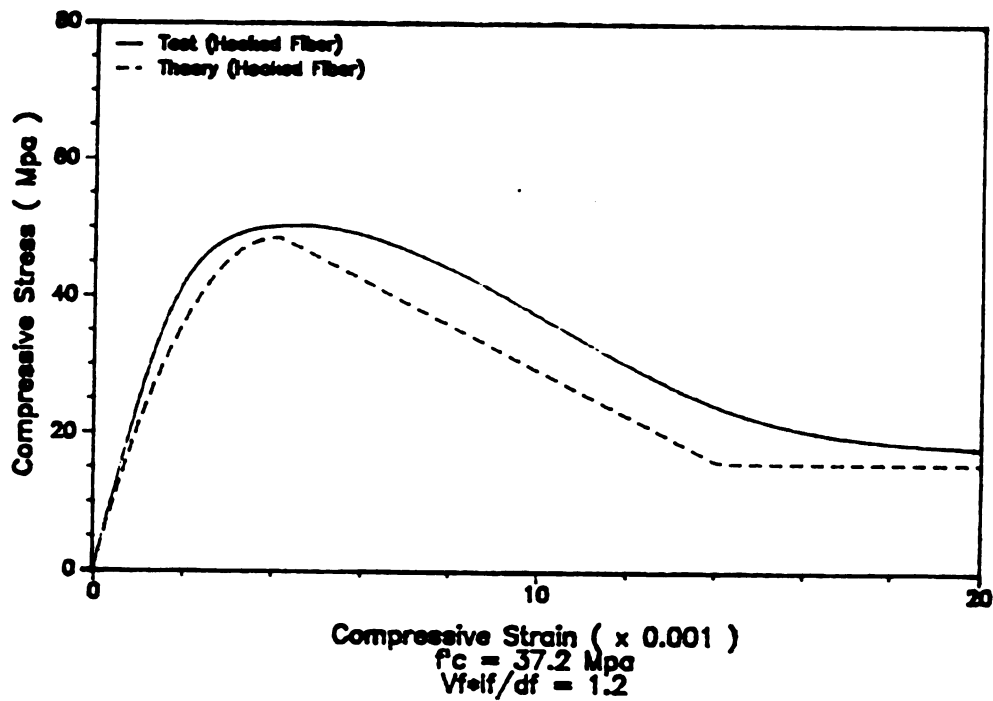


(e) Test Data from Reference 64 (Straight Fibers)

Figure 4.5 Analytical Model vs. Test (1 Mpa = 145 psi) (cont'd)

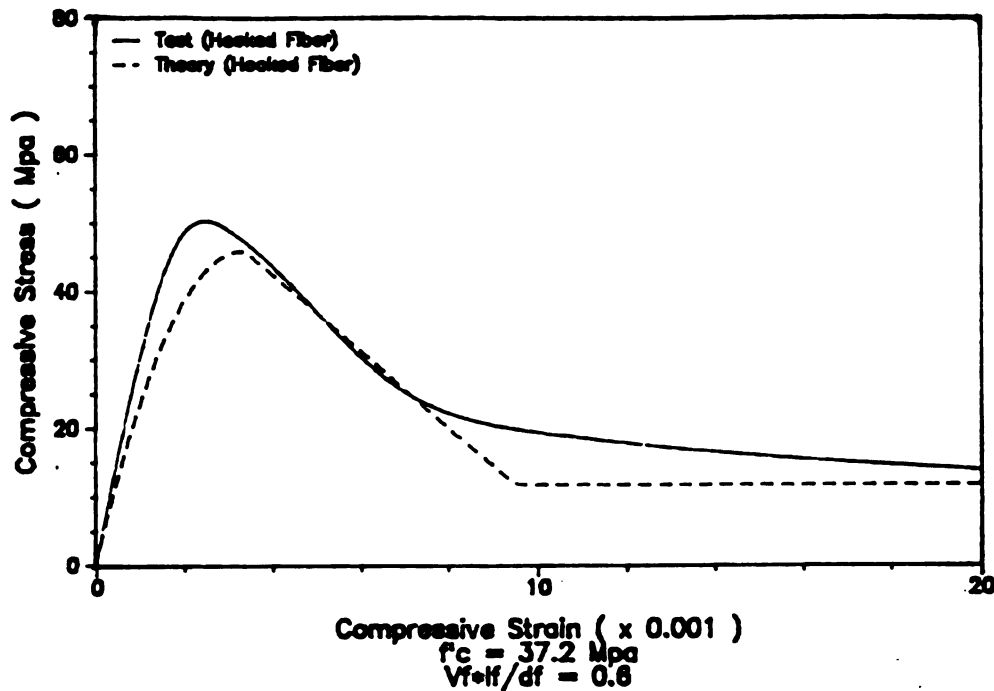


(f) Test Data from Reference 64 (Crimped Fibers)



(g) Test Data from Reference 64 (Hooked Fibers)

Figure 4.5 Analytical Model vs. Test (1 Mpa = 145 psi) (cont'd)



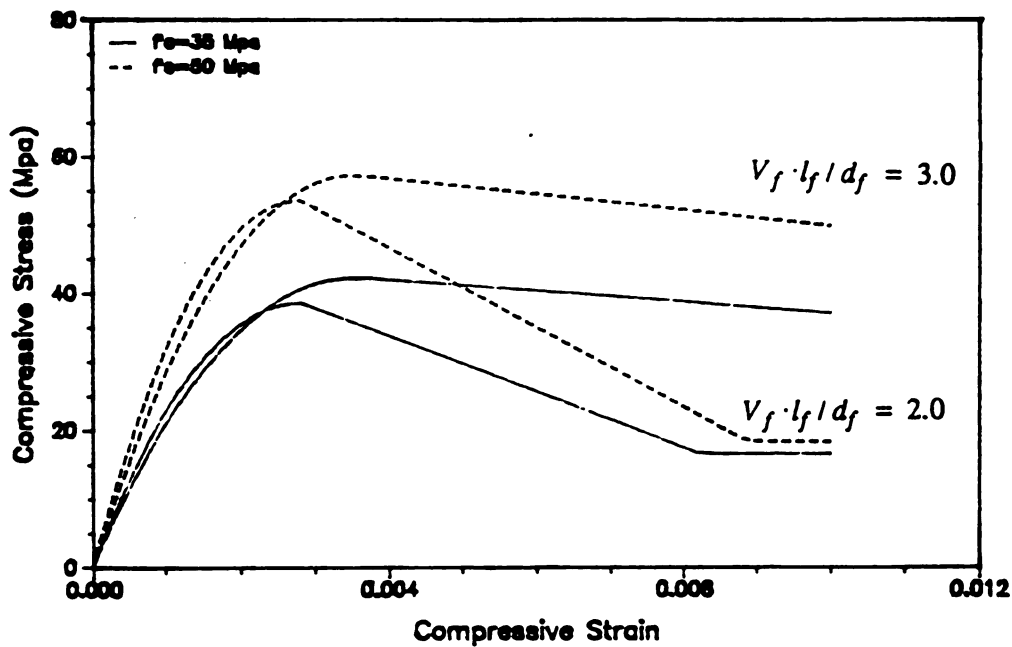
(h) Test Data from Reference 64 (Hooked Fibers)

Figure 4.5 Analytical Model vs. Test (1 Mpa = 145 psi) (cont'd)

Compression test results on concretes incorporating hooked steel fibers are also observed in Figures 4.5(g) and 4.5(h) to be closely predicted by the developed compressive constitutive model.

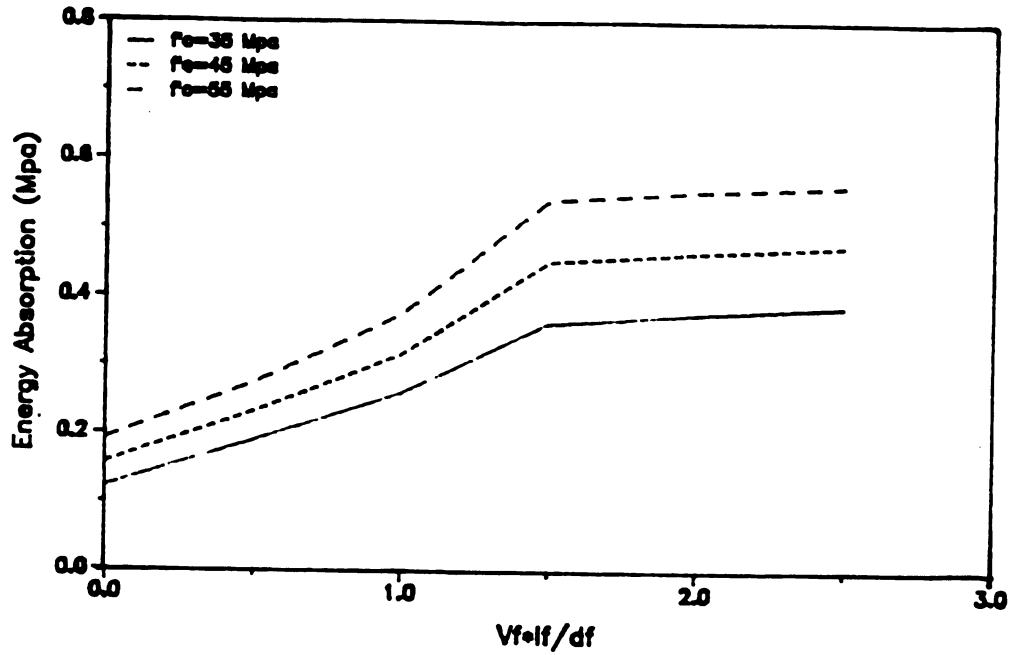
The developed compressive constitutive model of steel fiber reinforced concrete was also used for a numerical study on the effects of concrete compressive strength and fiber reinforcement index on the fibrous material behavior under compression. Figure 4.6(a) shows the overall constitutive performance of steel fiber reinforced concrete (with straight fibers) as influenced by the variations in steel fiber reinforcement index and compressive strength of concrete. Figure 4.6(b) shows the effects of these factors on the energy absorption capacity of fibrous concrete in compression (represented by the total area underneath the compressive stress-strain curve up to a strain of 0.01). Higher values of fiber

reinforcement index and concrete compressive strength are observed to produce significantly higher energy absorption capacities for fiber reinforced concrete. Figure 4.6(c) shows the tendency in strain at peak compressive stress to increase with increasing fiber reinforcement index in steel fiber reinforced concretes incorporating straight fibers. Finally, Figure 4.6(d) presents typical improvements in compressive performance of steel fiber reinforced concrete resulting from the use of hooked instead of straight fibers.

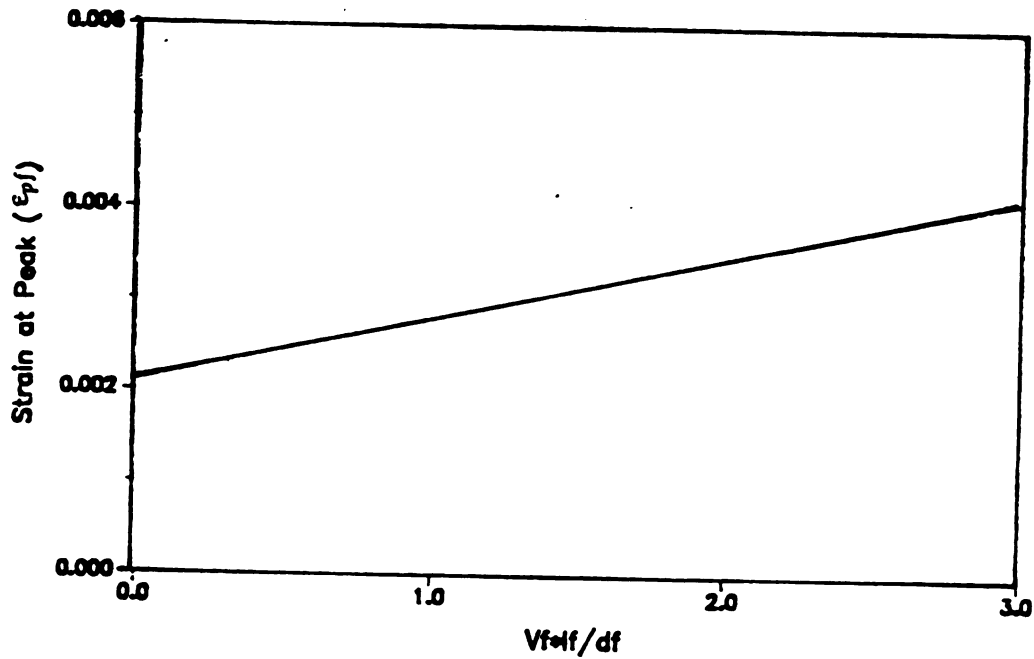


(a) Fiber Reinforcement Index (Straight Fibers)

Figure 4.6 Effects of Fiber Reinforcement Index and Concrete Compressive Strength on Compressive Behavior of SFRC as Predicted by the Proposed Constitutive Model (1 Mpa = 145 psi)

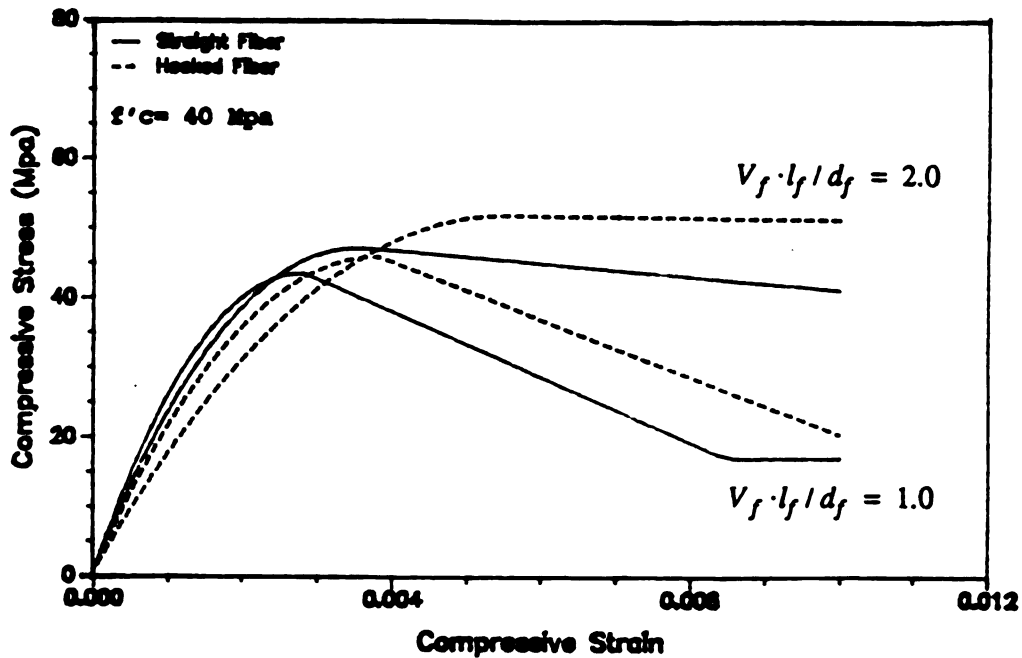


(b) Energy Absorption Capacity (Straight Fibers)



(c) Strain at Peak Stress (Straight Fibers)

Figure 4.6 Effects of Fiber Reinforcement Index and Concrete Compressive Strength on Compressive Behavior of SFRC as Predicted by the Proposed Constitutive Model (1 Mpa = 145 psi) (cont'd)



(d) Hooked vs. Straight Fibers

Figure 4.6 Effects of Fiber Reinforcement Index and Concrete Compressive Strength on Compressive Behavior of SFRC as Predicted by the Proposed Constitutive Model (1 Mpa = 145 psi) (cont'd)

#### 4.6 SUMMARY AND CONCLUSIONS

Reinforcement of concrete with randomly oriented short steel fibers increases the ultimate strength and especially the post-peak ductility and energy absorption capacity of concrete under compression. The effectiveness of steel fibers in enhancing concrete behavior under compression depends on the mix proportions of the matrix, the volume fraction, aspect ratio and deformation configurations of fibers, loading versus casting direction, specimen geometry, and rate of loading.

An empirical constitutive model was developed in this study for steel fiber reinforced concretes loaded in compression. This model accounts for the effects of fiber volume fraction, aspect ratio and type (straight vs. hooked) as well as the matrix compressive strength on the compressive behavior of steel fiber reinforced concrete. The model has been developed using results of ninety eight compression tests performed on 150 mm (6 in.) by 300 mm (12 in.) cylindrical concrete specimens with maximum aggregate sizes ranging from 9.5 mm (3/8 in.) to 19 mm (3/4 in.), incorporating straight or hooked fibers and loaded quasi-statically in the direction of casting.

The relatively simple empirical model developed in this study predicts experimental results (for fibrous concretes with relatively wide ranges of fiber and matrix variables) with a reasonable accuracy. More test results are needed for refining the model to consider the effects of maximum aggregate size, specimen geometry, loading versus casting direction, and the rate of loading.

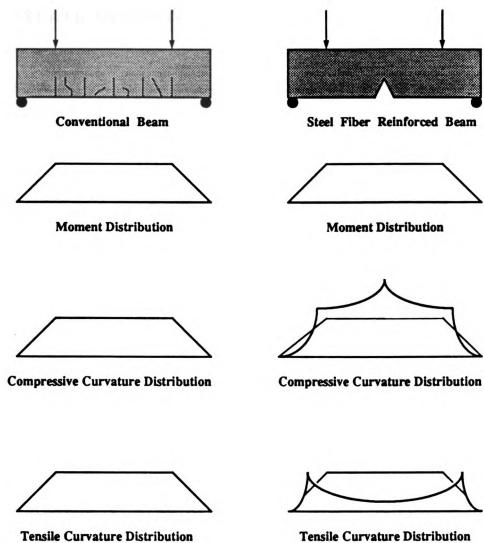
## CHAPTER 5

### FLEXURAL ANALYSIS OF STEEL FIBER REINFORCED CONCRETE

#### 5.1 INTRODUCTION

The improvements in SFRC behavior under compression and tension result in significantly higher improvements in the flexural strength and ductility of SFRC [24,41,64]. The flexural behavior of SFRC is typically marked by the formation of only one major crack of a critical section, a phenomenon that distinguishes the flexural behavior of SFRC beams from that of beams reinforced with conventional continuous bars (see Figure 5.1(a)). This implies that more damage is done to the cracked critical section and a concentration of curvature occurs in the vicinity of this section (Figure 5.1(b)). The critical section tends to suffer severe distortions and, after cracking, plane sections fail to remain plane in the vicinity of the critical section. As loading continues, the crack at the critical section begins to widen and this prompts the use of stress-crack relationships rather than stress-strain relationships on the tensile region of bending section. None of these features was considered in previous investigations [45-51].

Complete flexural load-deflection relationships are analytically constructed in this study through conducting a flexural analysis of the critical section, and using some assumptions regarding curvature distributions in the vicinity of the critical section. The predicted flexural load-deflection relationships are compared with experimental results, and the model is also used to conduct parametric studies on the effects of different matrix and fiber variables on the



(a) Conventional Beam

(b) Fiber Reinforced Beam

Figure 5.1 Crack Patterns and Possible Curvature Distributions

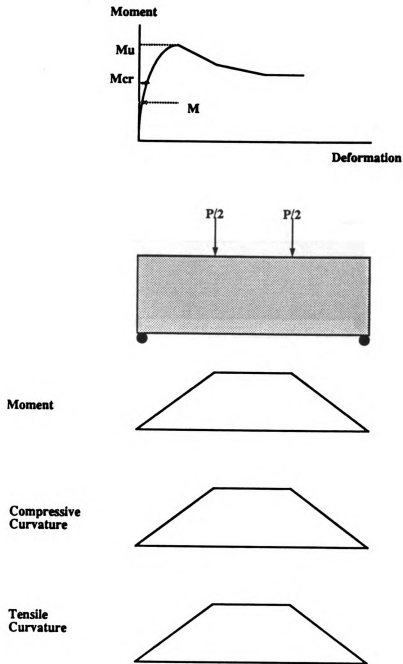
flexural performance of SFRC. The results of these parametric studies are evaluated using statistical analysis (by factorial design).

## 5.2 FLEXURAL ANALYSIS

The flexural analysis procedures developed for steel fiber reinforced concrete beams are described in this section. Attempts are made to consider the effects of cracking at the critical section on the release of tensile strains and the concentration of compressive strains in the vicinity of the critical section.

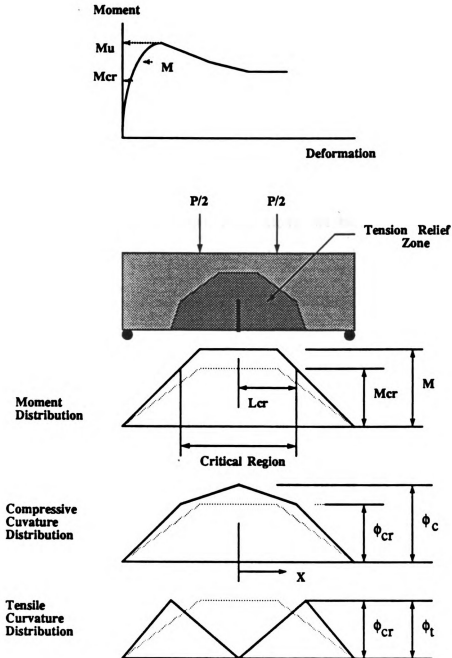
### 5.2.1 Curvature Distributions

Before the cracking the behavior of flexural beams can be regarded as elastic, and thus conventional beam theories are applicable. With increasing flexural loads the maximum tensile strain eventually reaches the tensile strain at peak tensile stress of steel fiber reinforced concrete, where the crack starts to open and this marks the first crack strength of the beam ( $P_{cr}$  in Figure 2.24). Up to this stage, the moment and curvature distributions are similar in shape (Figure 5.2(a)). Once one major crack starts to open at the critical section, tensile strains tend to be released near the crack, thus generally preventing the formation of another crack near the first crack. The opening of the crack on the tensile side will be accompanied by the concentration of compressive strains near the crack on the compressive side. Hence, upon cracking the distributions of moment, tensile strains and compressive strains cease to be similar in shape (see Figure 5.2(b)). In the post-cracking region, the pull-out action of fibers generally provides the beam with the capacity to resist increasing loads after cracking, and to maintain large fractions of its peak flexural load at large



(a) Before Cracking

Figure 5.2 Moment and Curvature Distributions



(b) After Cracking

Figure 5.2 Moment and Curvature Distributions (cont'd)

deformations in the post-peak region (Figure 2.24). Further widening of the crack with increasing deformations further disturbs the beam in the critical region, leading to increased concentration of compressive strains. The fact that only one crack appears in most beams subjected to flexural loads indicates that at a distance outside the critical section, where tensile strains drop below the cracking resistance, the curvature and strain distributions would tend to follow conventional elastic beam distributions. A region is defined in this investigation as the critical region (with a length  $2 \cdot L_{cr}$  along the beam span) in which the external moment along the beam is greater than or equal to the one corresponding to the first crack moment ( $M_{cr}$ ). Outside the critical region the elastic beam theory is assumed to be applicable. As the flexural load increases beyond the first-crack load, the critical region will spread outward continuously until the external load reaches its ultimate value.

The exact distributions of tensile and compressive strains in the critical region are rather complex. Simplifying assumptions have been used in this investigation in order to simulate the complex behavior in this region.

Once the beam reaches its ultimate flexural load and resistance starts to decrease with increasing deformations, the critical region is assumed to stabilize (in length), with curvature at the boundary assumed to stay constant at the first-crack value. Increased flexural deformations in the post-peak region, in spite of the continuous drop in load, lead to further increase in compressive strains in the critical region. Elastic flexural deformations outside critical region tend to decrease with drop in load in the post-peak phase of behavior. Hence, noting that at the boundaries of the critical region, curvatures are assumed to be constant, there is a tendency in deformations to increasingly concentrate near the center of the critical region. This concentration takes the form of crack widening and increased strains in tension and compression regions, respectively.

### 5.2.2 Analysis of the Critical Section

The crack shape at the critical section is assumed to be linear and symmetric about a plane normal to the beam longitudinal axis (see Figure 5.3).

As the crack opens, the tension part of the beam in the critical region continuously relieves its strains while compressive strains continue to increase. The increase in compressive strains after cracking is needed to satisfy the deformation compatibility requirements which would have been disturbed if, after cracking, the tensile and compressive strains were still assumed to be comparable (see Figures 5.4(a) and (b)). Thus, the crack opening angle ( $\theta_{cr}$  in Figure 5.4(b)) can be obtained by computing the difference in rotations associated with compressive and tensile strains in the critical region (Figure 5.4(b)):

$$\begin{aligned}\theta_{cr} &= \theta_c - \theta_t & (5.1) \\ &= \int_0^{L_\sigma} (\phi_c(x) - \phi_t(x)) dx;\end{aligned}$$

where

$\theta_{cr}$  = crack opening angle ;

$$\theta_c = \int_0^{L_\sigma} \phi_c(x) dx$$

= rotation of the compressive side of the beam

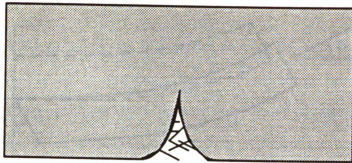
at the boundary of the critical region ;

$$\theta_t = \int_0^{L_\sigma} \phi_t(x) dx$$

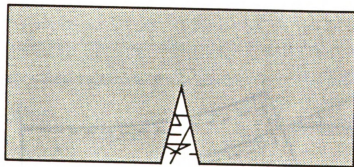
= rotation of the tensile side of the beam

at the boundary of the critical region

due to tensile curvature only;

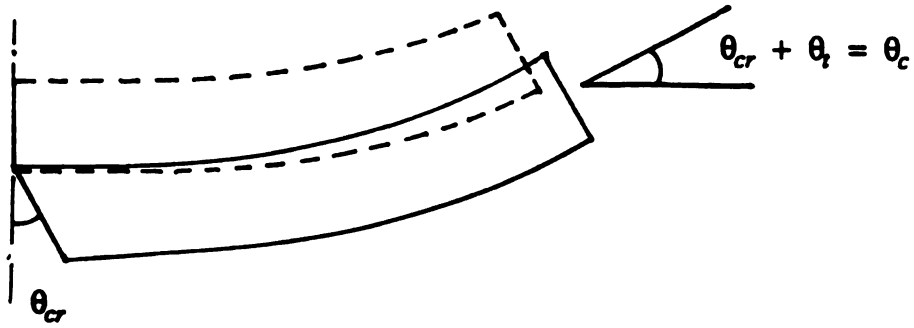


**(a) Actual Crack Shape**

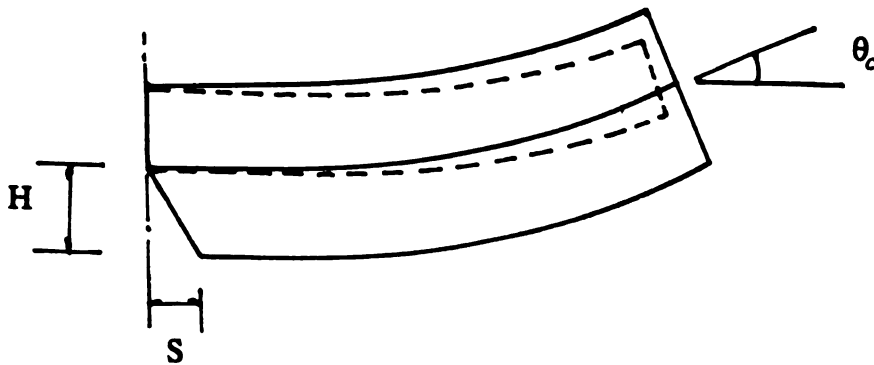


**(b) Assumed Crack Shape**

**Figure 5.3 Actual and Assumed Crack Shapes**



(a) Compressive Strain  $\approx$  Tensile Strain



(b) Compressive Strain  $>$  Tensile Strain

Figure 5.4 Deformation Compatibility after Cracking

$\phi_c, \phi_t$  = *compressive and tensile side*

*curvatures, respectively* ; and

$x$  = *distance from center (cracked section)* .

The tensile side curvature is assumed to vary linearly from zero at the crack to a value equal to the compressive side curvature at the boundary of the critical region. The assumed post-cracking distributions of compressive side and tensile side curvatures in the critical region are thus as follows:

$$\phi_c(x) = \frac{x}{L_{cr}} \cdot (\phi_c(L_{cr}) - \phi_c(0)) + \phi_c(0) ; \quad (5.2)$$

$$\phi_t(x) = \frac{x}{L_{cr}} \cdot \phi_t(L_{cr}) ; \text{ and}$$

$$\phi_c(L_{cr}) = \phi_t(L_{cr}) .$$

Incorporating the above curvatures into Equation (5.1) yields crack opening angle ( $\theta_{cr}$ ) as well as maximum crack opening ( $S$ ) at the extreme bottom layer of the critical section:

$$\theta_{cr} = 0.5 \cdot \phi_c(0) \cdot L_{cr} ; \text{ and} \quad (5.3)$$

$$S = H \cdot \theta_{cr} .$$

where:

$H$  = *crack depth (Figure 5.4(b))* .

The values of compressive side curvatures,  $\phi_c(0)$ , and crack depth,  $H$ , can be computed using a nonlinear flexural analysis of the cracked (critical) section, as described in the next section.

In flexural analysis of a complete beam, a step-by-step incremental approach was adopted. In each step, an increment is made in compressive side curvature at the critical section,  $\phi_c(0)$ , and then the crack depth ( $H$ ) is calculated using critical section nonlinear flexural analysis procedures (to be described later). This analysis needs input of crack opening angle ( $\theta_{cr}$ ) which depends on  $L_{cr}$ . The value of  $L_{cr}$ , however, can be computed after the critical section analysis is completed and the value of bending moment after curvature increment at the critical section is known. This condition requires a trial and adjustment (iterative) approach in which the analysis starts with the old value of  $L_{cr}$  at the end of the previous incremental step, and it would be adjusted until there is a tolerable difference between the starting and final values of  $L_{cr}$  in an iteration cycle. Total flexural deflection ( $\delta$ ) is computed by adding those resulting from flexural deformations, inside and outside of the critical region. Half of the beam span can be used for this purpose due to symmetry:

$$\delta = \int_0^{L_{cr}} \int_0^{\omega} \phi^c(\omega) d\omega dx + \int_{L_{cr}}^{L/2} \int_0^{\omega} \phi^c(\omega) d\omega dx \quad (5.4)$$

where:

$L$  = span of the beam ;

$x$  = distance from the critical section.

### 5.2.3 Nonlinear Flexural Analysis of the Critical (Cracked) Section

Curvature at the critical section is input incrementally, and then the equilibrium of axial forces at the section is satisfied through iterative selection of the neutral axis location. For any neutral axis location, given the curvature input value, the strain distributions can be obtained and using the tensile and compressive constitutive models of SFRC described in earlier Chapters, the tensile and compressive stresses and forces can be calculated. Iteration will be terminated when the calculated tensile and compressive forces balance each other (with a tolerable error). The informations regarding crack depth and opening, and other compressive side curvature, obtained from the critical section flexural analysis, can thus be used in overall analysis of the beam, as discussed in the previous section.

In the iterative approach to finding the new neutral axis position following curvature increment, first a lower bound neutral axis position (where the compressive force at section is larger than the tensile one) and an upper bound neutral axis position (where the tensile force exceeds the compressive one) are selected. Starting from the final position at the end of the previous step (Figure 5.5(a)), the lower bound is built by assuming a strain distribution with the new curvature but the crack depth corresponding to the previous step (Figure 5.5(b)). The upper bound is constructed with the new curvature, assuming an extreme compressive strain equal to that at the end of the previous step (Figure 5.5(c)).

Once the initial bracket was set up through the selection of lower and upper bound strain distributions for a given curvature, all the intermediate iterations leading to the equilibrium condition can be performed using the compressive strain at the top layer as the variable to be adjusted (noting that the neutral axis position can be easily computed if the values of curvatures and compressive strain at top are known). The iterations, involving the adjustment of the

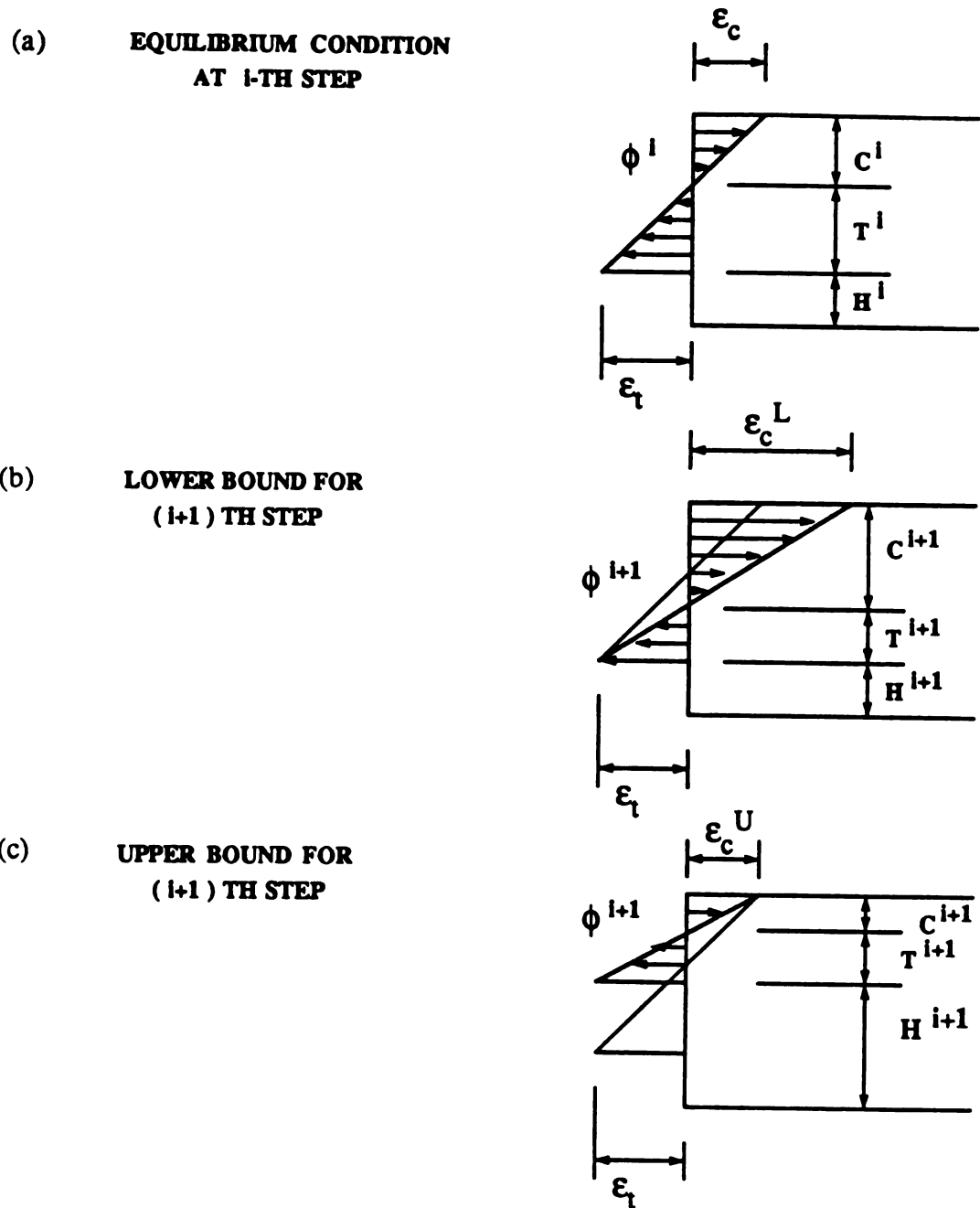
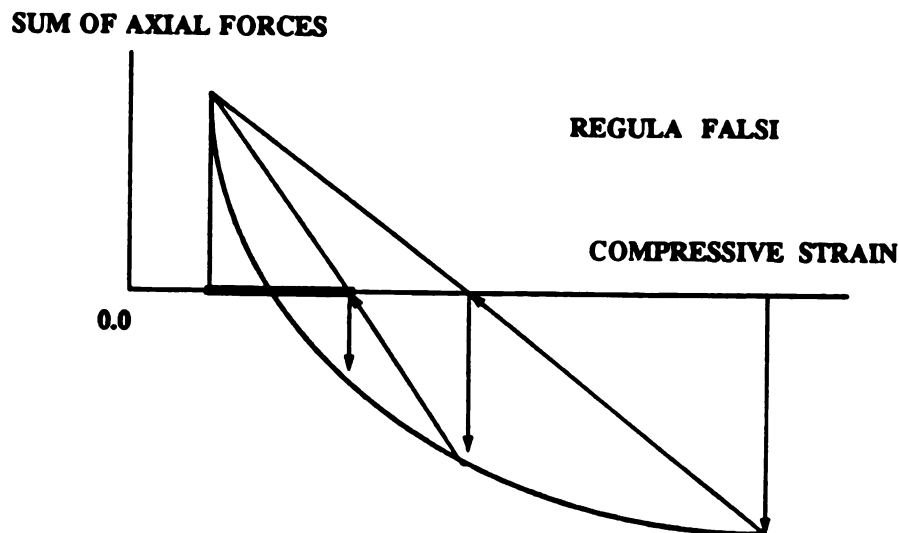


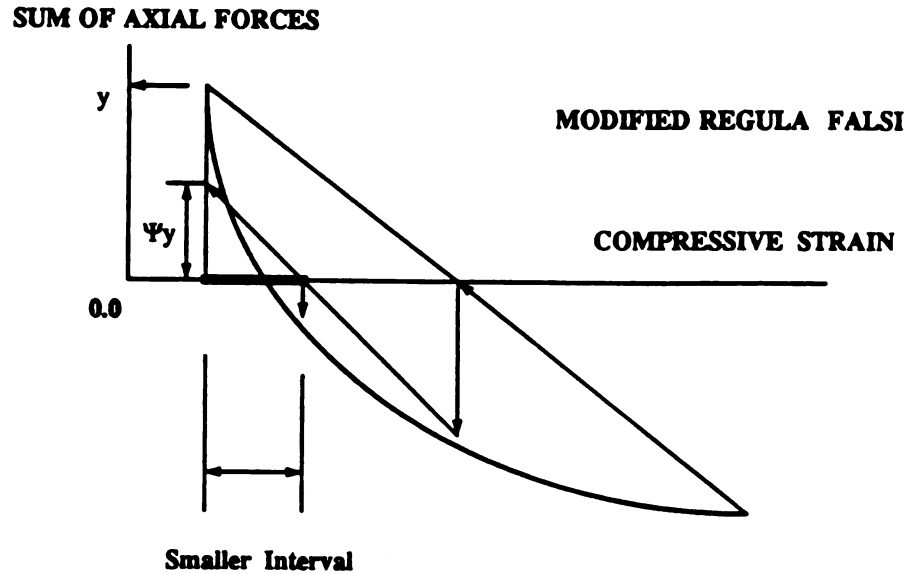
Figure 5.5 Estimation of the Initial Strain Configuration

extreme compressive strain at top for satisfying equilibrium were conducted using a Modified Regula-Falsi method [69]. In the conventional Regula-Falsi method (Figure 5.6(a)), the solutions (i.e., the compressive strain which makes the sum of tensile and compressive forces equal to zero) is obtained by gradually limiting the range within which the answer occurs. One side of the new range is the intersection of a line connecting points on the function curve corresponding to previous limits (with opposite signs of the function value) with the horizontal axis (corresponding to zero sum total of axial forces). In the Modified Regula-Falsi method (Figure 5.6(b)), however, the new side of the range within which the solution occurs is obtained as the intersection is with horizontal axis of a line connecting a point not on the function curve but at a location with  $\psi$  times the



(a) Regula-Falsi Method

Figure 5.6 Improvements of Regula-Falsi Method



(b) Modified Regula-Falsi Method

Figure 5.6 Improvements of Regula-Falsi Method (cont'd)

function value (with  $0 < \psi \leq 1.0$ , taken as 0.5 in this investigation) corresponding to one side of the previous range, with another point on the function curve of the other side of the range. With Modified Regula-Falsi method using  $\psi$  equal to 0.5, the number of iterations in finding equilibrium condition was reduced, when compared with the conventional Regula-Falsi method, by one-half to two-third. The maximum number of iterations in the Modified Regula-Falsi method typically varied between four to six.

#### 5.2.4 Comparison with Test Results

The next Chapter provides comprehensive discussions on the correlation of the proposed flexural analysis procedures for SFRC with test results. Some

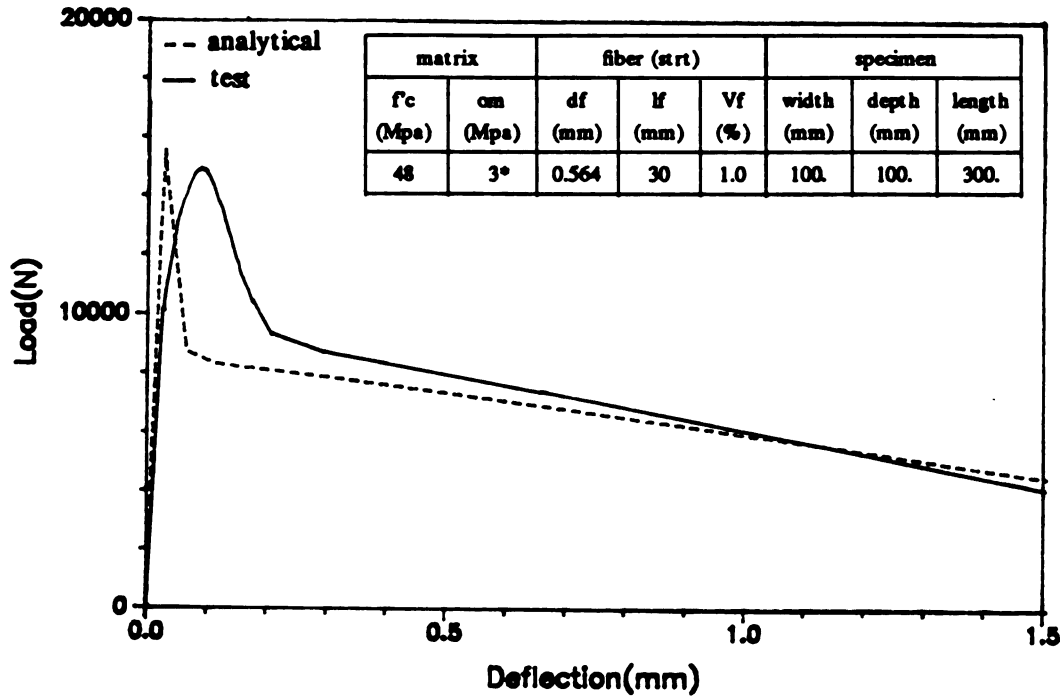
comparisons between the experimental flexural load-deflection curves reported in the literature and the predictions of the proposed analysis procedure are presented in this section.

Table 5.1 presents informations on the flexural test conditions considered for comparison with analytical results. Comparisons between experimental and analytical flexural load-deflection curves presented in Figures 5.7(a) to 5.7(c) are observed to be satisfactory.

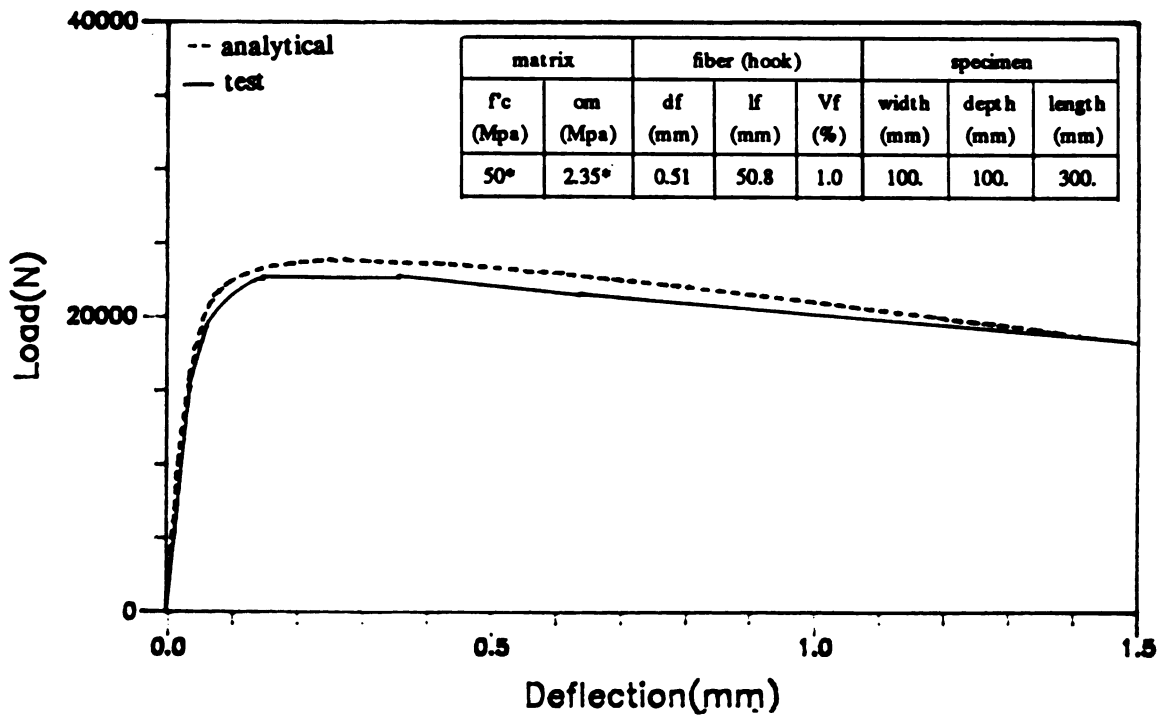
Table 5.1 Flextural Test Conditions

Ref.	matrix		fiber			specimen			loading
	comp. strength (Mpa)	tensile strength (Mpa)	diameter (mm)	length (mm)	Vf (%)	width (mm)	depth (mm)	length (mm)	
45	48	3 *	0.564	30	1.0	100.	100.	300.	4 pts.
76	50*	2.35*	0.53	31.8	1.0	100.	100.	300.	4 pts.
76	50*	2.35*	0.51	50.8	1.0	100.	100.	300.	4 pts.

\* Assumed Values

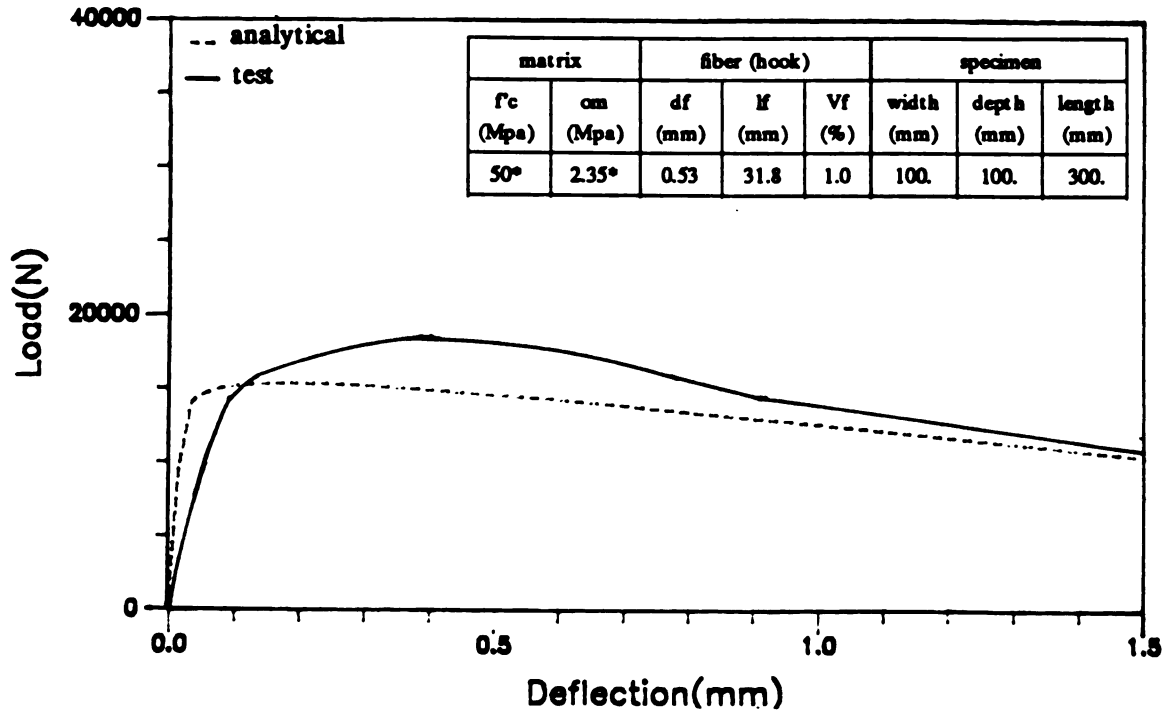


(a) Test Data from Reference 45



(b) Test Data from Reference 75

Figure 5.7 Comparisons between Experimental and Analytical Flexural Load-Deflection Curves



(c) Test Data from Reference 75

Figure 5.7 Comparisons between Experimental and Analytical Flexural Load-Deflection Curves (cont'd)

### 5.3 FLEXURAL BEHAVIOR OF CRITICAL (CRACKED) SFRC SECTION

Using the proposed analytical approach, flexural behavior of the critical section is investigated at different loading stages for two different steel fiber volume fractions (see Figure 5.8). The matrix and fiber properties used in this analytical study are also presented in Figure 5.8. Figure 5.8 shows that the increase in volume fraction of fibers from 0.5% to 1.2% increases the flexural strength and ductility of SFRC beams under flexure. Figure 5.9(a) and 5.9(b) show the profiles of strain and stress distributions along the depth of the critical section for two fiber volume fractions of the peak and post-peak points, respectively,

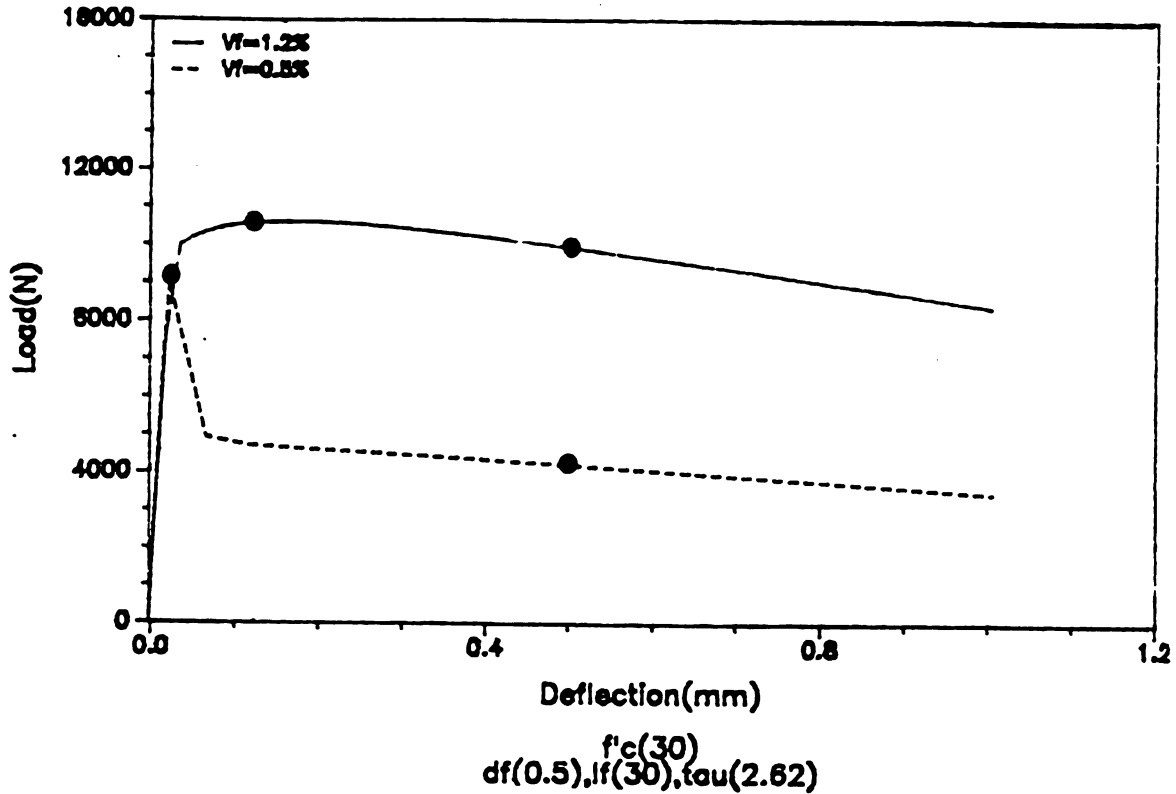
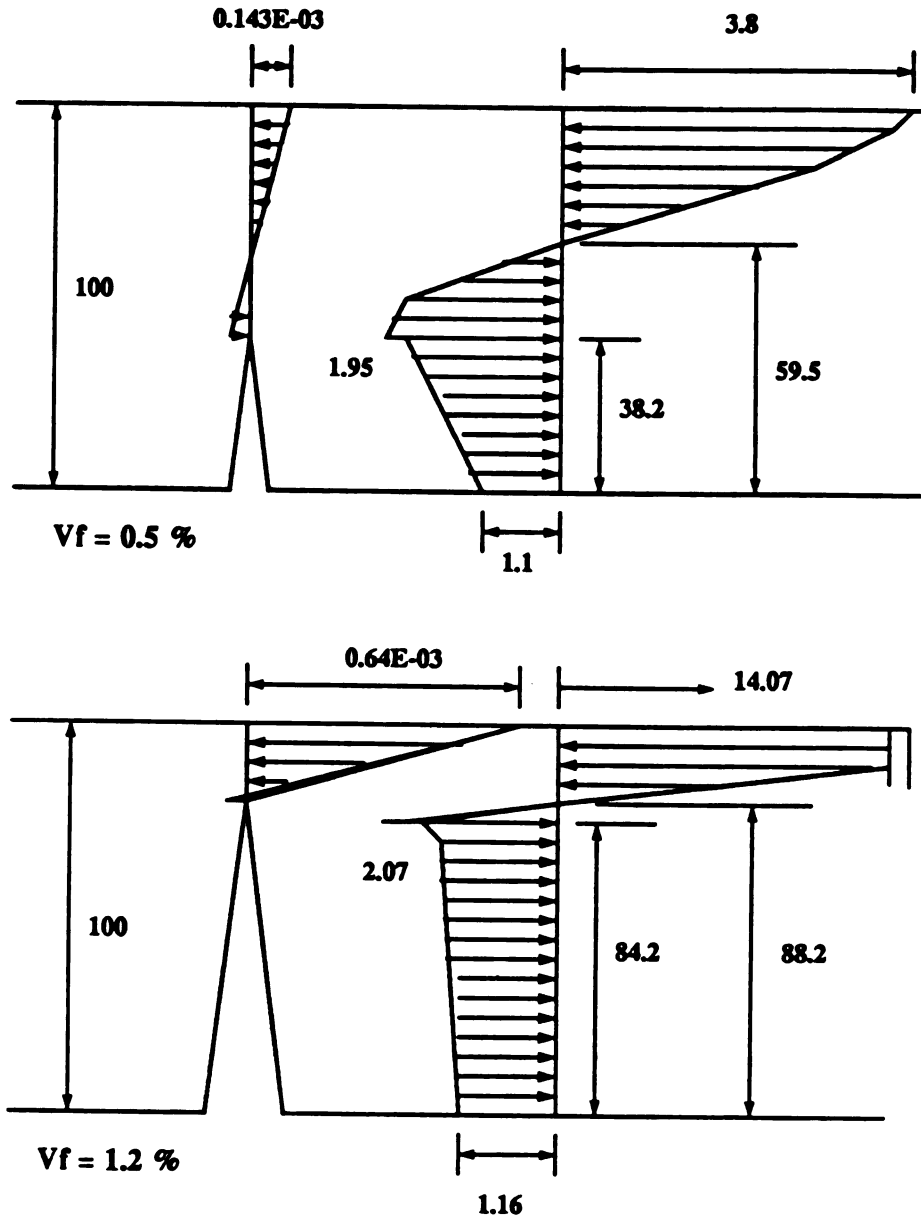


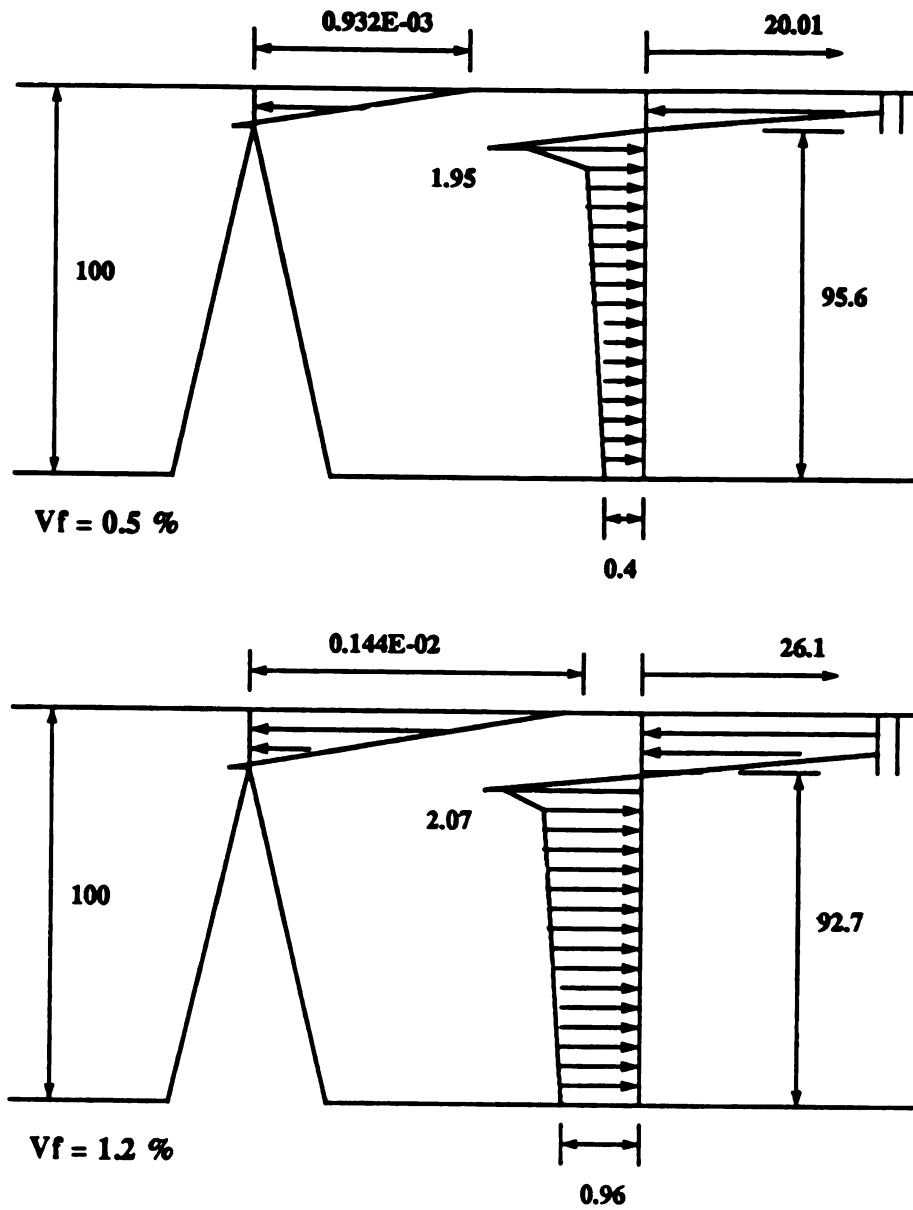
Figure 5.8 Typical Load-Deflection Curves ( $V_f = 0.5\%$  and  $1.2\%$ )

which are marked on curves in Figure 5.8. The post-peak point is chosen at a flexural deflection equal to 0.5 mm (0.02 in.). It is observed that in both cases the peak flexural load is attained when crack has already opened. Figure 5.8 shows that the load carrying capacity of the beam with 0.5% fiber volume fraction drops suddenly after peak, while the SFRC beam with 1.2% fiber volume fraction can maintain a major fraction of its peak flexural resistance in the post-peak region. Figure 5.9(b) shows that at a relatively large deformation in the post-peak region, where the crack has widened and penetrated deeply into the beam, the post-peak tensile resistance of SFRC seems to have an important effect on performance. At the relatively low fiber volume fraction of 0.5%, the tensile resistance provided by fibers bridging the crack is relatively small, leading to low flexural ductility; for the relatively high fiber volume fraction of 1.2%,



(a) Strain and Stress Distributions at Peak Load

Figure 5.9 Strain and Stress Distributions at the Critical Section



(b) Strain and Stress Distributions at Deflection equal to Five Times the Deflection at Peak Load

Figure 5.9 Strain and Stress Distributions at the Critical Section (cont'd)

however, fibers bridging the crack provide a desirable level of tensile (pull-out) resistance which give the beam a relatively high flexural ductility (i.e., capacity to resist major fractions of their flexural strength at relatively large post-peak deformations).

It is interesting to note, in regard to the stress distributions at peak flexural load, that flexural strength is reached in SFRC beams when the tensile behavior has already reached the post-peak conditions. The flexural strength of SFRC is thus dependent not only on the tensile strength of the material, but also on its post-peak tensile behavior. This partly illustrates why the increase in flexural strength resulting from fiber reinforcement is typically higher than the corresponding increases in tensile strength. One may also conclude from this discussion that the modulus of rupture computed using linear-elastic flexural analysis equations does not actually give a characteristic stress value which relates to the peak tensile strength of SFRC.

#### 5.4 A PARAMETRIC STUDY OF SFRC BEAM FLEXURAL BEHAVIOR

The objective of the parametric study presented in this section is to find the influential factors which determine the flexural behavior of steel fiber reinforced concrete. Two groups of factors were considered in this study (Figure 5.10): ten material-related factors (matrix tensile strength ( $\sigma_m'$ ), matrix compressive strength ( $f_c'$ ), crack opening at residual matrix strength in tension softening region ( $S_{cr}$ ), crack opening at zero matrix stress in tension softening region ( $S_{c0}$ ), fiber diameter ( $d_f$ ), fiber length ( $l_f$ ), fiber volume fraction ( $V_f$ ), fiber peak pull-out strength ( $\tau_u$ ), fiber slip at peak pull-out strength ( $S_{pk}$ ) and fiber slip at

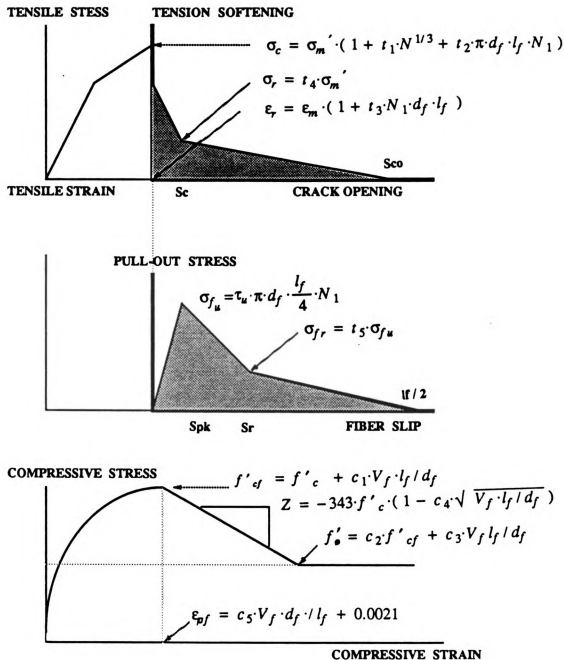


Figure 5.10 Material-Related and Constitutive Behavior-Related Factors

residual pull-out strength ( $S_r$ ) and ten constitutive behavior-related factors ( $t_1$  and  $t_2$  are parameters of composite peak tensile strength ( $\sigma_c$ ),  $t_3$  and  $t_4$  are parameters of matrix softening model,  $t_5$  is a parameter of fiber residual strength in post-peak pull-out region and  $c_1$  through  $c_5$  are parameters of compressive constitutive model).

The parametric study consists of analytically investigating the effects of changing the values of these factors (from "standard" values) on flexural load-deflection relationships. The "standard" values of the factors have been chosen either on the basis of test results or considering practical ranges applicable to steel fiber reinforced concrete. These "standard" values of the twenty factors considered in the parametric study are shown in Tables 5.2 and 5.3 (for material-related and constitutive behavior-related factors, respectively).

The effects of variations in different factors on the following aspects of the flexural behavior of SFRC beams were investigated analytically (see Figure 5.11): (1) peak load (P); (2) ductility (D), defined as the flexural resistance at a deflection equal to the span length divided by 150, measured from the deflection at peak load, divided by the peak flexural resistance; (3) toughness (A), defined as the area underneath the load-deflection curve in the post-peak region up to a flexural deflection equal to the span length divided by 150 from the deflection at ultimate load; and (4) the overall flexural behavior the variations of which (as a results of changes in the factors) were measured as:

$$V = \sum_{i=1}^{i=3} \gamma_i \cdot v_i^2 \quad (5.5)$$

where:

$V =$  overall flexural behavior ;

$\gamma_i$  = weighing coefficient for each factor ;

$$v_1 = \left( \frac{P_v - P_s}{P_s} \right);$$

$$v_2 = \left( \frac{D_v - D_s}{D_s} \right);$$

$$v_3 = \left( \frac{A_v - A_s}{A_s} \right);$$

$P$  = peak flexural load (Figure 5.11) ;

$D$  = ductility

=  $P / P_r$  ( see Figure 5.11 ) ; and

$A$  = toughness

= area under load-deflection curve

as defined in Figure 5.11 .

Considering the fact that  $v_1$ ,  $v_2$  and  $v_3$  explain discrepancies in pre-peak behavior, behavior between pre-peak and post-peak, and post-peak behavior, equal weights (weighing coefficient equal to 1.0) are given to each of these factors. The definition of ductility and toughness presented above have been developed based on the assumption that the pre-peak flexural deflection measurements in a number of the available test results have not been reasonably accurate. Large variations between the measured flexural stiffnesses provide the basis for this conclusion.

Conclusions regarding the significance of the effects of different factors on SFRC flexural behavior have been based on simple observations as well as statistical analyses based on  $2^k$  factorial designs [54]. For simple observations,

Table 5.2 Effects of Material-Related Factors

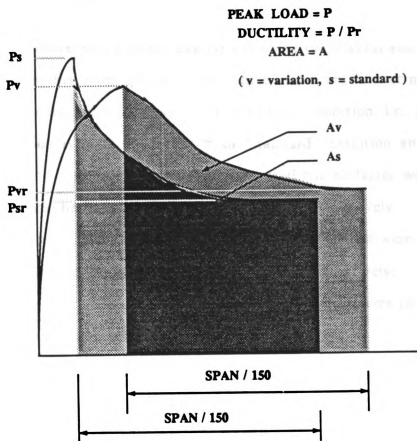
Factors	Standard Value	Variation	Maximum Normalized Differences *			
			Peak Load	Ductility	Toughness	Overall Behavior
$\sigma_m$	3	2 - 4	0.298	0.438	0.014	0.274
$f_c$	40	30 - 50	0.045	0.023	0.015	0.002
$S_e$	0.008	0.003 - 0.02	0.199	0.076	0.064	0.049
$S_o$	0.023	0.01 - 0.05	0.0	0.036	0.006	0.001
$d_f$	0.5	0.25 - 1.00	0.151	0.697	0.891	0.457
$l_f$	30	20 - 40	0.025	0.361	0.361	0.264
$V_f$	0.01	0.005 - 0.02	0.042	0.475	0.52	0.457
$\tau_m$	2.62	1.0 - 4.5	0.02	0.68	0.689	0.939
$S_{pk}$	0.025	0.01 - 0.05	0.031	0.015	0.011	0.001
$S_r$	2.8	1.0 - 5.0	0.0	0.531	0.322	0.32

\* Maximum Normalized Difference = Maximum absolute difference in a certain aspect of flexural behavior divided by "Standard Value" of that aspect due to changes in certain factor.

Table 5.3 Effects of Constitutive Behavior-Related Factors

Factors	Standard Value	Variation	Maximum Normalized Difference *			
			Peak Load	Ductility	Toughness	Overall Behavior
t1	0.138	0.069 - 0.207	0.001	0.004	0.002	0.0
t2	0.050	0.025 - 0.075	0.001	0.004	0.002	0.0
t3	0.35	0.175 - 0.525	0.023	0.059	0.021	0.004
t4	0.40	0.2 - 0.6	0.067	0.028	0.027	0.006
t5	0.3	0.15 - 0.45	0.0	0.291	0.097	0.016
c1	3.6	1.8 - 5.4	0.006	0.023	0.01	0.0
c2	0.12	0.06 - 0.18	0.0	0.0	0.0	0.0
c3	14.8	7.4 - 22.2	0.0	0.0	0.0	0.0
c4	0.66	0.33 - 0.99	0.0	0.0	0.0	0.0
c5	0.0007	0.0004 - 0.002	0.019	0.034	0.008	0.0

\* Maximum Normalized Difference = Maximum absolute difference in a certain aspect of flexural behavior divided by "Standard Value" of that aspect due to changes in certain factor



$$V = \sum_{i=1}^{i=3} \gamma_i \cdot v_i^2$$

$$v_1 = \left[ \frac{P_v - P_s}{P_s} \right];$$

$$v_2 = \left[ \frac{D_v - D_s}{D_s} \right];$$

$$v_3 = \left[ \frac{A_v - A_s}{A_s} \right];$$

Figure 5.11 Definitions of Four Different Criteria

the following strategy was selected; in each run, only one of the factors is varied and corresponding variations in any of the four aspects of flexural behavior introduced above were assessed analytically using the flexural analysis procedures developed in this investigation. Then these values are further normalized with respect to values corresponding to the "standard" condition, i.e., peak load from each variation is divided by that from "standard" condition and so on. The minimum and maximum values of each material-related factor were equal to 0.5 and 2.5 times the "standard" value of that factor, respectively. The lowest and highest values of the constitutive behavior-related factors were selected as 0.5 and 1.5 times the "standard" values of the factor, respectively. These limits on material-related and constitutive behavior-related factors were to represent practical conditions commonly encountered in SFRC.

The results are shown in Table 5.2 for material-related factors and in Table 5.3 for constitutive behavior-related factors. Figures 5.12 through 5.15 show typical flexural load-deflection relationships as influenced by variations in material-related factors (comparisons are made with the "standard" condition). The effects of the material-related and constitutive behavior-related factors on the flexural performance characteristics of SFRC are discussed in the following using the observations made of flexural load-deflection relationships (Figure 5.12) and also using statistical techniques based on  $2^k$  factorial designs.

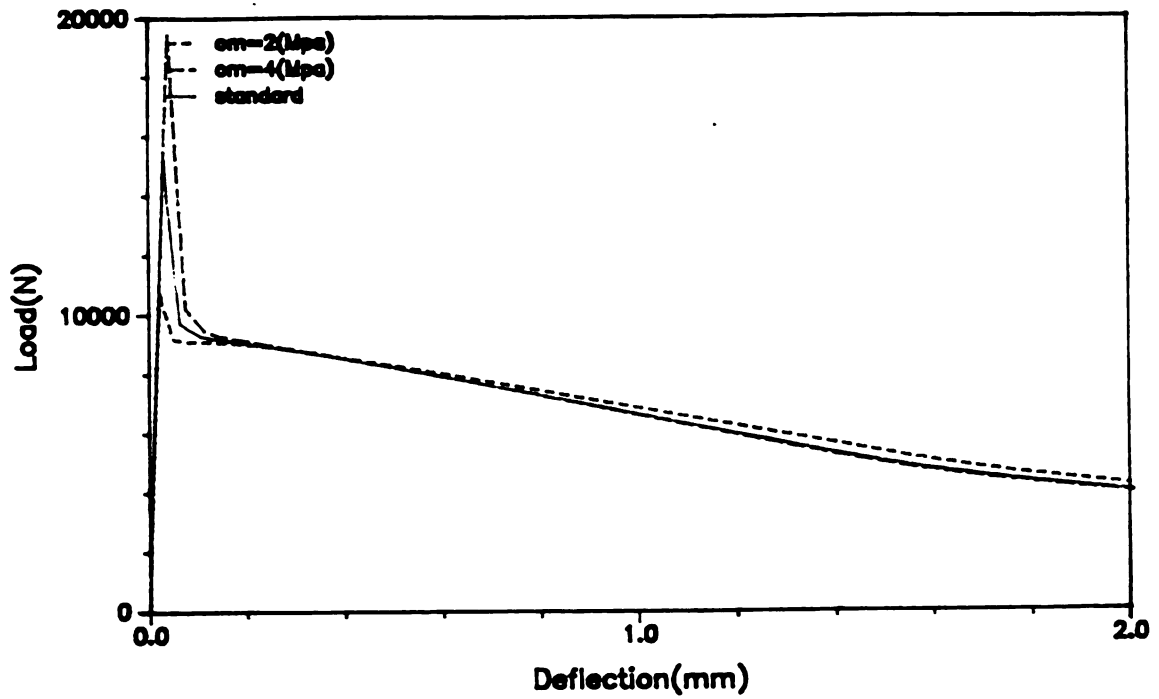
The ten material-related factors can be grouped in four different categories (Figure 5.10): (1) matrix strength (matrix tensile strength ( $\sigma_m'$ ) and matrix compressive strength ( $f_c'$ )); (2) matrix softening in tension (crack opening at post-peak residual tensile strength ( $S_{cr}$ ) and crack opening at post-peak zero tensile stress ( $S_{c0}$ )); (3) fiber dimensions (diameter ( $d_f$ ) and length ( $l_f$ )) and volume fraction ( $V_f$ ); and (4) fiber pull-out behavior (peak pull-out strength ( $\tau_u$ ), slip at peak pull-out strength ( $S_{pk}$ ) and slip at residual pull-out stress ( $S_r$ )). The

influences of factors in each of the above categories are discussed below.

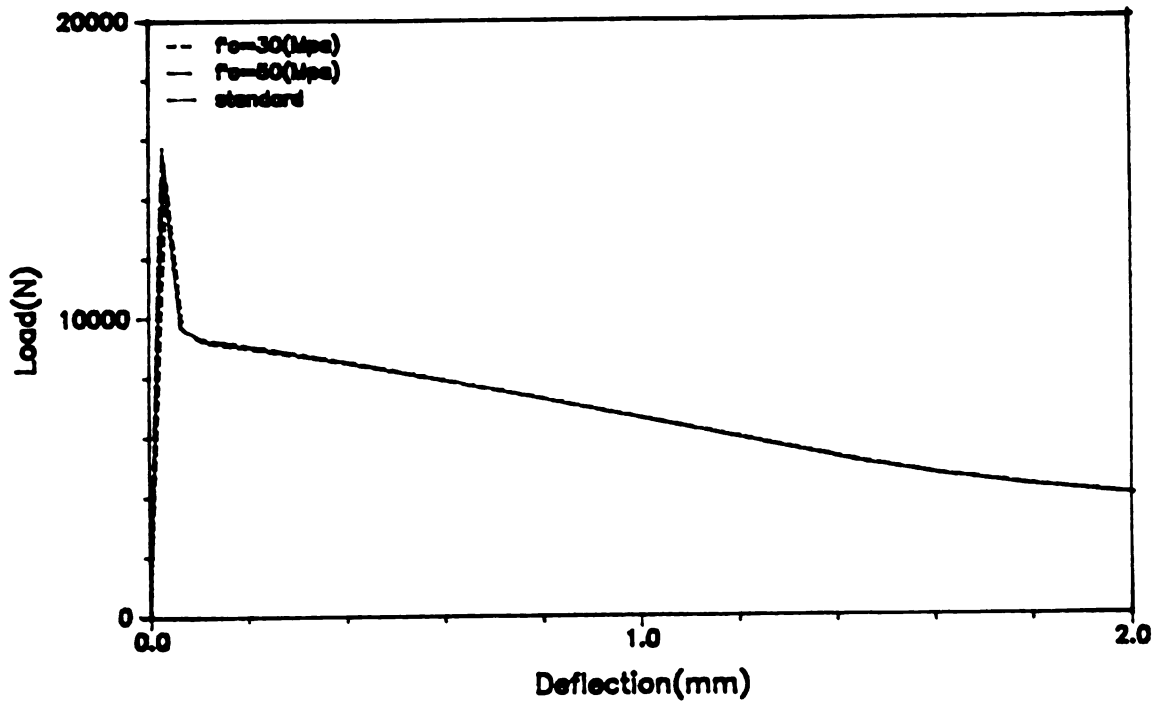
**Influence of Matrix Strength:** Figure 5.12(a) shows that increase (decrease) in matrix tensile strength ( $\sigma_m'$ ) increases (decreases) flexural strength. It is observed in this Figure, however, that matrix tensile strength has little influence on flexural toughness of SFRC. This is because in SFRC beam, as observed in previous section, the peak flexural strength of SFRC usually occurs when crack has already opened and has penetrated into the critical section. An increase in the matrix tensile strength can provide resistance against first crack opening, but as the crack widens and penetrates into the beam, the pre-peak behavior and peak tensile strength of steel fiber reinforced concrete tend to play less significant roles in deciding the post-peak flexural behavior of SFRC than the pull-out action of fibers bridging the crack.

Figure 5.12(b) shows that the compressive strength of plain concrete ( $f_c'$ ) has very little influence on the flexural behavior of SFRC. This is because pre-peak compressive constitutive behavior of SFRC is only partly utilized under flexure (due to the weak tensile strength of steel fiber reinforced concrete); the compressive strains at beam failure do not often reach the strain at peak compressive stress of SFRC.

The above qualitative observations regarding the effects of matrix strength characteristics are quantitatively verified in the first two rows of Table 5.2 (noting that a larger number is indicative of a larger effect of a certain factor on a certain aspect of flexural behavior). Comparison of numbers in the last column for the first two rows of Table 5.2 clearly indicates that the overall flexural performance characteristics of SFRC are much more sensitive to the tensile strength than to the compressive strength of the material.



(a) Effects of Matrix Tensile Strength

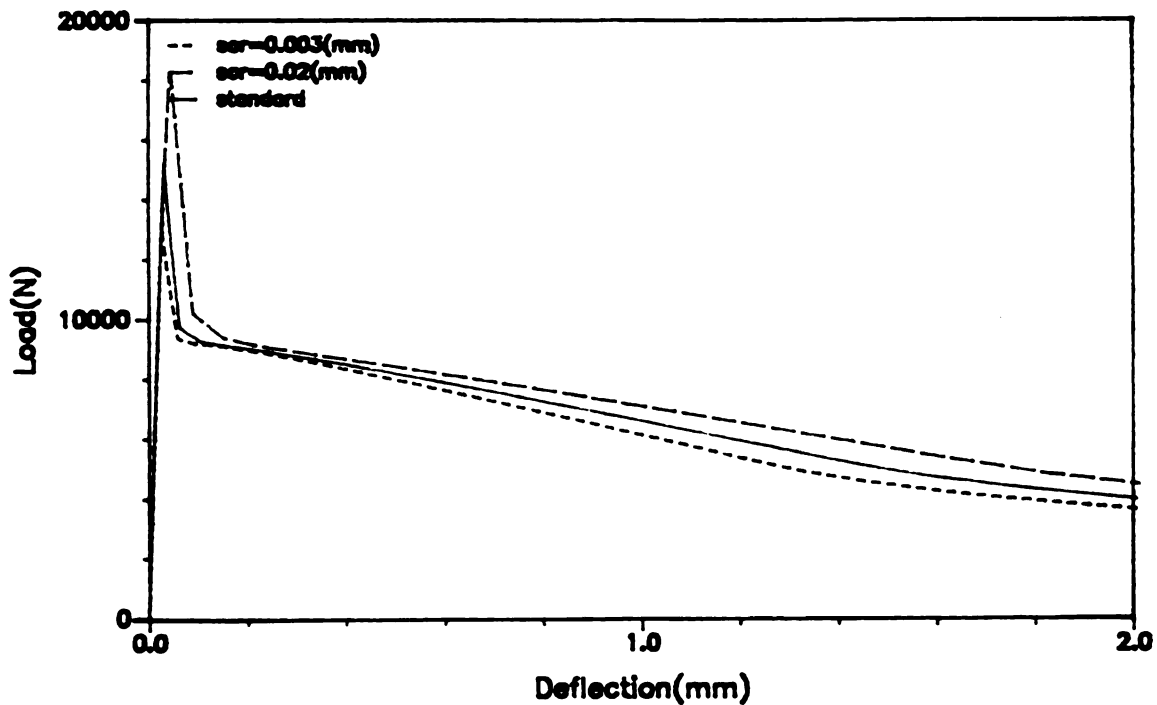


(b) Effects of Matrix Compressive Strength

Figure 5.12 Influence of Matrix Strength on Load-Deflection Curve

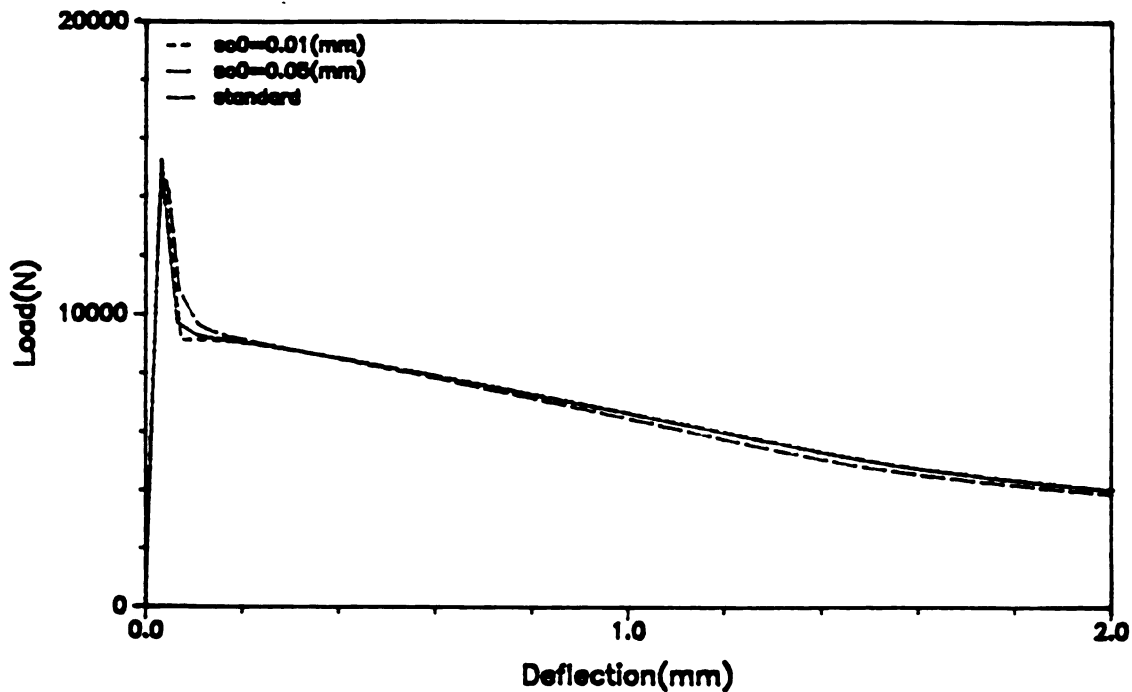
**Influence of Matrix Softening in Tension:** Figure 5.13(a) shows that the increase in crack opening at residual matrix tensile strength ( $S_{cr}$ ) increases the flexural strength and toughness of SFRC to some extent. Figure 5.13(b), on the other hand, shows negligible effects on flexural behavior of crack opening at zero matrix tensile stress ( $S_{c0}$ ). Contribution of the matrix tensile softening to flexural strength, ductility and toughness (Figure 5.13(a)) are indicative of relatively small crack openings across a part of the section in practically significant ranges of flexural behavior.

The above qualitative observations regarding the effects of the matrix tensile softening factors on flexural behavior are confirmed quantitatively in Table 5.2 (see rows 3 and 4).



(a) Effects of Crack Opening at Residual Matrix Tensile Strength

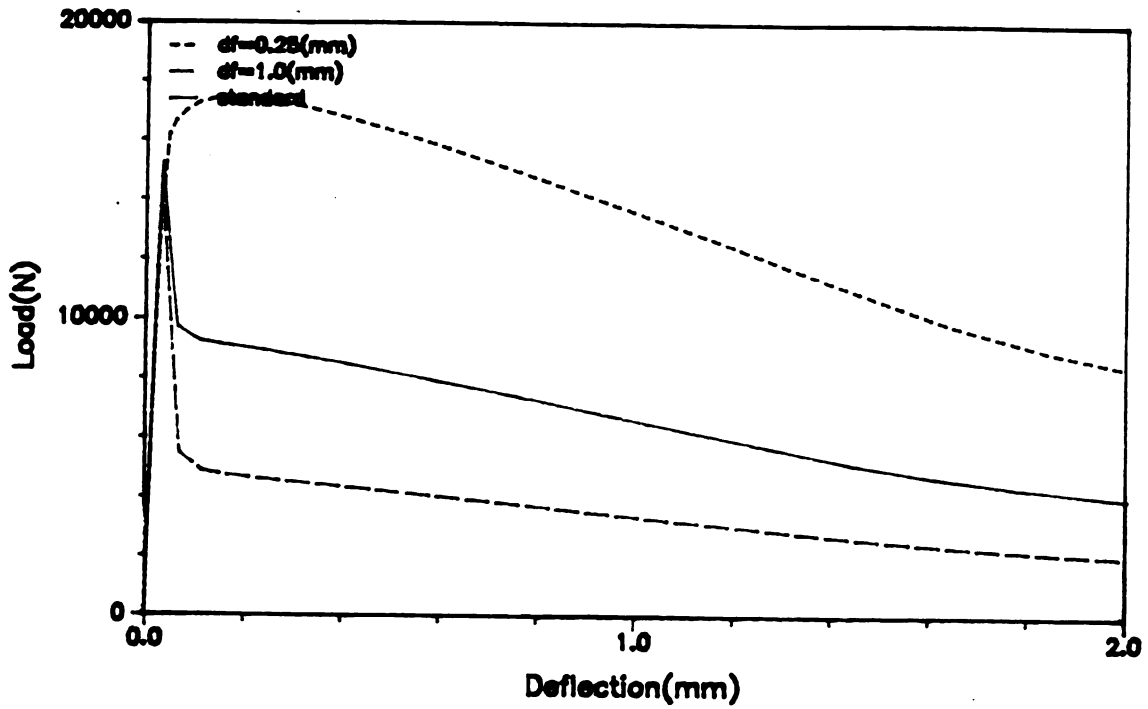
Figure 5.13 Influence of Matrix Softening in Tension on Load-Deflection Curve



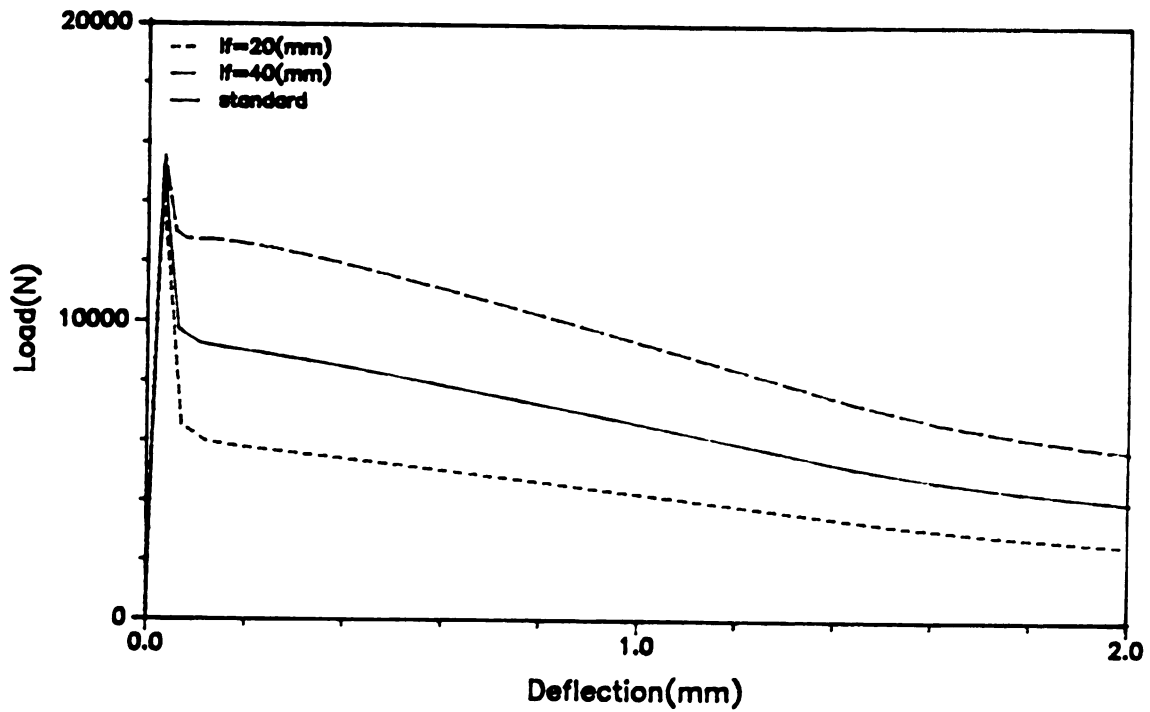
(b) Effects of Crack Opening at Zero Matrix Stress

Figure 5.13 Influence of Matrix Softening in Tension on Load-Deflection Curve (cont'd)

**Influences of Fiber Dimensions and Fiber Volume Fraction:** The effects of fiber diameter ( $d_f$ ) and fiber length ( $l_f$ ) at a fiber volume fraction of 1% are presented in Figures 5.14(a) and 5.14(b). Figure 5.14(a) shows that as the fiber diameter decreases, the peak flexural strength, ductility and toughness of SFRC increase. This may be attributed to the increase in the number of fibers per unit cross-sectional area and also in the available fiber-to-matrix interfacial bond area, which have favorable effects on flexural behavior at peak load and in the post-peak region. The increase in fiber length (Figure 5.14(b)), on the other hand, influences ductility, toughness but only to a relatively small extent the flexural strength of SFRC. The increase in fiber length for a given fiber volume fraction may reduce the number of fibers crossing unit cross-sectional area. Comparison of the effects of fiber diameter and length on flexural behavior in

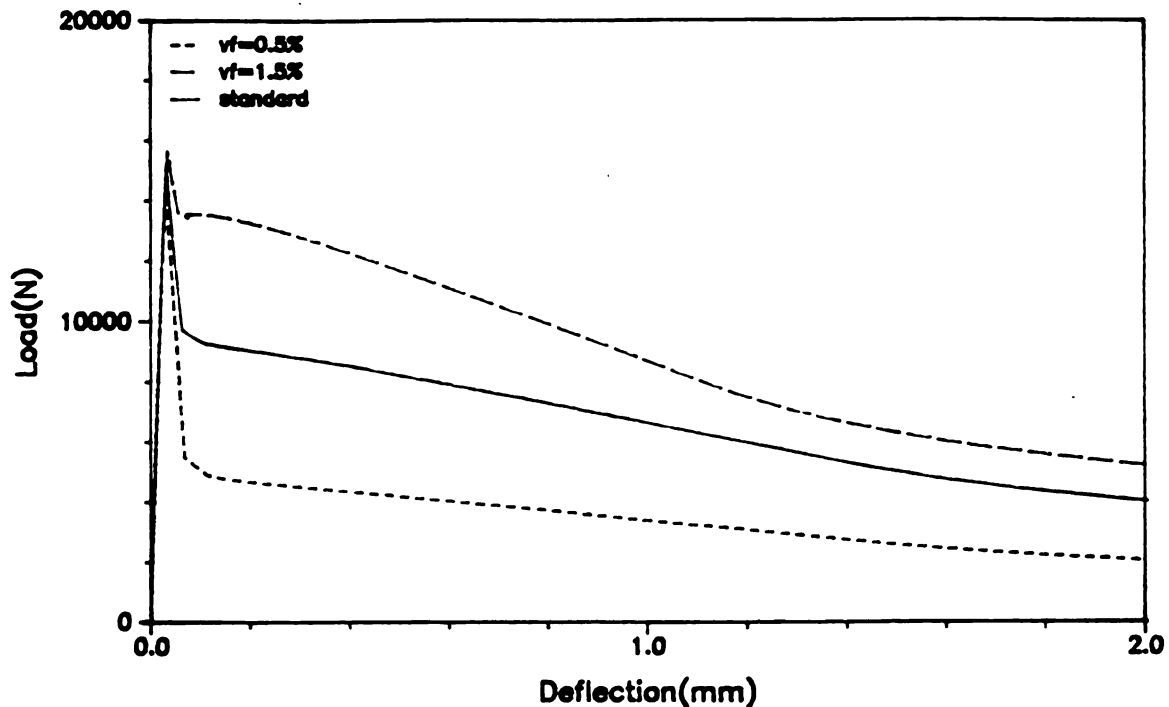


(a) Effects of Fiber Diameter



(b) Effects of Fiber Length

Figure 5.14 Influences of Fiber Dimensions and Fiber Volume Fraction



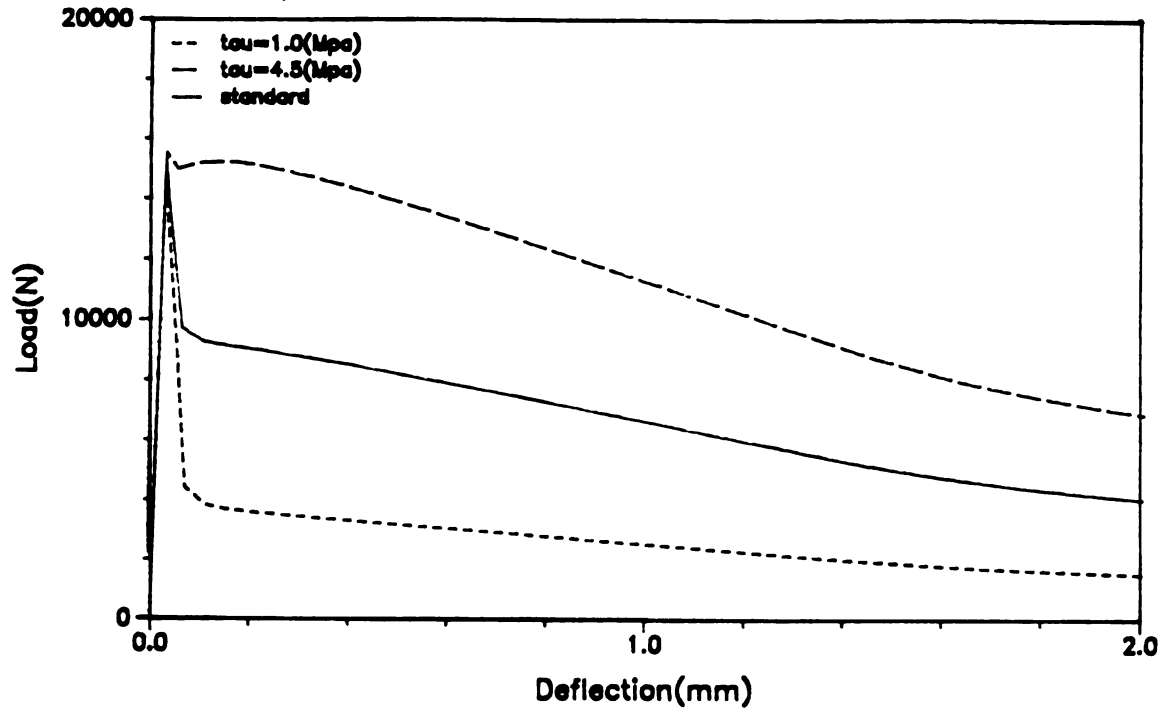
(c) Effects of Fiber Volume Fraction

Figure 5.14 Influences of Fiber Dimensions and Fiber Volume Fraction (cont'd)

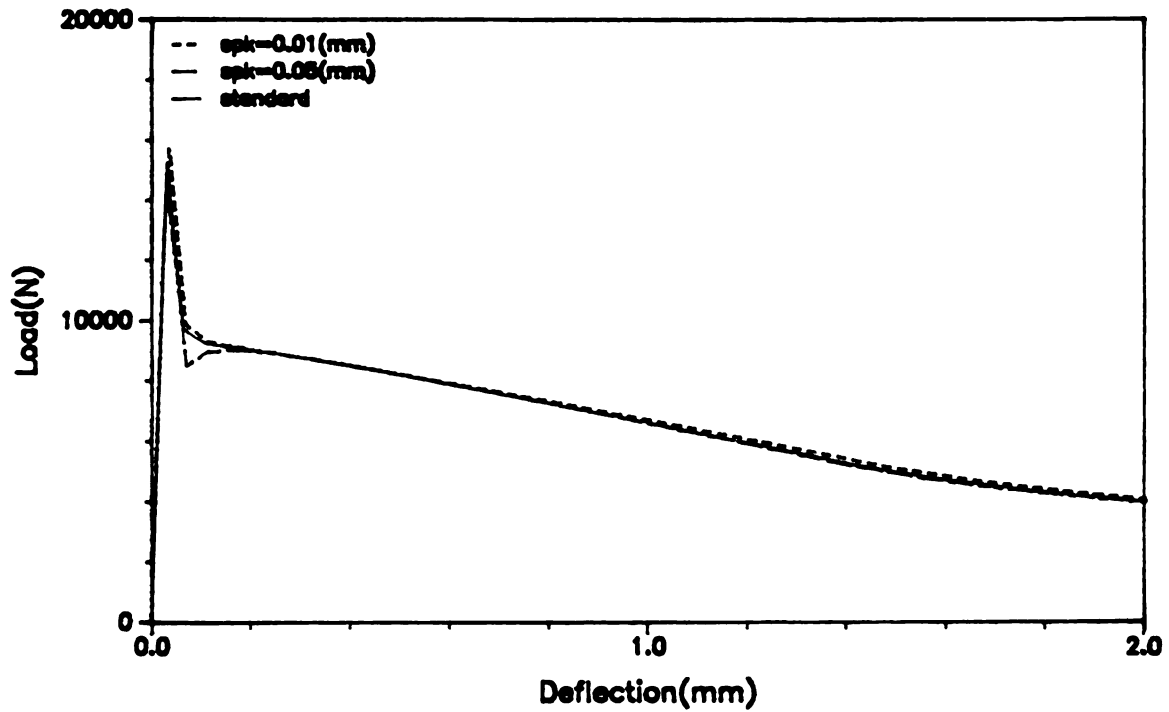
Table 5.2 (rows 5 and 6, respectively) confirms the fact that the flexural behavior of SFRC is more sensitive to variations in fiber diameter than those in fiber length.

Figure 5.14(c) illustrates the effects of fiber volume fraction ( $V_f$ ) on the flexural behavior of SFRC. The increase (decrease) in fiber volume fraction increases (decreases) the flexural ductility and toughness, and to some extent the flexural strength of SFRC. Table 5.2 (row 7) presents quantitative effects of fiber volume fraction on different aspects of the flexural behavior of SFRC; this factor is observed to have important effects on flexural behavior.

**Influence of Fiber Pull-Out Behavior:** Figure 5.15(a) shows that as the bond strength ( $\tau_u$ ) increases (decreases), the flexural ductility and toughness of SFRC tend to increase (decrease) significantly. The peak flexural strength is

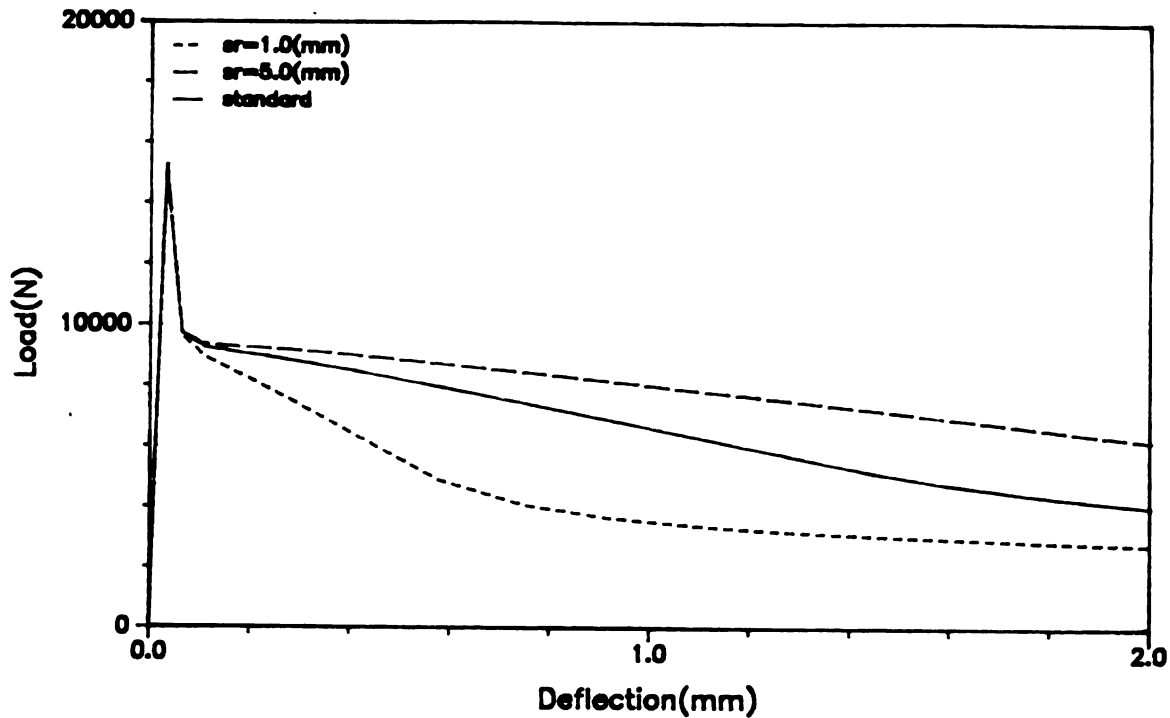


(a) Effects of Peak Fiber Pull-Out Strength



(b) Effects of Slip at Peak Fiber Pull-Out Strength

Figure 5.15 Influence of Fiber Pull-Out Behavior



(c) Effects of Slip at Residual Fiber Pull-Out Strength

Figure 5.15 Influence of Fiber Pull-Out Behavior (cont'd)

not much influenced by variations in bond strength. The significant effect of bond strength on post-peak flexural behavior of SFRC results from the fact that the pull-out action of steel fibers dominates the tensile behavior of cracked sections. Table 5.2 (row 8) quantitatively confirms the significant effects of the fiber-to-matrix bond strength on flexural ductility and toughness (and thus on the flexural behavior) of SFRC.

Slip at peak fiber pull-out strength ( $S_{pk}$ ) is observed in Figure 5.15(b) to have negligible effects on flexural behavior. This suggests that pull-out stiffness is not an important factor in deciding the flexural behavior of SFRC. Figure 5.15(c) shows that fiber slip at residual pull-out strength ( $S_r$ ) has relatively important effects on flexural ductility and toughness, but not on flexural strength of SFRC. Table 5.2 (rows 9 and 10) quantitatively confirms the above

observations regarding the effects of slip at peak fiber pull-out bond and at residual pull-out strength on the flexural behavior of SFRC.

As far as the constitutive behavior-related factors are concerned, Table 5.3 illustrates that factors such as  $t_3$  for composite peak tensile strength,  $t_4$  characterizing the plain matrix tensile softening behavior, and  $t_5$  deciding fiber pull-out resistance in the post-peak region, are the only factors with important effects on the flexural behavior of SFRC. The maximum changes due to variations in these factors occur in flexural ductility and toughness. Maximum changes, however, are below one-third of the values corresponding to "standard" conditions. These changes are relatively small when compared with those resulting from variations in influential material-related factors (which typically result in 70% to 80% variations in flexural performance characteristics). Table 5.4 summarizes the results of analyses based on  $2^k$  factorial design of Table 5.2 for the influence of material-related factors on flexural behavior. In Table 5.4, factors corresponding to higher numerical values are more influential than others in deciding a specific aspect of flexural behavior. According to this Table, matrix tensile strength ( $\sigma_m'$ ) is most influential in deciding the peak flexural load (P), while ductility (D), toughness (A) and overall flexural behavior (V) are most influenced by bond strength ( $\tau_u$ ). Except for factors such as matrix compressive strength ( $f_c'$ ), slip at peak pull-out strength ( $S_{pk}$ ), crack opening at residual matrix tensile strength ( $S_{cr}$ ) and matrix crack opening at zero stress ( $S_{co}$ ), the rest of material-related factors may be considered to have relatively important effects on the flexural behavior of SFRC.

The results of Table 5.2 and Table 5.4 are summarized in Table 5.5, which presents, in the order of significance, the influential material-related factors for each aspect of flexural behavior. This Table also shows the results obtained through simple observation of the flexural load-deflection curves.

Table 5.4 Effects of Material-Related Factors ( $2^k$  Factorial Design)

Factors	f - Values on Different Criteria (x 1000)			
	Peak Load	Ductility	Toughness	Overall Behavior
$\sigma_m$	1349	38	20712	20.14
$f_c$	22	0.32	249	0.19
$S_{cr}$	183	1.69	1889	0.08
$S_0$	0.71	0.0	489	0.02
$d_f$	383	161	706830	77
$l_f$	147	51	244490	34.4
$V_f$	244	91	425800	54.19
$\tau_u$	343	231	865120	84
$S_{pk}$	18	0.33	662	0.087
$S_r$	2.4	145	195130	60

Table 5.5 Effects of Material-Related Factors in Order

Criteria	Factors	Order					
		1	2	3	4	5	6
Peak Load	S.O *	$\sigma_m$	df	Scr	Vf	.....	.....
	2-k	$\sigma_m$	df	$\tau_u$	Vf	Sr	lf
Ductility	S.O.	$\tau_u$	Sr	df	lf	Vf	$\sigma_m$
	2-k	$\tau_u$	df	Sr	Vf	lf	$\sigma_m$
Toughness	S.O.	df	$\tau_u$	Vf	lf	Sr	.....
	2-k	$\tau_u$	df	Vf	lf	Sr	$\sigma_m$
Overall Behavior	S.O.	$\tau_u$	df	Vf	Sr	$\sigma_m$	lf
	2-k	$\tau_u$	df	Sr	Vf	lf	$\sigma_m$

\* Most important factor based on the "Simple Observation" of flexural load-deflection relationships.

It is interesting to note that generally similar results are obtained for the 2<sup>k</sup> factorial design and the simple observation of flexural load-deflection curves.

## 5.5 SUMMARY AND CONCLUSION

Under flexural loads, one major crack generally forms in steel fiber reinforced concrete at the critical section, in the vicinity of which a relief of tensile stresses occurs. After cracking, the critical section suffers severe distortions and thus plane sections do not remain plane in its vicinity. A flexural analysis procedure was developed which gives due consideration to the behavior at and near the critical (cracked) section.

The exact distributions of tensile and compressive strains in the critical region are rather complex. Some simplifying assumptions were made in order to simulate the flexural behavior at critical region. Before the crack starts to open, the moment and curvature distributions are similar in shape. As the flexural load increases beyond the first-crack load, the critical region is assumed to spread outward, and it stabilizes when the beam reaches its ultimate load, with curvature at the boundary of the critical region assumed to stay constant at the first-crack value. In the post-peak region, compressive strains in the critical region further increase while elastic flexural deformations outside critical region tend to decrease. This, together with the assumed constant values of curvature at the boundaries of the critical region, result in a tendency in deformations to increasingly concentrate near the center (cracked section) of the critical region.

The crack shape at the critical section is assumed to be linear and symmetric about a plane normal to the beam longitudinal axis. Assuming linear variations in compressive and tensile curvatures at the critical region (where the

tensile curvature is assumed to vary from zero at the crack to a value equal to the compressive side curvature at the boundary of the critical region), the crack opening angle could be obtained by computing the difference in rotations associated with compressive and tensile strains in the critical region. Maximum crack opening at the extreme bottom layer of the critical section could be obtained using this crack opening angle and the neutral axis position obtained by satisfying the equilibrium of tensile and compressive forces at the critical (cracked) section.

A step-by-step incremental approach was adopted for flexural analysis of SFRC beams. In each step, an increment is made in curvature on the compressive side of the cracked section, and numerical techniques (based on the Modified Regula-Falsi method) were used to iteratively decide the neutral axis position which satisfies equilibrium conditions. The tensile and compressive constitutive models of SFRC developed in this study were used in flexural analysis of the critical section. The assumptions described above were then used to derive the flexural behavior of complete beam using the critical section behavior at the end of each step.

Using the proposed analytical approach, the flexural behavior and stress profiles at the critical section were investigated at different loading stages with two different fiber volume fractions (0.5% and 1.2%). The results indicated that the peak flexural load at both fiber volume fractions is attained when the crack at critical section has already opened. This implies that flexural strength is reached in SFRC beams when the tensile behavior has already reached the post-peak region. The flexural strength of SFRC, therefore, seems to be dependent not only on the tensile strength of the material, but also on its post-peak tensile behavior. This further explains why the increase in flexural strength is typically higher than the corresponding increase in tensile strength for given fiber

reinforcement conditions. In addition, calculation of modulus of rupture based on linear-elastic flexural analysis equations does not seem to give a characteristic stress value which directly relates to the peak tensile strength of SFRC.

While a major fraction of the peak flexural resistance is maintained in the post-peak region for conditions with 1.2% fiber volume fraction, the load-carrying capacity with 0.5% fiber volume fraction drops suddenly in the post-peak regions.

The developed flexural analysis procedure was also used for a numerical parametric study on the influences of ten material-related and ten constitutive behavior-related factors on the flexural behavior of SFRC. The significance of these factors in deciding flexural performance characteristics was examined by simple observations of flexural load-deflection curves and also through statistical analysis based on  $2^k$  factorial design. The aspects of flexural behavior considered in this study were flexural peak load (P), ductility (D), toughness (A) and the overall flexural behavior of SFRC (V). The following conclusions could be derived using the results of this parametric study:

(1) The flexural strength of SFRC was most sensitive to the variation in matrix tensile strength.

(2) Ductility (D), toughness (A) and overall flexural behavior (V) are most influenced by fiber diameter and fiber pull-out strength.

(3) The effects on flexural behavior of the matrix compressive strength, crack opening at which matrix tensile stress diminishes, and fiber slip at peak pull-out load are negligible.

(4) Fiber dimensions (fiber diameter and fiber length) as well as fiber volume fraction have almost equally important effects on flexural behavior.

(5) While the matrix crack opening at residual matrix tensile strength has little effect on different aspects of flexural behavior, fiber slip at residual pull-out strength has relatively important effects on flexural ductility and overall flexural behavior of SFRC.

(6) Fiber-to-matrix bond strength ( $\tau_u$ ), fiber dimensions and volume fraction ( $d_f$ ,  $l_f$  and  $V_f$ ), matrix tensile strength ( $\sigma_m'$ ) and slip at residual pull-out strength ( $S_r$ ) are the most influential factors deciding the flexural behavior of SFRC.

(7) Similar observations were derived through analysis using  $2^k$  factorial design and also through simple observation of flexural load-deflection curves.

## CHAPTER 6

### INTERPRETATION OF FLEXURAL TEST RESULTS USING "SYSTEM IDENTIFICATION"

#### 6.1 INTRODUCTION

Flexural load-deflection relationships for steel fiber reinforced concrete are dependent on the tensile and compressive constitutive behavior of the material, which may be refined in the presence of strain gradients under flexural loads. Considering the relatively large amount of flexural test results available for steel fiber reinforced concrete, and the relative ease of conducting such tests (e.g., in comparison with direct tension tests), it seems to be important to develop techniques for interpreting the flexural test data in order to obtain basic information on the tensile and compressive constitutive behavior of steel fiber reinforced concrete. Obtaining basic information in constitutive behavior of the material from flexural test results may be called an "Inverse Problem."

"Inverse Problem" is solved in this investigation by using the method of "System Identification" [71]. Experimental test results on flexural load-deflection relationship are used to derive some material characteristic values related to the tensile constitutive behavior of SFRC. The derived values are then compared with analytically, and experimentally obtained values, and some discussions are made regarding the strain gradient effects on constitutive behavior of steel fiber reinforced concrete.

## 6.2 "SYSTEM IDENTIFICATION"

Most engineering problems are referred to as direct because a prediction of the output of a physical system is sought when the characteristics of the system and the input are known. In the "Inverse Problem," on the other hand, the response of the system to a given input is known from experiments and a mathematical model is to be found which will describe the material behavior.

In order to solve the "Inverse Problem" successfully, the mathematical models which can simulate both the physical flexural behavior of SFRC and constitutive behavior of the material must be well established. The characteristic material values in constitutive models are then adjusted until the best possible correlation is achieved between the predicted and measured response of SFRC under flexure. This process of selecting the form of the model and then, using measured test data, systematically adjusting the parameters based on a predefined criterion until the best correlation is achieved between the predicted and measured responses is called "System Identification."

A mathematical form for error function is needed to measure the correlation between test results and predictions of the mathematical model for a given set of characteristic values. The error function should be able to quantify the differences in important flexural characteristics of SFRC. If there are  $N$  parameters in the model, the error function can be viewed as an  $N$ -dimensional surface in a space with  $N+1$  dimensions (see Figure 6.1). "System Identification" deals with finding the location on the surface with minimum error, the coordinates of which will be the desired optimizing parameters. With good models of physical systems, resulting characteristic values of the optimum set will represent true behavior of the materials under the given loading system [71].

$$E = \sum_{i=1}^3 \omega_i \cdot e_i^2$$

$$e_1 = \left[ \frac{P_e - P_t}{P_e} \right];$$

$$e_2 = \left[ \frac{D_e - D_t}{D_e} \right];$$

$$e_3 = \left[ \frac{A_e - A_t}{A_e} \right];$$

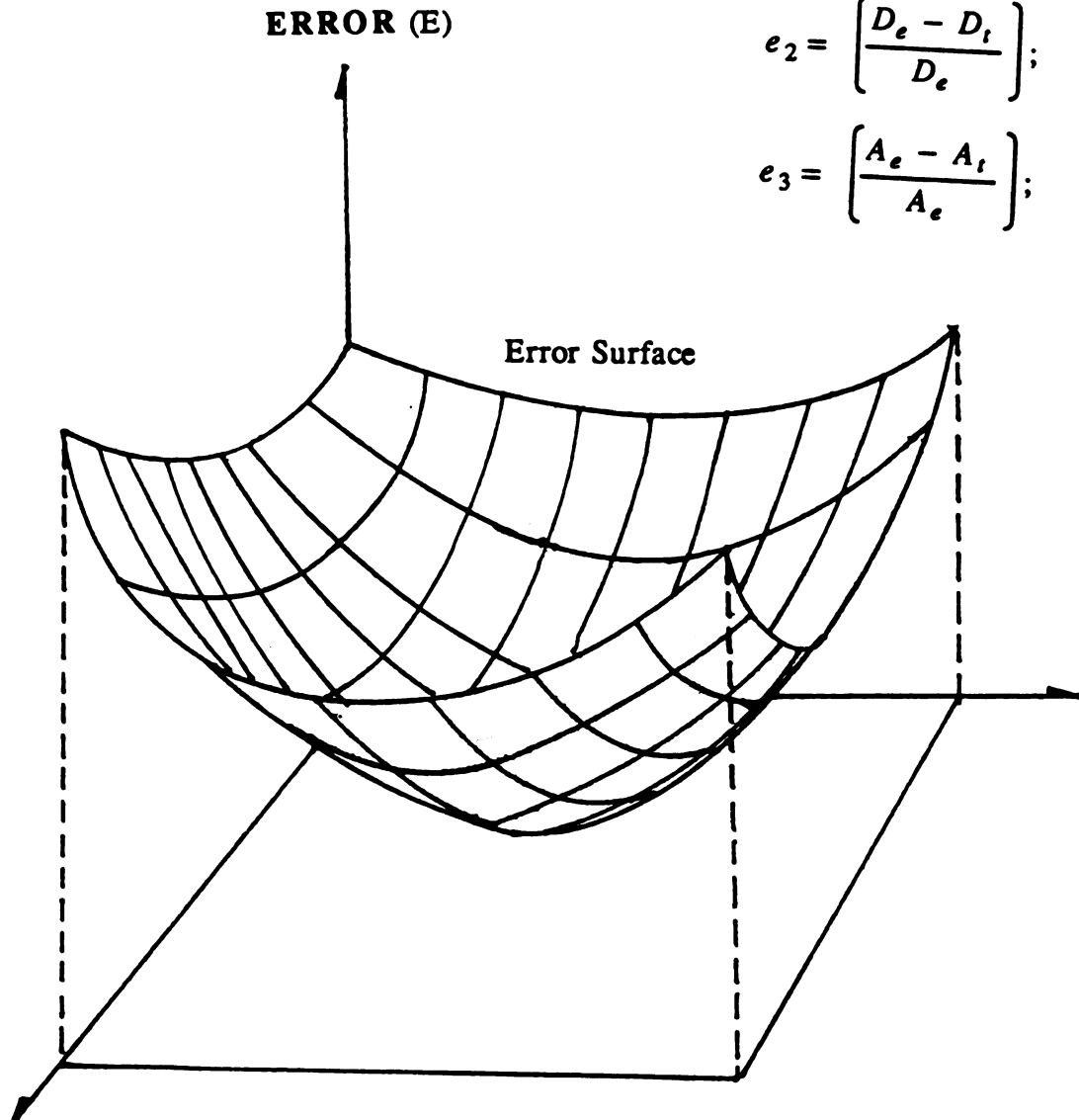


Figure 6.1 Error Surface in Parameter Space (Case of  $N = 2$ )

A mathematical optimization technique is needed to arrive successfully at this optimum point in error space. The method should be able to find correct search directions as well as minimum point in that direction with reasonable efficiency.

In this study, test results for steel fiber reinforced concrete beams subjected to flexural loading have been used to identify characteristic values of the tensile constitutive behavior of steel fiber reinforced concrete (using the tensile constitutive model of SFRC developed in this investigation which is partly based on a pull-out load-slip model for steel fibers). In order to simulate the steel fiber reinforced concrete behavior under flexural loading, compressive and tensile constitutive models of SFRC derived in previous Chapters were incorporated into the flexural analysis procedure developed in Chapter 5. An error function similar to the one defined in Chapter 5 for the measurement of overall flexural behavior of SFRC was applied to the flexural load-deflection relationships of steel fiber reinforced concrete. Three important characteristic parameters of the tensile constitutive behavior of SFRC were then selected out of the ten material-related and ten constitutive behavior-related factors related to the constitutive behavior of SFRC, and these three parameters were then optimized, while other factors were kept constants at "standard" values.

In the following sections, the process of "System Identification" will be illustrated and discussions will be made on the results of "System Identification" when applied to the flexural test results for SFRC.

### 6.3 DEFINITION OF ERROR FUNCTION

The error function (E) is defined to measure the correlation in overall flexural behavior between the experimentally measured and theoretically predicted load-deflection relationships. Based on discussions made in section 5.4 of Chapter 5, the characteristic values expressing the flexural behavior of SFRC are peak flexural load (P), flexural ductility (D), and flexural toughness (A). The differences in these characteristic values set the basis for computing the error between predicted and experimental flexural load-deflection relationships:

$$E = \sum_{i=1}^3 \omega_i \cdot e_i^2 \quad (6.1)$$

where:

$\omega_i$  = *weighing coefficient for each factor*

= 1.0 in this investigation ;

$$e_1 = \left[ \frac{P_e - P_t}{P_e} \right];$$

$$e_2 = \left[ \frac{D_e - D_t}{D_e} \right];$$

$$e_3 = \left[ \frac{A_e - A_t}{A_e} \right];$$

$P$  = *ultimate load (Figure 5.11) ;*

$D$  = *ductility*

=  $P / P_r$ , (see Figure 5.11) ;

$A$  = *toughness*

= *area under load-deflection curve*  
*as defined in Figure 5.11 .*

A desirable match between experimental and theoretical result is achieved when the value of this error function is minimized.

## 6.4 METHOD OF OPTIMIZATION

The error function derived in the previous section is an objective measure of how well the model fits the experimental data. The error function should be minimized in the N-parametric space. Nonlinear programming techniques should be used for this purpose. These techniques can be categorized in two groups: unconstrained and constrained. The nature of the present study suggests that the minimum point lies in the interior of the feasible region of the parameter space rather than on its boundary, and thus unconstrained nonlinear programs suit this problem.

An iterative minimization algorithm was used in the related unconstrained nonlinear programming approach. It starts at some arbitrary point  $\mathbf{x}_0$  in the parameter space (small bold letter implies vector in N-dimensional space, and capital bold letter implies matrix) and chooses a sequence of steps which will be taken, leading to the global minimum of a given function. The algorithm must be able to converge to a stationary point in the global sense and should also converge rapidly when it is in the neighborhood of a local minimum [72]. The iterative minimization approach adopted in this investigation is described below (see Figure 6.2).

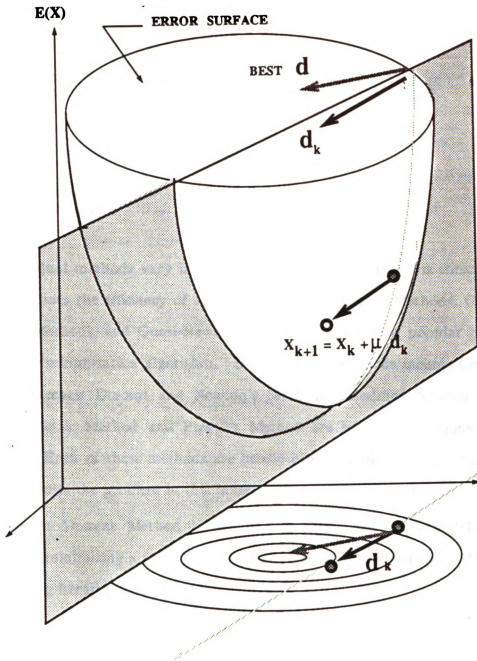


Figure 6.2 The Iterative Minimization Procedure

Starting from the point in the parameter space selected after  $k$  steps ( $\mathbf{x}_k$ ), choose the next point as follows:

$$\mathbf{x}_{k+1} = \mathbf{x}_k + \mu \cdot \mathbf{d} \quad (6.2)$$

where:

$\mathbf{d}$  = *direction search vector; and*

$\mu$  = *step length.*

Individual methods vary in their choice of  $\mu$  and  $\mathbf{d}$  and this choice in general determines the efficiency of the method. Basic Descent Methods, Conjugate Direction Methods, and Quasi-Newton Methods are the most popular ones used in iterative minimization algorithm. Basic Descent Methods include Coordinate Descent, Steepest Descent and Newton's Method. Modified Newton Method, Variable Metric Method and Powell's Method are examples of Quasi-Newton Methods. Each of these methods are briefly discussed in the following and the one which suits the problem in this investigation will be selected.

Steepest Descent Method is one of the oldest and most widely known method for minimizing a function of several variables. The method is defined by the following iterative algorithm:

$$\mathbf{x}_{k+1} = \mathbf{x}_k - \alpha_k \cdot \mathbf{g}_k \quad (6.3)$$

where  $\alpha_k$  is a non-negative scalar minimizing the function value  $f(\mathbf{x}_k - \alpha \cdot \mathbf{g}_k)$ , and  $\mathbf{g}_k$  is a gradient of the given function ( $\nabla f^T$ ). It can be shown that if  $f$  is a quadratic function, then for any initial point  $\mathbf{x}_0$ , the method converges to the

unique minimum point of function  $f$ .

Coordinate Descent, as its name implies, searches in the coordinate direction. By sequentially minimizing with respect to different components, a relative minimum of  $f$  might be ultimately determined. Convergence rate is, in general, slower compared to that of Steepest Descent Method.

The idea behind Newton's Method is that the function,  $f$ , may be minimized locally by approximating it as a quadratic function, and this approximate function then is minimized exactly. Near the point  $\mathbf{x}_k$  function  $f$  is approximated by the truncated Taylor series:

$$f(\mathbf{x}) = f(\mathbf{x}_k) + \nabla f(\mathbf{x}_k) \cdot (\mathbf{x} - \mathbf{x}_k) + \frac{1}{2} \cdot (\mathbf{x} - \mathbf{x}_k)^T \cdot \mathbf{F}(\mathbf{x}_k) \cdot (\mathbf{x} - \mathbf{x}_k) \quad (6.4)$$

Note that  $\mathbf{F}(\mathbf{x}_k)$  is the Hessian matrix and the right hand side is minimized at:

$$\mathbf{x}_{k+1} = \mathbf{x}_k - \mathbf{F}(\mathbf{x}_k)^{-1} \cdot \nabla f(\mathbf{x}_k)^T \quad (6.5)$$

This iteration method provides a good local convergence with an order of at least two ( i.e.  $|\mathbf{x}_{k+1} - \mathbf{x}^*| \leq |\mathbf{x}_k - \mathbf{x}^*|^2$  ), where  $\mathbf{x}^*$  is a true solution. Newton's method is then usually modified properly to accommodate the possible non-positive definiteness at regions remote from the solution.

Conjugate Direction Methods are analyzed mainly for quadratic problems. These methods have been proved to be extremely effective in dealing with general objective functions and are considered to be the best general purpose methods presently available. These methods assume the following quadratic function:

$$f = \frac{1}{2} \cdot \mathbf{x}^T \mathbf{Q} \mathbf{x} + \mathbf{b}^T \mathbf{x} + c \quad (6.6)$$

where  $\mathbf{Q}$  is positive definite. Using  $n$ -conjugate vectors  $( \left\{ \mathbf{d}_i \right\}_{i=1}^n )$  with respect to  $\mathbf{Q}$ , minimum of this function is found after  $n$  steps by generating the following sequence of  $\mathbf{x}_k$ :

$$\mathbf{x}_{k+1} = \mathbf{x}_k + \alpha_k \cdot \mathbf{d}_k ; \quad (6.7)$$

$$\alpha_k = - \frac{\mathbf{p}_k^T \mathbf{d}_k}{\mathbf{d}_k^T \mathbf{Q} \mathbf{d}_k} ; \text{ and}$$

$$\mathbf{p}_k = \mathbf{Q} \mathbf{x}_k - \mathbf{b}$$

Under the assumption that evaluation and inversion of the Hessian matrix is impractical or costly, the idea underlying Quasi-Newton Method is to use an approximation to the inverse Hessian in place of the true inverse that is required in Newtons Method. A basic iterative process takes the form of:

$$\mathbf{x}_{k+1} = \mathbf{x}_k - \alpha_k \cdot \mathbf{M}_k \mathbf{g}_k \quad (6.8)$$

where;

$$\mathbf{g}_k = \nabla f(\mathbf{x}_k)^T ; \text{ and}$$

$$\mathbf{M}_k = \text{symmetric } n \times n \text{ matrix}$$

$\alpha_k$  is chosen to minimize  $f(\mathbf{x}_{k+1})$  and  $\mathbf{M}_k$  is derived to be closer to inverse of the Hessian matrix.

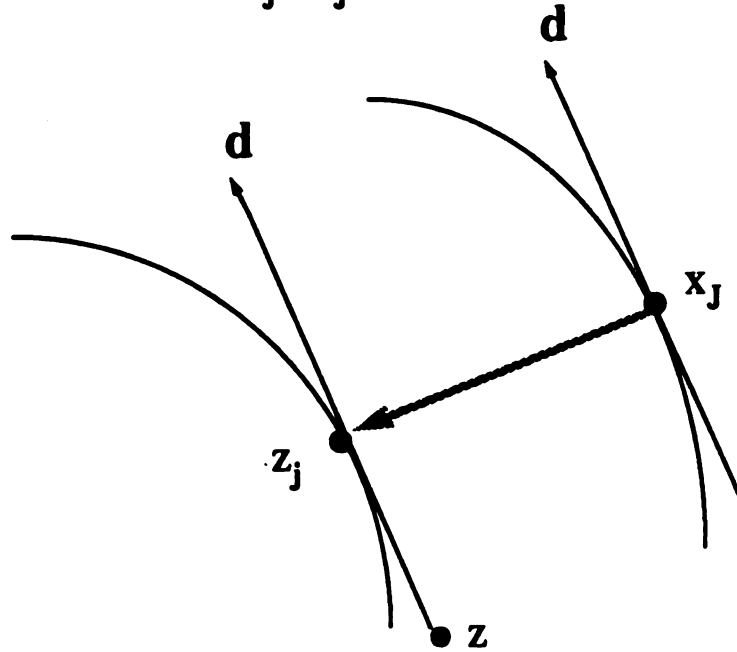
All methods described above require the use of the gradient vector, for which analytical expressions are assumed to exist. However, calculation of the gradient numerically rather than analytically may be desirable or even necessary. As the calculation of partial derivatives of  $f$  is, in general, at least as complicated as  $f$ , a method which avoids the calculation of derivatives has the possibility of being more efficient as well as having the advantage of being more convenient to use. One such method has been given by Powell [73]. This method uses the following two main theorems:

Theorem 1. Let  $f(\mathbf{x}) = \frac{1}{2} \cdot \mathbf{x}^T \mathbf{S} \mathbf{x} + \mathbf{b}^T \mathbf{x} + c$ , where  $\mathbf{S}$  is a symmetric and positive definite  $n \times n$  matrix. Let  $\mathbf{x}_j$  minimize  $f(\mathbf{x})$  in the direction  $\mathbf{d}$  and let  $\mathbf{z}$  be a point that is not on the line  $\mathbf{l} = \mathbf{x}_j + t \cdot \mathbf{d}$ . If  $\mathbf{z}_j$  minimizes  $f(\mathbf{x})$  on the line  $\mathbf{l} = \mathbf{z} + r \cdot \mathbf{d}$ , then the direction  $\mathbf{z}_j - \mathbf{x}_j$  is conjugate to  $\mathbf{d}$ .

Theorem 2. Let  $\mathbf{d}_k, k = 1, 2, \dots, m$  ( $\leq n$ ), be mutually conjugate. Then the global minimum of  $f(\mathbf{x})$  in  $m$ -dimensional space containing  $\mathbf{x}_1$  and the directions  $\mathbf{d}_k$  may be found by searching along each of these directions once only.

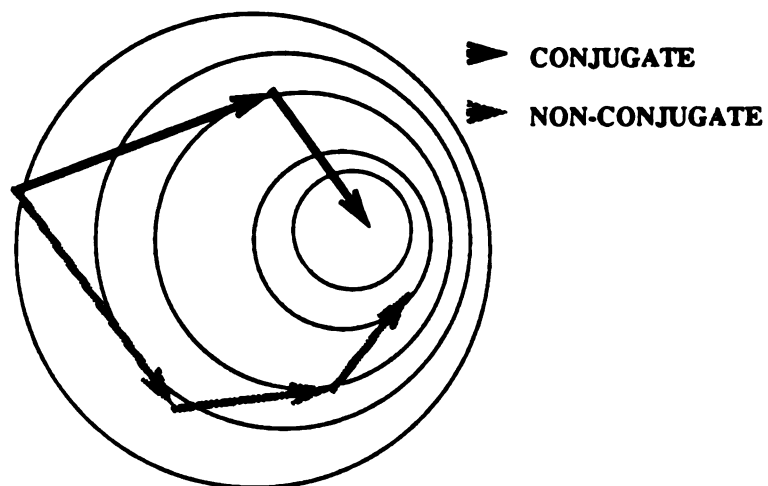
Figures 6.3(a) and (b) illustrate Theorem 1 and Theorem 2, respectively. Proofs for both theorems are given in Reference 74. The basic Powell's algorithm chosen for use in this study is presented below and it is followed by introducing a related modification regarding the choice of direction vectors.

**THEOREM 1:  $(z_j - x_j)$  IS CONJUGATE TO  $d$ .**



(a) Theorem 1

**THEOREM 2: THE GLOBAL MINIMUM OF A FUNCTION CAN BE FOUND BY SEARCHING ALONG EACH OF THE CONJUGATE DIRECTION ONCE ONLY.**



(b) Theorem 2

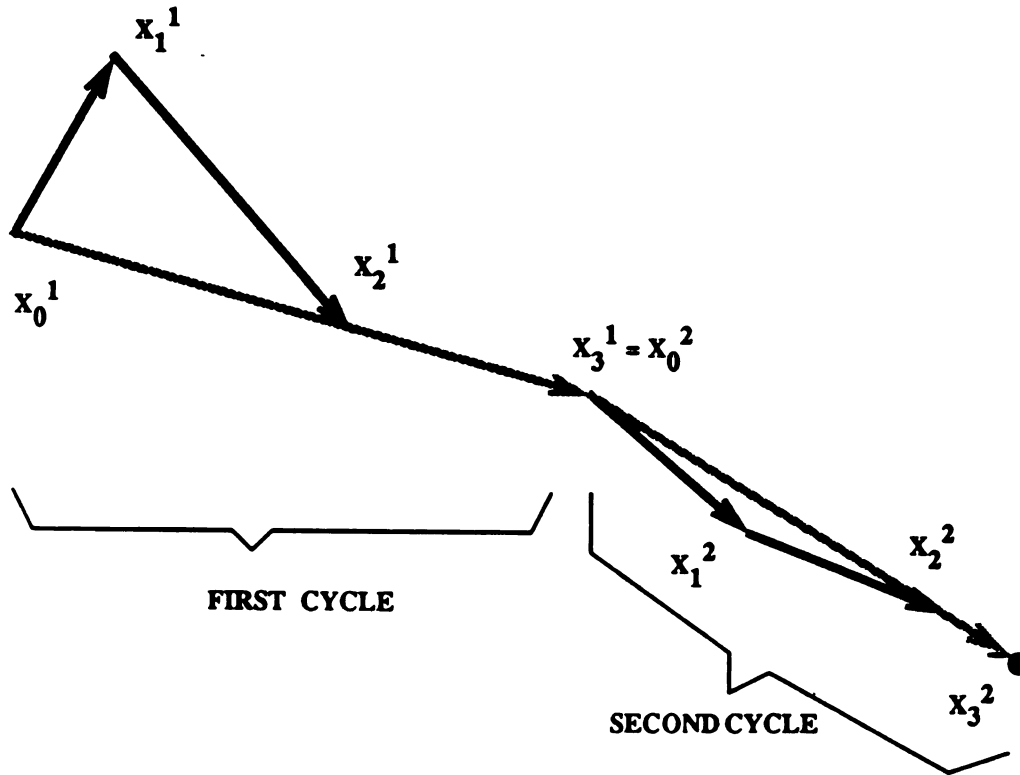
Figure 6.3 Main Theorems Used in Powell's Algorithm

The  $k^{\text{th}}$  iteration of this method starts with a current point  $\mathbf{x}_k$  and  $n$  directions,  $\mathbf{d}_{k,j}$ ,  $j = 1, 2, \dots, n$ . At the beginning,  $\mathbf{x}_1$  and  $\mathbf{d}_{1,j}$  are assumed to be given.

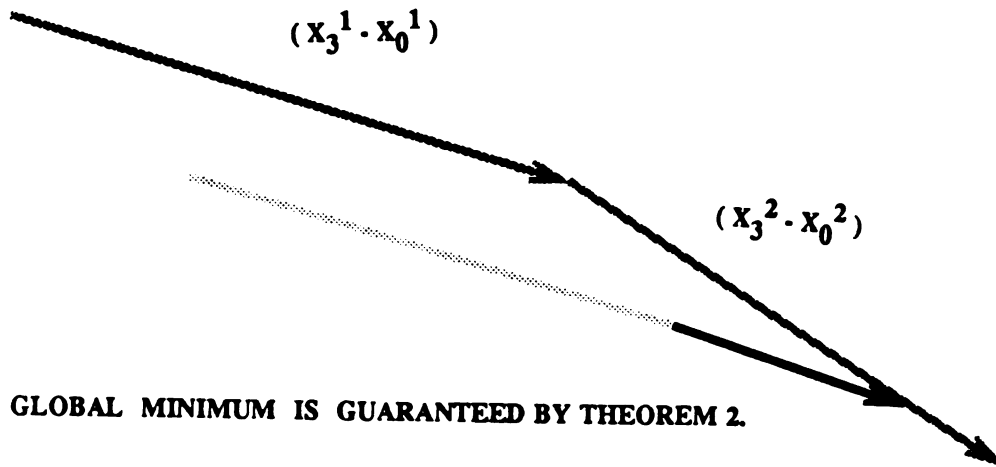
1. Let  $\mathbf{y}_{k,0} = \mathbf{x}_k$ .
2. Find  $\lambda_j^*$  which minimizes  $f(\mathbf{y}_{k,j-1} + \lambda_j \cdot \mathbf{d}_{k,j})$  and let  $\mathbf{y}_{k,j} = \mathbf{y}_{k,j-1} + \lambda_j^* \cdot \mathbf{d}_{k,j}$  for  $j = 1, 2, \dots, n$ .
3. Let  $\delta_k = \mathbf{y}_{k,n} - \mathbf{x}_k$ .
4. Find  $\lambda_n^*$  which minimizes  $f(\mathbf{y}_{k,n} + \lambda_n \cdot \delta_k)$  and let  $\mathbf{x}_{k+1} = \mathbf{y}_{k,n} + \lambda_n^* \cdot \delta_k$ .
5. Let  $\mathbf{d}_{k+1,j} = \mathbf{d}_{k,j+1}$ ,  $j = 1, 2, \dots, n-1$ , and  $\mathbf{d}_{k+1,n} = \delta_k$ . The direction  $\mathbf{d}_{k,1}$  is discarded in favor of a new direction  $\delta_k$ .
6. Go to step 1 and restart for  $(k + 1)^{\text{th}}$  step.

The  $k^{\text{th}}$  cycle which contains  $(n+1)$  subcycles for finding minimum along the given direction is schematically shown in Figure 6.4 for  $n = 2$ . In this Figure, superscripts and subscripts represent the subcycle number and iteration number in a certain subcycle, respectively.

The above Powell's algorithm produces  $n$  mutually conjugate directions in  $n$  iterations (i.e.,  $k = n$ ). The method, however, breaks down when the  $n$  directions for an iteration become linearly dependent. This happens if  $(\mathbf{y}_{k,n} - \mathbf{y}_{k,0})^T \cdot (\mathbf{y}_{k,1} - \mathbf{y}_{k,0})$  becomes zero. This implies that by discarding  $\mathbf{d}_{k,1}$  for  $(k + 1)^{\text{th}}$  step, one of the conjugate directions is lost and thus it never reaches minimum of the function. Powell [74] modified his basic method to overcome this type of difficulty by allowing a direction other than  $\mathbf{d}_{k,1}$  to be discarded after the  $k^{\text{th}}$  iteration. This modification, however, sometimes allows one of the mutually conjugate directions to be discarded, so that more than  $n$  iterations are required in order to find the minimum of a positive definite quadratic



(a) Iterative Procedure



GLOBAL MINIMUM IS GUARANTEED BY THEOREM 2.

(b) Conjugacy of Vectors  $(x_3^1 - x_0^1)$  and  $(x_3^2 - x_0^2)$

Figure 6.4 Main Theorems in Powell's Algorithm for  $N = 2$

function. The direction to be discarded, if any, is chosen using the condition that by discarding one of  $\mathbf{d}_{k,j}$ 's,  $j=1,2,\dots,n$ , the determinant of the matrix,  $[\mathbf{d}_{k,1}, \mathbf{d}_{k,2}, \dots, \mathbf{d}_{k,j-1}, \delta_k, \mathbf{d}_{k,j+1}, \dots, \mathbf{d}_{k,n}]$  is made as large as possible. For  $k^{\text{th}}$  iteration, it proceeds as follows :

1. Let  $\mathbf{y}_{k,0} = \mathbf{x}_k$  and for  $j=1,2,\dots,n$ , search from  $\mathbf{y}_{k,j-1}$  in the direction  $\mathbf{d}_{k,j}$  for a minimum at  $\mathbf{y}_{k,j}$ .
2. Find  $\Delta = \text{Max. } |f(\mathbf{y}_{k,j-1}) - f(\mathbf{y}_{k,j})| = |f(\mathbf{y}_{k,q-1}) - f(\mathbf{y}_{k,q})|$  where  $q$  is the value of  $j$  maximizing  $\Delta$  in  $j=1,2,\dots,n$ .
3. Define  $f_1 = f(\mathbf{y}_{k,0})$  and  $f_2 = f(\mathbf{y}_{k,n})$ . Then evaluate  $f_3 = f(2 \cdot \mathbf{y}_{k,n} - \mathbf{y}_{k,0})$ .
4. If either  $f_3 \geq 1$  or  $(f_1 - 2 \cdot f_2 + f_3) \cdot (f_1 - f_2 - \Delta)^2 \geq \frac{1}{2} \cdot \Delta \cdot (f_1 - f_3)^2$  then use old directions,  $\mathbf{d}_{k,j}$ ,  $j=1,2,\dots,n$ , for  $(k+1)^{\text{th}}$  iteration and put  $\mathbf{x}_{k+1} = \mathbf{y}_{k,n} = \mathbf{y}_{k+1,0}$ . Otherwise use rule 5.
5. Determine  $\mathbf{x}_{k+1}$  as in the  $k^{\text{th}}$  iteration of Powell's basic method, but take the directions of  $\left\{ \mathbf{d}_{k,1}, \mathbf{d}_{k,2}, \dots, \mathbf{d}_{k,q-1}, \mathbf{d}_{k,q+1}, \dots, \mathbf{d}_{k,n}, \delta_k \right\}$ . The supporting theorems and proofs are given in References 73 and 74.

In Powell's method,  $(n+1)$  line searches are needed to generate one conjugate direction. Therefore, to find the global minimum point (assuming that the given function is quadratic and positive definite) a total of  $n(n+1)$  line searches are required. Since in the Powell's method, the error function is being approximated by a quadratic function, it seems to be appropriate to use quadratic line search. In the present study, the method of quadratic line search described by Powell [73] has been used. This method basically discards one of three points

which is farthest from the turning point and then obtains a new current point by taking the specified distance in the given direction such that the function value is decreasing (see Figure 6.5). The newly found point and two existing points are then used to fit the quadratic curve, and the same procedures are repeated until the approximated minimum is within a satisfactory tolerance.

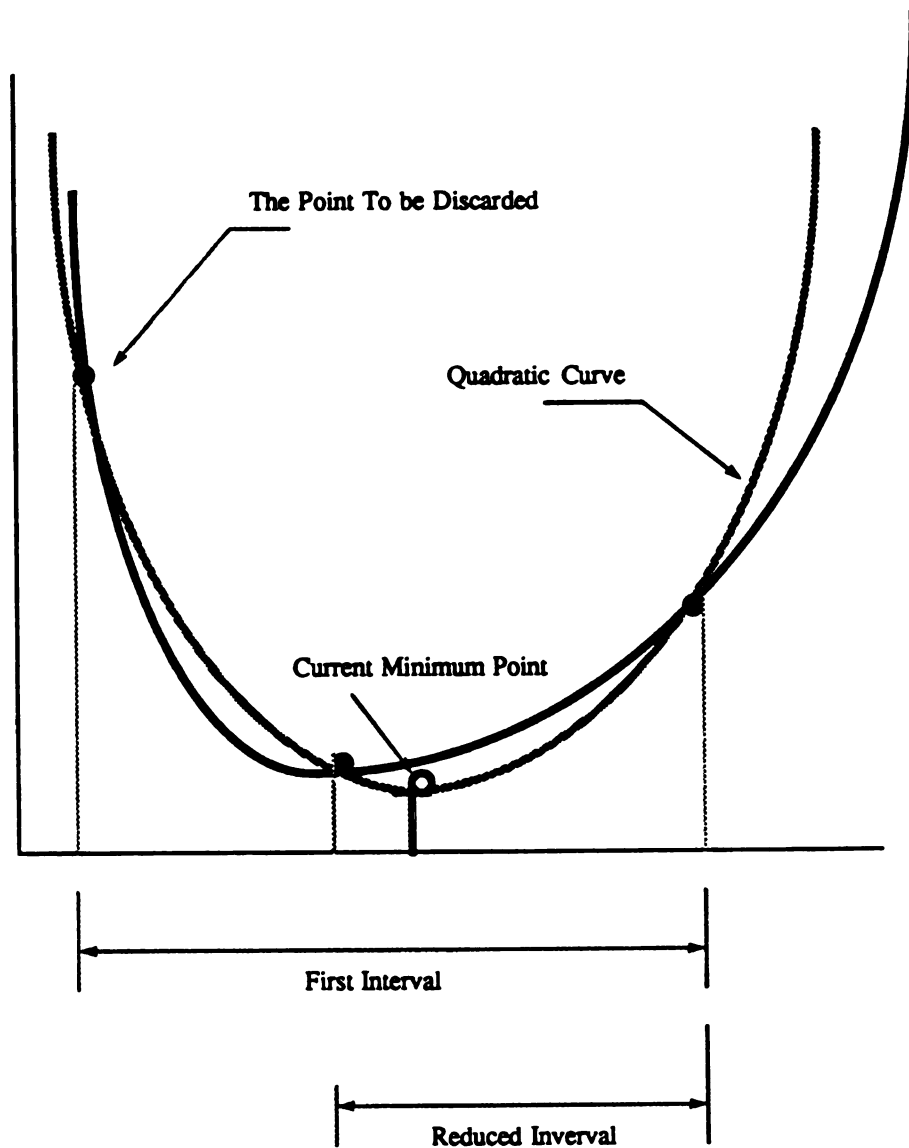


Figure 6.5 Quadratic Line Search

## 6.5 SELECTION OF PARAMETERS IN "SYSTEM IDENTIFICATION"

The flexural model contains ten material-related and ten constitutive behavior-related factors (see Figure 5.10). The variations in some of these factors have significant effects on the behavior of SFRC under flexure, while variations in other factors result in negligible effects on the flexural behavior of SFRC. Since it is not economical and practical to optimize all these factors in the process of "System Identification," factors whose variations result in significant effects on the flexural behavior of SFRC need to be selected as the "System Identification" parameters.

Chapter 5 has examined the influence of each factor on the flexural peak load ( $P$ ), flexural ductility ( $D$ ), flexural toughness ( $A$ ) and overall flexural behavior of steel fiber reinforced concrete ( $V$ ). It was observed that in the case of material-related factors, the fiber peak pull-out strength ( $\tau_u$ ), fiber diameter ( $d_f$ ), fiber length ( $l_f$ ), fiber volume fraction ( $V_f$ ), matrix tensile strength ( $\sigma_m'$ ), and fiber slip at residual pull-out strength ( $S_r$ ) are the most influential factors deciding the flexural behavior of SFRC. As far as the constitutive behavior-related factors are concerned, it was shown in Chapter 5 that their effects are negligible when compared with those of the material-related factors.

Among the six influential material-related factors, those representing fiber dimensions (i.e.,  $d_f$  and  $l_f$ ) as well as the volume fraction of fibers ( $V_f$ ) should be known inputs while analyzing some flexural test data obtained for SFRC. This further reduces the number of "System Identification" parameters and leaves only three material-related factors to be entered as parameters in "System Identification:" fiber peak pull-out strength ( $\tau_u$ ), fiber slip at residual pull-out strength ( $S_r$ ) and matrix tensile strength ( $\sigma_m'$ ). It is worth mentioning that

the tensile strength of SFRC can be determined once the values of these three factors are obtained through analysis of flexural test results using "System Identification."

## 6.6 RESULTS OF SYSTEM IDENTIFICATION

Table 6.1 summarizes conditions of the SFRC flexural tests considered for "System Identification," and also presents the optimized values of the three main parameters obtained from "System Identification." Figures 6.6(a) through 6.6(k) illustrate the comparisons between the experimentally obtained and theoretically optimized flexural load-deflection curves. Satisfactory correlations are observed in these Figures. From Table 6.1, the optimized values of three parameters are found to be larger than the values obtained from direct tension and material tests (see the comparison presented in Table 6.2). The experimental data presented in Table 6.2 are the averages obtained from several direct tension and fiber pull-out tests performed on materials comparable to those used in flexural tests. The matrix tensile strength ( $\sigma_m'$ ) and performance of fibers obtained from the analysis of flexural test results may be improved in comparison with those obtained from direct tension and pull-out tests due to the strain gradient effects under flexural loading condition, which generally lead to improved tensile performance of the material [27]. The improvements in pull-out performance in flexural test specimens over those obtained from single fiber pull-out tests may also be attributed to the positive effects of fiber reinforcement at the surrounding matrix (noting that single fiber pull-out tests are generally conducted using non-fibrous surrounding matrices) in flexural test specimens. Reference 27, using an analysis of experimental data, has also reported increase

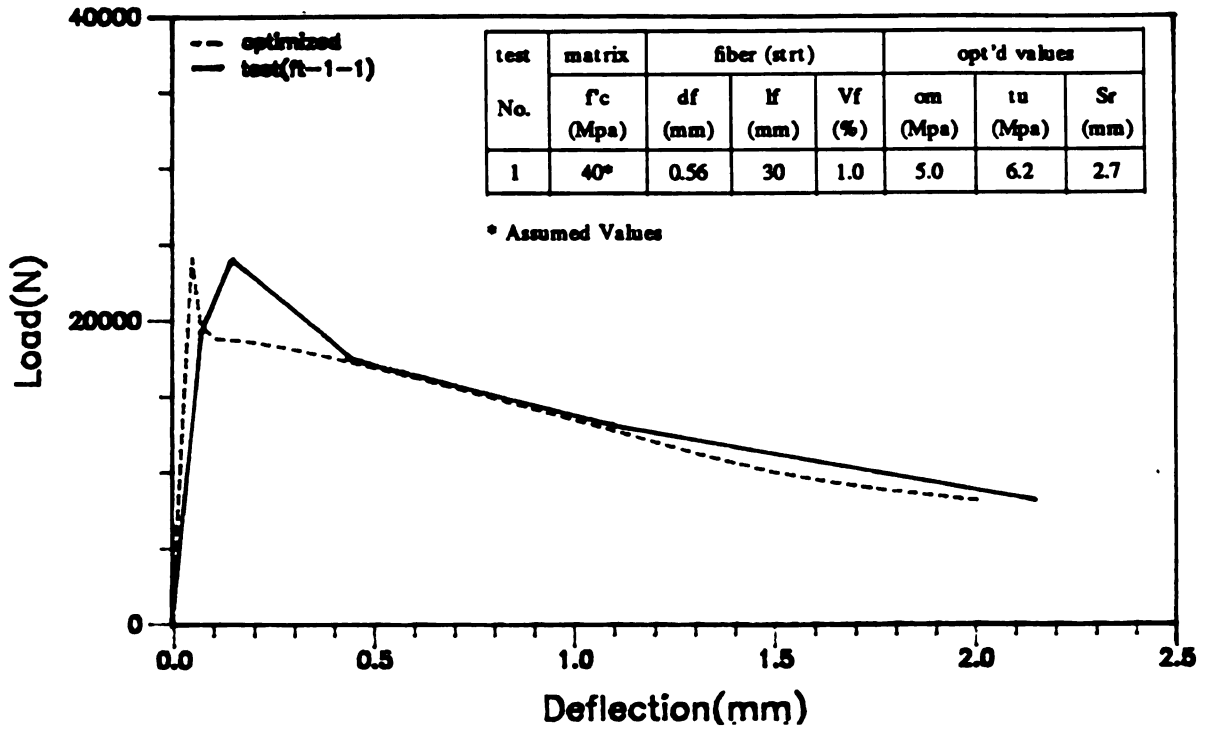
Table 6.1 Test Conditions and Optimized Values from System Identification.

Refs.	Test No.	Specimen			Fiber				f'c	Opt'd Values			Error	Iter. No.
		width	depth	length	type	df	lf	Vf		om'	tu	Sr		
44	1	100	100	300	strt	0.56	30	0.01	(40)	5.032	6.174	2.72	0.000456	4
	2	100	100	300	strt	0.56	30	0.015	(40)	5.895	5.036	3.441	0.000024	3
	3	100	100	300	strt	0.56	30	0.02	(40)	7.132	4.413	3.447	0.000011	6
45	4	100	100	300	strt	0.56	30	0.01	34.6	3.332	3.831	2.198	0.010869	6
	5	100	100	300	strt	0.56	30	0.015	34.6	4.649	3.933	3.121	0.000273	3
	6	100	100	300	strt	0.56	30	0.01	48	3.032	5.0	3.0	0.026306	2
	7	100	100	300	strt	0.56	30	0.01	24.7	2.564	2.752	2.56	0.000494	7
75	8	100	100	300	hook	0.5	30	0.01	(40)	3.444	9.291	3.085	0.000231	3
	9	100	100	300	hook	0.5	30	0.01	(40)	3.831	7.73	6.247	0.000967	4
	10	100	100	300	hook	0.5	30	0.01	(40)	3.695	5.371	2.957	0.004180	2
	11	100	100	300	hook	0.5	30	0.01	(40)	2.57	6.25	2.887	0.003061	3

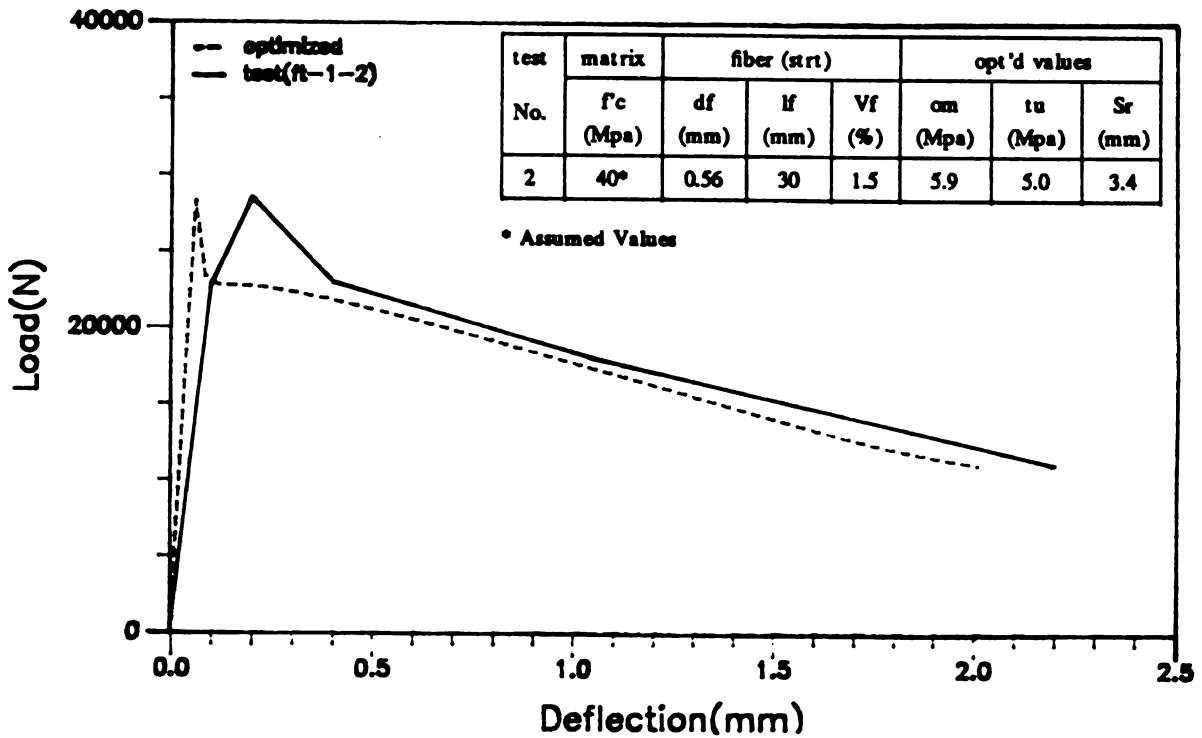
Values in parenthesis are assumed ones.

**Table 6.2 Comparison of the Tension Test Results with the Optimum Values of Parameters in Analysis of Flexural Test Results Using "System Identification."**

Refs. No.	Test No.	Fiber				$\sigma_m'$ ( $0.332\sqrt{f'c}$ )	Ratios		
		type	df	lf	vf		$\sigma_m^0/\sigma_m'$	$\tau_m^0/\tau_m$	$Sr^0/Sr$
44	1	str	0.56	30	0.01	2.1	2.4	2.35	0.97
	2	str	0.56	30	0.015	2.1	2.8	1.92	1.23
	3	str	0.56	30	0.02	2.1	3.4	1.68	1.23
45	4	str	0.56	30	0.01	1.95	1.7	1.45	0.97
	5	str	0.56	30	0.015	1.95	2.4	1.50	0.11
	6	str	0.56	30	0.01	2.30	1.32	1.90	1.07
	7	str	0.56	30	0.01	1.65	1.55	1.05	0.91
75	8	hook	0.5	30	0.01	2.1	1.63	2.07	1.10
	9	hook	0.5	30	0.01	2.1	1.82	1.72	2.23
	10	hook	0.5	30	0.01	2.1	1.76	1.20	1.05
	11	hook	0.5	30	0.01	2.1	1.22	1.35	1.03

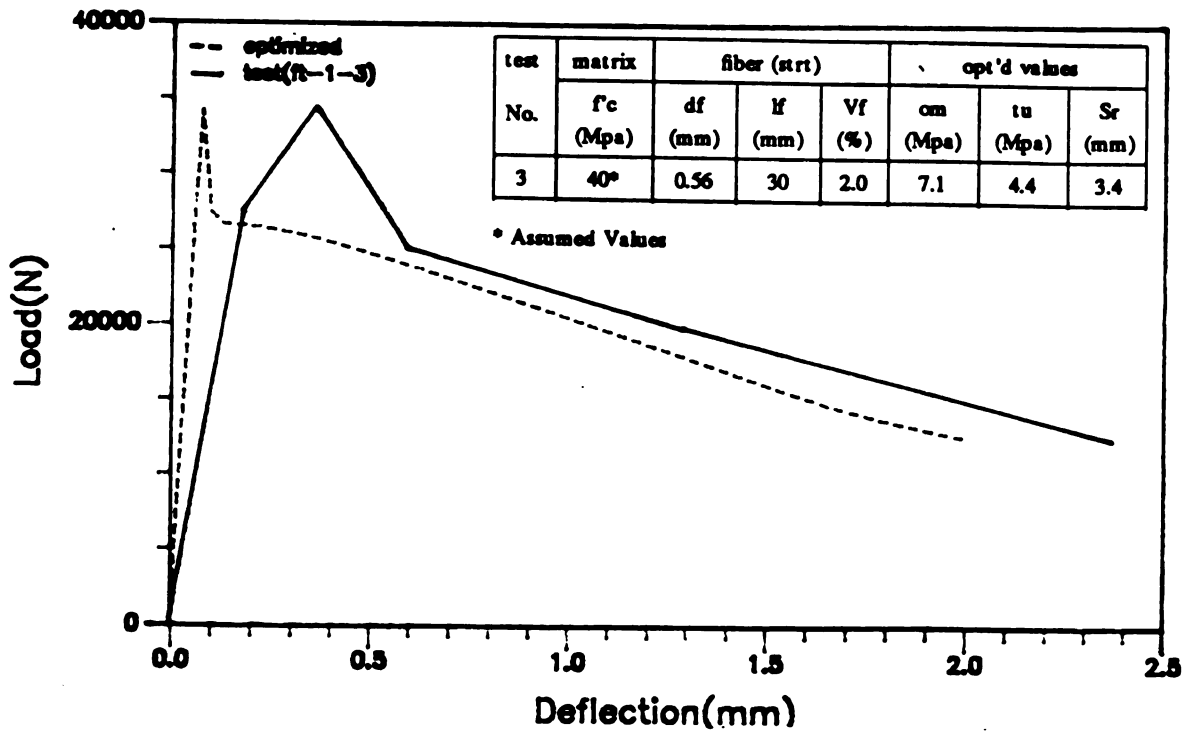


(a) Test Results from Reference 44

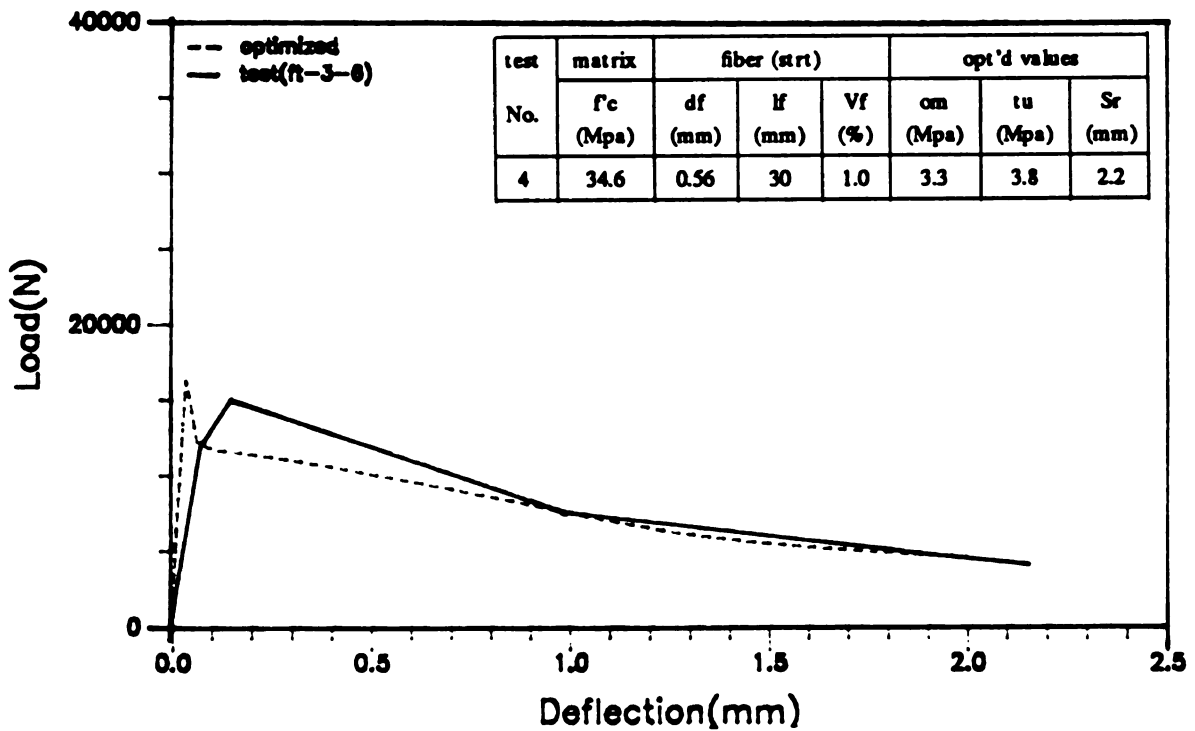


(b) Test Results from Reference 44

Figure 6.6 Comparisons between Experimentally Obtained and Theoretically Optimized Flexural Load-Deflection Curves

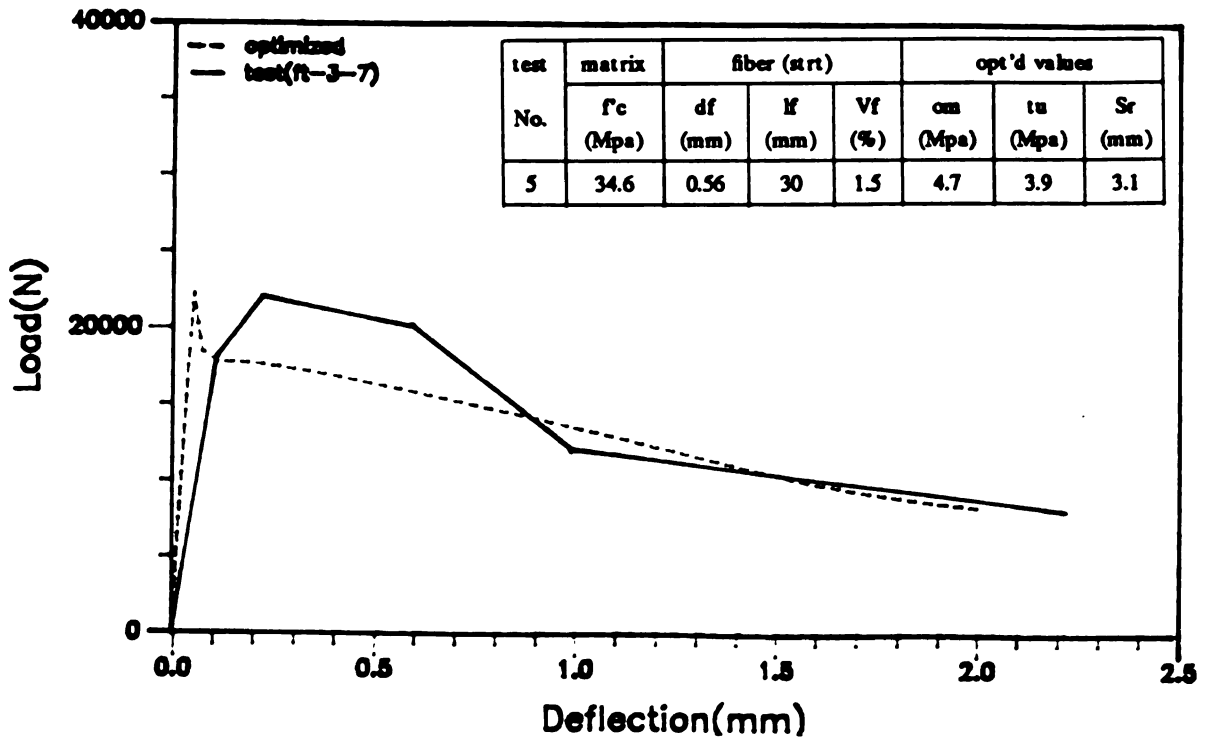


(c) Test Results from Reference 44

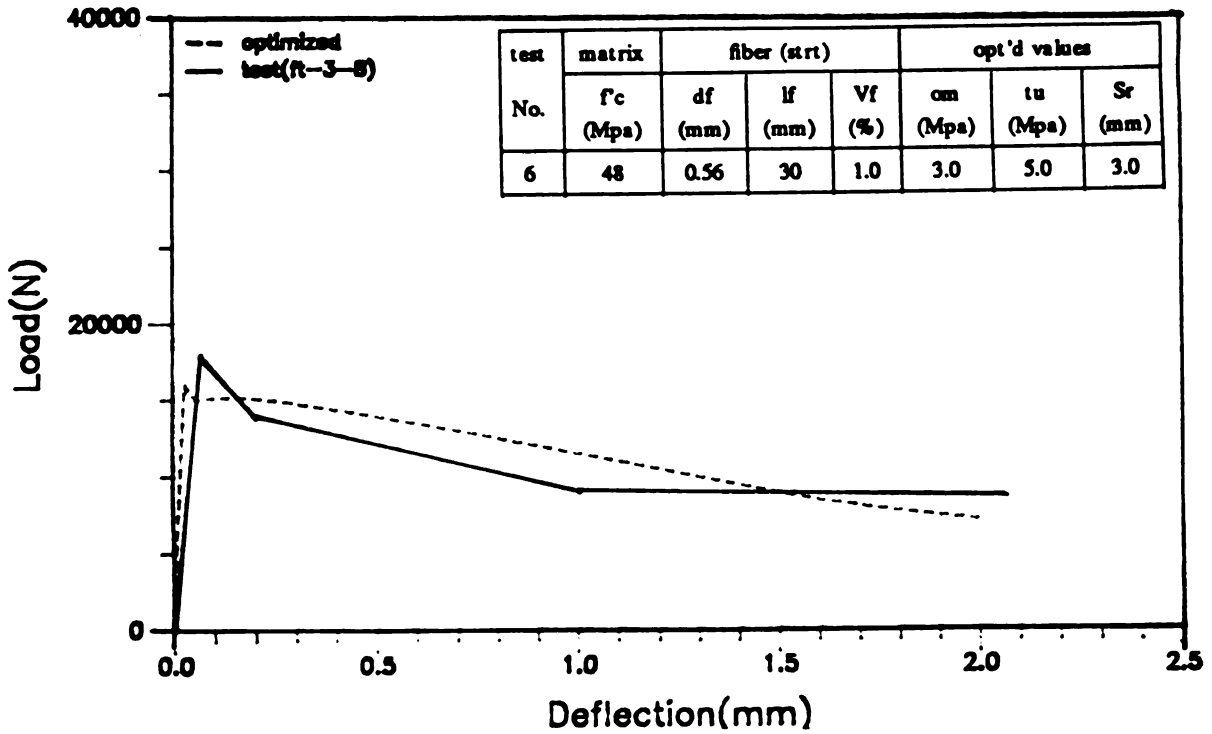


(d) Test Results from Reference 45

Figure 6.6 Comparisons between Experimentally Obtained and Theoretically Optimized Flexural Load-Deflection Curves (cont'd)

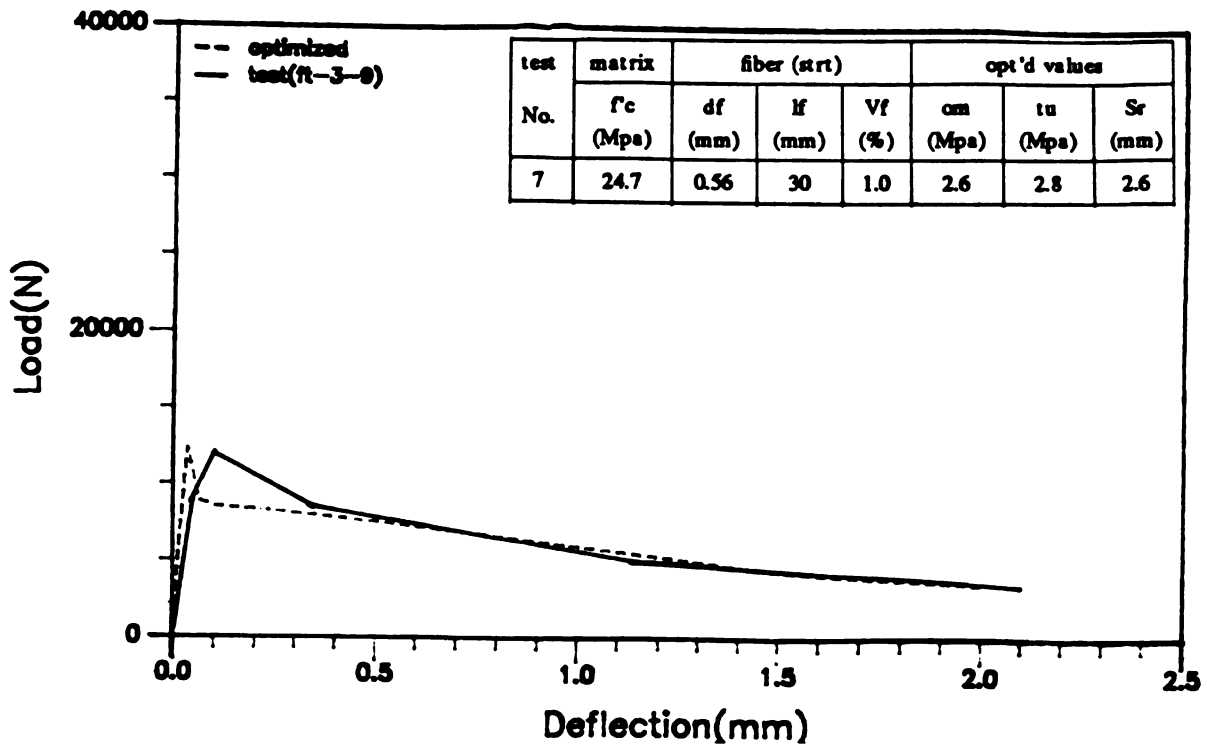


(e) Test Results from Reference 45

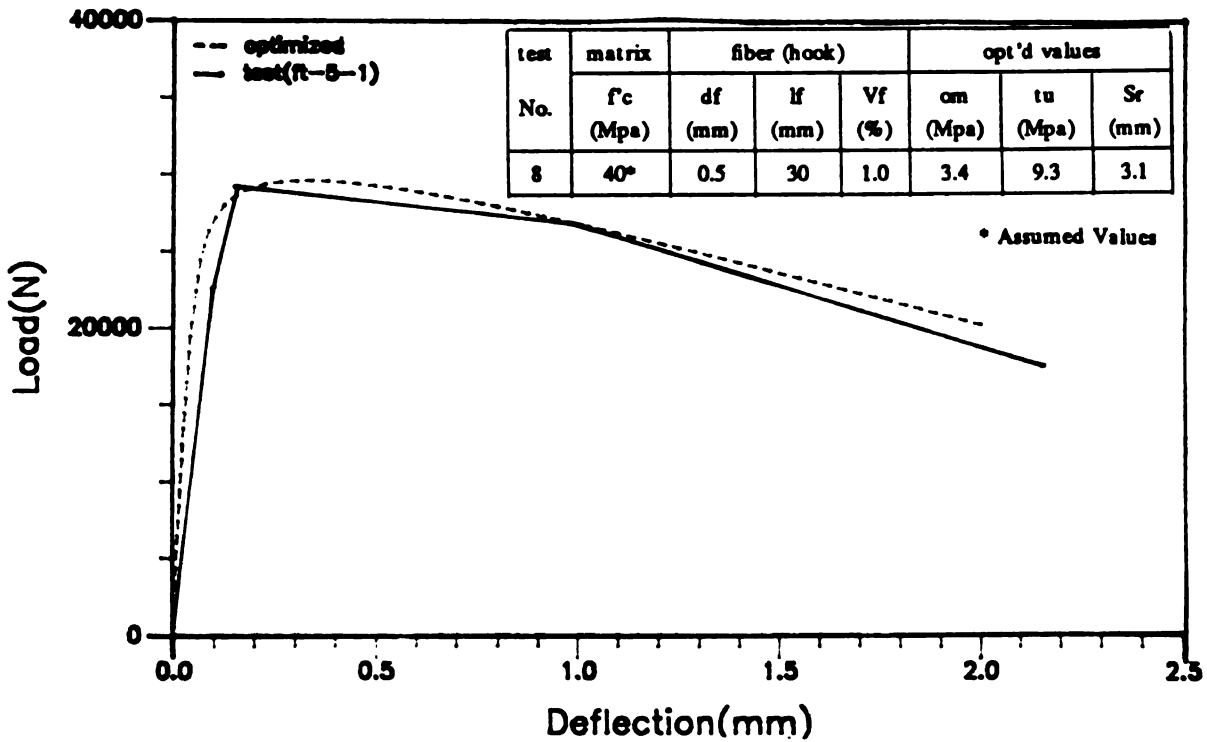


(f) Test Results from Reference 45

Figure 6.6 Comparisons between Experimentally Obtained and Theoretically Optimized Flexural Load-Deflection Curves (cont'd)

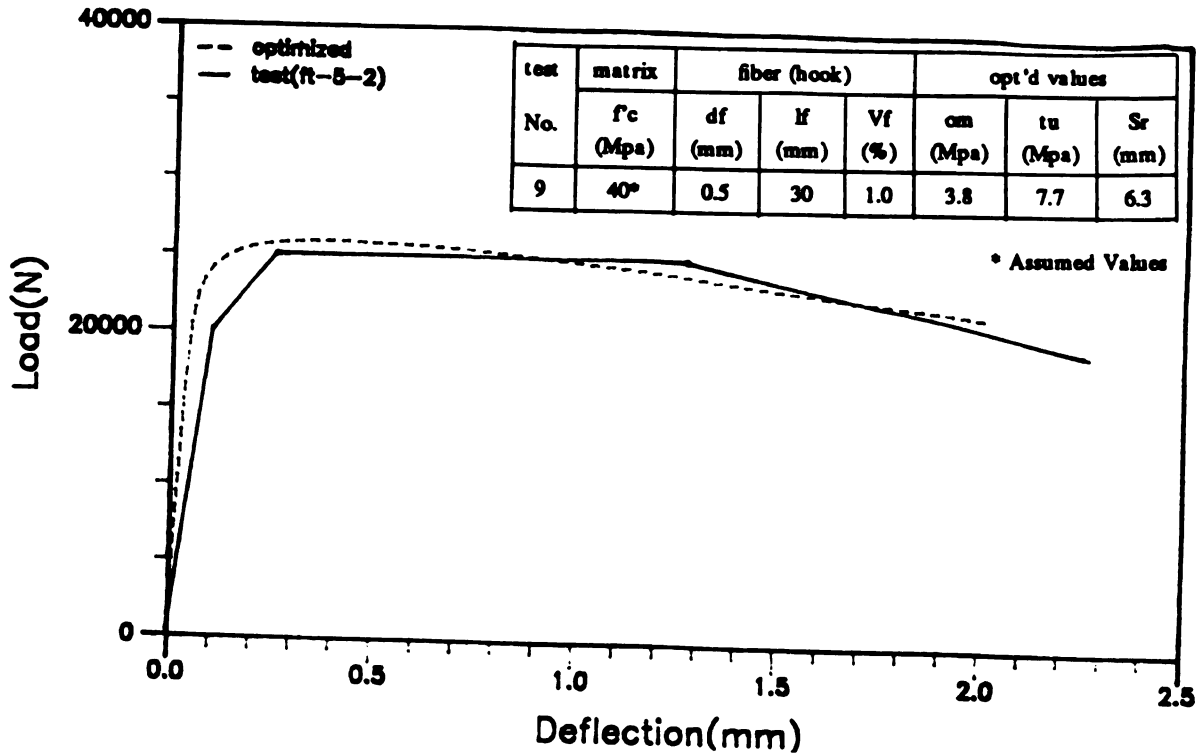


(g) Test Results from Reference 45

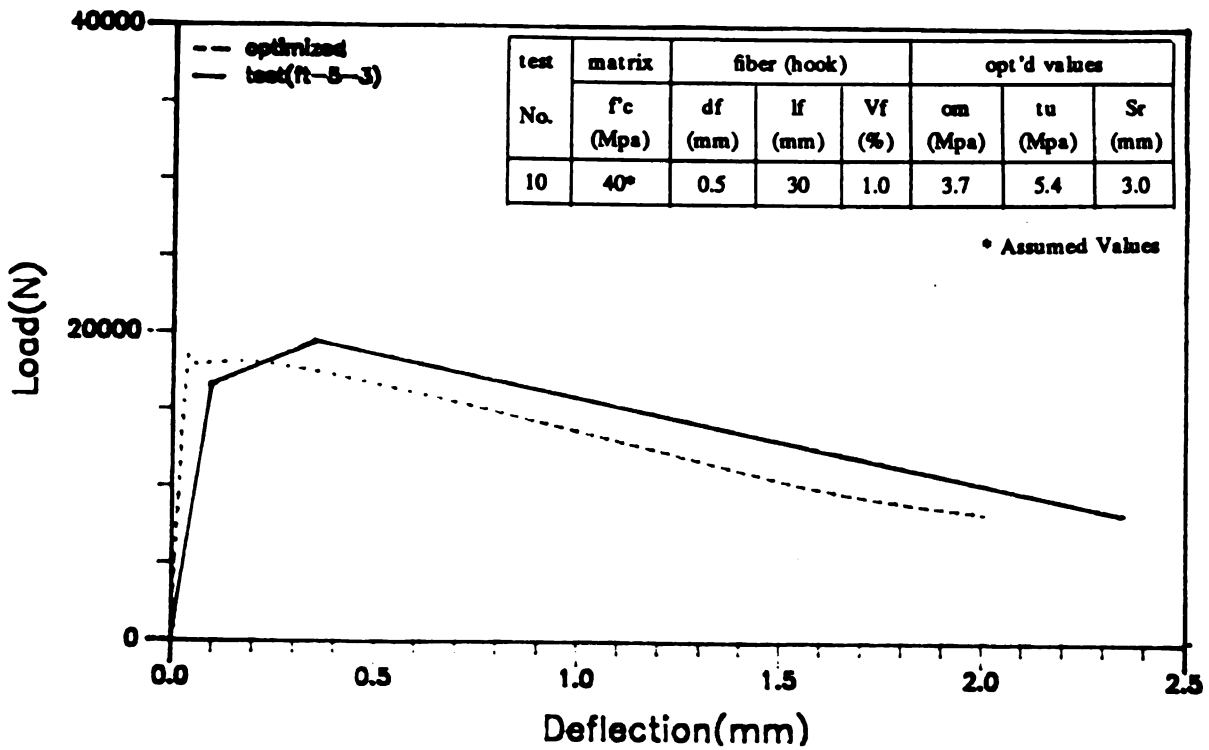


(h) Test Results from Reference 75

Figure 6.6 Comparisons between Experimentally Obtained and Theoretically Optimized Flexural Load-Deflection Curves (cont'd)

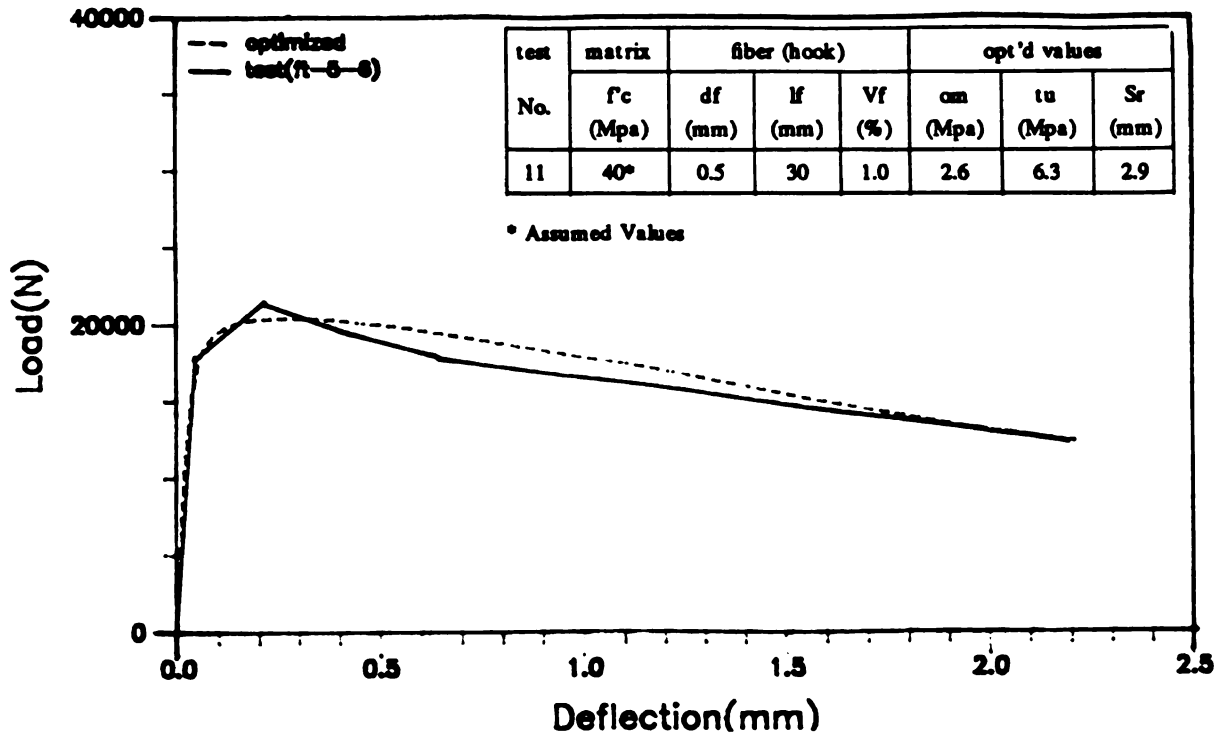


(i) Test Results from Reference 75



(j) Test Results from Reference 75

Figure 6.6 Comparisons between Experimentally Obtained and Theoretically Optimized Flexural Load-Deflection Curves (cont'd)



(k) Test Results from Reference 75

Figure 6.6 Comparisons between Experimentally Obtained and Theoretically Optimized Flexural Load-Deflection Curves (cont'd)

in pull-out strength under flexure when compared with pull-out strength under tension.

In Table 6.3, the tensile strengths of SFRC calculated using Equation 3.10 with the optimized values of parameters obtained from the analysis of flexural test data are compared with the corresponding predictions of Equation 3.10 with average values obtained from direct tension and fiber pull-out tests. The composite material tensile strengths obtained from flexural test results is observed to be larger than those obtained from direct tension and pull-out test results. The ratios of flexure-based to tension-based composite material tensile strengths are presented in the last column of Table 6.3. It is interesting that the average of these ratios is 1.82, which is close to the value of 1.87 obtained by taking the ratio of the matrix modulus of rupture ( $0.62 \cdot \sqrt{f_c'}$ ) to the matrix direct tensile

Table 6.3 Derived Tensile Strengths of Matrices and Composites in Direct Tension and "System Identification."

Ref. No.	Test No.	Matrix Tensile Strength		Ratios $\sigma_m^0 / f_r$	SFRC Tensile Strength (Eq. 3.10)		Ratios $\sigma_c^0 / \sigma_c$
		$\sigma_m^0$	$f_r (=0.62\sqrt{f_c})$		$\sigma_c^0$	$\sigma_c$	
44	1	5.03	3.92	1.28	6.85	2.87	2.39
	2	5.9	3.92	1.505	7.45	2.87	2.59
	3	7.13	3.92	1.82	8.42	2.87	2.9
45	4	3.32	3.64	0.91	4.45	2.71	1.64
	5	4.65	3.64	1.28	6.4	3.07	2.08
	6	3.03	4.29	0.706	4.47	3.08	1.451
	7	2.56	3.08	0.83	3.38	2.41	1.407
75	8	3.44	3.92	0.88	6.38	3.54	1.8
	9	3.83	3.92	0.98	6.31	3.54	1.782
	10	3.7	3.92	0.95	5.47	3.54	1.545
	11	2.57	3.92	0.65	4.56	3.54	1.288
Averages				1.008			1.82

strength ( $0.332 \cdot \sqrt{f'_c}$ ). This suggests that the tensile behavior of steel fiber reinforced concrete is also influenced by strain gradient in a manner similar to the tensile strength of plain concrete.

Large variations in the values of parameters ( $\tau_u$ ,  $\sigma_m$ , and  $S_r$ ) obtained from "System Identification" in Table 6.1 suggest that the highly variable (and unreliable) measurements of flexural deflections in the pre-peak region have some influence on the analysis of flexural test data using the "System Identification" approach. These variations may also partly result from the fact that some flexural test results reported in the literature were not accompanied by reliable information on basic material properties and thus some assumptions had to be made on these properties through the course of "System Identification."

## 6.7 SUMMARY AND CONCLUSION

The complexity and instability involved in testing cementitious materials under direct tension have led to wide spread use of flexural testing for the assessment of the tensile performance characteristics of cement-based materials. The analytical study presented in this Chapter was aimed at analyzing flexural test results for steel fiber reinforced concrete in order to derive information on the tensile constitutive behavior of the material.

An indirect method, "System Identification", was adopted for the analysis of flexural test results. "System Identification" is a process of selecting the form of the model (with a number of unknown parameters), and then systematically adjusting the parameters until, based on a predefined criterion, the best correlation is achieved between the predicted and measured responses. In this study, flexural test results were used to adjust characteristic parameters in the

constitutive model of SFRC. The flexural analysis procedure developed in Chapter 5, which incorporates tensile and compressive constitutive models of SFRC was employed to predict the flexural behavior of SFRC in the "System Identification" approach. The characteristic parameters initially considered consisted of ten material-related and ten constitutive behavior-related factors. The number of these parameters was reduced by selecting factors with significant effects on the overall flexural behavior of SFRC. These factors (parameters) were optimized through "System Identification." Based on the study performed in Chapter 5, six material-related factors ( $\tau_u$ ,  $d_f$ ,  $l_f$ ,  $V_f$ ,  $\sigma_m'$  and  $S_r$ ) were found to dominate the overall flexural behavior of SFRC, and considering the fact that fiber dimensions ( $d_f$  and  $l_f$ ) as well as the volume fraction of fibers ( $V_f$ ) are known inputs, the remaining three material-related factors ( $\tau_u$ ,  $\sigma_m'$  and  $S_r$ ) were entered as parameters in "System Identification."

In order to measure the correlation between the predicted and measured flexural load-deflection curves, an error function (E) which is defined in a similar manner as the function (V) measuring the overall flexural behavior of SFRC in Chapter 5, was established. The error function (E) takes into account differences between predicted and measured values of peak flexural strength (P), ductility (D), and toughness (A) of SFRC.

In order to find the optimum set of "System Identification" parameters which minimize the value of error function, a nonlinear programming technique based on Modified Powell's Method was used together with quadratic line search. The method iteratively searches for the minimum error point in the n-dimensional parameter space by producing n mutually conjugate directions in n subcycles and then discarding one of the mutually conjugate directions to avoid the linear dependency of direction vectors. The minimum points selected along these direction vectors eventually lead to the global minimum of a given error

function. The use of Modified Powell's Method has advantages over other methods in application to the specific problem of this study because it does not require the calculation of gradient vector for which analytical expressions should exist. The method could successfully produce the optimum set of parameters which lead to a satisfactory match between the measured and predicted flexural load-deflection relationships.

The values of parameters obtained from "System Identification" are, in most cases, larger than those derived from direct tension tests performed on SFRC. An analysis of the results indicated that:

(1) The matrix tensile strength ( $\sigma_m'$ ) and pull-out performance of fibers obtained from the analysis of flexural test results were superior to those obtained from direct tension and pull-out tests. This may be attributed to the strain gradient effects under flexural loads.

(2) The improvements in pull-out performance in flexural tests over those obtained from single fiber pull-out tests (where fibers are generally pulled out of non-fibrous matrices) may also be attributed to the positive effects of fiber reinforcement of the surrounding matrix in flexural test specimens.

(3) Tensile strength of SFRC obtained from the analysis of flexural test results is larger than tensile strength obtained from direct tension tests on SFRC. The tensile strength of SFRC under flexure was, on the average, 1.82 times the tensile strength of SFRC obtained from direct tension tests, which is comparable to the ratio of the modulus of rupture to direct tensile strength of plain concrete. This suggests that the tensile behavior of SFRC is influenced by strain gradient in a manner similar to the tensile strength of plain concrete.

(4) Large variations were observed in the values of parameters ( $\tau_u$ ,  $\sigma_m'$  and  $S_r$ ) obtained from "System Identification." This could result from both unreliable measurements of flexural deflections in the pre-peak region in

some test results reported in the literature, and also from the lack of information on some basic material properties for flexural tests conducted by other investigators.

## CHAPTER 7

### SUMMARY AND CONCLUSION

Reinforcement of concrete with randomly oriented short steel fibers improves the tensile strength, and the tensile and compressive toughness of the material. Fibers in cementitious matrices arrest and deflect the propagating microcracks. The debonding and pull-out action of fibers under tension, and the confinement of cementitious matrices by steel fibers under compression, are also important mechanisms leading to improvements in concrete behavior in the presence of steel fibers. Improvements in the flexural performance of concrete resulting from steel fiber reinforcement are direct consequences of the corresponding improvements in the tensile and compressive performance of the material.

In order to develop methods for analysis of reinforced concrete structures incorporating steel fibers, reliable tensile and compressive constitutive models are needed for fiber reinforced concrete. In many applications, SFRC is subjected to flexural forces and thus it is important to develop analytical techniques for predicting the flexural behavior of SFRC which account for the nonlinear stress distributions and the dominance of a cracked section in deciding the post-peak performance of SFRC.

This investigation dealt with three aspects of SFRC behavior: (1) compressive; (2) tensile; and (3) flexural. In the first phase of this investigation, summarized in Chapters 3 and 4, empirical constitutive models were developed for predicting the complete stress-deformation relationships of SFRC under tensile and compressive stresses. In Chapter 5, an analytical approach was developed

for simulating the flexural performance of SFRC, which incorporated the tensile and compressive constitutive models of SFRC developed in Chapters 3 and 4. Parametric studies were conducted using the developed constitutive models and flexural analysis procedures in order to assess the effects of different fiber and matrix properties on the performance characteristics of the composite material. Finally, the "System Identification" technique was used together with the developed flexural analysis procedure and constitutive models in order to derive information on the tensile behavior of SFRC using flexural test data.

Different phases of this investigation and the related conclusions are summarized below.

### **Tensile Constitutive Modeling**

Theoretical expressions were derived for the number of fibers per unit cross sectional area in fiber reinforced concrete as functions of fiber volume fraction and length, assuming that cross sectional boundaries are the only factors disturbing the 3-D random orientation of fibers. Measurements were made on fractured surfaces of steel fiber reinforced concrete specimens in order to assess the actual values for the number of fibers per unit area in steel fiber reinforced concrete. Nineteen steel fiber reinforced concrete specimens incorporating different fiber volume fractions and different fiber types were considered in this investigation. Statistical studies were conducted on the measured values of the number of fibers per unit area for determining the possible effects of fiber type and location on the number of fibers per unit area. Comparisons were also made between the theoretical and measured values of the number of fibers per unit area in order to determine the effects of reorientation of steel fibers inside concrete during vibration. Recommendations were made, based on the findings of this research, for approximating the number of fibers per unit area in steel fiber

reinforced concrete.

The following conclusions were derived from the results of this investigation:

(1) The type of steel fiber (straight vs. hooked) and the location in cross section with respect to the casting direction (top vs. bottom) did not have any statistically significant effect on the measured value of number of fibers per unit area.

(2) Vibration of steel fiber reinforced concrete seems to reorient the fibers, resulting in a tendency towards orienting the fibers in horizontal planes. This phenomenon illustrates the higher values for number of fibers per unit area in actual measurements when compared with theoretical predictions.

(3) The number of fibers per unit cross sectional area in steel fiber reinforced concrete after vibration is between the theoretical values derived for 3-D and 2-D random orientation conditions considering the boundary effects.

A refined concept ("interaction concept") was proposed for predicting the tensile strength of SFRC. This concept accounts for the partial mobilization of the fiber pull-out action (interfacial bond stresses) at the peak tensile strength of composite material, and also considers the microcrack arresting action of fibers and the consequent strengthening of matrix in the presence of steel fibers. The proposed "interaction concept" leads to an expression for predicting the tensile strength of steel fiber reinforced concrete, which incorporates some unknown coefficients to be determined empirically. These coefficients were decided in this study using a relatively large number of SFRC tensile strength test results.

The theoretical predictions based on the proposed "interaction concept", when compared with those of the commonly used composite material and spacing concepts, show a reasonable correlation with test results. More importantly, the relative matrix and fiber contributions to the composite material tensile

strength in the proposed "interaction concept" are representative of the physics of the composite material performance at peak tensile stress.

A constitutive model was also developed for predicting the pre-peak tensile stress-strain relationship as well as the post-peak tensile stress-deformation relationship of steel fiber reinforced concrete. The developed post-peak constitutive model accounts for the contributions of fibers crossing the critical section through their pull-out action as well as that of matrix in its post-peak softening range of behavior. Empirical fiber pull-out load-slip and matrix post-peak constitutive models were combined to derive the composite material post-peak tensile stress-deformation model. The pre-peak constitutive model of the composite material developed in this study was an empirical one based on the tension test results reported in the literature for steel fiber reinforced concrete. The proposed constitutive model is shown to compare reasonably well with tension test results performed on steel fiber reinforced concrete in both the pre- and post-peak regions.

### **Compressive Constitutive Modeling**

Reinforcement of concrete with randomly oriented short steel fibers increases the ultimate strength and especially the post-peak ductility and energy absorption capacity of concrete under compression. The effectiveness of steel fibers in enhancing concrete behavior under compression depends on the mix proportions of the matrix, the volume fraction, aspect ratio and deformation configurations of fibers, loading versus casting direction, specimen geometry, and rate of loading.

An empirical constitutive model was developed in this study for steel fiber reinforced concretes loaded in compression. This model accounts for the effects of fiber volume fraction, aspect ratio and type (straight vs. hooked), and the

matrix compressive strength, on the compressive behavior of steel fiber reinforced concrete. The model has been developed using results of ninety eight compression tests performed on 150 mm (6 in.) by 300 mm (12 in.) cylindrical concrete specimens with maximum aggregate sizes ranging from 9.5 mm (3/8 in.) to 19 mm (3/4 in.), incorporating straight or hooked fibers and loaded quasi-statically in the direction of casting.

The relatively simple empirical model developed in this study predicts experimental results (for fibrous concretes with relatively wide ranges of fiber and matrix variables) with a reasonable accuracy. More test results are needed for refining the model to consider the effects of maximum aggregate size, specimen geometry, loading versus casting direction, and the rate of loading.

### **Flexural Analysis of Steel Fiber Reinforced Concrete**

Under flexural loads, one major crack generally forms in steel fiber reinforced concrete at the critical section, in the vicinity of which a relief of tensile stresses occurs. After cracking, the critical section suffers severe distortions and thus plane sections do not remain plane in its vicinity. A flexural analysis procedure was developed which gives due consideration to the behavior at and near the critical (cracked) section.

The exact distributions of tensile and compressive strains in the critical region are rather complex. Some simplifying assumptions were made in order to simulate the flexural behavior at critical region. Before the crack starts to open, the moment and curvature distributions are similar in shape. As the flexural load increases beyond the first-crack load, the critical region is assumed to spread outward, and it stabilizes when the beam reaches its ultimate load, with curvature at the boundary of the critical region assumed to stay constant at the first-crack value. In the post-peak region, compressive strains in the critical

region further increase while elastic flexural deformations outside critical region tend to decrease. This, together with the assumed constant values of curvature at the boundaries of the critical region, result in a tendency in deformations to increasingly concentrate near the center (cracked section) of the critical region.

The crack shape at the critical section is assumed to be linear and symmetric about a plane normal to the beam longitudinal axis. Assuming linear variations in compressive and tensile curvatures at the critical region (where the tensile curvature is assumed to vary from zero at the crack to a value equal to the compressive side curvature at the boundary of the critical region), the crack opening angle could be obtained by computing the difference in rotations associated with compressive and tensile strains in the critical region. Maximum crack opening at the extreme bottom layer of the critical section could be obtained using this crack opening angle and the neutral axis position obtained by satisfying the equilibrium of tensile and compressive forces at the critical (cracked) section.

A step-by-step incremental approach was adopted for flexural analysis of SFRC beams. In each step, an increment is made in curvature on the compressive side of the cracked section, and numerical techniques (based on the Modified Regula-Falsi method) were used to iteratively decide the neutral axis position which satisfies equilibrium conditions. The tensile and compressive constitutive models of SFRC developed in this study were used in flexural analysis of the critical section. The assumptions described above were then used to derive the flexural behavior of complete beam using the critical section behavior at the end of each step.

Using the proposed analytical approach, the flexural behavior and stress profiles at the critical section were investigated at different loading stages with two different fiber volume fractions (0.5% and 1.2%). The results indicated

that the peak flexural load at both fiber volume fractions is attained when the crack at critical section has already opened. This implies that flexural strength is reached in SFRC beams when the tensile behavior has already reached the post-peak region. The flexural strength of SFRC, therefore, seems to be dependent not only on the tensile strength of the material, but also on its post-peak tensile behavior. This further explains why the increases in flexural strength is typically higher than the corresponding increase in tensile strength for given fiber reinforcement conditions. In addition, calculation of modulus of rupture based on linear-elastic flexural analysis equations does not seem to give a characteristic stress value which directly relates to the peak tensile strength of SFRC.

While a major fraction of the peak flexural resistance is maintained in the post-peak region for conditions with 1.2% fiber volume fraction, the load-carrying capacity with 0.5% fiber volume fraction drops suddenly in the post-peak regions.

The developed flexural analysis procedure was also used for a numerical parametric study on the influences of ten material-related and ten constitutive behavior-related factors on the flexural behavior of SFRC. The significance of these factors in deciding flexural performance characteristics was examined by simple observations of flexural load-deflection curves and also through statistical analysis based on  $2^k$  factorial design. The aspects of flexural behavior considered in this study were flexural peak load (P), ductility (D), toughness (A) and the overall flexural behavior of SFRC (V). The following conclusions could be derived using the results of this parametric study:

(1) The flexural strength of SFRC was most sensitive to the variation in matrix tensile strength.

(2) Ductility (D), toughness (A) and overall flexural behavior (V) are most influenced by fiber diameter and fiber pull-out strength.

(3) The effects on flexural behavior of the matrix compressive strength, crack opening at which matrix tensile stress diminishes, and fiber slip at peak pull-out load are negligible.

(4) Fiber dimensions (fiber diameter and fiber length) as well as fiber volume fraction have almost equally important effects on flexural behavior.

(5) While the matrix crack opening at residual matrix tensile strength has little effects on different aspects of flexural behavior, fiber slip at residual pull-out strength has relatively important effects on flexural ductility and overall flexural behavior of SFRC.

(6) Fiber-to-matrix bond strength ( $\tau_u$ ), fiber dimensions and volume fraction ( $d_f$ ,  $l_f$  and  $V_f$ ), matrix tensile strength ( $\sigma_m'$ ) and slip at residual pull-out strength ( $S_r$ ) are the most influential factors deciding the flexural behavior of SFRC.

(7) Similar observations were derived through analysis using  $2^k$  factorial design and also through simple observation of flexural load-deflection curves.

### **Interpretation of Flexural Test Results Using "System Identification"**

The complexity and instability involved in testing cementitious materials under direct tension have led to wide spread use of flexural testing for the assessment of the tensile performance characteristics of cement-based materials. The analytical study presented in this Chapter was aimed at analyzing flexural test results for steel fiber reinforced concrete in order to derive information on the tensile constitutive behavior of the material.

An indirect method, "System Identification", was adopted for the analysis of flexural test results. "System Identification" is a process of selecting the form of the model (with a number of unknown parameters), and then systematically adjusting the parameters until, based on a predefined criterion, the best

correlation is achieved between the predicted and measured responses. In this study, flexural test results were used to adjust characteristic parameters in the constitutive model of SFRC. The flexural analysis procedure developed in Chapter 5, which incorporates tensile and compressive constitutive models of SFRC was employed to predict the flexural behavior of SFRC in the "System Identification" approach. The characteristic parameters initially considered consisted of ten material-related and ten constitutive behavior-related factors. The number of these parameters was reduced by selecting factors with significant effects on the overall flexural behavior of SFRC. These factors (parameters) were optimized through "System Identification." Based on the study performed in Chapter 5, six material-related factors ( $\tau_u$ ,  $d_f$ ,  $l_f$ ,  $V_f$ ,  $\sigma_m'$  and  $S_r$ ) were found to dominate the overall flexural behavior of SFRC, and considering the fact that fiber dimensions ( $d_f$  and  $l_f$ ) as well as the volume fraction of fibers ( $V_f$ ) are known inputs, the remaining three material-related factors ( $\tau_u$ ,  $\sigma_m'$  and  $S_r$ ) were entered as parameters in "System Identification."

In order to measure the correlation between the predicted and measured flexural load-deflection curves, an error function (E) which is defined in a similar manner as the function (V) measuring the overall flexural behavior of SFRC in Chapter 5, was established. The error function (E) takes into account differences between predicted and measured values of peak flexural strength (P), ductility (D), and toughness (A) of SFRC.

In order to find the optimum set of "System Identification" parameters which minimize the value of error function, a nonlinear programming technique based on Modified Powell's Method was used together with quadratic line search. The method iteratively searches for the minimum error point in the n-dimensional parameter space by producing n mutually conjugate directions in n subcycles and then discarding one of the mutually conjugate directions to avoid

the linear dependency of direction vectors. The minimum points selected along these direction vectors eventually lead to the global minimum of a given error function. The use of Modified Powell's Method has advantages over other methods in application to the specific problem of this study because it does not require the calculation of gradient vector for which analytical expressions should exist. The method could successfully produce the optimum set of parameters which lead to a satisfactory match between the measured and predicted flexural load-deflection relationships.

The values of parameters obtained from "System Identification" are, in most cases, larger than those derived from direct tension tests performed on SFRC. An analysis of the results indicated that:

(1) The matrix tensile strength ( $\sigma_m'$ ) and pull-out performance of fibers obtained from the analysis of flexural test results were superior to those obtained from direct tension and pull-out tests. This may be attributed to the strain gradient effects under flexural loads.

(2) The improvements in pull-out performance in flexural tests over those obtained from single fiber pull-out tests (where fibers are generally pulled out of non-fibrous matrices) may also be attributed to the positive effects of fiber reinforcement of the surrounding matrix in flexural test specimens.

(3) Tensile strength of SFRC obtained from the analysis of flexural test results is larger than tensile strength obtained from direct tension tests on SFRC. The tensile strength of SFRC under flexure was, on the average, 1.82 times the tensile strength of SFRC obtained from direct tension tests, which is comparable to the ratio of the modulus of rupture to direct tensile strength of plain concrete. This suggests that the tensile behavior of SFRC is influenced by strain gradient in a manner similar to the tensile strength of plain concrete.

(4) Large variations were observed in the values of parameters ( $\tau_u$ ,  $\sigma_m$  and  $S_r$ ) obtained from "System Identification." This could result from both unreliable measurements of flexural deflections in the pre-peak region in some test results reported in the literature, and also from the lack of information on some basic material properties for flexural tests conducted by other investigators.

## LIST OF REFERENCE

1. ACI Committee 544, "State-of-the-Art Report on Fiber Reinforced Concrete," Report:ACI544, IR-82, American Concrete Institute, Detroit, May, 1982, pp.16
2. Shah, S.P. and Rangan, V., "Fiber Reinforced Concrete Properties," Journal of the American Concrete Institute, Feb. 1971, pp. 126-135.
3. Mangat, P.S., "Tensile Strength of Steel Fiber Reinforced Concrete," Cement and Concrete Research, 1976, Vol.6, pp. 245-252.
4. Shah, S.P., Stroeven, P., Dalhuisen, D. and van Stekelenburg, P., "Complete Stress-Strain Curves for Steel Fiber Reinforced Concrete in Uniaxial Tension and Compression," RILEM Symposium, 1978.
5. Fanella, D. and Naaman, A., "Stress-Strain Properties of Fiber Reinforced Mortar in Compression," Journal of the American Concrete Institute, Vol.82, No.4, July-August, 1985, pp475-483.
6. William, G.R., "The Effect of Steel Fibers on the Compressive Strength of Concrete," Fiber Reinforced Concrete, SP44-11, pp. 195-207.
7. Jindal, R.L., "Shear and Moment Capacities of Steel Fiber Reinforced Concrete Beams," Fiber Reinforced Concrete, SP81, American Concrete Institute, 1983, pp. 1-16.
8. Swamy, R.N. and Sa'ad A. Al-Ta'an, "Deformation and Ultimate Strength in Flexure of Reinforced Concrete Beams Made with Steel Fiber Concrete," Journal of the American Concrete Institute, Sept.-Oct. 1981, pp. 395-405.
9. Taketo Uomoto, "Shear Strength of Reinforced Concrete Beams with Fiber-Reinforcement," Journal of the American Concrete Institute, Sept.-Oct. 1981, pp. 395-405.
10. Gopalaratnam, V.S. and Shah, S.P., "Softening Response of Plain Concrete in Direct Tension," Journal of the American Concrete Institute, May-June 1985, pp. 310-323.
11. Diamond, S. and Bentur, A., "On Cracking in Concrete and Fiber Reinforced Cements," Application of Fracture Mechanics to Cementitious Composites, NATO-ARW, Sept. 4-7, 1984, pp. 87-140, Edited by Shah, S.P.
12. Gopalaratnam, V.S. and Shah, S.P., "Failure Mechanisms and Fracture of Fiber Reinforced Concrete," Proceedings of the Fiber Reinforced Concrete Symposium, ACI Convention, Baltimore, November 1986.
13. Shrive, N.G., "Compression Testing and Cracking of Plain Concrete," Magazine of Concrete Research, Vol.135, No.122, March 1983, pp. 27-39.
14. Craig, R., McConnell, J., Germann, H., Dib, N. and Kashani, F., "Behavior of Reinforced Fibrous Concrete Columns," American Concrete Institute, SP-81:Fiber Reinforced Concrete, 1981, pp. 69-105
15. Zollo, R.F., "An Overview of Progress in Applications of Steel Fiber Reinforced Concrete," Steel Fiber Concrete US-SWEDEN Joint Seminar (NSF-STU), Stockholm 3-5 June, 1985, Edited by Shah, S.P. and Skarendahl, A.
16. Gray, R.J. and Johnston, C.D., "The Measurement of Fibre-Matrix Interfacial Bond Strength in Steel Fiber Reinforced Cementitious Composites," RILEM, 1978, pp. 317-328.
17. Bentur, A., "Interfaces in Fibre Reinforced Cements," Materials Research Society Symposium, Proceedings, Vol.114, 1988, pp. 133-261.

18. Naaman, A. and Shah, S.P., "Pull-Out Mechanism in Steel Fiber Reinforced Concrete," *Journal of the Structural Division, ASCE*, Aug. 1976, pp. 1537-1549.
19. Narayanan, R. and Kareen-Palanjian, A.S., "Factors Influencing the Strength of Steel Fiber Reinforced Concrete," *RILEM Symposium*, 1978.
20. Pinchin, D.J., "Interfacial Contact Pressure and Frictional Stress Transfer in Steel Fibre Cement," *RILEM Symposium*, 1978, pp. 337-344.
21. Burakiewicz, A., "Testing of Fibre Bond Strength in Cement Matrix," *RILEM Symposium*, 1978, pp. 355-365.
22. Cancho, A.V. and Galvez V.S., "A Micromechanical Model for the Tensile Stress-Strain Curve of Fiber Reinforced Cements," *RILEM*, 1986.
23. Hannant, D.J., "Fiber Reinforced Cement and Concrete: Part 1; Theoretical Principles," *Concrete Society Current Practice Sheet*, No.92
24. Gopalaratnam, V.S. and Shah, S.P., "Micromechanical Model for the Tensile Fracture of Steel Fiber Reinforced Concrete," *RILEM Symposium, Proceedings*, 1986.
25. Walkus, B.R., Januszkiewicz, A. and Jeruzal, J., "Concrete Composites with Cut Steel Fiber Reinforcement Subjected to Uniaxial Tension," *ACI Journal*, October, 1979, pp. 1079-1093.
26. Lim, T.Y., Paramasivam, P. and Lee, S.L., "Analytical Model for Tensile Behavior of Steel-Fiber Concrete," *Journal of the American Concrete Institute (Material Journal)*, July-August 1987.
27. Swamy, R.N. and Mangat, P.S., "A Theory for the Flexural Strength of Steel Fiber Reinforced Concrete," *Cement and Concrete Research*, Vol.4, 1974, pp. 313-325.
28. Soroushian, P. and Bayasi, Z., "Prediction of the Tensile Strength of Fiber Reinforced Concrete: A Critique of the Composite Material Concept," *Fiber Reinforced Concrete, SP105*, American Concrete Institute, pp. 71-84.
29. Naaman, A.E. and McGarry, F.J., "Probabilistic Analysis of Fiber Reinforced Concrete," *Journal of the Engineering Mechanics*, Vol.100, No.EM2, April 1984, pp. 397-413.
30. Shah, S.P., "Strength Evaluation and Failure Mechanisms of Fiber Reinforced Concrete," *Proceedings of the International Symposium on Fiber Reinforced Concrete*, Dec. 16-19, 1987, Madras, India, pp. 1.3-1.9.
31. Pakotiprapha, B. and Lee, S.L., "Mechanical Properties of Cement Mortar with Randomly Oriented Steel Wires," *Magazine of Concrete Research*, Vol.26, No.86, March 1974, pp. 3-14.
32. Hughes, B.P., "Fibre Reinforced Concrete in Direct Tension," *Proceedings, ICE Conference on Fiber Reinforced Materials: Design and Engineering Applications*, London, March 1977.
33. Soroushian, P., Lee, C.D. and Bayasi, Z., "Fiber Reinforced Concrete: Theoretical Concepts and Structural Design," *Proceedings of the International Symposium on Fiber Reinforced Concrete*, Michigan State University, Feb. 1987, pp. 8.1-8.19.
34. Romualdi, J.P. and Mandel, J.A., "Tensile Strength of Concrete Affected by Uniformly Distributed Closely Spaced Short Lengths of Wire Reinforcement," *Journal of the American Concrete Institute*, Vol.61, June 1964, pp. 657-671.

35. Soroushian, P. and Lee, C.D., "Tensile Strength of Steel Fiber Reinforced Concrete: Correlation with Some Fiber Reinforcement Properties," *Journal of the American Concrete Institute* (Accepted for Publication).
36. Soroushian, P. and Lee, C.D., "Distribution and Orientation of Fibers in Steel Fiber Reinforced Concrete," *Journal of the American Concrete Institute* (Accepted for Publication).
37. Soroushian, P. and Lee, C.D., "Tensile and Compressive Constitutive Models for Steel Fiber Reinforced Concrete," *Proceedings, International Symposium on Steel Fiber Reinforced Concrete, London, U.K., 1989.*
38. Slate, F.O., "Stress-Strain Response and Fracture of a Concrete Model in Biaxial Loading," *Journal of the American Concrete Institute*, Aug. 1971, pp. 590-599.
39. Shah, S.P., "Internal Cracking and Strain-Softening Response of Concrete Under Uniaxial Compression," *Journal of the American Concrete Institute (Materials Journal)*, May-June 1987, pp. 200-212.
41. Soroushian, P. and Lee, C.D., "A Physical Simulation of the Fiber Reinforced Concrete Behavior under Compression," *Proceedings of International Symposium on Fiber Reinforced Concrete, Madras, India, Dec. 16-19, 1987*, pp. 1.3-1.9.
42. Parviz Soroushian, Ki-Bong Choi, and Abdulaziz Alhamad, "Dynamic Constitutive Behavior of Concrete," *Journal of the American Concrete Institute*, March-April 1986, pp. 251-259.
43. Kormeling, H.A., Reinhardt, H.W. and Shah, S.P., "Static and Fatigue Properties of Concrete Beams Reinforced with Continuous Bars and with Fibers," *Journal of the American Concrete Institute*, Jan.-Feb. 1980, pp. 36-43.
44. Cho, R. and Kobayashi, K., "Flexural Characteristics of Steel Fiber and Polyethylene Fibre Hybrid-Reinforced Concrete," *Composites*, April 1982, pp. 164-168.
45. Sakai, M. and Nakamura, N., "Analysis of Flexural Behavior of Steel Fiber Reinforced Concrete," *RILEM Symposium*, 1986.
46. Parameswaran, V.S. and Rajagopalan, K., "Strength of Concrete Beams with Aligned and Random Steel Fibre Micro-Reinforcement," *RILEM Symposium*, 1977, pp. 95-103.
47. Swift, D.G. and Smith, R.B.L., "The Physical Significance of the Flexure Test for Fibre Cement Composites," *RILEM Symposium*, 1978, pp. 463-478.
49. Rafagopalan, K., Parameswaran, V.S. and Pamaswamy, G.S., "Strength of Steel Fiber Reinforced Concrete Beams," *Indian Concrete Journal*, Jan. 1974, pp. 17-25.
50. Hughes, B.P. and Fattuhi, N.I., "Predicting the Flexural Strength of Steel and Polypropylene Fiber-Reinforced Cement-Based Beams," *Composites*, Jan. 1977, pp.57-61.
51. Laws, V. and Walton, P.L., "The Tensile-Bending Relationship for Fibre Reinforced Brittle Matrices," *RILEM Symposium*, 1978, pp. 429-438.
52. Johnston, C.D. and Coleman, R.A., "Strength and Deformation of Steel Fiber Reinforced Mortar in Uniaxial Tension," *An International Symposium; Fiber Reinforced Concrete, ACI, SP44*, pp. 178-193.
53. Lim, T.Y., Paramasivam, P., Mansur, M.A. and Lee, S.L., "Tensile Behavior of Steel Fibre Reinforced Cement Composites," *RILEM Symposium*, 1986.

54. Walpole, R.e. and Myer, R.H., "Probability and Statistics for Engineers and Scientists," McMillan Publishing Co., Reading, 1978.
55. Bonzel, J. and Schmidt, M., "Distribution and Orientation of Steel Fibers in Concrete and Their Influence on the Characteristics of Steel Fiber Concrete," Proceedings, RILEM Symposium on Fiber Reinforced Cement and Concrete, 1986.
56. Swamy, R.N. and Mangat, P.S., "Flexural Strength of Steel Fiber Reinforced Concrete," Proceedings, Institute of Civil Engineers, Part 2, Dec. 1974, pp. 701-707.
57. Fanella, D. and Krajcinovic, D., "Continuum Damage Mechanics of Fiber Reinforced Concrete," Journal of Engineering Mechanics, Vol.111, No.8, Aug. 1985, pp. 995-1009.
58. Hillerborg, A., "Numerical Methods to Simulate Softening and Fracture of Concrete," Fracture Mechanics of Concrete: Structural Application and Numerical Calculation, Edited by Sih, G.C. and Ditommaso, A.
59. Hughes, B.P. and Fattuhi, N.I., "Fibre Bond Strength in Cement and Concrete," Magazine of Concrete Research, Vol. 27, No.92, Sept. 1975, pp. 161-166.
60. Burakiewicz, A., "Testing of Fibre Bond Strength in Cement Matrix," RILEM Symposium on Fiber Reinforced Cement and Concrete, 1978
61. Stroeven, P., de Haan, Y.M. and Bouter, C., "Pull-Out Tests of Steel Fibers," RILEM Symposium, 1978
62. Gopalaratnam, V.S. and Abu-Mathkour, J., "Investigation of the Pull-Out Characteristics of Steel Fibers from Mortar Matrices," Proceedings of International Symposium on Fiber Reinforced Concrete, Dec. 16-19, 1987, Madras, India, pp. 2.201-2.211.
63. Naaman, A.E., Argon, A.S. and Moavenzadeh, F., "A Fracture Model for Fiber Reinforced Cementitious Materials," Cement and Concrete Research, Vol.3, 1973, pp.39-47.
64. Bayasi, Z., "Mechanical Properties and Structural Application of Steel Fiber Reinforced Concrete," Ph.D Thesis, Vol. II, Michigan State University, 1988.
65. Birkimer, D.L. and Hossley, J.R., "Comparison of Static and Dynamic Behavior of Plain and Fibrous-Reinforced Concrete Cylinders," Technical Report No.4-69, Dept. of Army, Ohio River Division Laboratories, Corps of Engineers, Dec. 1968.
66. Soroushian, P. and Bayasi, Z., "Optimum Use of Pozzolonic Materials in Steel Fiber Reinforced Concrete," Report No.88, Transportation Research Board 68th Annual Meeting, Jan. 22-26, 1989, Washington, D.C.
67. Scott, B.D., Park, R. and Priestley M.J.N., "Stress-Strain Behavior of Concrete Confined by Overlapping Hoops of Low and High Strain Rates," Journal of the American Concrete Institute, Jan.-Feb. 1982, pp. 13-27.
68. Soroushian, P. and Sim, J., "Axial Behavior of R/C Element under Dynamic Loads," Journal of the American Concrete Institute, Vol.83, No.6, Nov.-Dec. 1986, pp. 1018-1025.
69. Conte, S.D. and deBoor, C., "Elementary Numerical Analysis," McGraw-Hill Co., Reading, 1980.
70. Gopalaratnam, V.S. and Shah, S.P., "Properties of Steel Fiber Reinforced Concrete Subjected to Impact Loading," Journal of the American Concrete Institute, Jan.-Feb. 1986, pp. 117-126.

71. Stanton, J.F. and McNiven, H.D., "The Development of A Mathematical Model to Predict the Flexural Response of Reinforced Concrete Beams to Cyclic Loads, Using System Identification," Report No.UCB/EERC-70/02, Jan. 1979.
72. Luenberger, D.G., "Introduction to Linear and Nonlinear Programming," Addison-Wesley Publishing Company, Reading, Mass., 1973.
73. Powell, M.J.D., "An Efficient Method for Finding the Minimum of a Function of Several Variables Without Calculating Derivatives," Computer Journal, Vol.7, 1964.
74. Walsh, G.R., "Methods of Optimization," John Wiley and Sons Ltd., Reading, 1975.
75. Soroushian, P. and Ateff, K., "Mechanical Performance of Latex Modified Steel Fiber Reinforced Concrete," Report, Michigan State University, Feb. 1989.
76. Soroushian, P. and Mirza, F., "Effects of Different Steel Fibers on the Flexural Performance of SFRC," Report, Michigan State University, Mar. 1989.